Analysis and Design of MIMO Heterogeneous Cellular Networks

by

Mohammad Ghadir Khoshkholgh Dashtaki

B.S., University of Isfahan, 2006
M.S., Tarbiat Modares University, 2008

A THESIS SUBMITTED IN PARTIAL FULFILLMENT OF
THE REQUIREMENTS FOR THE DEGREE OF

DOCTOR OF PHILOSOPHY

in

The Faculty of Graduate and Postdoctoral Studies

(Electrical and Computer Engineering)

THE UNIVERSITY OF BRITISH COLUMBIA

(Vancouver)

August 2018

The following individuals certify that they have read, and recommend to the Faculty of Graduate and Postdoctoral Studies for acceptance, the dissertation entitled:

Analysis and Design of MIMO Heterogeneous Cellular Networks

submitted by Mohammad Ghadir Khoshkholgh Dashtaki in partial fulfillment of the requirements for

the degree of Doctor of Philosophy

in Electrical and Computer Engineering

Examining Committee:

Victor C. M. Leung, Electrical and Computer Engineering
Supervisor

Jane W. Wang, Electrical and Computer Engineering
Supervisory Committee Member

Lutz Hans-Joachim Lampe, Electrical and Computer Engineering
Supervisory Committee Member

Vijay Bhargava, Electrical and Computer Engineering
University Examiner

Frederick (Bruce) Shepherd, Computer Science
University Examiner

Abstract

The structure of cellular networks is under disruptive innovations as a response to the growth of data traffic demands and the emergence of new applications. On the one hand, cellular networks are evolving into complex infrastructures comprising of several tiers of base stations (BS), known as heterogenous cellular networks (HetNets). On the other hand, multiple-input multiple-output (MIMO) multi-stream (multiplexing) communications are deployed to improve the communication reliability and increase the transmission rate. A comprehensive network-level analysis of MIMO multiplexing HetNets in terms of influential system parameters is therefore required. This dissertation focuses on this matter and studies the network performance of several prominent MIMO multiplexing HetNets by adopting the powerful tool of stochastic geometry.

Unfortunately, the current literature lacks an accurate definition of the coverage probability in multiplexing systems, often considers simplistic cell association (CA) scenarios, and commonly provides the analytical results in numerically expensive forms. In general, these drawbacks render complexities in performance evaluation and hinder scalable system design. With these regards, this thesis aims at 1) analyzing the coverage performance from a link-level perspective; 2) considering the maximum signal-to-interference-plus-noise ratio (max-SINR) CA rule; and 3) deriving the network performance through easy-to-compute formulas.

Our analytical results are insightful and permits us to further explore various practical design issues. Specifically, thanks to compact formats and manageable computational costs of our analytical results, we are able to 1) comprehensively study the correlation across

data streams of a given communication link, and prove that this correlation undermines the coverage performance; 2) prove that in MIMO multiplexing HetNets growing the multiplexing gains reduces the coverage probability, thus diversity systems stands as the best option to maximize coverage probability; 3) investigate the relationship between spectral efficiency, multiplexing gains, and densification from a network-level perspective; 4) optimize the network in order to maximize aggregated multiplexing gains under prescribed coverage loss against the best possible coverage performance; and 5) explore the spectral efficiency optimization of the network subject to prescribed constraints.

Lay Summary

In recent years, the demands for wireless data traffic are exponentially growing thanks to the popularity of mobile video streaming and the proliferation of the data-hungry applications. Yet it is necessary to guarantee reliability of the data communications and the quality of service delivery. Accordingly, a dramatic shift in the design and deployment of cellular networks is taking place, which calls for the development of powerful mathematical tools that enable efficient, accurate, and scalable analysis and design of the network. These concerns are among the main focuses of this thesis.

We employ the mathematical tool of stochastic geometry to model and analyze the cellular networks in an analytically tractable approach. We then vigorously investigate various performance metrics of cellular networks that engineers require in order to properly design the network. We explore several of such practical design issues and provide several guidelines.

Preface

For all the chapters and corresponding papers, I conducted the literature survey on the related topics, identified the challenges, and performed the entire analytical developments and simulations. I wrote all the draft manuscripts for all my papers in a submission-ready format. My supervisor guided the research, validated the subject of the paper and the materials, and gave comments on improving the manuscripts. For those papers that Dr. Keivan Navaie and Prof. Kang G. Shin are the co-authors, I enjoyed their guidance as these individuals were kind enough to read the papers and apply their revisions mainly concerning with the language, and occasionally structure of the paper.

The list of publications that have resulted from the research documented in this thesis are presented in the following.

Two papers related to Chapter 2 have been published:

- Mohammad G. Khoshkholgh, Kang. G. Shin, Keivan Navaie, Victor C. M. Leung, "Coverage performance in multi-stream MIMO-ZFBF heterogeneous networks," *IEEE Transactions on Vehicular Technology*, vol. 66, no. 8, pp. 6801-6818, Aug. 2017.

- Mohammad G. Khoshkholgh and Victor C. M. Leung, "Closed-form approximations for coverage probability of multi-stream MIMO-ZFBF in HetNets," *IEEE Transactions on Vehicular Technology*, vol. 66, no. 11, pp. 9862–9879, Nov. 2017.

Two papers related to Chapter 3 have been published:

- Mohammad G. Khoshkholgh, Keivan Navaie, Kang. G. Shin, Victor C. M. Leung, "Coverage analysis of multi-stream MIMO HetNets with MRC receivers," *IEEE Transactions on Wireless Communications*, vol. 16, no. 12, pp. 7816–7833, Oct. 2017.

- Mohammad G. Khoshkholgh, Keivan Navaie, Kang. G. Shin, Victor C. M. Leung, "Coverage performance of MIMO-MRC in heterogeneous networks: a stochastic geometry perspective," in *Proc. of IEEE 84th Vehicular Technology Conference (VTC-Fall)*, 2016.

One paper related to Chapter 4 has been published:

- Mohammad G. Khoshkholgh and Victor C. M. Leung, "On the performance of MIMO-SVD multiplexing systems in HetNets: a stochastic geometry perspective," *IEEE Transactions on Vehicular Technology*, vol. 66, no. 9, pp. 8163-8178, Sep. 2017.

On the other hand, a minor part of Chapter 2 depends upon these three publications:

- Mohammad G. Khoshkholgh, Keivan Navaie, Kang. G. Shin, Victor C. M. Leung, "Cell association in dense heterogeneous cellular networks," *IEEE Transactions on Mobile Computing*, vol. 17, no. 5, pp. 1019-1032, 2017, May.

- Mohammad G. Khoshkholgh, Keivan Navaie, Kang. G. Shin, Victor C. M. Leung, "Coverage analysis of Max-SIR cell association in HetNets under Nakagami fading," *IEEE Transactions on Vehicular Technology*, vol. 67, no. 3, pp. 2420 - 2438, March, 2018

- Mohammad G. Khoshkholgh, Keivan Navaie, Kang. G. Shin, Victor C. M. Leung, "Performance evaluation of MISO-SDMA in heterogeneous networks with practical cell association," in *Proc. of IEEE 84th Vehicular Technology Conference (VTC-Fall)*, 2016.

I have also co-authored other research works which have been published or submitted for publication during my time as a Ph.D. student at UBC. These works as listed in Appendix C are not directly related to this work.

Table of Contents

Appendices

List of Figures

List of Abbreviations

3GPP	3rd Generation Partnership Project
2G	Second Generation
3G	Third Generation
4G	Forth Generation
5G	Fifth Generation
ASE	Area Spectral Efficiency
AWGN	Additive White Gaussian Noise
BEP	Bit-Error Probability
BS	Base Station
BPL	Bounded Path-Loss
CA	Cell Association
CDF	Cumulative Distribution Function
CCDF	Complementary Cumulative Distribution Function
CoMP	Coordinated Multi-Point Communication
CSI	Channel State Information
CSIR	Channel State Information at Receiver
CSIT	Channel State Information at Transmitter
CQI	Channel Quality Information
C-RAN	Cloud Radio Access Networks
D2D	Device-to-Device
DoF	Degrees of Freedom

FDD	Frequency Division Duplex
FDMA	Frequency Division Multiple Access
EiD	Equivalent-in-Distribution
ICI	Inter-Cell Interference
IUI	Inter-User Interference
LOS	Line-of-Sight
LTE	Long Term Evolution
LTE-A	LTE-Advanced
HetNets	Heterogenous Cellular Networks
Max-SINR	Maximum Signal-to-Interference-Plus-Noise Ratio
MIMO	Multiple-Input Multiple-Output
MISO	Multiple-Input Single-Output
MMSE	Minimum Mean Square Error
mmWave	Millimeter Wave
MRC	Maximum Ratio Combining
MRT	Maximum Ratio Transmission
NLOS	Non-Line-of-Sight
OSTBC	Orthogonal Space-Time Block Codes
PDF	Probability Density Function
PGFL	Probability Generating Functional
PPP	Poisson Point Process
PZF	Partial Zero-Forcing
SEP	Symbol Error Probability
SDMA	Spatial-Division Multiple Access
SIMO	Single-Input Multiple-Output
SINR	Signal-to-Interference-Plus-Noise Ratio
SISO	Single-Input Single-Output

SVD	Singular Value Decomposition
TDMA	Time Division Multiple Access
UE	User Equipment
ZFBF	Zero-Forcing Beamforming

List of Notations

$\boldsymbol{H}$	matrix
$\boldsymbol{s}$	vector
$(.)^T$	Transpose
$\|.\|$	l_2-norm
$\gtrsim$	lower-bound in an asymptotic sense
$\lesssim$	upper-bound in an asymptotic sense
$\approx\!\!\gtrsim$	almost lower-bound
$\approx\!\!\lesssim$	almost upper-bound
$(.)^\dagger$	conjugate transpose
$\mathbb{C}$	set of complex numbers
$\breve{\alpha}$	$\frac{2}{\alpha}$
$\mathbb{E}[.]$	expectation operator
$\mathrm{Var}[.]$	variance operator
$\lceil . \rceil$	ceiling operator
$K \geq 1$	number of tiers
Φ_i, $i \in \mathcal{K}$	locations of BSs in Tier i
x_i	location of BS x_i
$\Phi = \{\Phi_i\}_{\forall i}$	PPP set comprising the locations of all BSs
β	SINR threshold
$\Gamma(x)$	Gamma function, $\Gamma(x) = \int_0^\infty t^{x-1} e^{-t} \mathrm{d}t$
$C(\breve{\alpha})$	$\pi\Gamma(1+\breve{\alpha})$

$\lambda_i \geq 0$	density of BSs in Tier i
λ_U	density of UEs
$\mathcal{N}(a, b)$	Normal distribution with mean a and variance b
P_i	transmission power of BSs in Tier i
S_i	multiplexing gain in Tier i
$N^r \geq 1$	number of receive antennas
$N_i^t \geq 1$	number of transmit antennas at the BSs of Tier i
σ_i^2	AWGN power
$\delta^m(t)$	mth derivative of Dirac delta function
$l_i = 1, 2, \ldots, S_i$	data stream indices in a communication link in Tier i
$H_{x_i,l_i}^{\mathrm{ZFBF}}$	attending channel power gain under ZFBF
$H_{x_i,l_i}^{\mathrm{MRC}}$	attending channel power gain under MRC
$H_{x_i,l_i}^{\mathrm{SVD}}$	attending channel power gain under SVD
$H_{x_i,l_i}^{\mathrm{SIMO}}$	attending channel power gain under SIMO
$H_{x_i,l_i}^{\mathrm{MRT}}$	attending channel power gain under MRT
$H_{x_i,l_i}^{\mathrm{SDMA}}$	attending channel power gain under SDMA
$G_{x_i',l_i}^{\mathrm{ZFBF}}$	interfering channel power gain under ZFBF
$G_{x_i',l_i}^{\mathrm{MRC}}$	interfering channel power gain under MRC
$G_{x_i',l_i}^{\mathrm{SVD}}$	interfering channel power gain under SVD
$G_{x_i',l_i}^{\mathrm{SIMO}}$	interfering channel power gain under SIMO
$G_{x_i',l_i}^{\mathrm{MRT}}$	interfering channel power gain under MRT
$G_{x_i',l_i}^{\mathrm{SDMA}}$	interfering channel power gain under SDMA
$G \sim \chi_{2S}^2$	chi-squared random variable with DoF $2S$,
$\mathrm{SINR}_{x_i,l_i}^{\mathrm{ZFBF}}$	SINR on data stream l_i under ZFBF
$\mathrm{SIR}_{x_i,l_i}^{\mathrm{ZFBF}}$	SIR on data stream l_i under ZFBF
$\mathrm{SIR}_{x_i,l_i}^{\mathrm{MRC}}$	SIR on data stream l_i under MRC
$\mathrm{SIR}_{x_i,l_i}^{\mathrm{SVD}}$	SIR on data stream l_i under SVD

$\mathrm{SIR}_{x_i,l_i}^{\mathrm{MRT}}$	SIR on data stream l_i under MRT
$\mathrm{SIR}_{x_i,l_i}^{\mathrm{SDMA}}$	SIR on data stream l_i under SDMA
$\mathrm{SIR}_{x_i,l_i}^{\mathrm{SIMO}}$	SIR on data stream l_i under SIMO
$\mathcal{A}^{\mathrm{ZFBF}}$	association set under ZFBF
$\mathcal{A}^{\mathrm{MRC}}$	association set under MRC
$\mathcal{A}^{\mathrm{SVD}}$	association set under SVD
c^{ZFBF}	coverage probability under ZFBF
c^{MRC}	coverage probability under MRC
c^{SVD}	coverage probability under SVD
c^{SIMO}	coverage probability under SIMO
c^{MRT}	coverage probability under MRT
c^{SDMA}	coverage probability under SDMA
$\mathcal{L}_I(s)$	Laplace transform of random variable I
I^{l_i}	ICI on stream l_i
ϕ_{x_i,l_i}	un-ordered l_ith eigenvalue
$\phi_{x_i,\min}$	$\min_{l_i=1,2,\ldots,S_i} \phi_{x_i,l_i}$

Acknowledgments

I would like to express my sincere gratitude to my supervisor Prof. Victor C. M. Leung for his great support. His knowledge, advices, and work ethic are inspiring and his guidance has helped me in every stage of my research.

Also, I am grateful to the Natural Science and Engineering Research Council of Canada and the University of British Columbia for supporting this research through Vanier Graduate Canada Scholarship and a Four Year Doctoral Fellowship, respectively.

Finally, my sincere thanks goes to Dr. Keivan Navaie and Prof. Kang. G. Shin for their time and supports during my research.

Chapter 1

Introduction

Cellular networks are evolving into complex infrastructures by the deployment of diversified classes of base stations (BSs) with distinct technological and operational components. A typical 3G/4G cellular network comprises of the traditional tower-mounted macro BSs that are suitable for long-range communication and wide-area coverage. To stretch the coverage area of the network and also to increase the network capacity specially at hot-spots, e.g., shopping malls, stadiums, train stations, and airports, these standards permit the installation of operator-managed pico BSs and distributed antenna ports [2, 3]. On the other hand, short-range femto cells are often installed by the end users to eliminate the dead zones and gain much higher transmission rate [4]. This sophisticated structure of the current cellular networks is coined as a heterogeneous cellular network (HetNet); see Fig. 1.1 that illustrates an exemplary picture of HetNet, comprising of three macro cells overlayed with many pico cells, femto cells, and distributed antenna ports. On the other hand, to increase the capacity of cellular network several other disruptive technologies including multiple-input multiple-output (MIMO) communications [5], massive MIMO and mmWave communications [3, 6, 7], coordinated communications [8], and proximity aware device-to-device (D2D) networks [9] are introduced. Witnessing the crushing demands for mobile data traffic caused by the proliferation of data-hungry devices and applications, the evolution toward heterogeneity will accelerate.

Meanwhile, backed by decades of thorough investigations, MIMO communications have thus far been embodied in multiple IEEE 802.11 standards as well as in 3GPP LTE-Advanced [5, 10, 11]. Pervasive exploitations of sophisticated MIMO technologies in conjunction with

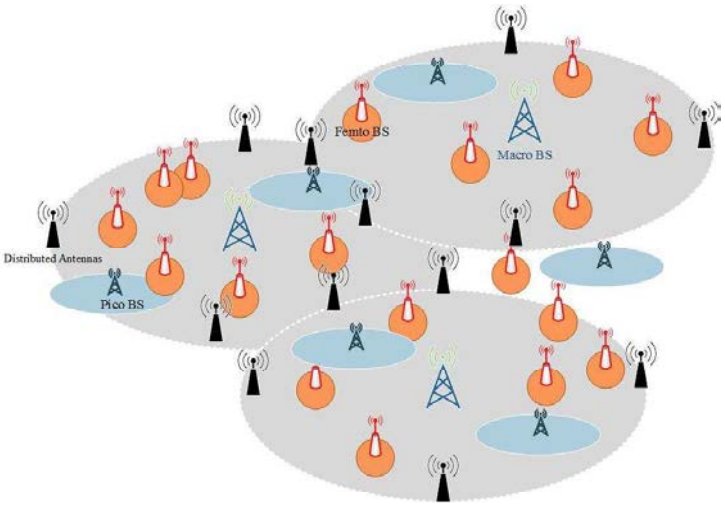

Figure 1.1: An exemplary picture of heterogenous cellular network (HetNet).

occurring densification in HetNets makes MIMO HetNet a key enabling communication paradigm. It is therefore envisioned that MIMO HetNets can smoothly deal with the occurring deluge of traffic demands [12], and thus are incorporated in the design and implementation of 4G/5G standards and beyond [3, 6].

The reason that MIMO communications are becoming so imperative in current and future cellular technologies should not however be surprising. It is in fact well established that such technologies are able to effectively harness diversity and multiplexing potentials of the wireless medium, attaining a colossal capacity (the maximum achievable data rate) gain as well as highly reliable communications (low symbol error rate) [13]. Importantly, these gains are achievable without necessitating higher transmission power and/or bigger chunk of wireless spectrum—which are usually limited in dense deployments as well as small-cells and D2D networks—compared to the single-antenna, a.k.a. SISO, counterpart systems [14]. In effect, the tremendous potentials of MIMO technologies can be comprehended through the decomposition of a point-to-point communication link by the aid of the singular value decomposition (SVD) method. In fading environments, this permits the simultaneous transmissions of as many streams as the minimum number of antennas that the transceivers at

either ends of the link are equipped with [15]. Consequently, multi-stream MIMO, or MIMO multiplexing, systems—whereby at each time instance a number of independent streams of data are transmitted on each communication link—are attractive for current and upcoming generations of high-capacity cellular systems.

Nevertheless, in the state-of-the-art research, there are several shortcomings regarding comprehensive performance evaluation of MIMO multiplexing systems from a *network-level perspective* [5]. Network-wise performance is of utmost importance when it comes to design and implementation of large-scale communication systems with millions of nodes. In fact, while in a single-cell system allocating the system resources is rather well-established, the same cannot be concluded from a network-wise performance context. For instance, in a single-cell system, decisions such as the number of antennas to be switched on/off, the number of user equipments (UEs) to be concurrently served, or choosing between multiplexing (using antennas for increasing data rate) and diversity (using antennas for increasing reliability) in order to maximize the capacity or similar objective functions are well investigated [5, 14, 16, 17], whereas in a multi-cell network, such decisions need sophisticated solutions based on network-wise performance metrics. In fact, while increasing the number of transmitted data streams in a single-cell system can be appealing and even locally optimal, it increases the inter-cell interference (ICI), almost with the same order, which could offset the effect of the former. It is, therefore, debatable whether strategies yielding higher capacity or better coverage from the perspective of local decisions result also in the network-wise optimality. We should also emphasize that even under the clustered-based solution, coordinated multi-point (CoMP) and networked MIMO [8], it is shown that the ultimate performance is quite sensitive to out-of-cluster interference [18, 19], so that regardless of the growth of the transmission power at the BSs the capacity stays flattened.

In light of the influential impact of ICI on the performance of MIMO HetNets, this dissertation is chiefly concerned with analyzing MIMO multiplexing systems under ICI.

This introductory chapter will start in Section 1.1 by reviewing key aspects of cellular net-

works, and the common modelling techniques researchers adopt to analyze the performance of cellular networks. We further pinpoint multiple drawbacks existing in the evaluation of MIMO communications under conventional cellular models. In Section 1.2, we introduce stochastic geometry and review important aspects of this theory that are relevant to the scope of this dissertation. In Section 1.3, we provide a comprehensive literature review. This section further discusses the research gaps we have spotted in the current literature, which serve as the main motivations behind this dissertation. Section 1.4 enumerates the key contributions of this thesis. Finally, the outline of the thesis is provided in Section 1.5.

1.1 MIMO Cellular Networks: Modelling and Analytical Approaches

In its simplest form, a wireless medium attenuates the transmitted signals quite proportional to the transmitter-receiver distance, what is known as distance-dependent path loss attenuation [14]. Because of path-loss attenuation, beyond a certain distance from the transmitter it becomes almost insurmountable for the receiver to distinguish information-bearing signals from the background noise. While it stands as an unfavorable outcome, this same phenomenon results in the desirable effect that two transmitters that are sufficiently far apart in space impose insignificant interference on each other. This forms the basis of frequency reuse in cellular networks, which permits the division of the service area into many disjoint cells. Therefore, although each cell is served by one BS, the time-frequency resources can be reused across adjacent cells [16].

However, other impairments of wireless channels, e.g., fading and ICI, restricts the coverage area of each cell. ICI is the aggregate impact of many interferers located at the adjacent cells utilizing the same time-frequency resources. Therefore, because of fading and ICI, network factors such as the locations of BSs, their transmit strategies (e.g., power allocation, sleep mode, and load balancing), the propagation environment, and also the receiver

structure (e.g., interference cancellation, MIMO scheme, and the like) are influential in understanding the network-level performance of cellular infrastructures.

In the following, we review various approaches that are commonly adopted in research communities to investigate the network-level performance.

1.1.1 Conventional Models for Cellular Networks

In a cellular system, a group of adjacent BSs attempt to provide seamless connection to a set of UEs. Commonly each UE is associated to only one BS [14, 16] as the serving BS. Nevertheless, via more sophisticated schemes such as coordinated communications or cloud radio access networks (C-RAN) [6, 20] it is possible to simultaneously transmit data to a single UE from several BSs.

Remark 1.1.1. *In this dissertation, we do not focus on coordinated communications and always assume that a UE receives information from one BS in each communication session. We shall however emphasize that the contributions of the thesis is straightforwardly applicable for those scenarios that each UE chooses the most proper BS/antenna ports from a set of candidate BSs. This scheme also falls into a BS cooperation strategy often referred transmission point selection [21] or dynamic cell selection [20, 22].*

In general, cell association (CA) is required in order to associate each UE to the best possible BS before the information transmission starts. CA could be as simple as connecting to the nearest BS to UEs or can be accomplished based on sophisticated optimization targeting a well-defined local or global objective function, for example, maximizing the net scheduled data rate (or a utility function) [23, 24, 25, 26]. Regardless of the conducted approach, in general one should expect that the CA procedure tessellates the network coverage area into several individual non-overlapping cells, each of which containing the potential positions of associated UEs.

Nota that in order to analyze the cellular systems, conventionally the traits of CA is

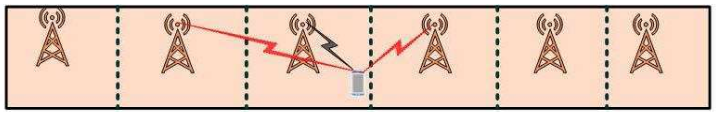

Figure 1.2: A one dimension Wyner model for cellular network.

represented via idealized layouts including Wayner model and hexagonal model [14, 16]. We briefly review these models in the following.

Wyner model

According to 1-d Wyner model [27], BSs are lined up horizontally at a fixed distance D, and each cell covers a rectangular coverage area as shown in Fig. 1.2. Obviously, this model is very simplistic, and may only be representable of a very narrow application of practical cellular networks. Further, under this topology, the interference is modelled quite unsophisticatedly by assuming that the victim UE, located in the coverage cell of the focused BS, realizes interference merely from its 1 or 2 immediate neighboring cells. The main reason for such a simplistic interference model in the Wyner model is the desire for solid information-theoretic analysis of cellular networks [28, 29]. Nevertheless, this approach is quite simplistic when it comes to providing a comprehensive understanding of the coverage probability and possible effects of CA mechanism.

Hexagonal Grid Model

The hexagonal grid model is regularly adopted to model the cellular networks [14, 16] to evaluate the performance of cellular systems. As also seen from Fig. 1.3, in this model, BS locations are in the centers of hexagonal grids. To manage the complexity of the model, it is a common practice to limit the model to 1 or 2 layers of BSs around the origin, resulting in a 7 BSs grid or 19 BSs grid system. Basically, analyzing statistics of signal-to-interference-plus-noise ratio (SINR) under this model is complicated and in many cases mathematically unamenable. Therefore, researchers often resort to extensive, time consuming simulations to

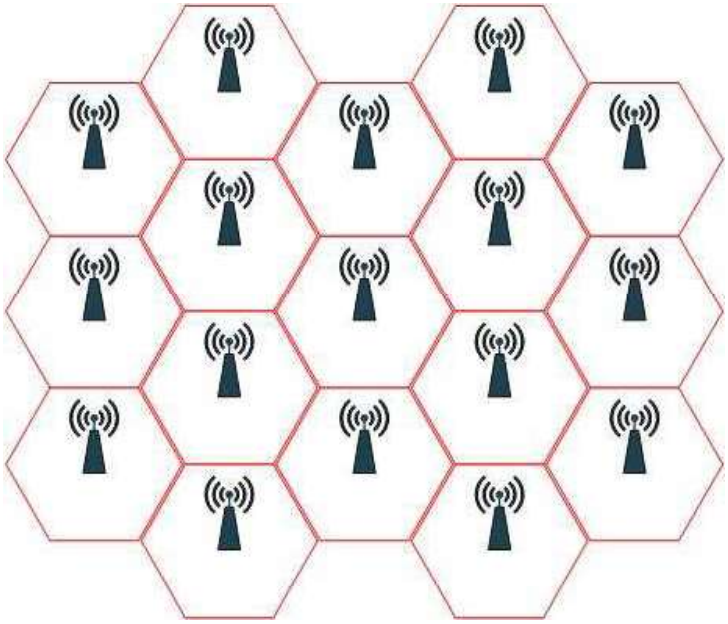

Figure 1.3: Hexagonal grid model for BS locations.

evaluate the coverage performance. While hardly being scalable, these sorts of simulations are prone to bugs and are inherently limited in their scope as it is hard to derive wide-range insights/guidelines required for adaptive system design. Note that one always benefits from availability of easily evaluated formulas of the network performance at least for sanity check of simulation and also tuning simulation parameters.

1.1.2 Performance Evaluation under Conventional Models

In order to evaluate the performance of cellular networks we need to formulate the SINR, as any other wireless communication networks [14, 16]. As a quintessential scenario, consider the cellular system shown in Fig. 1.4 consisting of N BSs, $BS_1, BS_2, \ldots BS_N$, using the same time-frequency resources. Assume we are interested in measuring the performance of a targeted UE located at the origin, which is assumed to be associated to BS_1 located at distance r_1. Due to wireless channel impact, the signal transmitted from the nth BS, B_n, undergoes an attenuation before impinging the UE's receive antenna. In the simplest

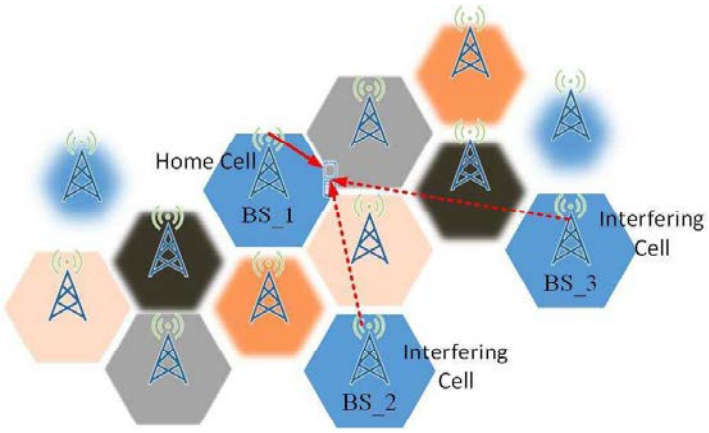

Figure 1.4: A cellular network comprising of supporting BS and interfering BSs.

form, the received power at the UE can be formulated as $P_{rn} = Ph_n r_n^{-\alpha}$, where P is the BS transmit power, which is assumed to be fixed and the same across BSs, $\alpha \in (2, 8)$ is the path-loss exponent, r_n is the distance of the interfering BS B_n from the UE and h_n denotes the random attenuation present in the channel which includes small-scale fading or possibly large-scale shadowing. Hence, the SINR at the victim UE is given as

$$\text{SINR} = \frac{Ph_1 r_1^{-\alpha}}{\sigma^2 + \sum_{n=2}^{N} Ph_n r_n^{-\alpha}}, \tag{1.1}$$

where σ^2 is the additive white Gaussian noise (AWGN) power at the receiver. In this formula, the term $\sum_{n=2}^{N} Ph_n r_n^{-\alpha}$ is actually the ICI, which, among other things, depends on the location of the interferers. One is then able to derive the distribution and various statistics of the SINR. One essential metric to describe the efficiency of the cellular network is the coverage probability, which by definition is the probability that the SINR (1.1) stays above a given threshold $\beta > 0$ [1, 14], i.e.,

$$c(\beta) = \mathbb{P}\left\{ \frac{Ph_1 r_1^{-\alpha}}{\sigma^2 + \sum_{n=2}^{N} Ph_n r_n^{-\alpha}} \geq \beta \right\}. \tag{1.2}$$

Remark 1.1.2 (Beyond Coverage Analysis). *From the definition* (1.2)*, it is apparent that the coverage probability is actually equivalent to the complementary cumulative distribution function (CCDF) of the SINR, and having it specified one is then able to derive other appealing performance metrics such as Ergodic capacity, effective capacity, energy efficiency, and spectral efficiency [14], [30]. This is because these performance metrics are functions of the CCDF of SINR. For example the Ergodic capacity,* $\overline{C}$*, is related to the CCDF of SINR through*

$$\overline{C} = \mathbb{E}\log\left(1+\mathrm{SINR}\right) = \int\limits_{v>0} \frac{c(v)}{1+v}\mathrm{d}v. \tag{1.3}$$

Furthermore, for given delay exponent $\theta \in \mathbb{R}^+$ *the effective capacity can be evaluated*

$$C(\theta) = \frac{-1}{\theta}\log \mathbb{E}e^{-\theta(1+\mathrm{SINR})} = 1 - \int\limits_{v<0\leq 1} c(v^{-\frac{1}{\theta}}-1)\mathrm{d}v. \tag{1.4}$$

Consequently, although throughout the thesis we often explore the coverage performance, it is straightforward to adopt the analysis to evaluate these performance metrics.

Note that assuming r_is are fixed/given, knowing the distribution of the fading is nearly sufficient to calculate the coverage probability. For the case of exponential distribution such a calculation is straightforward. However, this evaluation of the coverage probability is inherently limited and merely serves a particular scenario, e.g., the coverage probability on the cell boundary. On the other hand, if one desires to evaluate the coverage performance in a more generic setup, it is recommended to adjust the calculation, at least, as the following

$$c = \int\limits_{r_1} \ldots \int\limits_{r_n} \mathbb{P}\left\{\frac{Ph_1 r_1^{-\alpha}}{\sigma^2 + \sum\limits_{n=2}^{N} Ph_n r_n^{-\alpha}} \geq \beta\right\} \Xi(r_1, r_2, \ldots, r_n)\mathrm{d}r_1 \ldots \mathrm{d}r_n, \tag{1.5}$$

where $\Xi(r_1, r_2, \ldots, r_n)$ is a generic function that can capture the distribution of BSs with accordance to the hexagonal layout and implemented frequency reuse pattern. In this case, the coverage probability (1.5) is valid for any possible position of UEs in the cell and also any be-

havior of BSs (e.g., sleep mode) that affects distances through the function $\Xi(r_1, r_2, \ldots, r_n)$. Nevertheless, this analysis is cumbersome and difficult to proceed. Furthermore, the complexity of this approach dramatically increases for MIMO systems, which admit substantially more complex SINR formulas.

1.1.3 Is Evaluation of MIMO Communications Performance under Conventional Models Holistic?

Using analytical tools of random matrix theory, the performance evaluation of MIMO multiplexing systems is broadly focused and discussed in the literature [15, 31, 32]. Here we are not to review them as the literature is broad and is not in the main interest of this dissertation. Yet, we ought to highlight that the main focus of such literature has often been on the point-to-point—what we call *isolated*—scenarios. Although significant in its own right, such literature overlooks the incorporation of ICI that is imposed by other active communication links. As the dominant practice in previous cellular generations (2G/3G) recommended aggressive frequency reuse, it was quite acceptable to assume that interference is secondary factor compared to the other aspects of the communication systems such as intra-cell interference, fading, pecoding/decoding procedures, the availability of channel state information (CSI) at the receiver/transmitter, and the like. But, now that the trends of network configuration advocates heterogeneity, unprecedented densification, and aggressive frequency reuse, the impact of interference becomes more dominant and should be incorporated in the analysis.

Evaluation of the capacity and symbol error rate/probability (SEP) have been the main trends of the research community in order to understand the impact of interference on the performance of MIMO systems [33, 34, 35]. Nevertheless, a number of pressing drawbacks can be spotted in this literature:

- The main scopes are mainly on diversity systems, e.g, single-stream MIMO-SVD

communications, whereby in each time slot only one stream of data is transmitted [33, 34, 35]. Generally, it is not straightforward to extend the method and analysis of this literature to the cases of multi-stream (multiplexing) MIMO systems.[1] One reason is that in MIMO multiplexing systems the impinged signal quality across received data streams are statistically correlated.

- Generally, a handful of interferers — usually by neglecting the impact of path-loss attenuations and by assuming equal interference power on the victim receiver — are considered. This network model is inaccurate, and even far from the simplistic setup provided in Section 1.1.2. Thus, this approach cannot correctly model recent trends of cellular networks including HetNets. Furthermore, the existence of ICI, which itself behaves randomly, plays an integral role in inducing correlation among signals in MIMO multiplexing systems. This phenomenon substantially adds to the complexity of the analysis of multi-stream MIMO HetNets.

- Analytical results are provided in very complex forms of determinants of matrices the entries of which are special mathematical functions (e.g., hypergeometric functions) [33, 37, 38]. Besides restricting the scalability, such mathematical complexities hamper the applicability of the results to the practical cases where path-loss attenuations of the interfering signals are not deterministic, e.g., cellular networks.

- Even for such a simplified/unrealistic interference model, the capacity of multiplexing systems is actually considered as the main performance metric, and the evaluation of the coverage probability is occasionally focused; see, e.g., [39]. To understand the coverage probability in MIMO multiplexing systems, one needs to evaluate the CCDF of the scheduled data rate across data streams, which compared to the SISO systems (see Section 1.1.2) is prohibitively complex even for the simplistic isolated scenario.

We should, on the other hand, highlight that these drawbacks are becoming more pressing

[1] Comprehensive overviews of different MIMO communication techniques are provided in [5, 13, 36].

due to the random deployment of heterogenous BSs (e.g., plug-and-play installation of femto cells and distributed antenna ports [3, 6]), on/off status of BSs for managing sleeping modes, aggressive frequency reuse, many possible MIMO communication technologies one can choose from, unprecedented complexities in CA management, and large-scale system design based on network-level performance evaluation.

More than ever, efficient mathematical tools facilitating the comprehensive analysis of the network in terms of influential system parameters—required to effectually manage the adaptive designs and to gain engineering insights—are demanded.

To bridge the gaps, in this dissertation we aim to comprehensively evaluate the network-wise (spatial) performance of multi-stream MIMO systems in HetNets with the desire to provide computationally friendly expressions of the main performance metrics. To this end, we adopt powerful tools of stochastic geometry and Poisson point processes (PPP); see, e.g., [40, 41, 42] and references therein. Please refer to Appendix A for a brief overview of stochastic geometry.

1.2 Using Stochastic Geometry for Cellular Network Modeling

Stochastic geometry is a natural modelling tool for ad hoc and sensor networks as it captures their intrinsic spatial randomness [41, 43, 44]. In contrast, for modelling cellular networks that are mostly assumed to be spatially deployed according to an idealized grid layouts it seems rather unreasonable to adopt the stochastic geometry. Our goal in this section is to provide sufficient evidences backing up the suitability of stochastic geometry for the modeling, analysis, and design of cellular networks. We further discuss CA under stochastic geometry model.

1.2.1 Applications of Stochastic Geometry in Cellular Networks

Analyzing Cellular Networks

We first start by highlighting that stochastic geometry has been extensively adopted to analyze, design, and provide guidelines in cellular networks. The downlink of a single-tier cellular networks is generally the main focus in the literature [1, 45, 46]. With the main emphasis on load balancing, many of these works have also extended to multi-tier systems [47, 48, 49, 49, 50, 51, 52]. Cellular networks with MIMO antenna arrays and massive MIMO communications are investigated in [7, 53, 54, 55, 56, 57]. The impacts of CoMP, interference cancellation, and C-RAN on the performance of cellular networks are focused in [19, 58, 59, 60, 61, 62, 63]. Millimeter (mmW) based communication in cellular networks is characterized in [64, 65]. Furthermore, the impact of different path-loss model, line-of-sight, and shadowing are considered in [66, 67, 68, 69]. In [65, 70, 71] stochastic geometry tools are exploited to provide an analytically trackable account of blockage in cellular networks. Various simulations results are reported to corroborate the models. For the case of uplink communication, works of [72, 73, 74] investigate the partial power allocation and CA. On the other hand, stochastic geometry is found to be very handy to investigate handoff rate, impact of mobility, and interference correlation in cellular networks [55, 75, 76, 77, 78]. Furthermore, a great deal of research is devoted to comprehensively study self-organized cellular networks and D2D communications [79, 80, 81]. Moreover, issues such as relay-aided communications, full-duplex communications, physical layer security, and jamming are well investigated in [82, 83, 84, 85]

Design of Cellular Networks

Assume one is interested in investigating the effect of increasing multiplexing gain on the coverage performance of a MIMO multiplexing system. Traditionally, one assumes the locations of BSs to be known. However, instead of repeating the analysis for each and every

geographical setup of the cellular networks, it is also desirable to obtain a general performance analysis applicable to many analogous scenarios. In this way, the stochastic geometry analysis of the cellular network is not primarily concerned with the performance evaluation of a specific realization of the cellular network at a specific geographical location, for example a given city. Instead, a general analytical model that applies on average for all cellular network realizations in a particular wireless environment, for example countryside, downtown, or dense urban environment, is the main scope of this approach. This implies that from the analysis viewpoint, the exact locations of the BSs are basically considered unknown. However, there are plenty of rooms to customize this model in accordance to available information and measurement data. In effect, it is possible to distinguish between distinctive environments and network setups, such as different cities (Vancouver versus Toronto) or even different neighborhoods of a city (UBC campus against downtown of Vancouver). One can achieve this by adjusting influential system parameters, e.g., shadowing and blockage effects as well as density of BSs and blockages, based on available measurements.

We should also note that without the large-scale analysis of cellular networks, network-level optimizations can be overwhelmingly baffling simply because of the sheer number of network elements in HetNets that makes centralized instantaneous solutions impractical. Accordingly, stochastic geometry is gaining momentum providing concrete methodology required for adaptive design and drawing engineering guidelines in cellular networks. In its core, such an approach endorses the statistically optimized operation relying upon averaged performance that is usually formulated through stochastic geometry analysis. Such a statistical optimization empowers the designer to draw tradeoffs between complexity, signaling overhead, and performance since the statistical network parameters (e.g., distribution of channel gains, spatial distribution and intensity of network elements, and path-loss components) change on longer time scales. For instance, load balancing is heavily conducted through this technique [49, 51, 52]. Optimization of energy efficiency, energy harvesting, and BS sleeping mode for green cellular operations are vastly explored in the literature; see,

e.g., [86, 87, 88]. Also, system-level optimization for simultaneous wireless information and power transfer is the subject of [89]. Optimized coordination between D2D communications and cellular network is discussed in [80].

1.2.2 Is Stochastic Geometry a Right Tool?

So far, a great body of research results supports the practical values of stochastic geometry [90, 91]. Nevertheless, there might be skepticism regarding the accuracy of PPP for modelling the locations of Macro BSs [91]. This is because PPP models the position the BSs in the network plane almost indiscriminately, whereas in practice, Macro BSs are often placed far from each other. This issue is investigated further in [1], where the PPP assumption is shown to result in adequately precise characterization of Macro BSs. The PPP model is shown to provide a rather *pessimistic* bound on the coverage performance in contrast to other analytic methods such as hexagonal and lattice models that provide *optimistic* bounds. Large-scale measurements and industry-scale simulations in [90, 92, 93, 94, 95] also confirm that the PPP model results in sufficiently accurate estimation of the SINR distribution in cellular networks.

The authors in [96, 97] show that the spatial patterns exhibited by actual BS locations in different geographical places can be accurately fitted to random spatial patterns obtained via PPP analysis. Specifically, the results of [96] confirm the tight lower bound provided by the random network to the users SINR in simulations with actual BS locations. It is further shown in [90, 91, 97, 98] that typically a 1-3 (dB) SINR shift is enough to match the SIR distribution obtained under a PPP model with the one obtained from measurements or grid models. As a result, one is able to adjust the anticipated coverage probability from PPP analysis to the actual performance of the network by a suitable horizontal SIR shift. On the other hand, the results prove that the trends observed from measurements and also system-level simulations are exactly captured by the PPP analysis.

On the other hand, the analysis and simulation results presented in [99, 100] show that

any grid setting can be adequately modelled as a PPP simply because of the shadowing effect. This implies that any grid-based cellular model with strong shadowing effect is adequately representable by a PPP model without shadowing effect when the density of BSs in both models stays the same. Furthermore, work of [101] provides evidences behind log-normal model of shadowing from a stochastic geometry analysis.

Finally, adopting more sophisticated point process models such as determinantal point processes, such as Ginibre point process, one is able to properly account for repulsion among BSs of a class or across classes [95, 102]. This could be helpful when extra information regarding the deployment of BSs in particular regions is available. The downside of the analysis based on such sophisticated point processes is the substantial growth of the mathematical complexities.

1.2.3 Cell Association Under Stochastic Geometry Model

As we mentioned previously, under the grid model, CA is idealistically incorporated through the considered layout, e.g., hexagonal. However, to correctly model cellular network with stochastic geometry one needs to properly incorporate the traits of the CA mechanism [23]. In general, one can think of two main approaches to specify the CA procedure, as discussed in the following.

Range Expansion Cell Association

The most common approach is the closest-BS CA, which is basically the association of a UE to the BS that provides the maximum average received power [1, 23, 49]. Such an association leads to the Voronoi tessellation [44] of the network, i.e., the network coverage area is representable by non-overlapping mosaics each of which is associated with a BS containing all points that are closest to it. This approach is well-suited for single-tier networks as BSs have the same transmission power limit. Note that since fading fluctuations are averaged-out, the closes-BS CA rule circumvents the ping-pong effect, which makes it practically appealing.

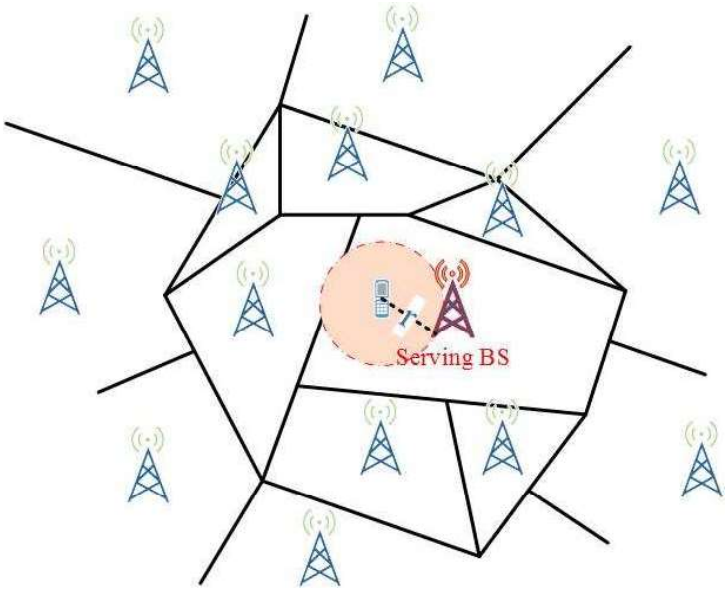

Figure 1.5: A single-tier cellular network modelled by PPP under the closest-BS CA rule.

Therefore, as far as the UE stays within the cell associated with the BS B, regardless of the UE's motion trait, it will always receive information from BS B. As also seen from Fig. 1.5, from the interference perspective, under this CA rule each UE actually produces an associated exclusion zone guaranteeing the the interfering BSs are farther to UE than the serving BS. From Fig. 1.5 we note that the typical UE is associated with the closest BS, with separation distance r meters. Therefore, all the interfering BSs are always farer than r meters. This induces a guard-zone around the UE. Note that the radius of this guard zone depends on the density of BSs, λ, through Rayleigh PDF $f(r) = 2\pi\lambda r e^{-\pi\lambda r^2}$ [1]

Nevertheless, the closest-BS CA rule could lead to severe performance damage in HetNets due to mismatch between the transmission power of BSs of different technologies. To deal with this issue and also facilitate traffic offloading from congested Macro BSs to small cells, a twisted version of the closest-BS CA rule is usually considered, whereby the received average power of each class of BSs is multiplied by an associated scaler parameter known as bias/weight. This method is termed as range-expansion CA and permits optimizing biases based on desired network performance or optimal traffic offloading [49, 52, 103]. In this

way, it is easily understandable that the closest-BS CA rule describes a special case of range expansion: the former is derived from the latter by choosing all biases equally.

Disadvantages of Range Expansion: Despite its practical merits and straightforward analytical advantages, range-expansion CA does not necessarily provide the maximization of the coverage probability/average data rate as it does not guarantee the maximization of the instantaneous SINR experienced at UEs. On the other hand and more relevant to the scope of this dissertation, for the particular case of MIMO HetNets the range-expansion systematically overlooks key features of physical (PHY) layer specifications of MIMO communications, including the precoding/decoding technique, the number of antennas, and the like in the stage of CA, as it treats all MIMO technologies indiscriminately.

As a plausible configuration scenario of 5G networks [3, 6], assume Tier 1 has massive MIMO technology while Tier 2 supports dense SISO communications. For these scenarios, under range expansion both tiers are treated similarly in the stage of CA, which is obviously oversimplifying. Under range expansion, it is not hard to imagine the scenarios that many massive MIMO BSs will end up staying often silent as each UE always finds a close-by femto base station for association. But, in reality while densified femto tier offers benefits by reducing transmission distance among pairs, massive MIMO tier also offers benefits through substantially large MIMO gains, which may be comparative to the former. Therefore, one can argue that if the CA policy is chosen properly, a more efficient usage of each tier's particular potentials can be achieved. One can address this issue, at least partially, via considering the max-SINR CA rule (see the following), as besides path-loss attenuations, it incorporates the traits of transmission/reception technologies in the stage of CA policy.

Maximum-SINR Cell Association

In comparison to range-expansion (or closest-BS) based CA rule, under the max-SINR CA rule each UE is attached to the BS that provides the maximum SINR across all BSs and classes of BSs. This implies that the serving BS may not necessarily be the closest BS to

the typical UE, which is also seen from Fig. 1.6. As seen from Fig. 1.6, the typical UE is associated with the BS that provides the highest post-processing SINR. In comparison to the closest-BS CA rule, here the serving BS may not be the closest BS. As a result, the interfering BSs can be closer to the UE than the serving BS.

To implement the max-SINR CA rule, at the start of each communication session each UE listens to pilots emitted from BSs and estimates channels. Then it estimates post-processed SINR values, and after sorting them, it chooses the most proper BS for association. Therefore, the max-SINR CA rule is actually suitable for instantaneous association policies: In each time instance that fading fluctuations and/or path-losses undergo new values, due for instance to mobility of UEs and/or activity factor of BSs, the typical UE should recalculate the post-processed SINR and connect to the BS that provides the strongest communication link.

Why Max-SINR CA Rule? In effect, from the literature of resource allocation in HetNets, which desires to apply CA based on resource allocation, transmission policy, and underlying scheduling procedure, it is well known that the range expansion is a very simplistic CA method, and far from the optimal policy (see [23, 24, 25, 26] for details). Such a literature shows that disjoint treatment of CA and resource allocation can substantially degrade the achievable performance of the network and undermine the potentials of HetNets. As a result, in this literature, the CA is decided upon, for example, solving properly designed complex optimization problem where the objective function and constraints are formulated based on (expected/estimated) SINR as a function of PHY layer specifications, transmission policies and scheduling procedures across tiers, see, e.g., [23, 24, 25, 26]. Unfortunately, such line of work is only applicable for a cluster of BSs with limited number of BSs. Therefore, the resultant policy can be deficient in thoroughly addressing the network-level implications. Admittedly, it is of vital importance to bring the aspects of this optimized CA into the network-level performance evaluation of HetNets. While it is dramatically complex and analytically intractable to model and analyze the traits of such locally optimization-driven CA approach

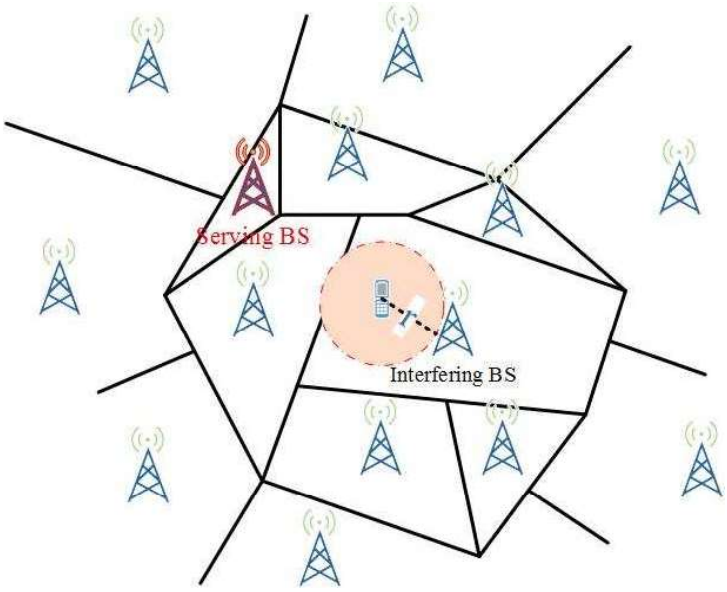

Figure 1.6: A single-tier cellular network modelled by PPP under the max-SINR CA rule.

in the stochastic geometry analysis of HetNets, it is yet possible to think of mimicking some of its traits through developing CA policies that permit the mathematical tractability. The max-SINR CA rule actually serves this goal. This should not, however, be regarded as a haphazard choice as the mentioned optimized-driven CA problems generally concentrate on maximizing a monotonically increasing function of SINR. Accordingly, stochastic analysis of the network based on the max-SINR CA rule can be regarded as an attempt to develop analytical tools allowing incorporation of some aspects of locally optimization-driven CA policies into the network-level performance evaluation of HetNets.

One may argue that the max-SINR CA rule complicates the network management in comparison to the range expansion, e.g., more frequent CA mechanisms and more pilot measurements. We could argue that by introducing many distinctly sophisticated technologies including dense small cells, massive MIMO, mmWave communications, and D2D communications in recent years, it is far from optimal to keep using the CA policies that are originally suitable for single-tier systems. On the other hand, the complex structure of future cellular systems calls for more complex network management and CA policies. Otherwise, the

expected performance boost that such technologies (e.g., dense small cells, massive MIMO, mmWave communications, and D2D communications) are expected to introduce may be partially degraded simply because of inappropriate, perhaps outdated, CA policy that in nature dose not distinguish and appreciate the distinctive traits of current technologies (e.g., dense small cells, massive MIMO, mmWave communications, and D2D communications).

Is Max-SINR CA Rule Implementable? It is also vital to note that the signaling overheads and computational complexities of max-SINR CA rule can be manageable in particular when the fading is slow (low mobility scenarios). Regardless of mobility/fading traits, although for the selection of the BS with the maximum SINR across all BSs many pilot measurements seems inevitable, in practice such measurements should be confined to only a number of adjacent BSs. This is mainly attributable to the simple observation that due to the severe path-loss attenuations distant BSs are less likely to preserve the required SINR thresholds. In reality, it is highly probable that one of the close-by BSs (not necessarily the closest one) preserves the best communication quality. Furthermore, for the sake of affordable handoff rate, it is more suitable to attach to a close-by BS than the too-distant BSs, as the chance that a far BS preserves the required SINR threshold for a couple of consequent communication sessions is rather vanishing.

Our Choice of CA

Regarding the important practical aspects of the max-SINR CA rule, we therefore concentrate mainly on this CA policy in this thesis. On the other hand, as we will also discuss in the literature review section, compared to the range expansion approach the literature of the max-SINR CA rule in MIMO multiplexing/diversity HetNets is unfortunately minuscule and little is known related to its performance and design issues.

1.3 Literature Review and Motivations of the Dissertation

1.3.1 Cellular SISO Communications

Various aspects of stochastic geometry for cellular networks have already been explored and reviewed in the previous section. In general, under the stochastic geometry analysis researchers often adopt the powerful technique of a probability generating functional (PGFL) for a straightforward evaluation of the SINR distribution [41, 42, 104, 105]; see Appendix A for more details.

Particularly, under Rayleigh fading in SISO systems, closed-form expressions of key performance metrics, including coverage probability, achievable rate (i.e., Ergodic capacity [14]), and area spectral efficiency (ASE), have been proposed [1, 47, 49]. Note that ASE by definition measures the accumulated throughput per unit area. In [47], the authors model the HetNets based on K classes of BSs each of which is independently modelled by a PPP. Their work is among the first to provide the coverage probability in a closed-form expression. The authors then extended their analysis to account for the impact of BSs loads on the coverage performance of HetNets in [51]. Further investigations regarding the impact of CA on the coverage probability are provided in [48]. The work of [49] investigates the selection of best biases for optimal load balancing based on long-term statistical network parameters, e.g., density of UEs and BSs. Furthermore, the authors of [106, 107] investigate the SINR process in HetNets and then evaluate the k-coverage probability, i.e., the probability that k BSs can potentially support the typical UE. The impact of CA on the coverage performance of HetNets is also investigated in [108]. The CA considered in [108] is specifically designed for load balancing, where the closest Macro BS is chosen when there is no femto BS in the vicinity of the UE that provides the highest SIR. The impact of CA on the network performance is also investigated in [109], where a heuristic association technique is also developed in order to

manage the CA according to statistical network parameters. The technique in [109] selects the associated tier for each UE based on a max-ratio association policy. Under this policy, for each UE a tier is selected such that the UEs distance to its nearest BS is smaller than that in other tiers, while its distance to the second-nearest BS in that tier is larger than that in other tiers. The closest BS of the selected tier is then considered as the serving BS. The work in [109] assumes that each tier has its own exclusive bandwidth.

Nevertheless, under more general fading distributions, such as Nakagami, and/or when the communication paradigms involve MIMO techniques, the effectiveness of the PGFL technique in providing easy-to-compute approximations of desirable network-level performance metrics partially collapses [42, 65, 105]. Many existing results in the related literature require numerical evaluations of two-fold infinite integrals of (two-fold) higher-order differentiations of complex functions [55, 110, 111, 112, 113] or a matrix norm of some matrices with entries of computationally expensive functions [114]. Assuming a general fading distribution, the authors in [113] obtain the coverage performance, which however requires complicated numerical integration over complex regions. By introducing a piece-wise linear approximation, the authors in [115] approximate the coverage probability of K-tier HetNets with Nakagami fading and noise through a summation of integrals. A recursive method is also developed to estimate the corresponding bounds of the integrations. Adopting a developed novel technique that permits the evaluations of functionals of PPP, [116] provides the SIR distribution under Nakagami fading. The coverage results are provided in integral formats of sophisticated functions. In [117], the authors develop a powerful moment generating method for approximating the SIR distribution of SISO systems under Nakagami fading. The derived moments require several improper integrations. Under this fading distribution, [94] studies the coverage probability of a single-tier cellular network when the BS deployment pattern is based on a Ginibre PP.

Remark 1.3.1 (Quantifying the Numerical Cost). *Throughout the thesis, when we discuss the numerical complexity of the analysis one should keep two particular regimes in*

mind: 1) the counterpart SISO system with exponential channel power gain; and 2) MIMO systems or SISO system under Nakagami-type channel power gain. Regime 1 represents the baseline of numerical complexity. In specific, we know that the coverage performance of regime 1 is generally expressable through (at most) an infinite integration which integrant is not represented in a higher-order differentiation form or the determinant of a matrix. We call this expression numerically friendly. Therefore, if we claim our analysis is also numerically friendly/affordable or is given in easy-to-compute expression, we implicitly mean that the format of the coverage probability is reminiscent of that of Regime 1. On the other hand, regarding Regime 2 if we argue that the analytical result is numerically heavy, we implicitly mean that the evaluation of the coverage probability requires the evaluation of several (more than one) infinite integrations while the integrand may also be given in complex forms comprising of either several higher-order differentiations or determinant forms. Accordingly, we are not quantifying the numerical complexity of the analysis from an algorithmic view point, but in the measure that whether it relies on evaluating the determinant of a matrix, higher-order differentiations, and couple of infinite integrations. Therefore, numerical complexity and numerical cost is treated similarly throughout the thesis. Finally, for the sake of fairness we generally refer to the communication scenarios of the mentioned regimes that are based on the main assumptions we also consider throughout the thesis: 1) independency of PPP sets; 2) independency of channel power gains of interfering BSs; 3) standard path-loss mode; and 4) either range expansion based CA or max-SINR CA. Therefore, we do not target the analytical complexity of the literature involving more sophisticated system model, e.g., Ginibri Point process.

1.3.2 MIMO Communications in Ad Hoc Networks

Our main focus in this dissertation is the stochastic geometry treatment of multi-stream MIMO HetNets. Our work is however related to the developments made in the literature of MIMO ad hoc communications too; see, e.g., [55, 62, 118, 119, 120, 121, 122, 123]. Note that

the analytical results of this literature may not necessarily fit with the model of this thesis due to existence of significant discrepancies between cellular and ad hoc networks (attributed to CA mechanisms and MAC protocols).

First, we review the single-stream MIMO communications. In [124], the authors focus on the evaluation of ergodic spatial capacity—accumulated ergodic capacity per unit area—in a single-input multiple-output (SIMO) random network. Therein, it is assumed that the receivers are designed to devote part of their receive array diversity for cancelling a number of dominant interferers (e.g., partial zero-forcing (PZF) receiver). Work of [121] also studies the transmission capacity — the maximum density of transmitters that fulfills the prescribed outage probability multiplied by the achievable throughput — of the SIMO system, when the receive filter is either PZF or minimum mean square error (MMSE). The conducted investigations in these works reveal that, by a careful design of PZF receiver, one can harness a proportional growth of the transmission capacity at most by the number of receive antennas. In [125], the CDFs of SIR of the MMSE filter in homogeneous, heterogenous, and also hierarchical PPP systems are calculated. The outage performance of the optimal combining in SIMO systems has also provided in [112, 126]. Furthermore, in [55, 78], the authors show that the inter-user interference causes a new source of correlation among the received signals in a multi-antenna receiver, which, in turn, degrades the diversity order of receive arrays.

For multi-stream MIMO systems, in [62, 118], the authors study the transmission capacity when the PZF receivers are designed to adaptively suppress interference. Further, work of [119] studies the outage probability and transmission capacity of MIMO multiplexing systems of sero-forcing beamforming (ZFBF), maximum ratio combining (MRC) as well as a diversity system of orthogonal space-time block codes (OSTBC), assuming that transmitters do not have access to channel state information CSI, i.e, open-loop MIMO. For this system, the authors pinpoint several advantages of ZFBF in enhancing the coverage performance of ad hoc networks, and further show that the multi-stream communications can actually outperform a single-stream ad hoc network. The authors then extend their analysis in [127]

to incorporate the multi-stream MMSE filters too. Work of [123] focuses on the examination of transmission capacity of ZFBF, antennas selection, and MRC diversity systems.

One of the main limiting aspect of the above literature is that the outage performance, and thus the transmission capacity, is merely studied from the perspective of a given stream — *stream-level* perspective. Put it in another word, the above literature simply assumes that the coverage probability of a data stream is equivalent to the coverage probability of the link. This is not, however, accurate. Specifically, while fading fluctuations across different streams (both related to interfering and desired signals) are generally independent, the interfering path-loss attenuations generated from the same set of interferers across data streams prompt correlation among data streams. We already know from works of [78, 112] that in SIMO ad hoc networks interference causes substantial correlation among impinged signals across receive antennas. Similar conclusions have also been reported in [55], where the interference correlation in space-time MIMO ad hoc networks was the focus. The authors observe that ignoring the interference correlation among antennas may in some cases substantially compromise the accuracy of the analysis.

However, in the multiplexing system, where each link runs a number of streams, the outage probability needs to be investigated from the perspective of the link — *link-level* perspective. In fact, as in the isolated scenario; see, e.g., [128, 129], the mutual information is the main indicator of the outage performance as the eigenvalues across data streams are heavily correlated [130, 131] even when interference is absent. In the non-isolated scenarios besides the correlation among eigenvalues there is another source of correlation: the common location of interfering BSs across data streams. Therefore, the method of the mentioned literature, which is based on a stream-level performance evaluation, is undoubtedly simplifying, and, to some levels, inaccurate. Thus, a comprehensive investigation of the link-level performance of multi-stream MIMO communication is crucial.

Interestingly, the importance of such analysis is partly recognized in the literature of ad hoc MIMO communications too. In [132], the authors study the link-level outage probability

of multi-stream MIMO-ZFBF receivers [14] when the transceivers are equipped with the same number of antennas. However, in this work the authors have heuristically substituted the actual covariance of the interference with the one in which fading is levelled out. Further, their result is based on a lower bound on the CCDF of mutual information, which was initially proposed by Foschini et. al. in [133]—this lower bound on the capacity essentially overlooks the correlation among eigenvalues of the link by substituting eigenvalues with a number of independent chi-squared random variables. The work of [134] also elaborates on some aspects of link-level coverage probability in random networks.

1.3.3 Cellular MIMO Communications

Assuming the CA rule of range expansion (see Section 1.2.3), [110, 114, 135] study the coverage performance and ASE of multiple-user spatial-division multiple access (SDMA) in MISO HetNets. In [114], the authors first derive the coverage probability through a L_1th norm of a well-packed matrix with entries derived through a recursive procedure. The results are then exploited to explore the optimal density of BSs in conjunction with the multiplexing gains of each tier in order to maximize ASE. The authors of [135] used the method of [114] and introduce a threshold-based range expansion in the downlink of SDMA systems. Work of [110] provides various heuristic CA procedures with respect to MIMO configurations, e.g., the number of equipped antennas at the BSs and the number of serviced UEs in the downlink. The authors then discuss optimal offloading based on the developed CA rules. The focus in [111] is the single Macro cell system overlaid by a number of multi-antenna femto cells. In [136, 137], the coverage performance of quantized beamforming system is estimated, and the results are used to adaptively share the feedback bits across users.

With multi-antenna receivers, the authors in [55, 73] focus on MRC and optimal combining in downlink and uplink of cellular networks, respectively. By exploiting the Gil-Pelaez inversion theorem, [138, 139] analyze the symbol error probability (SEP) of MIMO multiplexing systems. The impact of interference-driven correlation on dual-branch MRC receivers

in both ad hoc network and the downlink of a single-tier cellular network, is investigated in [112, 126]. Authors show that in comparison to ad hoc networks, in cellular communications a higher level of interference correlation across receive antennas is observable simply due to CA procedure. They also show that such interference correlation can substantially damage the diversity order of the receive arrays such that in many cases simple antenna selection combining can almost achieve the same coverage performance as does MRC or optimal combining.

Authors in [140] studied the bit error probability (BEP) of ZFBF with the aid of modelling ICI through the summation of an infinite number of Gaussian random variables, leading to a new mathematical technique referred Equivalent-in-Distribution (EiD). Therein BEP provided via twofold integral was shown to be simplified to a single integral formula when noise is neglected. The result was then extended in [141] to cover receive-diversity, multiplexing, and orthogonal space-time systems. In [142], the authors developed a new technique to model the ICI based on suitable Gaussian distribution in order to develop a unified framework for the evaluation of coverage probability and data rate of MIMO cellular systems. Closed-form expressions of the moments of the desired signal and ICI provided in [143], were further exploited to characterize spectral efficiency. Open-loop orthogonal space-time codes set the focus of the analysis in [55]. Their analysis covered the coverage probability of both interference blind MRC and optimal combining receiver techniques. Focusing on a single tier cellular network, MMSE and PZF beamforming schemes are investigated in [144].

In [86, 143, 145, 146, 147, 148], the authors adopt the theoretical results of [110, 114, 117] to optimize ASE and energy efficiency in uplink/downlink multi-user MIMO systems. The impact of beamforming schemes on energy-efficiency of MIMO downlink is investigated in [86]. Optimized offloading for controlling inter-cell interference utilizing coordinated MIMO communications was the subject of [147]. In [143], the coverage probability, spectral efficiency, and load balancing in MIMO systems is considered. [57] derives the ergodic capacity of several MIMO schemes in the downlink of a single-cell cellular network.

The works mentioned above assume range expansion for the CA policy. For the case of max-SINR CA rule (see Section 1.2.3), the work of [56] provides ordered results on the coverage, capacity, and ASE of MISO systems for qualitatively comparing several beamforming methods. Therein, the authors adopt stochastic ordering results to compare the coverage performance and ASE of SDMA and SISO systems. As far as we are aware, only this work studies MIMO HetNets under max-SINR CA rule, which indicates that many aspects of such configuration are missing in the state-of-the-art.

Despite these significant progresses in analyzing MIMO communications in HetNets, existing results are inadequate to comprehensively address the impact of multiplexing techniques on the coverage performance of HetNets. One reason is that the already existing results are mathematically very complex for numerical evaluations; see, e.g., [55, 56]. Commonly, the performance expressions in the literature of MIMO communications require single/double improper integrations of nested higher-order (as many as the number of antennas) derivatives of some numerically expensive functions such as hypergeometric functions (please refer to [126] for an example of the numerical algorithm). Unfortunately, the numerical complexities can become even more staggering when noise is included and also for large arrays. Such complexities may eventually overwhelm the desirable scalability for the particular purposes of system designs and engineering insights. We therefore set our goal to provide the coverage probability in numerically friendly expressions of the main system parameters. The obtained analytical results enable thorough investigations of densification and multiplexing gains in MIMO HetNets, some of which will be explored in the dissertation.

On the other hand, similar to the case of MIMO multiplexing in ad hoc networks, the above mentioned literature simply assumes that the coverage probability of a data stream is equivalent to the coverage probability of the link, which we already argue that it is not accurate. Consequently, we need to evaluate the coverage performance of MIMO multiplexing in HetNets from a *link-level* (that considers the reception of all the data steams) as opposed to the *stream-level or individual* (that considers the reception of a randomly selected data

stream) point of view.

Finally, note that the max-SINR CA rule is mainly studied for the SISO systems under exponential power gain in the literature; see, e.g., [47, 51, 106, 149, 150]. Note that there are a number of subtle differences between max-SIR CA rule in SISO systems and in MIMO systems, which do not allow straightforward extension of analytical results of the former to the latter: (1) as it is specified in [47, 51] in SISO systems the max-SIR CA rule is in effect equivalent to CA rule based on strongest *instantaneous* signal power. But this is actually not true in MIMO systems: the effective channel power gains on each data stream substantially differs from the channel matrix representing each communication link. In fact, as it is also pointed out in [56], in MIMO scenarios when a BS is the serving BS its fading distribution is essentially different than when it is an interfering BS, which is not the case of SISO systems. (2) In MIMO multiplexing systems, a communication link, which is physically represented by a channel matrix, is converted via precoding/decoding procedures into a number of data streams each with an associated post-processed SINR. Both, the CA and the coverage probability are then specified based on this post-processed channels. This, on the other hand, necessitates establishing a rule based on the quality of all the experienced SINR values across data streams received from a BS to decide upon CA, which differs from the SISO case.

In sum, observing these research gaps of the current literature, we aim at obtaining the coverage probability of MIMO multiplexing HetNets under the max-SINR CA rule.

1.4 Contributions and Results

Main Scope

This dissertation is mainly concerned with understanding the performance of MIMO multiplexing systems in HetNets. In effect, instead of concentrating on the resource allocation aspect of MIMO HetNets or improving beamforming techniques, we chiefly work toward

developing analytical tools for the purposes of investigating the coverage performance of MIMO multiplexing systems in large-scale cellular networks.

On the other hand, backed by the provided in-depth discussion in Section 1.2.2, throughout the thesis we assume that the stochastic geometry model is legitimate and acceptable. This is important as it allows us to entirely focus on the main goals of the thesis. This however does not mean that the thesis undermines the legitimate concerns regarding the accuracy of analysis for a particular configuration of the cellular network, for instance, in the downtown of Vancouver. We generally believe such concerns should be thoroughly covered in separate investigations. However, for such an investigation, assuming the empirical data is available, one still needs to access proper analytical tools beforehand, which is what this dissertation aims to provide.

Furthermore, our main focus is on the Sub-6 GHz (Microwave) spectrum, which substantially differs from mmWave communications that are strongly noise-limited, thanks to the strong link directionality [3, 6, 64, 65]. We also like to point out that 1) the stochastic-geometry investigation of mmWave communications commonly excludes the evaluation of a link-level performance, and usually focus is on stream-level analysis [3, 6, 64, 65]; 2) the techniques developed in [3, 6, 64, 65] usually rely upon incorporating the effect of (analog) beamforming through sectionized antennas with properly randomized antenna gains, which cannot correctly model the multiplexing systems; 3) [3, 6, 64, 65] usually assumes exponential distribution to model the post-processed channel power gain, which is not the case of the MIMO multiplexing systems where on each data stream Nakagami-type fading governs the fast fading propagation effect; 4) as far as we are aware of, the literature of mmWave communications commonly assume range expansion to model CA; and 5) the mmWave communications are severely vulnerable to blockages [70], so that it is acceptable to exclude non-LOS signals (could be originated from serving or interfering BSs) from analysis. In contrary, for many practical cases in the Sub-6 GHz, the LOS components are of secondary importance meaning that they could affect the performance solely when the network

is substantially densified [67].

On the other hand, in this thesis we adopt tools of stochastic geometry to study the scenario that a receiver is in the link-level coverage. We refer to it simply by coverage; unless otherwise specified. Our particular definition of link-level coverage implies the successful reception of all transmitted data streams of a link. This notion of coverage probability is known as *all-coverage probability* in the literature of isolated MIMO systems [128, 151]. We should emphasize that for those transceiver structures that the SER is related to the CCDF of the weakest data stream [128, 152, 153, 154], this definition of coverage probability is of course intuitive. However, as in the case of isolated scenarios other possible choices for specifying the coverage probability exist: *sum-coverage* and *any-coverage*. Regarding the former, a typical UE is assumed to be in coverage if the aggregate transmission data rate stays above a threshold. Regarding the latter, if the most powerful data stream of the link is undetectable, the link is assumed to be in outage. We in this dissertation mainly investigate the all-coverage probability. Note also that regardless of MIMO system structure, defining the coverage probability based on all-coverage notion has important practical implication too. In essence, it advocates the design of the network so that the UEs can successfully decode as many independent data streams as can be transmitted —i.e., no wastage of multiplexing gain.

The main scope of the analysis is devoted to the evaluation of the coverage probability. Nevertheless, recalling Remark 1.1.2, it is then a matter of straightforward manipulations to explore several other performance metrics such as spectral efficiency, capacity, and energy efficiency. When we want to provide concrete results, we explore spectral efficiency of the cellular network to demonstrate this point. On the other hand, we also broadly adopt the analytical results in order to explore various important design issues in MIMO multiplexing HetNets. Thanks to the numerically tractable form of our analytical results, such design problems permit us to draw interesting guidelines.

A Broad Goal

It is the goal of many researchers to seek analytical methods that simplify the analysis of wireless networks. For SISO systems and under practically fair assumptions, this goal is readily achieved. As a well-appreciated result, consider the downlink of a HetNet with K tiers of BSs, where $\beta > 1$ is the SIR threshold for successful transmission. Under the max-SIR CA rule, the coverage probability, c^{SISO}, is derived from the following [47]

$$c^{\text{SISO}} = \frac{\pi}{C(\alpha)\beta^{\alpha}}, \tag{1.6}$$

where $C(\alpha)$ only depends on the path-loss exponent α. As it is also discussed by the authors of [155], what (1.6) in essence provides is reminiscent of the comfort that the simple equation of bit error rate (BER) of BPSK modulation in Gaussian/fading channels provides. Analogous to modulation theory, using (1.6) the system designer is then well-equipped to design the network instead of resorting to try-and-fail exhaustive simulations.

Recalling from the modulation theory that for more sophisticated modulation/coding schemes the evaluation of the BER becomes dramatically more convoluted and less mathematically tractable, the same pattern in effect emerges in HetNets when the subject of the analysis shifts from SISO systems toward MIMO systems. Main complexities root in the fact that, as opposed to SISO scenarios, there are many MIMO techniques to choose from and each affects the signal propagation differently. On the other hand, the effective channel power gains deviate from the exponential distribution.

Thus, for MIMO multiplexing systems, we attempt to develop analytical tools that allow the network-level evaluation of key network metrics including the coverage probability hopefully with the same comfort that one enjoys in the analysis of counterpart SISO systems. As an example, for a MIMO-ZFBF system, assuming the multiplexing gain S and when UEs are equipped with $N^r \geq S$ antennas, we show that the coverage probability, c^{ZF}, is obtained

from

$$c^{\mathrm{ZF}} \leq \frac{\pi}{\tilde{C}(\alpha)\beta^{\alpha}}\Omega(S, N^r, \alpha), \tag{1.7}$$

where $\tilde{C}(\alpha)$ only depends on the path-loss exponent α and $\Omega(S, N^r, \alpha)$ is a function of multiplexing gain, path-loss exponent, and the number of receive antennas. Interesting similarity between SISO and MIMO formulas are evident. Further, while the MIMO system has much more complexities, our analysis is yet able to manage them and provide the key performance metric in numerically pleasing expression.

Therefore, a broad goal of this dissertation is to present the coverage probability of MIMO multiplexing systems in easy-to-compute and succinct expressions of the key network parameters. We desire to attain the same complexity as that resulting from network performance evaluation under SISO systems. We further aim to achieve this goal without sacrificing the accuracy of the analysis.

Main Contributions

We develop a comprehensive downlink model consisting of K tiers or classes of BSs, such as Macro-cells, femto-cells, pico-cells and distributed antennas. The BSs across tiers differ in terms of transmit power, deployment density, target SINR, number of transmit antennas, and multiplexing gains. We explore this model for popular MIMO multiplexing schemes, ZFBF, MRC, and SVD, by providing the coverage probability as the main performance metric. Regarding all-coverage probability and assuming the max-SINR CA rule, this dissertation provides the following contributions:

- For the case of ZFBF multiplexing HetNet:

    1. We obtain an upper- and a lower-bound on the link-level coverage probability. The upper-bound requires a single integration, while the lower-bound is in closed-form and has much lower computational complexity compared to the upper-bound. We also specify our results for the scenarios of full-multiplexing system, and the single-

stream communication (diversity system), and show that our results accurately predict the SISO system performance [47]. The conducted extensive simulations corroborate the analysis.

2. We also analytically prove that a single-stream communication has higher coverage performance than that of the multi-stream counterpart.

3. We investigate the impact of the cross-stream correlation on the coverage probability by introducing the *full-correlation* (FC) assumption, and derive the coverage probability under it. Specifically, we show that by averaging out the impact of interfering fading fluctuations the coverage probability results in the lower-bound on the coverage probability, which we also derive. Our simulations indicate that the induced performance gap, because of FC assumption, is slightly noticeable. As a result, it is safe to assume that in MIMO multiplexing systems data streams are fully correlated (from the coverage probability/SINR distribution perspective), which in some cases can substantially simplify the analysis of the network.

4. When the noise effect is negligible, i.e., in interference-limited systems, our coverage analysis does not rely upon the evaluation of integrals, and is given in a closed-form expression.

5. We exploit our analysis to investigate the interconnection between densification, multiplexing, and diversity in HetNets. We also formulate the spatial throughput of multiplexing systems when the quantized values of SINRs are available at the serving BSs through dedicated low-latency, error-free feedback channel with limited capacity. Our reported results show that by considering feedback channels with capacity up to 8 bits per frame per BS, the spatial throughput grows by at most 180% over the conventional 1-bit feedback system.

- For MIMO-MRC multiplexing systems, we also investigate the coverage probability. In comparison to ZFBF, under MRC the received data streams of a given communication

link interferes together as the receiver does not cancel out the cross-stream interference. Our analysis also incorporates the impact of inaccurate CSI at the receiver (CSIR). For this system:

1. We obtain an easy-to-compute, tight upper-bound on the network coverage probability in closed-form expression. Our analytical results—supported by extensive simulation—provide significant practical insights on the impact of densification on the link-level coverage performance. We then conclude that improvement in the network coverage performance and ASE by densification is subject to careful selection of multiplexing gains in different tiers, which is also observed for the case of MIMO-ZFBF multiplexing system. Besides, we quantify the trade-off between densification and multiplexing gains in multi-stream MRC systems. Our results indicate that increasing CSI inaccuracy compromises the coverage advantage of multi-stream over single-stream systems.

2. We demonstrate practical cases in which the high processing costs of ZFBF justifies using MRC, although ZFBF generally outperforms MRC in terms of coverage probability. We further provide quantitative insights on the coverage cost of adopting MRC compared to ZFBF.

3. We also analyze the cross-stream SIR correlation coefficient amongst multiple streams in a communication link. Our analysis provides quantitative insights on the impact of tiers' BSs density, path-loss exponent, CSI inaccuracy, and multiplexing gains on the SIR correlation among data streams. Besides exploring the coverage probability of MIMO-MRC under full-correlation assumption, we further discuss another extreme correlation scenario, no SIR correlation (NC) assumption, where all data streams of a communication link are deemed to be entirely uncorrelated. We show that the NC setting substantially over-estimates the coverage performance. Observing that the FC setting slightly underestimates

the coverage probability reconfirms the conclusion that in multiplexing systems the data streams can be regarded as nearly-fully correlated.

- We also derive the coverage probability of SVD systems. Compared to MRC and ZFBF schemes, under SVD the effective fading power gains across data streams are related the eigen-values of channel matrix. The distribution of eigenvalues deviates from chi-squared distribution, which is the case of MRC and ZFBF, and also causes new source of correlation across data streams. Both effects make the developed methods for ZFBF and MRC ineffective to derive the coverage probability under SVD. Our main contributions in this part are:

  1. Investigation of statistical correlation among streams caused by heterogenous interference. For the cases that the antennas are spatially uncorrelated, our analysis indicates that ICI causes path-loss driven correlation among data streams.
  2. In comparison to the general trend of the literature that provides the coverage probability of MIMO-SVD in terms of very complex forms of determinants of matrices where entries are special mathematical functions (e.g., hypergeometric functions), our coverage result in this part is given in closed-from expression with the same level of complexity of ZFBF as well as MRC.
  3. Our results also specify the regimes where increasing the number of antennas substantially improves the coverage performance. Highlighting the significance of channel state information at transmitter (CSIT) in HetNets, we then demonstrate substantial grows of the coverage performance under full multiplexing SVD systems compared to ZFBF and MRC systems.

1.5 Thesis Outline

The rest of this thesis is organized as follows:

- In Chapter 2, we introduce a K-tier PPP model for MIMO-ZFBF multiplexing HetNets in downlink. We present the signal model, formulate the SINR, and define the all-coverage probability. We further elaborate on extending the max-SINR CA rule based on all-coverage probability. In this chapter, we first derive the coverage probability of staggering computational complexity, which also stands as a motivation for the consequent analysis of the chapter. To tackle the computational burden, we then develop a lower-bound and an upper-bound on the coverage probability. We further introduce notion of full-correlation (FC) assumption and prove that the lower-bound on the coverage probability coincides with the coverage probability under FC assumption. We also analytically prove that in HetNets increasing the number of transmitted data streams reduces the coverage performance. Further, we derive the coverage probability for interference-limited scenario. We also extend our analysis for the case of spectrum-sharing D2D HetNets and show how one can adjust the equivalent noise power based on the D2D communication parameters. Furthermore, in this chapter we discuss the coverage performance when path-loss exponents across tiers are different. We also explore a practical version of max-SINR CA rule whereby a limited number of BSs are available for CA. To derive the coverage probability for this practical CA rule we use the FC assumption. Last, this chapter discusses the extension of the analysis for several pertinent MIMO systems such as SDMA and maximum ratio transmission (MRT).

- The approach of Chapter 3 is quite similar to Chapter 2. In this chapter the main focus is on MRC multiplexing systems. However, here we extend the analysis to quantify the cross-stream SIR correlation coefficient. We derive this parameter and evaluate the impact of many important system parameters and inaccurate CSIR on it. We further quantify the relationship between ASE, coverage probability, multiplexing gains, densification, and CSIR inaccuracy. Since ZFBF outperforms MRC in HetNets, we elaborate on scenarios that MRC provides a more efficient receiver choice by taking the receiver complexity into account. This chapter also introduces the no-correlation

(NC) assumption scenario, which is actually the method of the literature, to derive another upper-bound on the coverage probability. We observe that NC assumption substantially over-estimates the coverage probability. We analytically prove that the growth of cross-stream SIR correlation decreases the coverage probability.

- Our analysis in Chapter 2 and Chapter 3 assumes that the CSIT is unavailable. In Chapter 4, we alleviate this assumption and focus on the scenario of full CSIT. The coverage analysis of SVD systems are notoriously complex even for simple cases of isolated systems. We in this chapter develop analytical tools allowing an accurate estimation of the coverage probability based on the PDF of the min eigenvalue distribution of central Wishart matrix. We also explore the cross-stream SIR correlation in SVD systems. This chapter shows the great benefit of CSIT from a network-level perspective. In effect, we observe that full multiplexing SVD can increase the coverage performance compared to MRC by up to 1000 per cent. Also, SVD systems demonstrate great potentials in improving the coverage probability by increasing the number of transmit antennas, whereas the coverage performance of ZFBF and MRC based systems are nearly constant.

- Chapter 5 summarizes the contributions of the thesis and outlines areas of future research.

- Appendix A provides a short discussion on stochastic geometry and main analytical tools which are often used throughout the thesis. Appendix B proves two important Lemmas, which we often refer to, when deriving the coverage probability.

Chapter 2

Analysis and Design of Multi-Stream MIMO-ZFBF Receivers in HetNets

2.1 Introduction

The pioneering work of [47] proposes a flexible approach for modeling K-tier HetNets through a K spatially and spectrally coexisting tiers, each with its own BSs. BSs are distributed in 2-d plane through K tiers of independent PPPs. In conjunction with the max-SINR CA rule, the authors derive key system performance metrics, including coverage probability as a function of the main influential system parameters in a closed-form expression, which is undeniably hard to achieve under conventional cellular models, e.g., grid/hexagonal model.

In this chapter, we aim at extending the proposed in [47] to a multi-stream MIMO HetNet, and investigate its coverage performance and explore several aspects of this configuration. Our focus is on open-loop—no CSIT— MIMO-ZFBF. This scheme is practically attractive due to its straightforward implementation, low computational complexity, and almost zero feedback overhead [36]. Regarding this model, we attempt to accomplish three specific goals:

1. The first goal concerns the lack of numerically suitable formula(s) for the evaluation of the coverage probability of MIMO multiplexing systems, particularly ZFBF receivers. In fact, the model [47] is adopted by the same authors in [56] to investigate the coverage probability of a multi-user MISO, a.k.a SDMA-ZFBF, donwlink in a HetNet. However, the authors only provide ordering results implying that the coverage performance of a single-user MISO is higher than SISO counterpart system, while both systems provide

higher coverage performance than multi-user MISO system. The main shortcoming of this work is that the derived coverage provability for the considered MIMO system has a staggering high computational complexity, making it almost unsuitable for numerical analysis. Furthermore, their method is not straightforwardly extendable for multi-stream MIMO communication scenarios. As we already mention in Chapter 1, the complex analytical results are quite persistent in the stochastic geometry analysis of MIMO systems. We therefore believe it is of high priority to invest in developing analytical tools that conceivably scale down the computational burden of the analysis without sacrificing accuracy.

2. On the other hand, in the context of ad hoc networks, the literature shows several advantages of ZFBF in enhancing the coverage performance [119]. The authors in [119] prove that multi-stream communications can actually outperform a single-stream ad hoc network. In light of this finding, one may then argue that the same trends can hold in MIMO HetNets by noticing the convergence, albeit partial, of HetNets toward ad hoc networks, for instance through *random* installation of remote antenna ports, relays, and small cells.[2] It is, therefore, necessary to investigate:

   - Whether or not the multi-stream MIMO schemes, such as ZFBF, are of practical significance in enhancing the coverage performance of HetNets;
   - Whether in MIMO HetNets, cell densification and high multiplexing gains should be practiced simultaneously in all tiers;
   - If new techniques are needed to evaluate, whether excessive densification is preferable to increase multiplexing gains.

   Thanks to the developed analysis, these questions and similar design issues can be thoroughly addressed by devising suitable optimization solutions. In this chapter, we

[2] Apart from such analogies, significant discrepancies between these two networks exists which can be due to the corresponding CA mechanisms governing HetNets, as well as centralized TDMA/FDMA MAC protocols, which are commonly practiced in infrastructure-based configurations.

explore several of such design issues, highlighting important aspects of the MIMO multiplexing systems and providing various guidelines.

3. Finally, as mentioned in Chapter 1, one of the main limiting aspect of the literature of MIMO multiplexing systems, e.g., [62, 118, 123, 127], is that the outage performance is merely studied from the perspective of a given stream — *stream-level* perspective. This is not accurate due to the common location of interfering BSs across the data streams of a link. Thus, in multiplexing systems, where each link runs a number of streams, the outage probability needs to be investigated from the perspective of the link — *link-level* perspective. In this chapter we provide a notion of link-level coverage probability and build over the analysis.

We shall also emphasize that the method developed in this chapter is general enough and will be exploited/extended to investigate many other prominent MIMO systems. Some direct extensions are pinpointed in this chapter. Other relevant ones which require extra elaborations or adoption of more sophisticated steps are covered in the other chapters of this dissertation.

The rest of the chapter is organized as follows. The system model and main assumptions are presented in Section 2.2. Coverage performance is analyzed in Section 2.3. We then present an approximation of the coverage probability by introducing the FC assumption in Section 2.4, followed by investigating the impact of multiplexing gain on the coverage performance in Section 2.5. Section 2.6 discuses the coverage probability of the interference-limited system. In Section 2.7, we present the simulation and numerical results. In Section 2.8, we discuss several pertinent system design and explore performance evaluation of the network via numerical studies. In Section 2.9 we provide various extensions of the provided analysis. The extensions include: 1) spectrum sharing in MIMO HetNets, 2) non-homogenous path-loss environment, 3) a more practical version of the max-SINR CA mechanism, 4) other MIMO techniques. The provided extensions are to demonstrate how the analysis can be

exploited to discuss relevant MIMO communication scenarios, thus we exclude full-fledged investigations of the subjects. The chapter is finally concluded in Section 3.7.

2.2 System Model and Assumptions

2.2.1 Network Model

Consider the downlink communication of a K-tier heterogeneous cellular networks. The HetNet is comprised of $K \geq 1$ tiers of randomly located BSs in which the BSs of Tier $i \in \mathcal{K}$ are spatially distributed according to a homogenous PPP, Φ_i, with spatial density, $\lambda_i \geq 0$. A brief introduction to PPP is available in Appendix A. Parameter λ_i is the number of BSs per unit area [47]. We further assume that Φ_i, $i \in \mathcal{K}$ are mutually independent. For the ease of exposition we also denote $\Phi = \{\Phi_i\}_{\forall i}$. UEs are also randomly positioned across the network and form a PPP, Φ_U, independent of Φ, with given density λ_U. According to Slivnayak's Theorem [40, 41] (see also Theorem A.1.2 and Definition A.1.6 in Appendix A) and due to the stationarity of the point processes, the spatial performance of the network can be obtained from the perspective of a typical UE positioned at the origin.

Time is slotted and, similar to [47, 50, 55, 56], we assume that at each given resource block (e.g., time slot) only one UE is served per active cell. In cases where more than one UE is associated with a given BS, UEs will be scheduled across resource blocks (e.g., time slots, sub-carriers). We also assume that UEs are equipped with N^r antennas.

Each Tier i is fully characterized by the corresponding spatial density of BSs, λ_i, the transmission power of BSs, P_i W, the SINR threshold, β_i, the number of the transmit antennas BSs possess, N_i^t, the number of scheduled streams $S_i \leq \min\{N_i^t, N^r\}$ (also referred to as *multiplexing gain* [118, 119, 156]), and the associated noise power σ_i^2. As [47, 50, 56], we assume that SINR thresholds $\beta_i \geq 1$, only for analytical purposes—more details regarding this assumption is provided in Remark 2.3.2.

2.2.2 Signal Model

Let a typical UE be associated with BS x_i, transmitting S_i data streams. The received signal, $\boldsymbol{y}_{x_i} \in \mathbb{C}^{N^r \times 1}$, is

$$\boldsymbol{y}_{x_i} = \|x_i\|^{-\frac{\alpha}{2}} \boldsymbol{H}_{x_i} \boldsymbol{s}_{x_i} + \sum_{j \in \mathcal{K}} \sum_{x_j \in \Phi_j \setminus x_0} \|x_j\|^{-\frac{\alpha}{2}} \boldsymbol{H}_{x_j} \boldsymbol{s}_{x_j} + \boldsymbol{w}_i, \tag{2.1}$$

where $\forall x_i, i \in \mathcal{K}$, $\boldsymbol{s}_{x_i} = [s_{x_i,1} \dots s_{x_i,S_i}]^T \in \mathbb{C}^{S_i \times 1}$, $s_{x_i,l_i} \sim \mathcal{CN}(0, P_i/S_i)$ is the transmitted signal corresponding to stream l_i in Tier i, $\boldsymbol{H}_{x_i} \in \mathbb{C}^{N^r \times S_i}$ is the fading channel matrix between BS x_i and the typical UE, with entries independently drawn from $\mathcal{CN}(0,1)$, i.e., Rayleigh fading. Also, $\boldsymbol{w}_i$ stands for the background noise which is assumed to be additive, Gaussian, and white.

In our model, we assume that the transmitted signals are independent of the channel matrices. In (2.1), $\|x_i\|^{-\alpha}$ is the distance-dependent path-loss attenuation, where $\|x_i\|$ is the Euclidian distance between BS x_i and the origin, and $\alpha > 2$ is the path-loss exponent. We also assume perfect CSI is available at the receiver (i.e., CSIR), which is attainable by dedicating enough pilot transmission.

Remark 2.2.1 (Large-Scale Shadowing). *Our model does not explicitly include the impact of large-scale shadowing. Nevertheless, under certain conditions it is quite straightforward to include its impact in the analysis. Assume shadowing is i.i.d., i.e., shadowing gains across BSs of a tier are i.i.d.. Further, let χ_{x_i} be the shadowing effect between BS x_i and the typical UE so that $\mathbb{E}[\chi_{x_i}^{\check{\alpha}}] < \infty$, where $\check{\alpha} = 2/\alpha$. Therefore, according to the results of [50, 100, 157], one then is able to simply scale the densities as $\lambda_i \to \lambda_i \mathbb{E}[\chi_{x_i}^{\check{\alpha}}]$ in order to incorporate the impact of the shadowing. For instance when χ_{x_i} is governed by the log-normal distribution as $\chi_{x_i} \sim 10^{\mathcal{N}(\overline{\chi}_i, \mathrm{Var}(\chi_i))}$, where $\mathcal{N}(\overline{\chi}_i, \mathrm{Var}(\chi_i))$ stands for a Normal distribution with finite mean $\overline{\chi}_i$ and variance $\mathrm{Var}(\chi_i)$, it is straightforward to confirm that*

$$\mathbb{E}[\chi_{x_i}^{\check{\alpha}}] = e^{\frac{\log 10}{5} \frac{\overline{\chi}_i}{\alpha} + 0.5 (\frac{\log 10}{5} \frac{\mathrm{Var}(\chi_i)}{\alpha})^2} < \infty. \tag{2.2}$$

Note that under this particular choice of shadowing, the PPP sets Φ_is stay homogeneous, which is desirable. Nevertheless, when shadowing is spatially correlated (e.g., large buildings probably impose the same shadowing effect on adjacent BSs) [16], or it does affect the fading characteristics, resulting a composite fading distribution [158, 159, 160, 161], the analysis becomes substantially more intricate as the net effect of shadowing manipulates the Poisson sets Φ_is which are demonstrating distance-dependent inhomogeneity. Among suitable approaches permitting to deal with the possible analytical complexities one can suggest 1) considering more realistic path-loss model that includes LOS/NLOS components (this approach can to some levels account for the source of shadowing in cellular networks); 2) modeling the correlated shadowing through a suitable clustered point process (therefore, BSs that falling into the same cluster have the same shadowing gain); and 3) considering more regular Point models, e.g., Manhatan Poisson line process, to account for street-type structure of cities. Our main focus in this thesis does not include such scenarios.

2.2.3 SINR Formulation

As [118, 119], we focus on the scenario in which the CSIT is unavailable, and hence the BSs of each Tier i simply turn on S_i transmit antennas, where the transmit power P_i is equally divided among the transmitted data streams. Such a simple pre-coding scheme is often categorized as *open-loop*, see, e.g., [118, 119]. In this chapter, we analyze a dominant open-loop technique *viz.* ZFBF at the receiver.

A typical UE utilizes the CSIR, $\boldsymbol{H}_{x_i}$, to mitigate the inter-stream interference to successfully decode the l_ith stream. The typical UE obtains matrix $(\boldsymbol{H}_{x_i}^{\dagger}\boldsymbol{H}_{x_i})^{-1}\boldsymbol{H}_{x_i}^{\dagger}$, and then multiplies the conjugate of its l_ith column by the received signal in (2.1). The post-processing SINR associated with the l_ith stream is then obtained from [119] as

$$\mathrm{SINR}_{x_i,l_i}^{\mathrm{ZF}} = \frac{\frac{P_i}{S_i}\|x_i\|^{-\alpha}H_{x_i,l_i}^{\mathrm{ZF}}}{\sum\limits_{j\in\mathcal{K}}\sum\limits_{x_j\in\Phi_j\setminus x_i}\frac{P_j}{S_j}\|x_j\|^{-\alpha}G_{x_j,l_i}^{\mathrm{ZF}}+\sigma_i^2}. \tag{2.3}$$

The numerator is the effective power of the attending/intending signal per stream after post-processing, and the denominator is the ICI plus AWGN power. The intending channel power gain associated with the l_ith data stream, $H^{\mathrm{ZF}}_{x_i,l_i}$, and the ICI caused by $x_j \neq x_i$ on data stream l_i, $G^{\mathrm{ZF}}_{x_j,l_i}$, are chi-squared random variables (r.v.) with Degree-of-Freedom (DoF) $2(N^r - S_i + 1)$, and $2S_j$, respectively. Note that for each l_i, $H^{\mathrm{ZF}}_{x_i,l_i}$ and $G^{\mathrm{ZF}}_{x_j,l_i}$ are independent r.v.s. Further, $H^{\mathrm{ZF}}_{x_i,l_i}$ (resp. $G^{\mathrm{ZF}}_{x_j,l_i}$) and $H^{\mathrm{ZF}}_{x_i,l}$ (resp. $G^{\mathrm{ZF}}_{x_j,l}$) are i.i.d. for $l \neq l_i$. In (2.3), for a given communication link, $\mathrm{SINR}^{\mathrm{ZF}}_{x_i,l_i}$, are identically, but *not* independently, distributed across streams, which roots in the path-loss attenuations. We discuss this issue with more details in Section 2.4.

Remark 2.2.2 (Beyond ZFBF). *As mentioned in 2.1, in addition to its practical simplicity, ZFBF provides mathematical tractability, which is hard to achieve in non-linear MIMO-based techniques. However, the analytical tools developed in this chapter are to some extents general enough to be adopted to study some other pertinent MIMO systems, e.g., space-division multiple access (SDMA). As a rule of thumb, one is able to use the analysis of this chapter quite straightforwardly if the system under the scrutiny admits the same SINR formulation of* (2.3)*. The main characteristics that should be maintained in order to successfully achieve this goal is that the SINR should 1) include Nakagami-type fading distribution in attending and/or interfering signals, 2) maintain the statistical independence of numerator and denominator, and 3) involve no intra-cell interference. Nevertheless, when the SINR formula demonstrates non-Nakagami-type fading (e.g., under SVD processing as is covered in Chapter 4), the receiver suffers from intra-stream interference (e.g., MRC system which is covered in Chapter 3), and correlation between the numerator and denominator (e.g., correlated received antennas or the quantized beamforming), one is then required to substantially upgrade the analysis of this chapter.*

Remark 2.2.3 (Receive Antenna Correlation). *In reality, both of the intending and interfering channel matrices may demonstrate degrees of row correlation because of spatial antenna correlation at the receiver side [14, 37, 162, 163]. Such a phenomenon renders*

substantial analytical complications as 1) $H^{\mathrm{ZF}}_{x_i,l_i}$ and $G^{\mathrm{ZF}}_{x_j,l_i}$ are now correlated governed by the eigenvalues of intending and interfering channel matrices and associated correlated matrices, 2) the intending channel power gain $H^{\mathrm{ZF}}_{x_i,l_i}$ behaves as a mixture of generalized chi-squared r.v.s (comprised of Gauss hypergeometric functions, see, e.g., [164]), which are less tractable than the chi-squared r.v.. Both of these issues cause substantial complexities, hampering the analytical investigation of the coverage probability. More sophisticated tools facilitating the investigation of antenna correlation on the network-level performance are then required.

2.2.4 Coverage Probability in Multi-Stream MIMO Cellular Communications

The coverage probability of a single-stream MIMO communication is directly related to the CCDF of the SINR. More specifically, for Tier i, the coverage probability is the probability that the SINR stays above a given SINR threshold β_i. In the case of multiple streams however, depending on the transceiver structure and/or Quality-of-Service (QoS) requirements, evaluation of the coverage probability becomes more complex. For instance, in some transceivers, the coverage probability is related to the CCDF of the weakest data stream [128, 152, 153, 154]. This is the main subject of this thesis, whereby a UE is considered covered if all of its streams are successfully decoded. As the isolated scenarios [128, 151] case, this interpretation of the coverage is referred to *all-coverage probability*, which is formally defined in the following:

Definition 2.2.1 (All-Coverage Probability). *In a multi-stream MIMO system, a UE is considered covered if all of its streams are successfully decoded.*

All-coverage probability, in effect, encourages the transmission of as many independent data streams in each tier that the system is able fully decode, i.e., no wastage of multiplexing gain.

Having our interpretation of coverage specified, what remaines is to specify the CA:

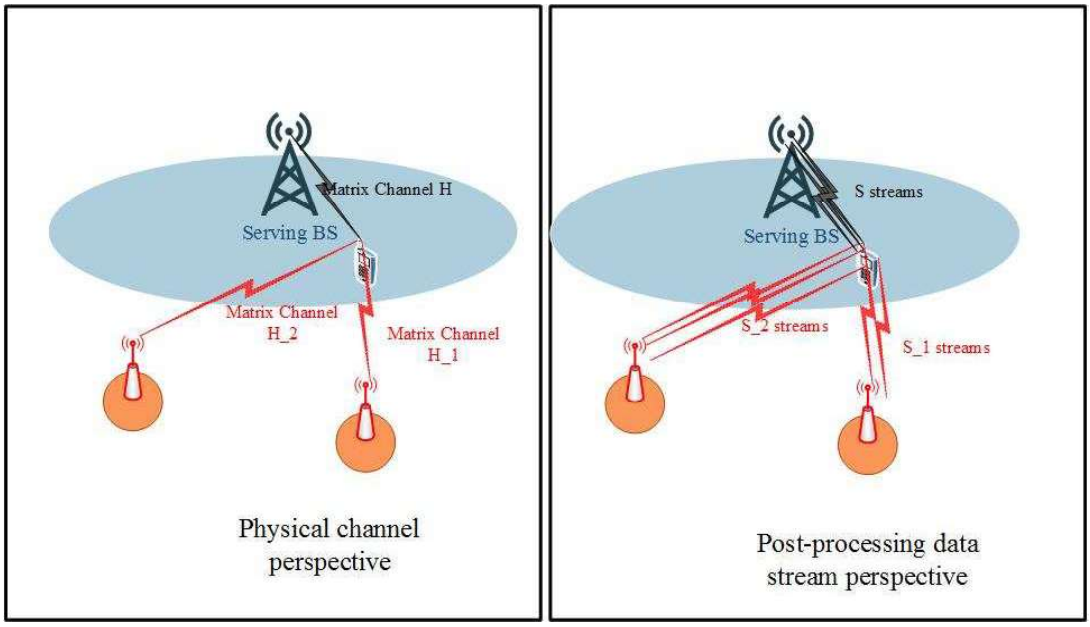

Figure 2.1: Post-processed MIMO multiplexing scenario.

Definition 2.2.2 (Max-SINR Cell Association under All-Coverage Probability). *The typical UE is associated to the BS through which the weakest SINR across the streams is larger than the corresponding SINR threshold, β_i. Accordingly, the typical UE is considered in the coverage area if $\mathcal{A}^{\mathrm{ZF}}$ is nonempty, where*

$$\mathcal{A}^{\mathrm{ZF}} = \left\{ \exists i \in \mathcal{K} : \max_{x_i \in \Phi_i} \min_{l_i = 1,\ldots,S_i} \mathrm{SINR}^{\mathrm{ZF}}_{x_i,l_i} \geq \beta_i \right\}. \tag{2.4}$$

Let $c^{\mathrm{ZF}} = \mathbb{P}\{\mathcal{A}^{\mathrm{ZF}} \neq \emptyset\}$ denote the all-coverage probability.

Remark 2.2.4. *The max-SINR CA mechanism introduced in Definition 2.2.2 is practically influential as it allows the typical UE staying always associated with a single BS across all data streams, adhering to the fact that all the data streams are basically originated from a single BS* (2.1)*. This is also shown in Fig. 2.1. This illustration shows the equivalence between the signal model based on channel matrices and the post-processed association model. Since the coverage performance depends upon the post-processed SINR values, it is important to specify the association based on the status of the link and not each individual data stream.*

If coverage probability per stream is considered, one may encounter occasions that the typical UE simultaneously receives data from several BSs (as with non-vanishing probability different unique BSs can provide strongest SIR value on different data streams), which obviously is not the reality of the signal model in (2.1).

Remark 2.2.5 (Load Balancing). *By load balancing, one is able to manipulate the CA (by including artificial biases) to more aggressively offload traffic a from heavily-loaded tier (usually Macro BSs) into small cells [49, 110]. This is an effective approach to compensate for higher transmission power of Macro BSs form a network-level perspective. This approach to load balancing is heavily investigated under the range expansion CA rule (see Section 1.2.3 for details). Although the max-SINR CA rule does not specifically address load balancing in HetNets, it is but straightforward to incorporate such design issue into the analysis. As an example, assume parameters* $0 \leq \rho_i \leq 1$ *are the association biases such that* $\sum_i \rho_i = 1$. *The (modified) max-SINR CA rule is then constructed as*

$$\mathcal{A}^{\mathrm{ZF}} = \left\{ \exists i \in \mathcal{K} : \max_{x_i \in \Phi_i} \rho_i \min_{l_i = 1, \ldots, S_i} \mathrm{SINR}^{\mathrm{ZF}}_{x_i, l_i} \geq \beta_i \right\}. \tag{2.5}$$

Applying $\beta_i \to \frac{\beta_i}{\rho_i}$, *one simply attains the conventional max-SINR CA rule* (2.5), *where parameters* β_i*s are variable that need to be optimally evaluated based on the particular design agenda and system constraints.*

Our main goal in the rest of this chapter is to evaluate c^{ZF} in a computationally friendly expression, which is not a trivial task. This is because 1) associated with each data stream, the fading fluctuation of the intended signal is chi-squared, which is not as amendable to analysis as the exponential distribution, 2) the existence of noise, and finally 3) the correlation of the SINR values across data streams of a communication link, which has roots in the common location of interferers across data streams, i.e., as seen from (2.3), the same path-loss attenuation $\|x_j\|^{-\alpha}$ from interfering BS $x_j \neq x_i$, which is random due to the random location of BS x_j, is realized across data streams l_i.

2.2.5 Characterization of Inter-Cell Interference

The denominator of (2.3) represents the aggregate ICI imposed from concurrent transmissions in adjacent cells. The ICI on stream l_i is given by

$$I^{l_i} \triangleq \sum_{j\in\mathcal{K}} \sum_{x_j\in\bigcup_j \Phi_j\setminus x_i} \frac{P_j}{S_j}\|x_j\|^{-\alpha} G^{\mathrm{ZF}}_{x_j,l_i} \tag{2.6}$$

which is a shot noise process [104, Section III-A] (see Section A.2 in Appendix A), and is entirely characterized by its Laplace transform $\mathcal{L}_{I^{l_i}}(t)$ (A.9). It is straightforward to show that

$$\begin{aligned}
\mathcal{L}_{I^{l_i}}(t) &= \mathbb{E}e^{-tI^{l_i}} && (2.7)\\
&= \mathbb{E}_{\Phi}\mathbb{E}_{\{G^{\mathrm{ZF}}_{x_j,l_i}\}_{x_j,\forall x_j}} \prod_{j\in\mathcal{K}} \prod_{x_j\in\Phi_j\setminus x_i} e^{-t\frac{P_j}{S_j}\|x_j\|^{-\alpha} G^{\mathrm{ZF}}_{x_j,l_i}} && (2.8)\\
&= \prod_{j\in\mathcal{K}} \mathbb{E}_{\Phi_j} \prod_{x_j\in\Phi_j\setminus x_i} \mathbb{E}_{G^{\mathrm{ZF}}_{x_j,l_i}} e^{-t\frac{P_j}{S_j}\|x_j\|^{-\alpha} G^{\mathrm{svd}}_{x_j,l_i}} && (2.9)\\
&= e^{-t^{\check{\alpha}}\tilde{C}(\alpha)\sum\limits_j \lambda_j (\frac{P_j}{S_j})^{\check{\alpha}}\mathbb{E}[(G^{\mathrm{ZF}}_{x_j,l_i})^{\check{\alpha}}]}, && (2.10)
\end{aligned}$$

where $\tilde{C}(\alpha) = \pi\Gamma(1-\check{\alpha})$ and $\Gamma(a) = \int\limits_0^\infty t^{a-1}e^{-t}dt$ is the standard Gamma function. The last step is because of [104, Eq. 8] (see also Example A.2.2 in Appendix A). Since $G^{\mathrm{ZF}}_{x_j,l_i}$ is chi-squared with DoF $2S_j$, then $\mathbb{E}(G^{\mathrm{ZF}}_{x_j,l_i})^{\check{\alpha}} = \frac{\Gamma(\check{\alpha}+S_j)}{\Gamma(S_j)}$. Using this, (2.10) is finally reduced to

$$\mathcal{L}_{I^{l_i}}(t) = e^{-t^{\check{\alpha}}\Lambda(\boldsymbol{S})}, \tag{2.11}$$

where letting $\boldsymbol{S} = (S_1, S_2, \ldots, S_K)$, we have

$$\Lambda(\boldsymbol{S}) \triangleq \tilde{C}(\alpha)\sum_{j\in\mathcal{K}} \lambda_j \left(\frac{P_j}{S_j}\right)^{\check{\alpha}} \frac{\Gamma(\check{\alpha}+S_j)}{\Gamma(S_j)}. \tag{2.12}$$

Remark 2.2.6. *Under the max-SINR CA rule interfering BSs can be closer to the typical UE*

than the serving BS [47, 56]. This, in turn, implies that in comparison to the range expansion CA, here for the evaluation of $\mathcal{L}_{I^{l_i}}(t)$ *in* (2.10) *the inclusion of an exclusion zone around the typical UE is unnecessary. We are actually in favor of this characteristic of max-SINR CA rule, as it permits formulating the Laplace transform of ICI in* (2.11) *in a form suitable for analytical purposes—observing that* $\mathcal{L}_{I^{l_i}}(t)$ *is explicitly formulated through variable* t *has favorable analytical consequences. In comparison, under the closest-BS CA rule, the Laplace transform of ICI can at best be formulated in an integral formula, impossible to explicitly formulate it as a function of variable* t*. This leads to complications in deriving the coverage probability in analytically favorable expressions.*

2.3 Analyzing the Coverage Performance

Our main goal in this chapter is to provide computationally affordable expressions for the coverage probability. Let us first state these two following Lemmas, which are broadly exploited in the analysis of this chapter and the consequent chapters.

Lemma 2.3.1. *For a r.v.* H *distributed according to* χ^2_{2M} *with CCDF* $\overline{F}_H(z) = e^{-z}\sum_{m=0}^{M-1}\frac{z^m}{m!}$*, the inverse Laplace transform of* $\overline{F}_H(z)$ *is* $\mathcal{L}^{-1}_{\overline{F}_H(z)}(t) = \sum_{m=0}^{M-1}\frac{1}{m!}\delta^{(m)}(t-1)$*, where* $\delta^{(m)}(t)$ *is the* m*th derivative of the Dirac delta function. Furthermore, there holds*

$$\int_0^\infty \frac{\mathcal{L}^{-1}_{\overline{F}_H(z)}(t)}{t^{\check{\alpha}}}\mathrm{d}t = \sum_{m=0}^{M-1}\frac{\Gamma(\check{\alpha}+m)}{\Gamma(\check{\alpha})\Gamma(m+1)}. \tag{2.13}$$

Proof. See Appendix B.1. □

Lemma 2.3.2. *Consider a shot noise process,* $I = \sum_{j\in\mathcal{K}} I_j$*, where* $I_j = \sum_{x_j\in\Phi_j} P_j\|x_j\|^{-\alpha}H_{x_j}$*, and* H_{x_j}*s are i.i.d. random variables distributed according to* $\chi^2_{2S_j}$*. Assume* H *is distributed according to* χ^2_{2S} *and is independent of* H_{x_j}*s. Then, for a given real parameter* $\Delta \geq 0$ *there*

holds

$$\mathbb{P}\left\{H \geq \Delta I\right\} = \int_0^\infty \mathcal{L}^{-1}_{\overline{F}_H(z)}(t) e^{-t^{\check{\alpha}} \Delta^{\check{\alpha}} \Lambda(\boldsymbol{S})} \mathrm{d}t, \tag{2.14}$$

where $\mathcal{L}^{-1}_{\overline{F}_H(z)}(t)$ *is the inverse Laplace transform of the CCDF of r.v.* H *as given in Lemma 2.3.1.*

Proof. See Appendix B.2. □

We now use the above lemmas to drive the coverage probability c^{ZF} in the following proposition.

Proposition 2.3.1. *The coverage probability of a multi-stream MIMO-ZFBF multiplexing HetNet is*

$$c^{\mathrm{ZF}} = \sum_{i \in \mathcal{K}} 2\pi\lambda_i \int_0^\infty r_i \sum_{m_i^1=0}^{N^r - S_i} \cdots \sum_{m_i^{S_i}=0}^{N^r - S_i} \frac{(-1)^{m_i^1 + \ldots + m_i^{S_i}}}{m_i^1! \ldots m_i^{S_i}!}$$

$$\times \int_0^\infty \frac{\partial^{m_i^1} \ldots \partial^{m_i^{S_i}} \Xi^{\mathrm{ZF}}(r_i, t_1, \ldots, t_{S_i})}{\partial {t_1}^{m_i^1} \ldots \partial {t_{S_i}}^{m_i^{S_i}}}\Big|_{t_{l_i}=1, \forall l_i} r_i \mathrm{d}r_i, \tag{2.15}$$

where

$$\Xi^{\mathrm{ZF}}(r_i, t_1, \ldots, t_{S_i}) = e^{-r_i^2 \frac{\tilde{C}(\alpha)}{S_i} \left(\frac{S_i \beta_i}{P_i}\right)^{\check{\alpha}} \sum_{j=1}^{K} \lambda_j \left(\frac{P_j}{S_j}\right)^{\check{\alpha}} \mathbb{E}_{\{G^{\mathrm{ZF}}_{j,l_i}\}_{l_i}} \left[\left(\sum_{l_i=1}^{S_i} G^{\mathrm{ZF}}_{j,l_i} t_{l_i}\right)^{\check{\alpha}}\right] - \beta_i \frac{S_i}{P_i} r_i^{\alpha} \sigma_i^2 \sum_{l_i=1}^{S_i} t_{l_i}}. \tag{2.16}$$

Proof. The coverage probability is defined in (2.2.2). Let denote $r_i = \|x_i\|$. According to [47, Lemma 1], and assuming $\beta_i \geq 1$, $\forall i$ the coverage probability is obtained as

$$\begin{aligned}
c^{\mathrm{ZF}} &= \mathbb{P}\left\{ \max_{\bigcup_{i \in \mathcal{K}} x_i \in \Phi_i} \min_{l_i = 1, \ldots, S_i} \mathrm{SINR}^{\mathrm{ZF}}_{x_i, l_i} \geq \beta_i \right\} && (2.17)\\
&= \sum_{i \in \mathcal{K}} \mathbb{E} \sum_{x_i \in \Phi_i} 1\left(\min_{l_i = 1, \ldots, S_i} \mathrm{SINR}^{\mathrm{ZF}}_{x_i, l_i} \geq \beta_i \right) && (2.18)\\
&\overset{(a)}{=} \sum_{i \in \mathcal{K}} 2\pi\lambda_i \int_0^\infty r_i \mathbb{P}\left\{ \min_{l_i = 1, \ldots, S_i} \mathrm{SINR}^{\mathrm{ZF}}_{x_i, l_i} \geq \beta_i \right\} \mathrm{d}r_i && (2.19)
\end{aligned}$$

$$\overset{(b)}{=} \sum_{i\in\mathcal{K}} 2\pi\lambda_i \int_0^\infty r_i \mathbb{E}_\Phi \prod_{l_i=1}^{S_i} \mathbb{P}\left\{\mathrm{SINR}_{x_i,l_i}^{\mathrm{ZF}} \geq \beta_i \middle| \Phi\right\} \mathrm{d}r_i, \tag{2.20}$$

where Step (a) is due to Slivnyak's Theorem and Campbell's Theorem, and Step (b) is because conditioned on process Φ, the SINR expressions across streams are statistically independent. Now we use Lemma 2.3.2 to express probability $\mathbb{P}\left\{\mathrm{SINR}_{r_i,l_i}^{\mathrm{ZF}} \geq \beta_i \middle| \Phi\right\}$ through the inverse Laplace transform of the CCDF of the intended fading gain of stream l_i (see Lemma 2.3.1). Doing so, for a given r_i we then write

$$\begin{aligned}
&\mathbb{P}\left\{\mathrm{SINR}_{r_i,l_i}^{\mathrm{ZF}} \geq \beta_i \middle| \Phi\right\} \\
&\quad = \mathbb{P}\left\{ H_{r_i,l_i}^{\mathrm{ZF}} \geq \beta_i \frac{S_i}{P_i} r_i^\alpha \sigma_i^2 + \beta_i \frac{S_i}{P_i} r_i^\alpha \sum_{j\in\mathcal{K}} \sum_{x_j\in\Phi_j\setminus x_i} \frac{P_j}{S_j} \|x_j\|^{-\alpha} G_{x_j,l_i}^{\mathrm{ZF}} \middle| \Phi \right\} && (2.21) \\
&\quad \overset{(a)}{=} \int_0^\infty \mathcal{L}_{\overline{F}_{H_i^{\mathrm{ZF}}}}^{-1}(t_i) e^{-t_i\beta_i \frac{S_i}{P_i} r_i^\alpha \sigma_i^2} \mathbb{E}_{\{G_{x_j,l_i}^{\mathrm{ZF}}\}} e^{-t_i\beta_i \frac{S_i}{P_i} r_i^\alpha \sum_{j\in\mathcal{K}} \sum_{x_j\in\Phi_j\setminus x_i} \frac{P_j}{S_j}\|x_j\|^{-\alpha} G_{x_j,l_i}^{\mathrm{ZF}}} \mathrm{d}t_i && (2.22) \\
&\quad \overset{(b)}{=} \int_0^\infty \mathcal{L}_{\overline{F}_{H_i^{\mathrm{ZF}}}}^{-1}(t_i) e^{-t_i\beta_i \frac{S_i}{P_i} r_i^\alpha \sigma_i^2} \prod_{j\in\mathcal{K}} \prod_{x_j\in\Phi_j\setminus x_i} \mathbb{E}_{G_{x_j,l_i}^{\mathrm{ZF}}} e^{-t_i\beta_i \frac{S_i}{P_i} r_i^\alpha \frac{P_j}{S_j}\|x_j\|^{-\alpha} G_{x_j,l_i}^{\mathrm{ZF}}} \mathrm{d}t_i, && (2.23)
\end{aligned}$$

where Step (a) is due to Lemma 2.3.2. As r.v. H_i^{ZF} is distributed according to $\chi^2_{2(N^r-S_i+1)}$ with CCDF $\overline{F}_{H_i^{\mathrm{ZF}}}(z) = e^{-z} \sum_{m_i=0}^{N^r-S_i} \frac{z^{m_i}}{m_i!}$, based on Lemma 2.3.1 the inverse Laplace transform of CCDF $\overline{F}_{H_i^{\mathrm{ZF}}}(z)$ is $\mathcal{L}_{\overline{F}_{H_i^{\mathrm{ZF}}}}^{-1}(t_i) = \sum_{m_i=0}^{N^r-S_i} \frac{1}{m_i!}\delta^{(m_i)}(t-1)$ where $\delta^{(m_i)}(t)$ is the m_i-th derivative of the Dirac's Delta function. In Step (b) we use the independency among the interfering links H_{x_j} $\forall x_j, j$. Now, substitute (2.23) into (2.20) and apply some straightforward manipulations, to obtain

$$\begin{aligned}
c^{\mathrm{ZF}} = \sum_{i\in\mathcal{K}} 2\pi\lambda_i \int_0^\infty r_i \mathbb{E}_\Phi \prod_{l_i=1}^{S_i} \int_0^\infty \mathcal{L}_{\overline{F}_{H_i^{\mathrm{ZF}}}}^{-1}(t_i) e^{-t_i\beta_i \frac{S_i}{P_i} r_i^\alpha \sigma_i^2} \\
\times \prod_{j\in\mathcal{K}} \prod_{x_j\in\Phi_j\setminus x_i} \mathbb{E}_{G_{x_j,l_i}^{\mathrm{ZF}}} e^{-t_i\beta_i \frac{S_i}{P_i} r_i^\alpha \frac{P_j}{S_j}\|x_j\|^{-\alpha} G_{x_j,l_i}^{\mathrm{ZF}}} \mathrm{d}t_i \mathrm{d}r_i. \qquad (2.24)
\end{aligned}$$

(2.24) is then expressible as

$$c^{\mathrm{ZF}} = \sum_{i\in\mathcal{K}} 2\pi\lambda_i \int_0^\infty r_i \mathrm{d}r_i \mathbb{E}_\Phi \int_0^\infty \ldots \int_0^\infty e^{-\beta_i \frac{S_i}{P_i} r_i^\alpha \sigma_i^2 \sum_{l_i=1}^{S_i} t_{l_i}} \prod_{l_i=1}^{S_i} \mathcal{L}^{-1}_{\overline{F}_{H_i^{\mathrm{ZF}}}}(t_{l_i})\mathrm{d}t_{l_i} \tag{2.25}$$

$$\times \left(\prod_{j\in\mathcal{K}} \prod_{x_j\in\Phi_j\setminus x_i} \prod_{l_i=1}^{S_i} \mathbb{E}_{G^{\mathrm{ZF}}_{x_j,l_i}} e^{-\beta_i \frac{S_i}{P_i} r_i^\alpha \frac{P_j}{S_j} \|x_j\|^{-\alpha} G^{\mathrm{ZF}}_{x_j,l_i} t_{l_i}} \right)$$

$$\overset{(a)}{=} \sum_{i\in\mathcal{K}} 2\pi\lambda_i \int_0^\infty r_i \mathrm{d}r_i \mathbb{E}_\Phi \int_0^\infty \ldots \int_0^\infty e^{-\beta_i \frac{S_i}{P_i} r_i^\alpha \sigma_i^2 \sum_{l_i=1}^{S_i} t_{l_i}} \prod_{l_i=1}^{S_i} \mathcal{L}^{-1}_{\overline{F}_{H_i^{\mathrm{ZF}}}}(t_{l_i})\mathrm{d}t_{l_i} \tag{2.26}$$

$$\times \left(\prod_{j\in\mathcal{K}} \prod_{x_j\in\Phi_j\setminus x_i} \mathbb{E}_{G^{\mathrm{ZF}}_{x_j}} \prod_{l_i=1}^{S_i} e^{-\beta_i \frac{S_i}{P_i} r_i^\alpha \frac{P_j}{S_j} \|x_j\|^{-\alpha} G^{\mathrm{ZF}}_{x_j,l_i} t_{l_i}} \right),$$

where Step (a) is because $G^{\mathrm{ZF}}_{x_j,l_i}$s are i.i.d. across streams l_i. Now, due to the independency of PPP sets Φ_js, c^{ZF} is further reduced to

$$c^{\mathrm{ZF}} = \sum_{i\in\mathcal{K}} 2\pi\lambda_i \int_0^\infty r_i \mathrm{d}r_i \int_0^\infty \ldots \int_0^\infty e^{-\beta_i \frac{S_i}{P_i} r_i^\alpha \sigma_i^2 \sum_{l_i=1}^{S_i} t_{l_i}} \prod_{l_i=1}^{S_i} \mathcal{L}^{-1}_{\overline{F}_{H_i^{\mathrm{ZF}}}}(t_{l_i})\mathrm{d}t_{l_i} \tag{2.27}$$

$$\times \left(\prod_{j\in\mathcal{K}} \mathbb{E}_{\Phi_j} \prod_{x_j\in\Phi_j\setminus x_i} \mathbb{E}_{G^{\mathrm{ZF}}_{x_j}} e^{-\beta_i \frac{S_i}{P_i} r_i^\alpha \frac{P_j}{S_j} \|x_j\|^{-\alpha} \sum_{l_i=1}^{S_i} G^{\mathrm{ZF}}_{x_j,l_i} t_{l_i}} \right)$$

$$\overset{(a)}{=} \sum_{i\in\mathcal{K}} 2\pi\lambda_i \int_0^\infty r_i \mathrm{d}r_i \int_0^\infty \ldots \int_0^\infty e^{-r_i^2 \tilde{C}(\alpha) \left(\frac{S_i\beta_i}{P_i}\right)^{\check{\alpha}} \sum_{j=1}^{K} \lambda_j \left(\frac{P_j}{S_j}\right)^{\check{\alpha}} \mathbb{E}_{G_j^{\mathrm{ZF}}} \left[\left(\sum_{l_i=1}^{S_i} G^{\mathrm{ZF}}_{j,l_i} t_{l_i} \right)^{\check{\alpha}} \right]} \tag{2.28}$$

$$\times \prod_{l_i=1}^{S_i} \mathcal{L}^{-1}_{\overline{F}_{H_i^{\mathrm{ZF}}}}(t_{l_i}) e^{-\beta_i \frac{S_i}{P_i} r_i^\alpha \sigma_i^2 t_{l_i}} \mathrm{d}t_{l_i},$$

$$= \sum_{i\in\mathcal{K}} 2\pi\lambda_i \int_0^\infty r_i \mathrm{d}r_i \int_0^\infty \ldots \int_0^\infty \tag{2.29}$$

$$\times \prod_{l_i=1}^{S_i} e^{-r_i^2 \frac{\tilde{C}(\alpha)}{S_i} \left(\frac{S_i\beta_i}{P_i}\right)^{\check{\alpha}} \sum_{j=1}^{K} \lambda_j \left(\frac{P_j}{S_j}\right)^{\check{\alpha}} \mathbb{E}_{G_j^{\mathrm{ZF}}} \left[\left(\sum_{l_i=1}^{S_i} G^{\mathrm{ZF}}_{j,l_i} t_{l_i} \right)^{\check{\alpha}} \right]} \mathcal{L}^{-1}_{\overline{F}_{H_i^{\mathrm{ZF}}}}(t_{l_i}) e^{-\beta_i \frac{S_i}{P_i} r_i^\alpha \sigma_i^2 t_{l_i}} \mathrm{d}t_{l_i},$$

where Step (a) is due to PGL (see (A.4)) of shot noise process (see (A.2.2)). Now, recalling that $\mathcal{L}^{-1}_{\overline{F}_{H_i^{\mathrm{ZF}}}}(t_i) = \sum_{m_i=0}^{N^r-S_i} \frac{1}{m_i!} \delta^{(m_i)}(t-1)$, along with applying B.3, the desired result follows.

□

Remark 2.3.1 (Other Notions of Coverage in MIMO Multiplexing Systems). *As discussed in Chapter 1 besides all-coverage probability one can also consider any-coverage and sum-coverage too. The former is defined as*

$$c_{\text{any}}^{\text{ZF}} = \mathbb{P}\left\{ \max_{\bigcup_{i\in\mathcal{K}} x_i\in\Phi_i} \max_{l_i=1,\ldots,S_i} \text{SINR}_{x_i,l_i}^{\text{ZF}} \geq \beta_i \right\}, \tag{2.30}$$

which implies that to announce coverage it is enough to have the best data stream to be received successfully. Under the latter, the coverage is defined as

$$c_{\text{sum}}^{\text{ZF}} = \mathbb{P}\left\{ \max_{\bigcup_{i\in\mathcal{K}} x_i\in\Phi_i} \sum_{l_i=1,\ldots,S_i} \text{SINR}_{x_i,l_i}^{\text{ZF}} \geq \beta_i \right\}. \tag{2.31}$$

For the case of any-coverage taking some primarily steps we can express the any-coverage probability as a function of all-coverage probability as follows:

$$\begin{aligned} c_{\text{any}}^{\text{ZF}} &= 1 - \mathbb{P}\left\{ \max_{l=1_i,\ldots,S_i} \text{SIR}_{x_i,l_i}^{\text{ZF}} < \beta_i \right\} && (2.32)\\ &= \sum_{i\in\mathcal{K}} 2\pi\lambda_i \int_0^\infty r_i \mathbb{E}_\Phi \left(1 - \mathbb{P}\left\{\text{SIR}_{x_i}^{\text{ZF}} \geq \beta_i \middle| \Phi\right\}\right) \mathrm{d}r_i && (2.33)\\ &= \sum_{i\in\mathcal{K}} 2\pi\lambda_i \sum_{l_i=1}^{S_i} \binom{S_i}{l_i} (-1)^{l_i+1} \int_0^\infty r_i \mathbb{E}_\Phi \prod_{l_i'=1}^{l_i} \mathbb{P}\left\{\text{SIR}_{x_i,l_i'}^{\text{ZF}} \geq \beta_i \middle| \Phi\right\} \mathrm{d}r_i. && (2.34) \end{aligned}$$

The inner integral is then represented in the form similar the integral encountered in (2.20)*. What is remained is to take the same steps provided in thr proof of Proposition 2.3.1 to derive any-coverage probability.*

Nevertheless, the case of sum-coverage is more involved and exact evaluation needs separate analysis. A simple approximation however can be introduced based on the any-coverage

and all-coverage probabilities:

$$c_{\text{sum}}^{\text{ZF}} \approx 0.5c_{\text{any}}^{\text{ZF}} + 0.5c_{\text{all}}^{\text{ZF}}. \tag{2.35}$$

To achieve this approximation one can note that for m identical but dependent r.v.s $Z_1, Z_2, \dots Z_M$ *we have* $M \min_m Z_m \leq \sum_m Z_m \leq M \max_m Z_m$. *Therefore,* $\mathbb{P}\{\min Z_m > R/M\} \leq \mathbb{P}\{\sum_m Z_m > R\} \leq \mathbb{P}\{\max Z_m > R/M\}$. *Using this we then approximate* $\mathbb{P}\{\sum_m Z_m > R\}$ *through the mean of the upper-bound and lower bound. Note that* (2.35) *is heuristic, one is on the other hand able to approximate sum-coverage probability by Gaussian distribution after deriving the first and second moments of r.v.* $\sum_{l_i=1,\dots,S_i} \text{SINR}_{x_i,l_i}^{\text{ZF}}$.

Remark 2.3.2 (Analytical Significance of Assumption $\beta_i \geq 1$ $\forall i$). *In the proof of Proposition 1 (see second step in* (2.20)*) we exploit the assumption* $\beta_i \geq 1$ $\forall i$ *to convert the probability of event*

$$\left\{ \max_{\bigcup_{i\in\mathcal{K}} x_i\in\Phi_i} \min_{l_i=1,\dots,S_i} \text{SINR}_{x_i,l_i}^{\text{ZF}} \geq \beta_i \right\}$$

into its equivalent form

$$\mathbb{E} \sum_{i\in\mathcal{K}} \sum_{x_i\in\Phi_i} 1\left(\min_{l_i=1,\dots,S_i} \text{SINR}_{x_i,l_i}^{\text{ZF}} \geq \beta_i \right).$$

We here remark on the legitimacy of this step with more details.

Let us fist consider the counterpart SISO system with exponential power fading gain and max-SINR CA rule. Under the assumption $\beta_i \geq 1$ $\forall i$, *it is proved in [47, Lemma 1] that for this SISO system the coverage probability is accurately equivalent to the probability of whether or not there is a BS that can support the typical UE with the required SIR threshold. However, for the case of* $\beta_i < 1$ *this statement partially tumbles, as there are now possibilities that more than one BS can tentatively support the typical UE, which is also referred to by the k-coverage in [106, 107]. Yet, via simulations the authors in [47] observe that for SIR thresholds as small as -6 dB the derived coverage probability under the assumption* $\beta_i \geq 1$ $\forall i$

still stays accurate.

On the other hand, for this SISO system when the assumption $\beta_i \geq 1$ is applicable but the fading distribution on the attending link is changed to a Nakagami-type, which is actually covered by the SINR formula in (2.3) *too, it is argued in [56, Section IV-B] that there is a slight chance that more than one BS can support the typical UE. For such scenario, if the average power of the fading of the attending channel is much higher than that of the fading of the interfering channel, we expect that the likelihood of having more than 1 BS supporting the typical UE grows. Therefore, the coverage probability can be larger than one.*

Now consider our model. Let us denote $X = \sum_i \sum_{x_i \in \Phi_i} 1(\min_{l_i=1,\dots,S_i} \mathrm{SIR}^{\mathrm{ZF}}_{x_i,l_i})$ as the number of BSs that can support the typical UE, which is lower-bounded by a Poisson r.v. with mean value $\mu = \mathbb{E}[X] = c^{\mathrm{ZF}}$. This implies that $\mathbb{P}\{X > 1\} \leq 1 - \mu e^{-\mu} - e^{-\mu}$, which the right-hand-side is a monotonically increasing function of μ. Simulation result in Fig. 2.2 indicates that for $\mu \in [0, 1]$ (note that μ is equivalent to the coverage probability, therefore we are technically interested in applicable range $\mu \in [0, 1]$) almost surely we have $\mathbb{P}\{X > 1\} < 0.3$. This implies that it is generally safe to assume that the second step in (2.20) *is legitimate. We explore the impact of SINR thresholds on the coverage probability with more details in Section 2.7 via simulations.*

As seen, Proposition 2.3.1 has a substantial analytical intractability, which in turn leads to undesirable high computational complexity. In particular, apart from improper integration, the complexity has mainly rooted in the nested higher-order differentiations of the function $\Xi^{\mathrm{ZF}}(r_i, t_1, \dots, t_{S_i})$, which is not expressed explicitly in term of variables $t_1, \dots, t_{S_i}$. Therefore, in the rest of this section we set our goal to scale down on the computational complexity of Proposition 2.3.1, hopefully without sabotaging the desirable accuracy.

Proposition 2.3.2 (Upper-Bound). *Define*

$$\phi_n^m \triangleq \sum_{n'=1}^{n} (-1)^{n'} \binom{n}{n'} \prod_{u=0}^{m-1} (\breve{\alpha} n' - u). \tag{2.36}$$

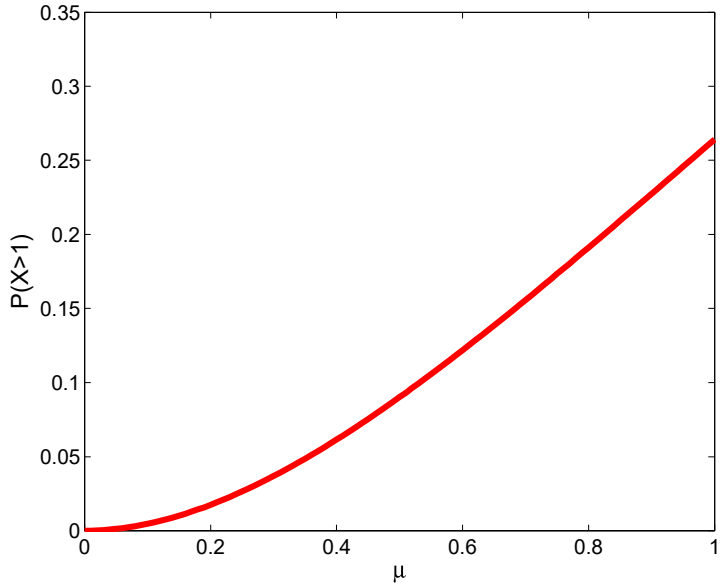

Figure 2.2: $\mathbb{P}\{X > 1\}$.

The coverage probability of MIMO-ZFBF is then upper-bounded by

$$c^{\mathrm{ZF}} \leq \sum_{i\in\mathcal{K}} 2\pi\lambda_i \int_0^{\infty} e^{-\beta_i \frac{S_i^2}{P_i} r_i^{\alpha}\sigma_i^2} e^{-r_i^2\left(\frac{S_i^2\beta_i}{P_i}\right)^{\breve{\alpha}}\Lambda(\boldsymbol{S})} \left(1 + \sum_{m_i=1}^{N^r-S_i}\sum_{m_i'=0}^{m_i} \frac{(-1)^{m_i'}\binom{m_i}{m_i'}}{m_i!}\left(\beta_i\frac{S_i}{P_i}r_i^{\alpha}\sigma_i^2\right)^{m_i-m_i'}\right.$$

$$\left.\times\left[1 + \sum_{n=1}^{m_i'} \frac{\phi_n^{m_i'}}{n!}\left(\frac{S_i^2\beta_i}{P_i}\right)^{n\breve{\alpha}} \frac{\Lambda(\boldsymbol{S})^n}{S_i^n} r_i^{2n}\right]\right)^{S_i} r_i \mathrm{d}r_i. \tag{2.37}$$

Proof. To tackle the computational complexity of (2.15), we start by working on expression $\mathbb{E}_{\{G_{j,l_i}^{\mathrm{ZF}}\}_{l_i}}\left[(\sum_{l_i=1}^{S_i} G_{j,l_i}^{\mathrm{ZF}} t_{l_i})^{\breve{\alpha}}\right]$ in function $\Xi^{\mathrm{ZF}}(r_i, t_1, \ldots, t_{S_i})$ (2.16). To that end, we attempt to lower-bound it by noting that the function $g(v) = v^{\breve{\alpha}}$, $v \geq 0$, is concave, and thereafter applying Jensen's inequality [165] yields

$$\mathbb{E}_{\{G_{j,l_i}^{\mathrm{ZF}}\}_{l_i}}\left[\left(\sum_{l_i=1}^{S_i} G_{j,l_i}^{\mathrm{ZF}} t_{l_i}\right)^{\breve{\alpha}}\right] = S_i^{\breve{\alpha}}\mathbb{E}_{\{G_{j,l_i}^{\mathrm{ZF}}\}_{l_i}}\left[\left(\frac{1}{S_i}\sum_{l_i=1}^{S_i} G_{j,l_i}^{\mathrm{ZF}} t_{l_i}\right)^{\breve{\alpha}}\right] \tag{2.38}$$

$$\geq S_i^{\check{\alpha}} \mathbb{E}_{\{G_{j,l_i}^{\mathrm{ZF}}\}_{l_i}} \left[\frac{1}{S_i} \sum_{l_i=1}^{S_i} (G_{j,l_i}^{\mathrm{ZF}} t_{l_i})^{\check{\alpha}} \right] \tag{2.39}$$

$$= S_i^{\check{\alpha}-1} \sum_{l_i=1}^{S_i} \mathbb{E}_{G_j^{\mathrm{ZF}}} \left[(G_{j,l_i}^{\mathrm{ZF}})^{\check{\alpha}} \right] t_{l_i}^{\check{\alpha}} \tag{2.40}$$

$$= S_i^{\check{\alpha}-1} \frac{\Gamma(S_j + \check{\alpha})}{\Gamma(S_j)} \sum_{l_i=1}^{S_i} t_{l_i}^{\check{\alpha}}, \tag{2.41}$$

where the last step is because G_j^{ZF} is chi-squared with $2S_j$ DoF. We now substitute (2.41) into (2.30), and use the introduced parameter $\Lambda(\boldsymbol{S})$ in (2.12) to reach the following upper-bound on the coverage probability

$$c^{\mathrm{ZF}} \leq \sum_{i \in \mathcal{K}} 2\pi\lambda_i \int_0^\infty r_i \mathrm{d}r_i \int_0^\infty \cdots \int_0^\infty e^{-\beta_i \frac{S_i}{P_i} r_i^\alpha \sigma_i^2 \sum_{l_i=1}^{S_i} t_{l_i}} \times \prod_{l_i=1}^{S_i} \mathcal{L}^{-1}_{\overline{F}_{H_i^{\mathrm{ZF}}}}(t_{l_i}) \mathrm{d}t_{l_i} e^{-r_i^2 \left(\frac{S_i^2 \beta_i}{P_i} \right)^{\check{\alpha}} \frac{\Lambda(\boldsymbol{S})}{S_i} \sum_{l_i=1}^{S_i} t_{l_i}^{\check{\alpha}}} \tag{2.42}$$

$$= \sum_{i \in \mathcal{K}} 2\pi\lambda_i \int_0^\infty r_i \mathrm{d}r_i \int_0^\infty \cdots \int_0^\infty \prod_{l_i=1}^{S_i} \left(e^{-r_i^2 \left(\frac{S_i^2 \beta_i}{P_i} \right)^{\check{\alpha}} \frac{\Lambda(\boldsymbol{S})}{S_i} t_{l_i}^{\check{\alpha}}} e^{-\beta_i \frac{S_i}{P_i} r_i^\alpha \sigma_i^2 t_{l_i}} \mathcal{L}^{-1}_{\overline{F}_{H_i^{\mathrm{ZF}}}}(t_{l_i}) \mathrm{d}t_{l_i} \right) \tag{2.43}$$

$$= \sum_{i \in \mathcal{K}} 2\pi\lambda_i \int_0^\infty r_i \mathrm{d}r_i \prod_{l_i=1}^{S_i} \left(\int_0^\infty e^{-\beta_i \frac{S_i}{P_i} r_i^\alpha \sigma_i^2 t_i} \mathcal{L}^{-1}_{\overline{F}_{H_i^{\mathrm{ZF}}}}(t_i) e^{-r_i^2 \left(\frac{S_i^2 \beta_i}{P_i} \right)^{\check{\alpha}} \frac{\Lambda(\boldsymbol{S})}{S_i} t_i^{\check{\alpha}}} \mathrm{d}t_i \right) \tag{2.44}$$

$$= \sum_{i \in \mathcal{K}} 2\pi\lambda_i \int_0^\infty r_i \mathrm{d}r_i \left(\int_0^\infty e^{-\beta_i \frac{S_i}{P_i} r_i^\alpha \sigma_i^2 t_i} \mathcal{L}^{-1}_{\overline{F}_{H_i^{\mathrm{ZF}}}}(t_i) e^{-r_i^2 \left(\frac{S_i^2 \beta_i}{P_i} \right)^{\check{\alpha}} \frac{\Lambda(\boldsymbol{S})}{S_i} t_i^{\check{\alpha}}} \mathrm{d}t_i \right)^{S_i}, \tag{2.45}$$

where the last two steps are due to the fact that r.v.s $\{H_{l_i}^{\mathrm{ZF}}\}_{l_i}$ are i.i.d.. Now, putting the expression for the inverse of CCDF $\overline{F}_{H_i^{\mathrm{ZF}}}$ from (B.1) along with the identity (B.2), we derive a closed-form expression for the inner integral in (2.45) as the following:

$$\int_0^\infty e^{-\beta_i \frac{S_i}{P_i} r_i^\alpha \sigma_i^2 t_i} \mathcal{L}^{-1}_{\overline{F}_{H_i^{\mathrm{ZF}}}}(t_i) e^{-r_i^2 \left(\frac{S_i^2 \beta_i}{P_i} \right)^{\check{\alpha}} \frac{\Lambda(\boldsymbol{S})}{S_i} t_i^{\check{\alpha}}} \mathrm{d}t_i$$

$$= \sum_{m_i=0}^{N^r - S_i} \frac{1}{m_i!} \int_0^\infty e^{-\beta_i \frac{S_i}{P_i} r_i^\alpha \sigma_i^2 t_i} e^{-r_i^2 \left(\frac{S_i^2 \beta_i}{P_i} \right)^{\check{\alpha}} \frac{\Lambda(\boldsymbol{S})}{S_i} t_i^{\check{\alpha}}} \delta^{(m_i)}(t_i - 1) \mathrm{d}t_i \tag{2.46}$$

$$= \sum_{m_i=0}^{N^r-S_i} \frac{(-1)^{m_i}}{m_i!} \frac{d^{m_i}}{dt_i^{m_i}} e^{-\beta_i \frac{S_i}{P_i} r_i^{\alpha} \sigma_i^2 t_i} e^{-r_i^2 \left(\frac{S_i^2 \beta_i}{P_i}\right)^{\breve{\alpha}} \frac{\Lambda(\boldsymbol{S})}{S_i} t_i^{\breve{\alpha}}} \Big|_{t_i=1} \tag{2.47}$$

$$= e^{-\beta_i \frac{S_i}{P_i} r_i^{\alpha} \sigma_i^2} e^{-r_i^2 \left(\frac{S_i^2 \beta_i}{P_i}\right)^{\breve{\alpha}} \frac{\Lambda(\boldsymbol{S})}{S_i}} + \sum_{m_i=1}^{N^r-S_i} \frac{(-1)^{m_i}}{m_i!} \sum_{m_i'=0}^{m_i} \binom{m_i}{m_i'}$$

$$\times \frac{d^{m_i-m_i'}}{dt_i^{m_i-m_i'}} e^{-\beta_i \frac{S_i}{P_i} r_i^{\alpha} \sigma_i^2 t_i} \Big|_{t_i=1} \frac{d^{m_i'}}{dt_i^{m_i'}} e^{-r_i^2 \left(\frac{S_i^2 \beta_i}{P_i}\right)^{\breve{\alpha}} \frac{\Lambda(\boldsymbol{S})}{S_i} t_i^{\breve{\alpha}}} \Big|_{t_i=1}, \tag{2.48}$$

where the last step is because of the Leibnitz's formula. By borrowing [166, Eq. (15)] and applying some manipulations we then have the following result on the second derivative term in (2.48):

$$\frac{d^{m_i'}}{dt_i^{m_i'}} e^{-r_i^2 \left(\frac{S_i^2 \beta_i}{P_i}\right)^{\breve{\alpha}} \frac{\Lambda(\boldsymbol{S})}{S_i} t_i^{\breve{\alpha}}} \Big|_{t_i=1} = e^{-r_i^2 \left(\frac{S_i^2 \beta_i}{P_i}\right)^{\breve{\alpha}} \frac{\Lambda(\boldsymbol{S})}{S_i}} \sum_{n=1}^{m_i'} \frac{\phi_n^{m_i'}}{n!} \left(r_i^2 \left(\frac{S_i^2 \beta_i}{P_i}\right)^{\breve{\alpha}} \frac{\Lambda(\boldsymbol{S})}{S_i} \right)^n, \quad m_i \geq 1, \tag{2.49}$$

where $\phi_n^{m_i'}$ is given in (2.36). Applying (2.49) into (2.48), we then have

$$(2.48) = e^{-\beta_i \frac{S_i}{P_i} r_i^{\alpha} \sigma_i^2 - r_i^2 \left(\frac{S_i^2 \beta_i}{P_i}\right)^{\breve{\alpha}} \frac{\Lambda(\boldsymbol{S})}{S_i}} \left(1 + \sum_{m_i=1}^{N^r-S_i} \sum_{m_i'=0}^{m_i} \frac{(-1)^{m_i'} \binom{m_i}{m_i'}}{m_i!} \right.$$

$$\left. \left(\beta_i \frac{S_i}{P_i} r_i^{\alpha} \sigma_i^2\right)^{m_i-m_i'} \left(1 + \sum_{n=1}^{m_i'} \frac{\phi_n^{m_i'}}{n!} \left(\left(\frac{S_i^2 \beta_i}{P_i}\right)^{\breve{\alpha}} \frac{r_i^2 \Lambda(\boldsymbol{S})}{S_i} \right)^n \right). \right. \tag{2.50}$$

The final result in then in order by plugging (2.50) into (2.45). □

Importantly, the provided upper-bound on the coverage probability in (2.37) has an acceptable computational burden. In effect, it poses the same level of computational complexity that does the case of SISO system in [47]. On the other hand, this upper-bound captures the impact of many important system parameters, including density of BSs, multiplexing gains, transmission powers, SIR thresholds, and noise power. It is therefore suitable for network-level performance evaluation and also deriving system engineering insights, if one desires.

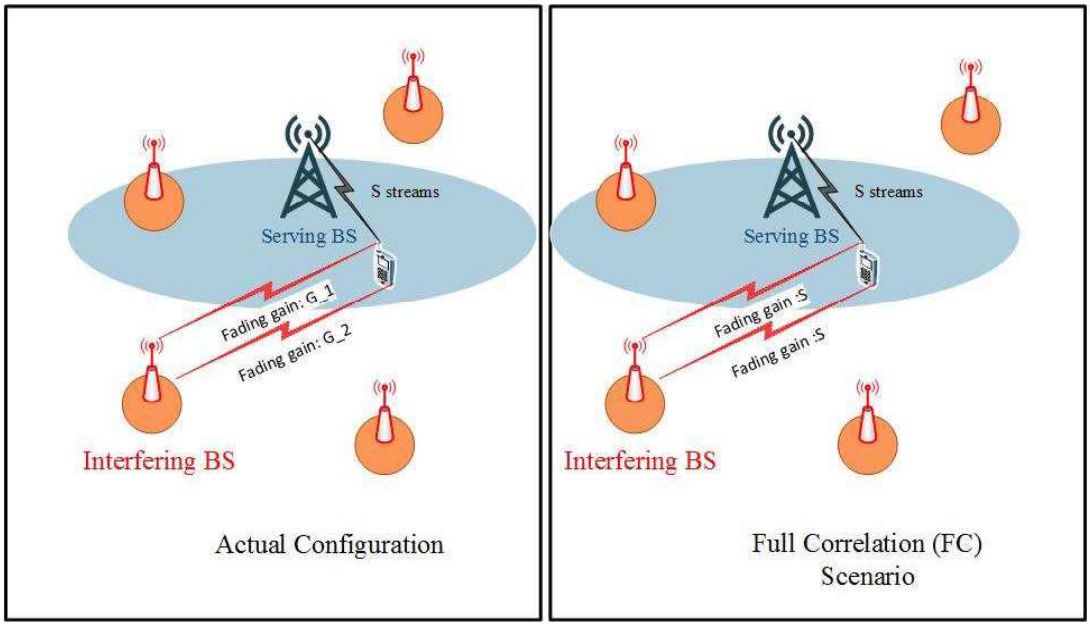

Figure 2.3: Full-correlation (FC) scenario.

2.4 Full-Correlation (FC) Assumption

In the previous section, we derived a numerically feasible upper-bound on the coverage probability. It is still possible to further reduce the numerical complexity, which is persuaded in this section. As a useful byproduct, the conducted analysis leads us shedding some lights on the impact of the cross-stream interference correlation on the coverage performance of the multiplexing system, which happens to be useful in explaining several behaviors of the multiplexing system we are exploring in the rest of this chapter. Note that throughput this thesis we frequently revisit the method developed in this section as an effective method to derive the coverage probability of sophisticated MIMO multiplexing systems, which otherwise is rather impossible to investigate in a numerically affordable approach.

First note that one of the main reasons that the analytical evaluation of the coverage probability in multi-stream systems is challenging is due to the cross-stream interference correlation that is chiefly induced by the common location of interferers. In fact, as seen from Fig. 2.3, path-loss fluctuation $\|x_j\|^{-\alpha}$ caused by the interfering BS x_j is the same

across different data streams of the communication link which is also evident from (2.3). As seen from Fig. 2.3, the location of BSs in both scenarios are the same, the only difference is that under the FC assumption all interfering streams are fully correlated. However, due to independency of fading fluctuations across interfering data streams, the net effect of interfering signals across data streams fluctuates around $\|x_j\|^{-\alpha}$, which causes the SINR values to stay partially correlated among streams. Such a partial cross-stream correlation is generally hard to manage, rendering mathematical intractability as witnessed above. To bypass it, in this section we heuristically assume that the ICI values across data streams are fully correlated:

Definition 2.4.1 (Full-Correlation (FC) Assumption). *Assume the typical UE is associated with BS x_i. Further, let's replace the interfering fading gain $G^{\mathrm{ZF}}_{x_j,l_i}$ with its average value $\mathbb{E}_{G^{\mathrm{ZF}}_{x_j,l_i}} = S_j$. Under FC assumption, ICI is then formulated as*

$$I^{\mathrm{FC}} = \sum_{j\in\mathcal{K}} \sum_{x_j\in\Phi_j/x_i} P_j \|x_j\|^{-\alpha}. \tag{2.51}$$

Moreover, the post-processing SINR on data stream l_i is approximated as

$$\mathrm{SINR}^{\mathrm{ZF-FC}}_{x_i,l_i} = \frac{\frac{P_i}{S_i}\|x_i\|^{-\alpha} H^{\mathrm{ZF}}_{x_i,l_i}}{I^{\mathrm{FC}} + \sigma_i^2}. \tag{2.52}$$

Now, denote $H^{\mathrm{ZF}}_{x_i,\min} \triangleq \min_{l_i=1,\ldots,S_i} H^{\mathrm{ZF}}_{x_i,l_i}$. Under the max-SINR CA rule and FC assumption, the typical UE is then stated to be in coverage if set

$$\mathcal{A}^{\mathrm{ZF-FC}} = \left\{ \exists i \in \mathcal{K} : \max_{x_i\in\Phi_i} \frac{\frac{P_i}{S_i}\|x_i\|^{-\alpha} H^{\mathrm{ZF}}_{x_i,\min}}{I^{\mathrm{FC}} + \sigma_i^2} \geq \beta_i \right\}, \tag{2.53}$$

is not empty, the probability of which is denoted by $c^{\mathrm{ZF-FC}}$. As it is seen, contrary to (2.5), in (2.53) the determining quality of the desired signal is effectively encapsulated into the r.v. $H^{\mathrm{ZF}}_{x_i,\min}$. We use the statistics of $H^{\mathrm{ZF}}_{x_i,\min}$ the following proposition to provide a closed-from expression for the coverage probability.

Proposition 2.4.1 (FC Assumption). *Define*

$$\overline{\sum}_{i,\boldsymbol{k}} \triangleq \sum_{k_0+k_2+\ldots+k_{N^r-S_i}=S_i-1} \binom{S_i-1}{k_0,k_2,\ldots,k_{N^r-S_i}}, \tag{2.54}$$

and

$$\tilde{S}_i(\boldsymbol{k}) \triangleq N^r - S_i + 1 + \sum_{l=0}^{N^r-S_i} l k_l. \tag{2.55}$$

Furthermore, let

$$\Lambda^{\mathrm{FC}} \triangleq \tilde{C}(\alpha) \sum_{j=1}^{K} \lambda_j P_j^{\breve{\alpha}}. \tag{2.56}$$

Thus, the coverage probability under FC assumption is obtained from

$$c^{\mathrm{ZF-FC}} = \sum_{i\in\mathcal{K}} \overline{\sum_{i,\boldsymbol{k}}} \sum_{u=0}^{\tilde{S}_i(\boldsymbol{k})-1} \frac{2\pi\lambda_i(-1)^u S_i^{u+1}\Gamma(\tilde{S}_i(\boldsymbol{k}))}{\Gamma(S_i)u!\prod_{l=0}^{N^r-S_i}(l!)^{k_l}} \left(\varphi_{0i}^0 + \sum_{m_i=1}^{u}\sum_{m_i'=0}^{m_i} \frac{(-1)^{m_i'}}{m_i!}\binom{m_i}{m_i'} \right.$$

$$\left. \times \left(\beta_i \frac{S_i}{P_i}\sigma_i^2\right)^{m_i-m_i'} \varphi_{0i}^{m_i-m_i'} + \sum_{m_i=1}^{u}\sum_{m_i'=0}^{m_i}\sum_{n=1}^{m_i'} \frac{(-1)^{m_i'}\binom{m_i}{m_i'}(\Lambda^{\mathrm{FC}})^n \phi_n^{m_i'}\varphi_{0i}^{m_i-m_i'}}{m_i!n!\left(\frac{S_i\beta_i}{P_i}\right)^{-n\breve{\alpha}}\left(\beta_i\frac{S_i}{P_i}\sigma_i^2\right)^{m_i'-m_i}} \right), \tag{2.57}$$

where

$$\varphi_{ni}^m \triangleq \int_0^\infty r_i^{m\alpha+2n+1} e^{-\beta_i\frac{S_i^2}{P_i}r_i^\alpha\sigma_i^2} e^{-r_i^2\left(\frac{S_i^2\beta_i}{P_i}\right)^{\breve{\alpha}}\Lambda^{\mathrm{FC}}} \mathrm{d}r_i. \tag{2.58}$$

Proof. To prove the proposition, we first note that the PDF of r.v. $H_{i,\min}^{\mathrm{ZF}}$ is represented by

$$f_{H_{i,\min}^{\mathrm{ZF}}}(h) = \frac{d}{dh}\left(\int_h^\infty e^{-g}\frac{g^{N^r-S_i}}{\Gamma(N^r-S_i)}dg\right)^{S_i} \tag{2.59}$$

$$= S_i e^{-h}\frac{h^{N^r-S_i}}{\Gamma(N^r-S_i)}\left(\int_h^\infty e^{-g}\frac{g^{N^r-S_i}}{\Gamma(N^r-S_i)}dg\right)^{S_i-1} \tag{2.60}$$

$$= S_i\left(e^{-h}\sum_{l=0}^{N^r-S_i}\frac{h^l}{l!}\right)^{S_i-1}\frac{h^{N^r-S_i}e^{-h}}{\Gamma(N^r-S_i)} \tag{2.61}$$

$$= \frac{S_i}{\Gamma(N^r - S_i)} e^{-S_i h} \overline{\sum}_{i,\boldsymbol{k}} \frac{h^{\tilde{S}_i(\boldsymbol{k})-1}}{\prod_{l=0}^{N^r-S_i} (l!)^{k_l}}, \tag{2.62}$$

where the last step is due to multi-nominal expansion. The PDF (2.62) admits the CCDF

$$\overline{F}_{H^{\mathrm{ZF}}_{i,\min}}(h) = \overline{\sum}_{i,\boldsymbol{k}} \frac{S_i \Gamma(\tilde{S}_i(\boldsymbol{k})) \sum_{u=0}^{\tilde{S}_i(\boldsymbol{k})-1} \frac{(S_i h)^u}{u!} e^{-S_i h}}{\Gamma(N^r - S_i) \prod_{l=0}^{N^r-S_i} (l!)^{k_l}}. \tag{2.63}$$

The inverse Laplace transform of CCDF $\overline{F}_{H^{\mathrm{ZF}}_{i,\min}}(h)$ is also obtained from

$$\mathcal{L}^{-1}_{\overline{F}_{H^{\mathrm{ZF}}_{i,\min}}}(z) = \overline{\sum}_{i,\boldsymbol{k}} \frac{S_i \Gamma(\tilde{S}_i(\boldsymbol{k})) \sum_{u=0}^{\tilde{S}_i(\boldsymbol{k})-1} \frac{S_i^u}{u!} \delta^{(u)}(z - S_i)}{\Gamma(N^r - S_i) \prod_{l=0}^{N^r-S_i} (l!)^{k_l}}. \tag{2.64}$$

Now, under the same logics put forth in the proof of Proposition 2.3.1, and using Lemma 2.3.2 and the obtained expression $\mathcal{L}^{-1}_{\overline{F}_{H^{\mathrm{ZF}}_{i,\min}}}(z)$ in (2.64), we then evaluate the coverage probability under the FC assumption as the following:

$$c^{\mathrm{ZF-FC}} = \sum_{i\in\mathcal{K}} \mathbb{E} \sum_{x_i\in\Phi_i} 1\left(\frac{\frac{P_i}{S_i}\|x_i\|^{-\alpha} H^{\mathrm{ZF}}_{x_i,\min}}{I^{\mathrm{FC}} + \sigma_i^2} \geq \beta_i \right) \tag{2.65}$$

$$= \sum_{i\in\mathcal{K}} 2\pi\lambda_i \int_0^\infty r_i \mathbb{E}_\Phi \int_0^\infty \mathcal{L}^{-1}_{\overline{F}_{H^{\mathrm{ZF}}_{i,\min}}}(t_i) e^{-t_i\beta_i \frac{S_i}{P_i} r_i^\alpha \sigma_i^2} \times \prod_{j\in\mathcal{K}} \prod_{x_j\in\Phi_j/x_i} e^{-t_i\beta_i \frac{S_i}{P_i} r_i^\alpha P_j \|x_j\|^{-\alpha}} \mathrm{d}t_i \mathrm{d}r_i \tag{2.66}$$

$$= \sum_{i\in\mathcal{K}} 2\pi\lambda_i \int_0^\infty r_i \mathrm{d}r_i \int_0^\infty e^{-\beta_i \frac{S_i}{P_i} r_i^\alpha \sigma_i^2 t_i} \mathcal{L}^{-1}_{\overline{F}_{H^{\mathrm{ZF}}_i}}(t_i) e^{-r_i^2 \left(\frac{S_i\beta_i}{P_i}\right)^{\check{\alpha}} \Lambda^{\mathrm{FC}} t_i^{\check{\alpha}}} \mathrm{d}t_i \tag{2.67}$$

$$= \sum_{i\in\mathcal{K}} \overline{\sum}_{i,\boldsymbol{k}} \sum_{u=0}^{\tilde{S}_i(\boldsymbol{k})-1} \frac{2\pi\lambda_i (-1)^u S_i^{u+1}}{\Gamma(S_i) u!} \frac{\Gamma(\tilde{S}_i(\boldsymbol{k}))}{\prod_{l=0}^{N^r-S_i} (l!)^{k_l}}$$

$$\times \int_0^{\infty} r_i \mathrm{d}r_i \frac{d^u}{dt_i^u} e^{-\beta_i \frac{S_i}{P_i} r_i^{\alpha} \sigma_i^2 t_i} e^{-r_i^2 \left(\frac{S_i \beta_i}{P_i}\right)^{\check{\alpha}} \Lambda^{\mathrm{FC}} t_i^{\check{\alpha}}} \Big|_{t_i = S_i}. \tag{2.68}$$

Applying the Leibnitz's formula along with [166, Eq. (15)], similar to what was done in (2.49), the desired result then follows. □

Recall from Definition 2.4.1 that under the FC assumption we let the interference across data streams stay totally correlated. We now scrutinize the relationship between the coverage performance under the FC assumption and the actual coverage performance. This allows us to better grasp the impact of ICI-driven cross-stream SIR correlation on the coverage probability.

Proposition 2.4.2. *FC assumption yields a lower-bound of the coverage probability.*

Proof. We derive a lower-bound on the coverage probability by upper-bounding the term $\mathbb{E}_{G_{j,l_i}^{\mathrm{ZF}}}\left[(\sum_{l_i=1}^{S_i} G_{j,l_i}^{\mathrm{ZF}} t_{l_i})^{\check{\alpha}}\right]$ as the sequel. Note that the function $g(v) = v^{\check{\alpha}}$, $v \geq 0$, is concave. Consequently, by applying Jensen's inequality [165] along with some mathematical manipulations, we can show that

$$\mathbb{E}_{G_j^{\mathrm{ZF}}}\left[\left(\sum_{l_i=1}^{S_i} G_{j,l_i}^{\mathrm{ZF}} t_{l_i}\right)^{\check{\alpha}}\right] \leq \left(\sum_{l_i=1}^{S_i} \mathbb{E}_{G_j^{\mathrm{ZF}}}\left[G_{j,l_i}^{\mathrm{ZF}}\right] t_{l_i}\right)^{\check{\alpha}} \tag{2.69}$$

$$= S_i^{\check{\alpha}} \left(\sum_{l_i=1}^{S_i} t_{l_i}\right)^{\check{\alpha}}, \tag{2.70}$$

where the last step is because G_{j,l_i}^{ZF} is chi-squared with $2S_j$ DoFs. Using (2.70) in (2.30), the following lower-bound on the coverage probability is obtained:

$$c^{\mathrm{ZF}} \geq \sum_{i \in \mathcal{K}} 2\pi\lambda_i \int_0^{\infty} r_i \mathrm{d}r_i \int_0^{\infty} \cdots \int_0^{\infty} e^{-\beta_i \frac{S_i}{P_i} r_i^{\alpha} \sigma_i^2 \sum_{l_i=1}^{S_i} t_{l_i}} \prod_{l_i=1}^{S_i} \mathcal{L}^{-1}_{\overline{F}_{H_i^{\mathrm{ZF}}}}(t_{l_i}) \mathrm{d}t_{l_i}$$

$$\times e^{-r_i^2 \tilde{C}(\alpha) \left(\frac{S_i \beta_i}{P_i}\right)^{\check{\alpha}} \sum_{j=1}^{K} \lambda_j P_j^{\check{\alpha}} \left(\sum_{l_i=1}^{S_i} t_{l_i}\right)^{\check{\alpha}}}, \tag{2.71}$$

On the other hand, using LGF of the PPP, the expression (2.71) can be (reversely) expanded as (see also (A.9))

$$
\begin{aligned}
(2.71) \;=\; & \sum_{i\in\mathcal{K}} 2\pi\lambda_i \int_0^\infty r_i \mathrm{d}r_i \int_0^\infty \dots \int_0^\infty e^{-\beta_i \frac{S_i}{P_i} r_i^\alpha \sigma_i^2 \sum_{l_i=1}^{S_i} t_{l_i}} \prod_{l_i=1}^{S_i} \mathcal{L}^{-1}_{\overline{F}_{H_i^{\mathrm{ZF}}}}(t_{l_i})\mathrm{d}t_{l_i} && (2.72)\\
& \times \left(\prod_{j\in\mathcal{K}} \mathbb{E}_{\Phi_j} \prod_{x_j\in\Phi_j\setminus x_i} e^{-\beta_i \frac{S_i}{P_i} r_i^\alpha P_j \|x_j\|^{-\alpha} \sum_{l_i=1}^{S_i} t_{l_i}} \right) && (2.73)\\
& = \sum_{i\in\mathcal{K}} 2\pi\lambda_i \int_0^\infty r_i \mathrm{d}r_i \int_0^\infty \dots \int_0^\infty e^{-\beta_i \frac{S_i}{P_i} r_i^\alpha \sigma_i^2 \sum_{l_i=1}^{S_i} t_{l_i}} \prod_{l_i=1}^{S_i} \mathcal{L}^{-1}_{\overline{F}_{H_i^{\mathrm{ZF}}}}(t_{l_i})\mathrm{d}t_{l_i} && (2.74)\\
& \times \left(\prod_{j\in\mathcal{K}} \mathbb{E}_{\Phi_j} \prod_{x_j\in\Phi_j\setminus x_i} \prod_{l_i=1}^{S_i} e^{-\beta_i \frac{S_i}{P_i} r_i^\alpha P_j \|x_j\|^{-\alpha} t_{l_i}} \right) && (2.75)\\
& = \sum_{i\in\mathcal{K}} 2\pi\lambda_i \int_0^\infty r_i \mathbb{E}_\Phi \prod_{l_i=1}^{S_i} \int_0^\infty \mathcal{L}^{-1}_{\overline{F}_{H_i^{\mathrm{ZF}}}}(t_i) e^{-t_i\beta_i \frac{S_i}{P_i} r_i^\alpha \sigma_i^2} && (2.76)\\
& \times \prod_{j\in\mathcal{K}} \prod_{x_j\in\Phi_j\setminus x_i} e^{-t_i\beta_i \frac{S_i}{P_i} r_i^\alpha P_j \|x_j\|^{-\alpha}} \mathrm{d}t_i \mathrm{d}r_i && (2.77)\\
& \overset{(a)}{=} \sum_{i\in\mathcal{K}} 2\pi\lambda_i \int_0^\infty r_i \mathbb{E}_\Phi \prod_{l_i=1}^{S_i} \mathbb{P}\Bigg\{ H^{\mathrm{ZF}}_{r_i,l_i} \geq \beta_i \frac{S_i}{P_i} r_i^\alpha \sigma_i^2 && (2.78)\\
& + \beta_i \frac{S_i}{P_i} r_i^\alpha \sum_{j\in\mathcal{K}} \sum_{x_j\in\Phi_j\setminus x_i} P_j \|x_j\|^{-\alpha} \big| \Phi \Bigg\} dr_i && (2.79)\\
& \overset{(b)}{=} \sum_{i\in\mathcal{K}} 2\pi\lambda_i \int_0^\infty r_i \mathbb{E}_\Phi \prod_{l_i=1}^{S_i} \mathbb{P}\Bigg\{ H^{\mathrm{ZF}}_{r_i,l_i} \geq \beta_i \frac{S_i}{P_i} r_i^\alpha \sigma_i^2 + I^{\mathrm{FC}} \big| \Phi \Bigg\} dr_i && (2.80)\\
& = \sum_{i\in\mathcal{K}} 2\pi\lambda_i \int_0^\infty r_i \mathbb{E}_\Phi \mathbb{P}\Bigg\{ \bigcap_{l_i=1}^{S_i} \left\{ \frac{\frac{P_i}{S_i}\|x_i\|^{-\alpha} H^{\mathrm{ZF}}_{x_i,l_i}}{I^{\mathrm{FC}} + \sigma_i^2} \geq \beta_i \big| \Phi \right\} \Bigg\} dr_i && (2.81)\\
& = \sum_{i\in\mathcal{K}} 2\pi\lambda_i \int_0^\infty r_i \mathbb{E}_\Phi \mathbb{P}\Bigg\{ \min_{l_i=1,\dots,S_i} \frac{\frac{P_i}{S_i}\|x_i\|^{-\alpha} H^{\mathrm{ZF}}_{x_i,l_i}}{I^{\mathrm{FC}} + \sigma_i^2} \geq \beta_i \big| \Phi \Bigg\} dr_i && (2.82)\\
& = c^{\mathrm{ZF-FC}}, && (2.83)
\end{aligned}
$$

where Step (a) is due to Lemma B.2, and in Step (b) we notice (2.51). □

The result of Proposition 2.4.2 is interesting, as it implies that ICI-driven cross-stream

SIR correlation renders a smaller coverage probability in the multi-stream MIMO-ZFBF communication. This is because when the ICI becomes more correlated (or equivalently when the impinged signals at the receive antennas become more correlated) the potential diversity order of receive antennas deteriorates.

On the other hand, our simulation results in Section 2.7 show that the FC assumption actually *slightly* underestimates the actual coverage probability. This implies that one can simply assume, without damaging the accuracy of the analysis, that ICI across data streams of a typical communication link is fully correlated. In fact, it is straightforward to show that the Laplace transform of interference under FC assumption is $\mathcal{L}_{I^{\mathrm{FC}}}(t) = e^{-t^{\check{\alpha}}\Lambda^{\mathrm{FC}}}$, where Λ^{FC} is given in (2.56). Comparing this with the actual Laplace transform of ICI (2.11) and noting that $\Lambda^{\mathrm{FC}}\Gamma(1+\check{\alpha}) \leq \Lambda(\boldsymbol{S})$ (see (2.109)), we observe that since $\Gamma(1+\check{\alpha}) < 2! = 2$ the Laplace transform under the FC assumption slightly smaller than that of the actual Laplace transform.

Since the provided expression of the coverage probability under FC assumption in Proposition 2.4.1 has more manageable computational evaluation, this last observation makes the analysis of multiplexing systems even more tractable.

2.5 Impact of Multiplexing gain on the Coverage Performance

By increasing the multiplexing gains, one may come upon 1) a decrease of DoF of the intending signal (lowering diversity gain of each stream and its effective power), 2) growing the effective interference fading power, and 3) a lower likelihood of preserving the retrievability of the all transmitted data streams, recalling that the association and coverage is based on the minimum SINR among all transmitted streams of a communication link. It is then surmisable that the growth of multiplexing gains should lead to a decline of the coverage probability. In this section, we study the impact of increasing multiplexing gain on the

coverage probability.

We first discuss some especial cases of the multiplexing system: SISO, single-stream, i.e, $S_i = 1\ \forall i$ or diversity/SIMO, and full-multiplexing (full-MUX), i.e., $S_i = N^r = N_i^t\ \forall i$.

Corollary 2.5.1 (SISO scenario). *When $N^r = 1$, Proposition 2.3.2 implies that*

$$c^{\mathrm{SISO}} = \sum_{i\in\mathcal{K}} 2\pi\lambda_i \int_0^\infty r_i e^{-\frac{\beta_i}{P_i} r_i^\alpha \sigma_i^2} e^{-r_i^2 \left(\frac{\beta_i}{P_i}\right)^{\breve{\alpha}} \Lambda^{\mathrm{SISO}}} \mathrm{d}r_i,$$

in which

$$\Lambda^{\mathrm{SISO}} \triangleq C(\alpha) \sum_{j=1}^{K} \lambda_j P_j^{\breve{\alpha}} \tag{2.84}$$

where $C(\alpha) \triangleq \tilde{C}(\alpha)\Gamma(1+\breve{\alpha})$. This expression coincides with the result of [47, Theorem 1]. Note that c^{SISO} is the exact coverage probability.

Corollary 2.5.2 (Diversity/SIMO System). *For the case of a single-stream setting, i.e, $S_i = 1\ \forall i$, Proposition 2.3.2 simplifies to*

$$c^{\mathrm{ZF}} = \sum_{i\in\mathcal{K}} 2\pi\lambda_i \Bigg(\hat{\varphi}_{0i}^0 + \sum_{m_i=1}^{N^r-1} \sum_{m_i'=0}^{m_i} \frac{(-1)^{m_i'} \binom{m_i}{m_i'} \varphi_{0i}^{m_i-m_i'}}{m_i! \left(\frac{\beta_i}{P_i}\sigma_i^2\right)^{m_i'-m_i}}$$

$$+ \sum_{m_i=1}^{N^r-1} \sum_{m_i'=0}^{m_i} \sum_{n=1}^{m_i'} \frac{(-1)^{m_i'} \binom{m_i}{m_i'} (\Lambda^{\mathrm{SIMO}})^n \phi_n^{m_i'} \hat{\varphi}_{0i}^{m_i-m_i'}}{m_i! n! \left(\frac{\beta_i}{P_i}\right)^{-n\breve{\alpha}} \left(\frac{\beta_i}{P_i}\sigma_i^2\right)^{m_i'-m_i}} \Bigg), \tag{2.85}$$

where

$$\Lambda^{\mathrm{SIMO}} \triangleq \tilde{C}(\alpha)\Gamma(1+\breve{\alpha}) \sum_{j=1}^{K} \lambda_j P_j^{\breve{\alpha}} = \Lambda^{\mathrm{SISO}}, \tag{2.86}$$

and

$$\hat{\varphi}_{ni}^m \triangleq \int_0^\infty r_i^{m\alpha+2n+1} e^{-\frac{\beta_i}{P_i} r_i^\alpha \sigma_i^2} e^{-r_i^2 \left(\frac{\beta_i}{P_i}\right)^{\breve{\alpha}} \Lambda^{\mathrm{SIMO}}} \mathrm{d}r_i. \tag{2.87}$$

Here, (2.85) stands as the exact coverage probability.

Note that Corollary 2.5.1 and Corollary 2.5.2 are the actual coverage probabilities as for

$S_i = 1$ the inequality (2.41) reduces to the equality.

Corollary 2.5.3 (Full-MUX System). *Let assume $N_i^t \geq N^r \ \forall i$. For the Full-MUX system, whereby $S_i = N^r \ \forall i$, Proposition 2.3.2 can be used to show that the coverage probability is upper-bounded by*

$$c^{\mathrm{ZF}} \leq \sum_{i \in \mathcal{K}} 2\pi\lambda_i \int_0^{\infty} r_i e^{-\frac{\beta_i (N^r)^2}{P_i} r_i^{\alpha} \sigma_i^2} e^{-r_i^2 \left(\frac{\beta_i (N^r)^2}{P_i}\right)^{\check{\alpha}} \tilde{\Lambda}} \mathrm{d}r_i, \tag{2.88}$$

where $\tilde{\Lambda} \triangleq \frac{\Gamma(N^r + \check{\alpha})}{(N^r)^{\check{\alpha}} \Gamma(N^r)} \Lambda^{\mathrm{SIMO}}$.

Intuitively, the distribution of the fading of the desired signal remains exponential irrespective of the growth of N^r, while the strength of the interfering signals proportionally grows with N^r. Besides, N^r data streams must be simultaneously decoded successfully to declare the coverage, which is very unlikely to happen for larger values of N^r, thus by growing N^r the coverage probability of full-MUX decreases. This statement can also be seen by closely scrutinizing Corollary 2.5.3. To that end, we can argue that the impact of N^r on parameter $\tilde{\Lambda}$ is quite circumscribable, since due to $\frac{\Gamma(N^r + \check{\alpha})}{\Gamma(N^r)} \lesssim (N^r)^{\check{\alpha}}$ [78] and noticing that $\Lambda^{\mathrm{SIMO}} = \Lambda^{\mathrm{SISO}}$ (see Corollary 2.5.1 and Corollary 2.5.2), there holds

$$\Gamma(1 + \check{\alpha}) \Lambda^{\mathrm{SISO}} < \tilde{\Lambda} \lesssim \Lambda^{\mathrm{SISO}}. \tag{2.89}$$

As Λ^{SISO} does not depend on N^r, it is straightforward to see that (2.88) reduces by N^r. We formally, state that:

Corollary 2.5.4. *For the all-coverage probability and under max-SINR CA rule, the SISO system has a higher coverage probability than the full-MUX system, which its coverage probability declines by increasing the number of antennas at the receiver.*

Now we formally prove that the growth of multiplexing gain leads to a reduction of the coverage probability:

Proposition 2.5.1 (Impact of Multiplexing Gains on Coverage). *By growing the multiplexing gain, the coverage probability can decline. It implies that the diversity system has a higher coverage probability than the multiplexing system.*

Proof. First consider the cases of full-MUX and diversity system. We prove that the coverage probability under the former is smaller than the latter. We then extend the proof for the general case.

Consider full-MUX scenario and a generic multiplexing system under the FC assumption. Note that under the FC assumption the coverage probability is slightly underestimated. We then note two evidences: firstly, it is helpful to spot subtle similarities between the provided expressions of the coverage probability in Proposition 2.4.1 and Corollary 2.5.2. In effect, as $\Gamma(1+\check{\alpha})\Lambda^{\mathrm{FC}} = \Lambda^{\mathrm{SIMO}}$ holds, we can argue that from a network-level perspective a single-stream scenario and the FC assumption expose nearly the same level of ICI from the eye of a typical UE. Secondly, in the diversity scenario the fading on the intended channel is distributed as $\chi^2_{2N^r}$. (Note that under the FC assumption the determining fading is governed by $H^{\mathrm{ZF}}_{x_i,\min} = \min_{l_i=1,\ldots,S_i} \chi^2_{2(N^r-S_i+1)}$.) Using these two observations, it is then conceivable to claim that transmitting multi-stream of data can result in a smaller coverage. To confirm this argument, we firstly write

$$\begin{aligned}
\overline{F}_{H^{\mathrm{ZF}}_{x_i,\min}}(z) &= \left(\overline{F}_{\chi^2_{2(N^r-S_i+1)}}(z)\right)^{S_i} && (2.90)\\
&\leq \overline{F}_{\chi^2_{2(N^r-S_i+1)}}(z) && (2.91)\\
&\leq \overline{F}_{\chi^2_{2N^r}}(z), \qquad\qquad \forall z \geq 0 && (2.92)
\end{aligned}$$

where the last inequality is attributable to stochastic ordering results, see, e.g., [56]. Using this and knowing that under the FC assumption the coverage probability is nearly equal to the actual coverage probability, we then have

$$c^{\mathrm{ZF}} \approx c^{\mathrm{ZF-FC}} \qquad (2.93)$$

$$= 2\pi \sum_i \lambda_i \int_0^\infty z \mathbb{E}_{I^{\mathrm{FC}}} \overline{F}_{H^{\mathrm{ZF}}_{x_i,\min}} \left(\frac{S_i \beta_i}{P_i} z^\alpha \sigma_i^2 + \frac{S_i \beta_i}{P_i} z^\alpha I^{\mathrm{FC}} \right) dz \tag{2.94}$$

$$\leq 2\pi \sum_i \lambda_i \int_0^\infty z \mathbb{E}_{I^{\mathrm{FC}}} \overline{F}_{H^{\mathrm{ZF}}_{x_i,\min}} \left(\frac{\beta_i}{P_i} z^\alpha \sigma_i^2 + \frac{\beta_i}{P_i} z^\alpha I^{\mathrm{FC}} \right) dz \tag{2.95}$$

$$\leq 2\pi \sum_i \lambda_i \int_0^\infty z \mathbb{E}_{I^{\mathrm{FC}}} \overline{F}_{\chi^2_{2N^r}} \left(\frac{\beta_i}{P_i} z^\alpha \sigma_i^2 + \frac{\beta_i}{P_i} z^\alpha I^{\mathrm{FC}} \right) dz \tag{2.96}$$

$$\overset{(a)}{=} 2\pi \sum_i \lambda_i \int_0^\infty z \mathbb{E}_{\Phi} \overline{F}_{\chi^2_{2N^r}} \Bigg(\frac{\beta_i}{P_i} z^\alpha \sigma_i^2 \tag{2.97}$$

$$+ \frac{\beta_i}{P_i} z^\alpha \mathbb{E}_{\{G^{\mathrm{ZF}}_{x_j,l_i}\}} \sum_{j \in \mathcal{K}} \sum_{x_j \in \Phi_j \setminus x_i} \frac{P_j}{S_j} \|x_j\|^{-\alpha} G^{\mathrm{ZF}}_{x_j,l_i} \Bigg) dz \tag{2.98}$$

$$\overset{(b)}{\leq} 2\pi \sum_i \lambda_i \int_0^\infty z \mathbb{E}_{\Phi} \mathbb{E}_{\{G^{\mathrm{ZF}}_{x_j,l_i}\}} \overline{F}_{\chi^2_{2N^r}} \Bigg(\frac{\beta_i}{P_i} z^\alpha \sigma_i^2 \tag{2.99}$$

$$+ \frac{\beta_i}{P_i} z^\alpha \sum_{j \in \mathcal{K}} \sum_{x_j \in \Phi_j \setminus x_i} \frac{P_j}{S_j} \|x_j\|^{-\alpha} G^{\mathrm{ZF}}_{x_j,l_i} \Bigg) dz \tag{2.100}$$

$$\overset{(c)}{=} 2\pi \sum_i \lambda_i \int_0^\infty z \int_0^\infty e^{-\frac{\beta_i}{P_i} z^\alpha \sigma_i^2 t_i} \mathcal{L}^{-1}_{\overline{F}_{\chi^2_{2N^r}}}(t_i) e^{-z^2 \left(\frac{\beta_i}{P_i}\right)^{\check{\alpha}} \Lambda(\boldsymbol{S}) t_i^{\check{\alpha}}} \mathrm{d}t_i \tag{2.101}$$

$$\overset{(d)}{\lesssim} 2\pi \sum_i \lambda_i \int_0^\infty z \int_0^\infty e^{-\frac{\beta_i}{P_i} z^\alpha \sigma_i^2 t_i} \mathcal{L}^{-1}_{\overline{F}_{\chi^2_{2N^r}}}(t_i) e^{-z^2 \left(\frac{\beta_i}{P_i}\right)^{\check{\alpha}} \Gamma(1+\check{\alpha}) \Lambda^{\mathrm{FC}} t_i^{\check{\alpha}}} \mathrm{d}t_i, \tag{2.102}$$

where in Step (a) we plug (2.51), in Step (b) we use Lemma B.2 to write

$$\overline{F}_{\chi^2_{2N^r}} \left(\frac{\beta_i}{P_i} z^\alpha \sigma_i^2 + \frac{\beta_i}{P_i} z^\alpha \mathbb{E}_{\{G^{\mathrm{ZF}}_{x_j,l_i}\}} \sum_{j \in \mathcal{K}} \sum_{x_j \in \Phi_j \setminus x_i} \frac{P_j G^{\mathrm{ZF}}_{x_j,l_i}}{S_j \|x_j\|^\alpha} \right) \tag{2.103}$$

$$= \int_0^\infty e^{-\frac{\beta_i}{P_i} z^\alpha \sigma_i^2 t_i} \mathcal{L}^{-1}_{\overline{F}_{\chi^2_{2N^r}}}(t_i) e^{-\frac{\beta_i}{P_i} z^\alpha \mathbb{E}_{\{G^{\mathrm{ZF}}_{x_j,l_i}\}} \sum_{j \in \mathcal{K}} \sum_{x_j \in \Phi_j \setminus x_i} \frac{P_j G^{\mathrm{ZF}}_{x_j,l_i}}{S_j \|x_j\|^\alpha}} \mathrm{d}t_i \tag{2.104}$$

$$\leq \int_0^\infty e^{-\frac{\beta_i}{P_i} z^\alpha \sigma_i^2 t_i} \mathcal{L}^{-1}_{\overline{F}_{\chi^2_{2N^r}}}(t_i) \mathbb{E}_{\{G^{\mathrm{ZF}}_{x_j,l_i}\}} e^{-\frac{\beta_i}{P_i} z^\alpha \sum_{j \in \mathcal{K}} \sum_{x_j \in \Phi_j \setminus x_i} \frac{P_j G^{\mathrm{ZF}}_{x_j,l_i}}{S_j \|x_j\|^\alpha}} \mathrm{d}t_i \tag{2.105}$$

$$= \mathbb{E}_{\{G^{\mathrm{ZF}}_{x_j,l_i}\}} \overline{F}_{\chi^2_{2N^r}} \left(\frac{\beta_i}{P_i} z^\alpha \sigma_i^2 + \frac{\beta_i}{P_i} z^\alpha \sum_{j \in \mathcal{K}} \sum_{x_j \in \Phi_j \setminus x_i} \frac{P_j G^{\mathrm{ZF}}_{x_j,l_i}}{S_j \|x_j\|^\alpha} \right). \tag{2.106}$$

In Step (c), we apply Lemma B.2. Step (d) is, finally, because using [78, Eq. (3)] we can write

$$\begin{aligned}\Lambda(\boldsymbol{S}) &= \tilde{C}(\alpha)\sum_{j=1}^{K}\lambda_j\left(\frac{P_j}{S_j}\right)^{\breve{\alpha}}\frac{\Gamma(S_j+\breve{\alpha})}{\Gamma(S_j)} &(2.107)\\ &\gtrsim \Gamma(1+\breve{\alpha})\tilde{C}(\alpha)\sum_{j=1}^{K}\lambda_j\left(\frac{P_j}{S_j}\right)^{\breve{\alpha}}{S_j}^{\breve{\alpha}} &(2.108)\\ &= \Gamma(1+\breve{\alpha})\Lambda^{\mathrm{FC}}. &(2.109)\end{aligned}$$

Now, knowing that $\Gamma(1+\breve{\alpha})\Lambda^{\mathrm{FC}} = \Lambda^{\mathrm{SIMO}}$, we then conclude that the expression in Step (d) is actually the coverage probability of the single-stream system. This proves that the coverage performance of diversity system is larger than full-MUX.

Now, consider the general scenario.

$$\begin{aligned}c^{\mathrm{ZF}} &\approx c^{\mathrm{ZF-FC}} &(2.110)\\ &= 2\pi\lambda_i\int_0^{\infty} z\mathbb{E}_{I^{\mathrm{FC}}}\overline{F}_{H^{\mathrm{ZF}}_{x_i,\min}}\left(\frac{S_i\beta_i}{P_i}z^{\alpha}\sigma_i^2+\frac{S_i\beta_i}{P_i}z^{\alpha}I^{\mathrm{FC}}\right)dz &(2.111)\\ &+ 2\pi\sum_{i'\neq i}\lambda_{i'}\int_0^{\infty} z\mathbb{E}_{I^{\mathrm{FC}}}\overline{F}_{H^{\mathrm{ZF}}_{x_{i'},\min}}\left(\frac{S_{i'}\beta_{i'}}{P_{i'}}z^{\alpha}\sigma_{i'}^2+\frac{S_{i'}\beta_{i'}}{P_{i'}}z^{\alpha}I^{\mathrm{FC}}\right)dz. &(2.112)\end{aligned}$$

On the other hand, using stochastic ordering results we can show that for general multiplexing system by growing the multiplexing gain in Tier i the CCDF of $H^{\mathrm{ZF}}_{x_i,\min}$ is upper-bounded as

$$\begin{aligned}\overline{F}_{H^{\mathrm{ZF}}_{x_i,\min}}(z) &= (\overline{F}_{\chi^2_{2(N^r-S_i+1)}}(z))^{S_i} &(2.113)\\ &\leq (\overline{F}_{\chi^2_{2(N^r-S_i+1)}}(z))^{S_i+1} &(2.114)\\ &\leq (\overline{F}_{\chi^2_{2(N^r-S_i+2)}}(z))^{S_i+1}, \qquad \forall z\geq 0. &(2.115)\end{aligned}$$

As the case of full-MUX, one is able to apply the same lines developed above to show that by adding to the multiplexing gain in Tier i expression (2.111) declines. On the other hand,

due to (2.109) we can conclude that $\Lambda(\boldsymbol{S})$ is an increasing function of multiplexing gains. Therefore, by increasing S_i, (2.112) also reduces. These two statements then prove that by increasing S_i the coverage probability declines, which proves the proposition. □

2.6 Interference-Limited Scenario

Aggressive frequency reuse and densification make the operating point of HetNet lend toward interference-limited regime, i.e., negligible background noise. This can be exploited, as we see in the following, to substantially simplify the analysis of the multiplexing system.

Proposition 2.6.1. *For an interference-limited system, the coverage probability of the MIMO-ZFBF multiplexing system is upper-bounded as*

$$c^{\mathrm{ZF}} \leq \frac{\pi}{\tilde{C}(\alpha)} \sum_{i\in\mathcal{K}} \frac{\lambda_i \left(\frac{P_i}{S_i^2\beta_i}\right)^{\breve{\alpha}} \left(\Gamma_i^{\mathrm{ZF}}\right)^{S_i}}{\sum_{j\in\mathcal{K}} \lambda_j \left(\frac{P_j}{S_j}\right)^{\breve{\alpha}} \left(\frac{\Gamma(\frac{\breve{\alpha}}{S_i}+S_j)}{\Gamma(S_j)}\right)^{S_i}}, \tag{2.116}$$

where

$$\Gamma_i^{\mathrm{ZF}} \triangleq \sum_{m_i=0}^{N^r-S_i} \frac{\Gamma(\frac{\breve{\alpha}}{S_i}+m_i)}{\Gamma(\frac{\breve{\alpha}}{S_i})\Gamma(1+m_i)}. \tag{2.117}$$

Proof. Consider (2.30), and let $\sigma_i^2 = 0\ \forall i$, to attaint

$$c^{\mathrm{ZF}} \leq \sum_{i\in\mathcal{K}} 2\pi\lambda_i \int_0^\infty r_i \mathrm{d}r_i \int_0^\infty \dots \int_0^\infty \prod_{l_i=1}^{S_i} \mathcal{L}^{-1}_{\overline{F}_{H_i^{\mathrm{ZF}}}}(t_{l_i})\mathrm{d}t_{l_i} \tag{2.118}$$

$$\times e^{-r_i^2\tilde{C}(\alpha)\left(\frac{S_i\beta_i}{P_i}\right)^{\breve{\alpha}} \sum_{j=1}^{K}\lambda_j\left(\frac{P_j}{S_j}\right)^{\breve{\alpha}} \mathbb{E}_{\{G^{\mathrm{ZF}}_{j,l_i}\}}\left[\left(\sum_{l_i=1}^{S_i} G^{\mathrm{ZF}}_{j,l_i} t_{l_i}\right)^{\breve{\alpha}}\right]} \tag{2.119}$$

$$= \sum_{i\in\mathcal{K}} 2\pi\lambda_i \int_0^\infty \dots \int_0^\infty \prod_{l_i=1}^{S_i} \mathcal{L}^{-1}_{\overline{F}_{H_i^{\mathrm{ZF}}}}(t_{l_i})\mathrm{d}t_{l_i} \int_0^\infty r_i \tag{2.120}$$

$$\times e^{-r_i^2\tilde{C}(\alpha)\left(\frac{S_i\beta_i}{P_i}\right)^{\breve{\alpha}} \sum_{j=1}^{K}\lambda_j\left(\frac{P_j}{S_j}\right)^{\breve{\alpha}} \mathbb{E}_{\{G^{\mathrm{ZF}}_{j,l_i}\}}\left[\left(\sum_{l_i=1}^{S_i} G^{\mathrm{ZF}}_{j,l_i} t_{l_i}\right)^{\breve{\alpha}}\right]} \mathrm{d}r_i \tag{2.121}$$

$$= \sum_{i\in\mathcal{K}} \frac{\pi}{\tilde{C}(\alpha)} \lambda_i \left(\frac{P_i}{S_i\beta_i}\right)^{\breve{\alpha}} \int_0^{\infty} \cdots \int_0^{\infty} \frac{\prod_{l_i=1}^{S_i} \mathcal{L}^{-1}_{\overline{F}_{H_i^{\mathrm{ZF}}}}(t_{l_i})\mathrm{d}t_{l_i}}{\sum_{j\in\mathcal{K}} \lambda_j \left(\frac{P_j}{S_j}\right)^{\breve{\alpha}} \mathbb{E}_{\{G^{\mathrm{ZF}}_{j,l_i}\}} \left[\left(\sum_{l_i=1}^{S_i} G^{\mathrm{ZF}}_{j,l_i} t_{l_i}\right)^{\breve{\alpha}}\right]}, \quad (2.122)$$

Direct evaluation of (2.122) is complex, and hence we use the arithmetic-geometric inequality for deriving an upper-bound. Thus,

$$c^{\mathrm{ZF}} \leq \sum_{i\in\mathcal{K}} \frac{\pi\lambda_i \left(\frac{P_i}{S_i\beta_i}\right)^{\breve{\alpha}}}{\tilde{C}(\alpha)} \int_0^{\infty} \cdots \int_0^{\infty} \frac{\prod_{l_i=1}^{S_i} \mathcal{L}^{-1}_{\overline{F}_{H_i^{\mathrm{ZF}}}}(t_{l_i})\mathrm{d}t_{l_i}}{\sum_{j\in\mathcal{K}} \lambda_j \left(\frac{P_j}{S_j}\right)^{\breve{\alpha}} \mathbb{E}_{\{G^{\mathrm{ZF}}_{j,l_i}\}} \left[S_i^{\breve{\alpha}} \left(\prod_{l_i=1}^{S_i} G^{\mathrm{ZF}}_{j,l_i} t_{l_i}\right)^{\frac{\breve{\alpha}}{S_i}}\right]} \quad (2.123)$$

$$= \sum_{i\in\mathcal{K}} \frac{\frac{\pi}{\tilde{C}(\alpha)} \left(\frac{P_i}{S_i\beta_i}\right)^{\breve{\alpha}} \frac{\lambda_i}{S_i^{\breve{\alpha}}}}{\sum_{j=1}^{K} \lambda_j \left(\frac{P_j}{S_j}\right)^{\breve{\alpha}} \mathbb{E}_{\{G^{\mathrm{ZF}}_{j,l_i}\}} \prod_{l_i=1}^{S_i} (G^{\mathrm{ZF}}_{j,l_i})^{\frac{\breve{\alpha}}{S_i}}} \int_0^{\infty} \cdots \int_0^{\infty} \prod_{l_i=1}^{S_i} \frac{\mathcal{L}^{-1}_{\overline{F}_{H_i^{\mathrm{ZF}}}}(t_{l_i})\mathrm{d}t_{l_i}}{t_{l_i}^{\frac{\breve{\alpha}}{S_i}}} \quad (2.124)$$

$$= \sum_{i\in\mathcal{K}} \frac{\frac{\pi}{\tilde{C}(\alpha)} \left(\frac{P_i}{S_i\beta_i}\right)^{\breve{\alpha}} \frac{\lambda_i}{S_i^{\breve{\alpha}}}}{\sum_{j=1}^{K} \lambda_j \left(\frac{P_j}{S_j}\right)^{\breve{\alpha}} \left(\mathbb{E}_{G^{\mathrm{ZF}}_{j,1}} (G^{\mathrm{ZF}}_{j,1})^{\frac{\breve{\alpha}}{S_i}}\right)^{S_i}} \left(\int_0^{\infty} \frac{\mathcal{L}^{-1}_{\overline{F}_{H_i^{\mathrm{ZF}}}}(t_{l_i})}{t_i^{\frac{\breve{\alpha}}{S_i}}} \mathrm{d}t_i\right)^{S_i}. \quad (2.125)$$

where the last step is due to the fact that r.v.s $G^{\mathrm{ZF}}_{x_j,l_i}$ are i.i.d. across streams. Since H_i^{ZF} is a chi-squared r.v. with $2(N^r - S_i + 1)$ DoF, applying Lemma B.1 completes the proof. □

The bound presented in Proposition (2.6.1) reflects the effect of system parameters including multiplexing gains, S_is, deployment densities, λ_i, and transmission powers, P_i, on the the coverage performance. Note that by substituting $\sigma_i^2 = 0\ \forall i$ in (2.3) for $\sigma_i^2 = 0$ we obtain:

$$c^{\mathrm{ZF}} \leq \sum_{i\in\mathcal{K}} 2\pi\lambda_i \int_0^{\infty} e^{-r_i^2 \left(\frac{S_i^2\beta_i}{P_i}\right)^{\breve{\alpha}} \Lambda(\boldsymbol{S})} \left(1 + \sum_{m_i=1}^{N^r-S_i} \frac{(-1)^{m_i}}{m_i!} \left[1 + \sum_{n=1}^{m_i} \frac{\phi_n^{m_i}}{n!} \left(\frac{S_i^2\beta_i}{P_i}\right)^{n\breve{\alpha}} \frac{\Lambda^n(\boldsymbol{S})}{S_i^n} r_i^{2n}\right]\right)^{S_i} r_i \mathrm{d}r_i. \quad (2.126)$$

In general, it is hard to derive (2.116) from this expression. This is because the derivation of Proposition 2.3.2 is based on Jensen's inequality while here we exploit arithmetic-geometric inequality.

Interestingly, for the case of SISO, $N_i^t = N^r = 1\ \forall i$, the upper-bound (2.116) reduces to the expression previously derived in [47, Corollary 1] for the counterpart SISO system.

Using Proposition (2.6.1), the coverage performance for Tier i is upper-bounded as

$$c_i^{\mathrm{ZF}} \leq \frac{\frac{\pi\lambda_i}{\tilde{C}(\alpha)} \left(\frac{P_i}{S_i}\right)^{\breve{\alpha}} \beta_i^{-\breve{\alpha}} S_i^{-\breve{\alpha}} \left(\Gamma_i^{\mathrm{ZF}}\right)^{S_i}}{\sum_{j\in\mathcal{K}} \lambda_j \left(\frac{P_j}{S_j}\right)^{\breve{\alpha}} \left(\frac{\Gamma(\frac{\breve{\alpha}}{S_i}+S_j)}{\Gamma(S_j)}\right)^{S_i}}. \tag{2.127}$$

Further, by considering per-stream coverage probability as the performance metric (see, e.g., [55, 118, 120]), and following the same lines of arguments in the proof of Proposition 2.6.1, one can also show that the coverage probability per stream l_i is

$$c_{i,l_i}^{\mathrm{ZF}} \leq \frac{\pi}{\tilde{C}(\alpha)} \frac{\lambda_i \left(\frac{P_i}{S_i}\right)^{\breve{\alpha}} \beta_i^{-\breve{\alpha}} \Gamma_i^{\mathrm{ZF}}}{\sum_{j\in\mathcal{K}} \lambda_j \left(\frac{P_j}{S_j}\right)^{\breve{\alpha}} \frac{\Gamma(\breve{\alpha}+S_j)}{\Gamma(S_j)}}. \tag{2.128}$$

In the upper-bound, the effect of the ICI imposed from tier $j \neq i$ is shown to be represented solely through $\frac{\Gamma(\breve{\alpha}+S_j)}{\Gamma(S_j)}$ which is independent of S_i. Since $\frac{\Gamma(\frac{\breve{\alpha}}{S_i}+S_j)}{\Gamma(S_j)} \leq \frac{\Gamma(\breve{\alpha}+S_j)}{\Gamma(S_j)}$, multiplexing gain S_i could reduce the negative effect of higher multiplexing gain S_j, on the link performance compared to the given stream performance due to the dependency of SIR values among the streams. *A direct conclusion is that performance of a given stream of a communication link does not necessarily represent the entire picture of the communication link performance.* Further, the multiplexing gain S_i affects the intended signal strength in (2.127) via $S_i^{-\breve{\alpha}} \left(\Gamma_i^{\mathrm{ZF}}\right)^{S_i}$ that is dependent on $N^r - S_i + 1$ which is the available DoF for transmitting each stream of data. Comparing (2.127) with (2.128), one can see that by considering the per-stream coverage as the performance metric, this effect is overlooked.

2.7 Simulation and Numerical Results

In this part, we examine the accuracy of the proposed approximations of the coverage probability. We further study the impact of various system parameters on the coverage probability as well as spectral efficiency in order to shed some light on the effects of densification, mul-

tiplexing gains, and propagation environment.

The simulation results are based on Monte Carlo technique. We randomly produce BSs based on given densities in a dick with radius 10,000 meters, and repeat the procedure for 40,000 times. Each time, fading matrices are randomly produced based of Rayleigh fading distribution. We set $P_1 = 50$ W, $P_2 = 10$ W, $N_1^t = 16$, and $N_2^t = 16$ which are generally kept fixed during the simulation experiments. Other parameters are assumed to be variable and their particular values will be specified in each experiment. Note that in our simulations, density is measured as the number of nodes per square meter.

Impact of SINR Thresholds

In Fig. 2.4 (resp. Fig. 2.5) we plot the coverage probability vs. SINR threshold β_2 (resp. β_1). First, we observe from both figures that by growing the SINR thresholds the coverage probability decreases, which is expected as the higher is the SINR thresholds, the smaller is the chance of successfully decoding all the transmitted data streams. Further, as seen, the upper-bound and lower-bound (associated with the FC assumption) are both very accurate for $\beta_i \geq 1$. We also observe that, except the case of $\lambda = 10^{-3}$ and $N^r = 8$ in Fig. 2.5, both the upper-bound and the lower-bound preserve acceptable level of accuracy for SINR thresholds as small as 0.5. These observations are in line with the provided discussion in Remark 2.3.2.

Interestingly, we note that, to our main interest which includes $\beta_i \geq 1$, under FC assumption the coverage probability is slightly lower-bounded, therefore, in multiplexing systems it is safe to assume that from the coverage probability perspective the data streams are fully correlated.

On the other hand, from both Fig. 2.4 and Fig. 2.5 we observe that when $N^r = 8$, depending on the SINR thresholds, the coverage probability may increase/decrease by densifying Tier 1. In fact, as seen from Fig. 2.4 we observe that when $\beta_2 \gtrapprox 5$ by densifying Tier 1 the coverage probability improves. In contrary, from Fig. 2.5 we see that when $\beta_1 \lessapprox 3$

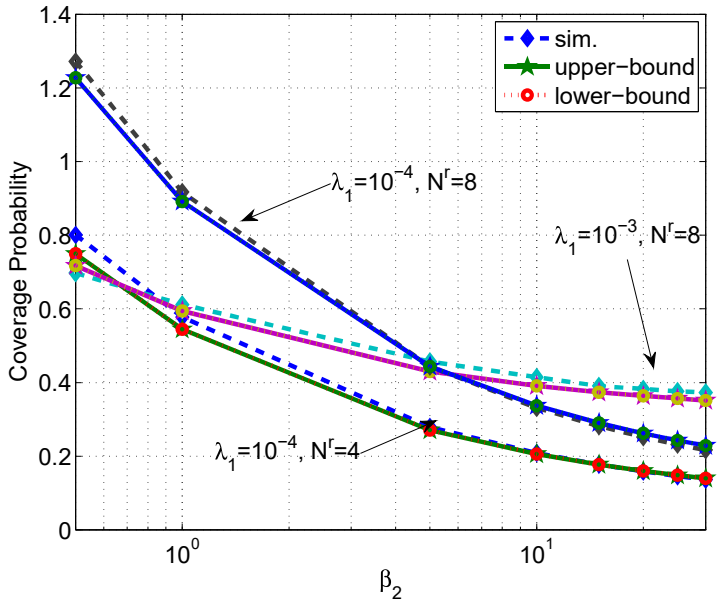

Figure 2.4: Coverage probability *vs.* β_2 when $\beta_1 = 5$. Parameters are: $S_1 = S_2 = 2$, $\sigma^2 = 10^{-10}$ and $\lambda_2 = 10^{-3}$.

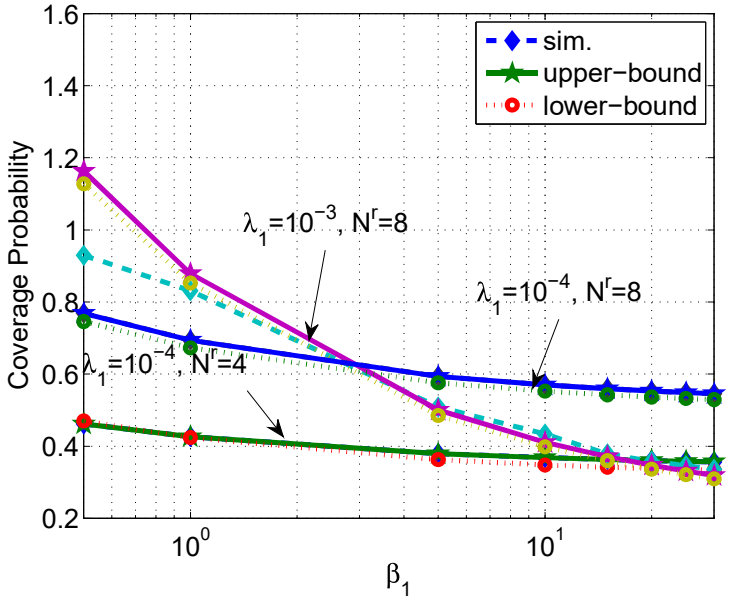

Figure 2.5: Coverage Probability *vs.* β_1 when $\beta_2 = 2.5$. Parameters are: $S_1 = S_2 = 2$, $\sigma^2 = 10^{-10}$ and $\lambda_2 = 10^{-3}$.

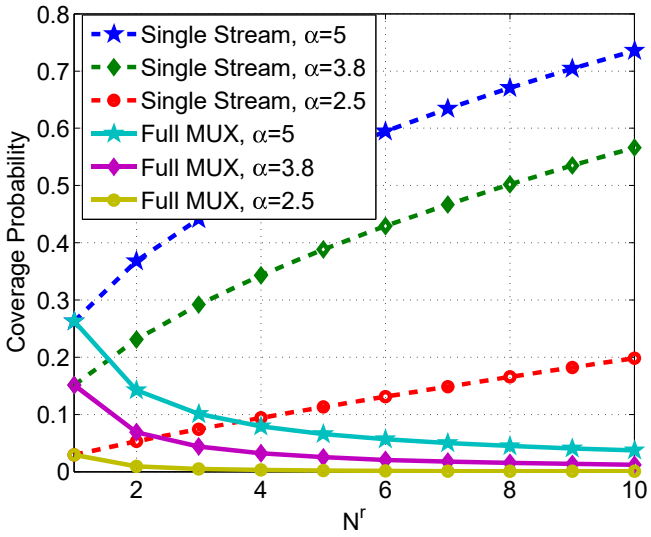

Figure 2.6: Coverage probability *vs.* N^r. Parameters are: $\sigma^2 = 10^{-8}$, $\lambda_1 = 10^{-4}$, $\lambda_2 = 10^{-3}$, $\beta_1 = 5$, and $\beta_2 = 2.5$.

by densifying Tier 1 the coverage probability improves. This implies that densification should be practiced with accordance to other system parameters, for this example SINR thresholds, otherwise it may not lead to what we expect it to achieve (i.e., improving the coverage probability). We explore this issue in more depth in Section 2.8.

Impact of Number of Receive Antennas

From Fig. 2.4 and Fig. 2.5, we further observe that by increasing the number of receive antennas from $N^r = 4$ to $N^r = 8$ the coverage probability improves, attributable to a higher diversity potential of larger arrays. However, as Fig. 2.4 shows, by growing β_2 the benefit of using larger arrays at the receiver declines. In the contrary, Fig. 2.5 indicates that almost 156% coverage growth is introduced by doubling the number of antennas at the receiver, but the gain stays nearly stable despite the growth of β_1.

To better assess the impact of N^r on the coverage probability, Fig. 2.6 demonstrates the coverage probability of the diversity system (see Corollary 2.5.2) vs. N^r for several choices of path-loss exponent, α. As seen, by growing N^r the coverage probability increases. In fact, the

DoF of the desired signal proportionally grows by N^r, while the fading power distribution of the interfering signals remains exponential with mean value one irrespective of N^r. However, the growth of the coverage probability by N^r is not linear. This is apprehensible referring to Corollary 2.5.2. Superficially, Corollary 2.5.2 implies that because of $(-1)^{m_i}$ the terms involved in the outer summation partially cancel out each other, leading to a sub-linear growth of the coverage probability by N^r.

Furthermore, this illustration demonstrates that by increasing the path-loss exponent α, the coverage probability increases as parameter Λ^{SIMO} in (2.86) is a decreasing function of α. Intuitively, for smaller values of α many not-too-close interfering BSs can pose substantial interference making the victim receiver more susceptible to ICI, which, conceivably, leads to a disappointingly small coverage performance. In contrary, for large values of α, only a handful number of nearby interfering BSs may impose sufficiently powerful ICI at the victim UE.

Fig. 2.6 also demonstrates that the coverage probability of the SISO system (see Corollary 2.5.1) is smaller than that of the single-stream system, while it is higher than that of the full-MUX system (see Corollary 2.5.3). These results are inline with what Corollary 2.5.4 and Proposition 2.5 also anticipate. In effect, in the SISO system the fading of both the desired signal and the interfering signals are exponential, so compared to the single-stream system there is no diversity available to be exploited. On the other hand, under the full-MUX system, while the desired fading is exponentially distributed with mean 1, as the SISO scenario, the interfering fading is chi-squared with DoF $2N^r$, which is much more powerful than the exponential gain with mean 1. Besides, in the full-MUX system, to declare coverage, N^r number of data streams should be received successfully, which is way less probable to happen in comparison with the case of the SISO system.

Finally, as in the single-stream scenario, this illustration shows that by increasing the path-loss exponent α the coverage probability of the full-MUX system increases. However, it is seen that in this case the impact of α is not as significant as the case of single-stream

scenario. Furthermore, its impact reduces by the growth of N^r.

Note that when α is large a number of closed-by interferers are sufficient to cause outage. However, the existence of such close-by interferers can also result in large ICI correlation across receive antennas, reducing the diversity of the array. Consequently, as α increases the benefits of receive diversity reduces. To combat such negative effect one way is to increase the number of receive antennas, which the results of Fig. 2.6 support it.

Impact of Deployment Densities and Multiplexing Gains

Fig. 2.7 (resp. Fig. 2.8) shows the coverage probability vs. λ_2 (resp. λ_1) when $\beta_2 = 2.5$ and $\beta_1 = 5$. Both of the figures confirm the accuracy of our analysis (see also Remark 2.3.2) for a wide range of deployment densities and multiplexing gains. Specifically, we notice that the relative gaps between the simulation result and the upper-bound and lower-bound are almost indistinguishable.

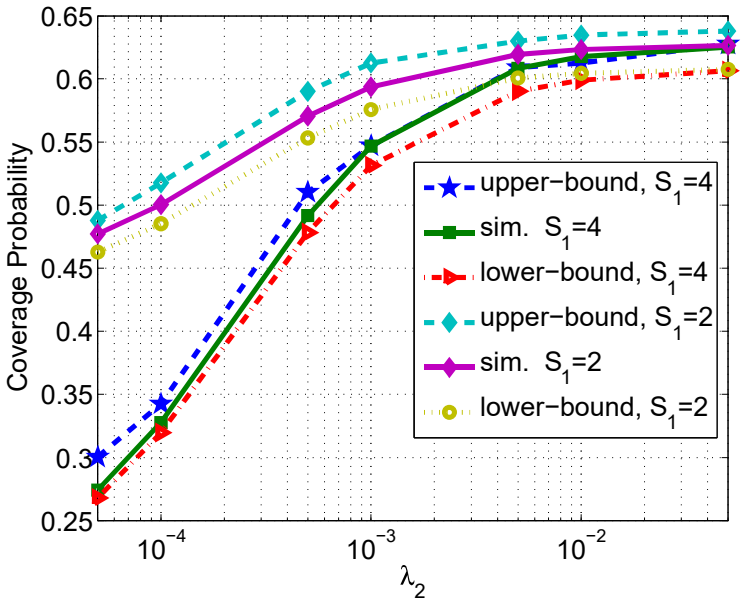

Figure 2.7: Coverage probability *vs.* λ_2 when $\lambda_1 = 10^{-4}$. Parameters are: $N^r = 8$, $S_2 = 2$, $\sigma^2 = 10^{-10}$, $\beta_2 = 2.5$ and $\beta_1 = 5$.

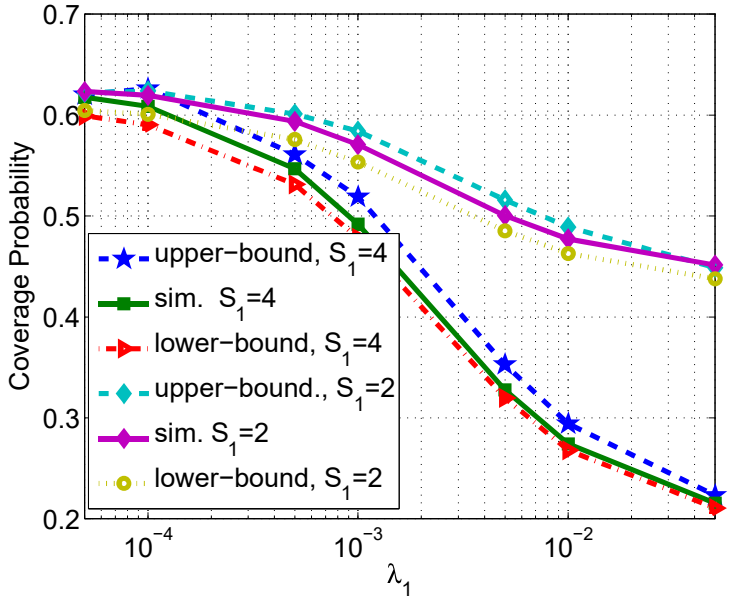

Figure 2.8: Coverage probability *vs.* λ_1 when $\lambda_2 = 5 \times 10^{-3}$. Parameters are: $N^r = 8$, $S_2 = 2$, $\sigma^2 = 10^{-10}$, $\beta_2 = 2.5$ and $\beta_1 = 5$.

On the other hand, both of the figures show that by increasing the multiplexing gains in Tier 1, the coverage probability declines, which is also predicted by Proposition 2.5. This is because by growing S_1 it becomes less likely to simultaneously decode all the transmitted streams successfully. Yet, from Fig. 2.7 and Fig. 2.8, we obviously recognize that the reduced coverage probability by the growth of S_1 depends on the deployment densities. In fact, Fig. 2.7 reveals that the detrimental effect of increasing S_1 can be entirely compensated for by substantially densifying Tier 2. This is an important observation, as it implies that densifying Tier 2 allows the growth of multiplexing gain in Tier 1 without undermining the coverage probability. This is because, by increasing λ_2 the typical UE will be more probably associated with a BS from Tier 2, and the resultant association will be probably successful due to its small multiplexing gain.

However, from Fig. 2.8 we observe that if one is to increase the multiplexing gain of Tier 1, this is not recommended if this tier is to be densified too. As seen, only when Tier 1 is

sparse increasing its multiplexing gain is rather harmless to the coverage probability.

Comparison with Grid Layout and the Closest-BS CA rule

In this part, we compare the coverage performance under PPP model with the max-SINR CA rule with the grid layout and also the PPP model with the closest-BS CA rule. Regarding the grid layout, we position the BSs of Tier 2 in accordance to the PPP model, but the BSs of Tier 1 is positioned according to a hexagonal layout. The number of BSs of Tier 1, and thus the associated cell coverage of each BS, is then obtained based on density λ_1. On the other hand, under the closest-BS CA rule we let UEs attach to the closest BS.

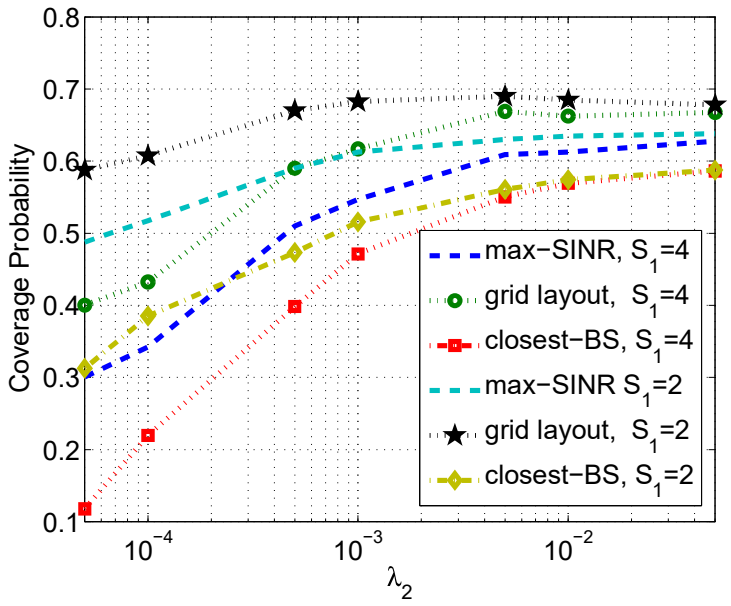

Figure 2.9: Coverage probability *vs.* λ_2 when $\lambda_1 = 10^{-4}$. Parameters are: $N^r = 8$, $S_2 = 2$, $\sigma^2 = 10^{-10}$, $\beta_2 = 2.5$ and $\beta_1 = 5$.

In Fig. 2.9 and Fig. 2.10, we demonstrate the results. As seen from both figures, the PPP model underestimates the coverage performance of the grid layout, where the gap reduces by growing the density. The curves demonstrate the consistency of PPP model in predicting the pattern observed under the grid layout for different multiplexing gains and also density

of BSs.

On the other hand, the max-SINR CA rule outperforms the closest-BS CA rule where the performance gap is more appreciable when the density of BSs is small. In fact, by growing the density both CA rules converge as with higher probability the BS that provides the maximum SINR is also the closest BS.

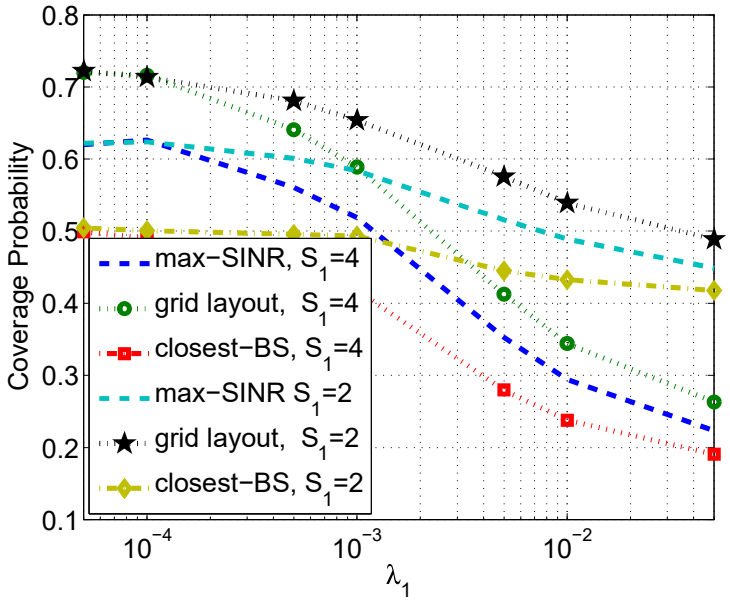

Figure 2.10: Coverage Probability *vs.* λ_2 when $\lambda_1 = 10^{-4}$. Parameters are: $N^r = 8$, $S_2 = 2$, $\sigma^2 = 10^{-10}$, $\beta_2 = 2.5$ and $\beta_1 = 5$.

Impact of Noise

In Fig. 2.11, we study the impact of noise power on the coverage probability. We observe that our analysis predicts the coverage probability very accurately. In this illustration we also include "No-Noise" scenario obtained from Proposition 2.6.1. As seen, for as larger as $\sigma^2 = 10^{-6}$ (resp. $\sigma^2 = 10^{-4}$) the operating regime is accurately representable by the interference-limited system (see Section 2.6) when $\lambda_1 = 10^{-4}$ (resp. $\lambda_1 = 10^{-3}$).

Remark 2.7.1. *Regarding the observation made from Fig. 2.11, we, therefore, in the rest*

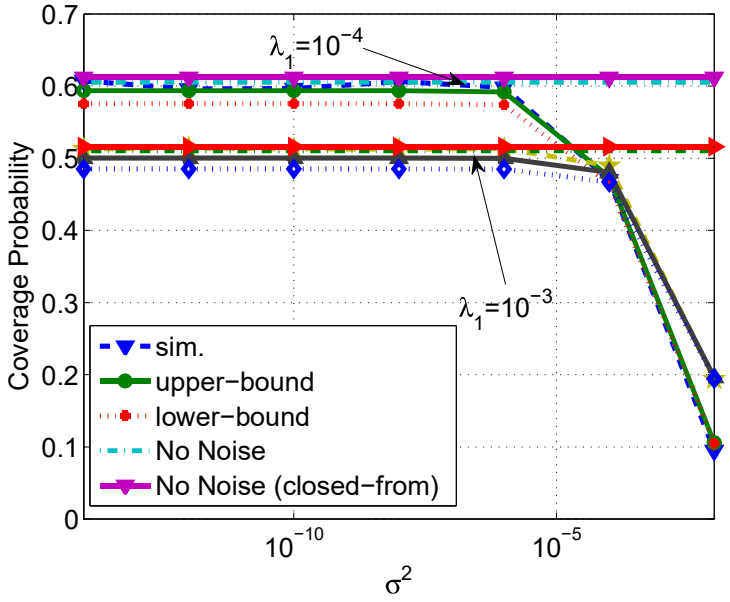

Figure 2.11: Coverage probability *vs.* σ^2. Parameters are: $S_1 = 2$, $S_2 = 2$, $\lambda_2 = 10^{-3}$, $\beta_1 = 5$, and $\beta_2 = 2.5$.

of this thesis generally discard the impact of noise, and assume that the operating point of the network is well modelled by the interference-limited system.

Remark 2.7.2 (Application to the Spectrum Sharing Systems). *The result of Fig. 2.11 is insightful, as it implies that sharing the cellular spectrum with other services such as D2D communications [9], [79] may not affect the coverage performance of MIMO HetNets as far as the power of the imposed inter-service interference—assuming is modelled as the background noise—does not exceed a threshold. Such a policy can substantially simplify the network management, as by knowing only a parameter—permissible noise power threshold—it is possible to decouple the management of cellular and D2D networks. However, such an approach requires modelling the effect of D2D network via background noise. In Section 2.9.1, we briefly look at this issue and discuss it with more details.*

2.8 Design Issues and Performance Evaluation

2.8.1 Optimizing the Accumulated Multiplexing Gains

Proposition 2.5.1 implies that the growth of the multiplexing gains can lead to a lower coverage probability (see also Fig. 2.8 and Fig. 2.7). Nevertheless, in some cases it is yet possible to increase the multiplexing gains subject to a given coverage constraint with respect to the diversity system, which according to Fig. 2.6 yields the maximum attainable coverage performance. In fact, one may desire to increase the multiplexing gains as much as possible subject to a coverage penalty against the diversity systems. Here, we look into such a design issue by deploying the following optimization problem:

$$O_1: \quad \max_{S_1,S_2}(S_1+S_2) \tag{2.129}$$

$$s.t. \quad c^{\mathrm{SIMO}} - c^{\mathrm{ZF}} \leq \xi_1, \tag{2.130}$$

where the objective is the total number of transmitted data streams in the network. Threshold ξ_1 stands for the maximum permissible coverage loss against the SIMO counterpart system due to the growth of the multiplexing gains. In Fig. 2.12, we show the numerical results of this optimization problem when $\xi_1 = 0.05$ for several values of the deployment densities. Interestingly, we observe that one can still practice MIMO communications with large multiplexing gains across tiers without undermining the coverage probability. But, inline with what Fig. 2.7 and Fig. 2.8 also imply, it is important to choose multiplexing gains across tiers judiciously according to deployment densities. Specifically, Fig. 2.12-(a) demonstrates that by growing λ_2, it is possible to increase S_1. However, if one densifies Tier 1 too, the permissable S_1 should be smaller, so that the high value of S_1 is only suitable when Tier 2 is super dense. On the other hand, Fig. 2.12-(b) indicates that it is ill-advised to simultaneously grow density of Tier 2 and its multiplexing gain. Moreover, by densifying Tier 1, the multiplexing gain in Tier 2 should decrease. In effect, when the multiplexing

gain of a tier increases, it is getting harder to preserve acceptable coverage probability, thus, one ought to densify the other tier to compensate for the induced loss. As a general rule of thumb, a recommended practice is to densify the tier that is practicing a lower multiplexing gain such that the sparser tier be able to transmit a larger number of data streams.

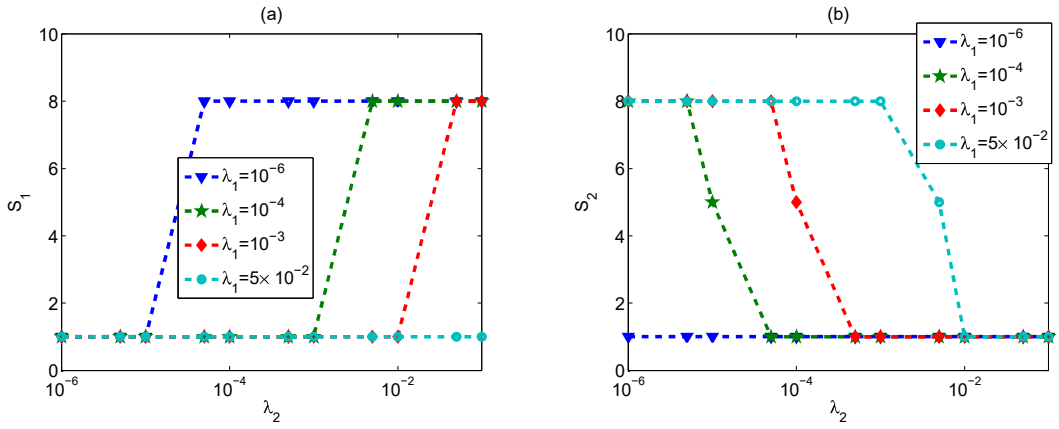

Figure 2.12: (a): Maximum number of data streams in Tier 1 *vs.* λ_2 that guarantees $c^{\text{SIMO}} - c^{\text{ZF}} \leq 0.05$. (b): Maximum number of data streams in Tier 2 *vs.* λ_2 that guarantees $c^{\text{SIMO}} - c^{\text{ZF}} \leq 0.05$. Parameters are: $N^r = 8$, $\sigma^2 = 10^{-10}$, $\beta_2 = 2.5$ and $\beta_1 = 5$.

2.8.2 Joint Optimization of Densities and SINR Thresholds

In Section 2.7, we stress the importance of proper system design pursuing densification with accordance to the SINR thresholds. Accordingly, it is appealing to inspect if it is possible to optimally choose the SINR thresholds and deployments densities, subject to a prescribed coverage requirement. Here, for an illustrative example, we seek such a design issue by solving the following optimization problem:

$$O_2: \quad \max_{\beta_1 \geq 1, \beta_2 \geq 1, \lambda_1 \geq 0, \lambda_2 \geq 0} \sum_{i=1}^{2} \lambda_i S_i c_i^{\text{ZF}} \log(1+\beta_i) \tag{2.131}$$

$$s.t. \quad c^{\text{ZF}} \geq \xi_2, \tag{2.132}$$

$$\lambda_{\min} \leq \lambda_i \leq \lambda_{\max}, \quad i = 1, 2. \tag{2.133}$$

In O_2, the objective function is ASE, see also [56]. ASE is an essential performance metric which indicates efficiency of spectral usage throughout the coverage area of a wireless network. The data rate that a BS of Tier i can support a covered UE with $S_i \log(1+\beta_i)$. This is because when UE is covered all the transmitted data streams are recoverable successfully. On the other hand, ξ_2 is the coverage probability constraint; $\lambda_{\min}$ and $\lambda_{\max}$ are respectively the minimum and maximum allowable deployment densities. Note that in this formulation we enforce $\beta_i \geq 1$, to insure that the coverage probability is accurately predictable by our analysis.

In Fig. 2.13,[3] we depict the best deployment densities for various multiplexing gains when $\lambda_{\min} = 10^{-7}$ and $\lambda_{\max} = 10$. Here, we set $\xi_2 = 0.9$. As it is seen from Fig. 2.13-(a), by growing S_1 the best policy is to reduce the density of Tier 1. Furthermore, by increasing S_2 the network can accommodate a denser Tier 1. On the other hand, Fig. 2.13-(b) implies that by growing S_1 the best policy is to increase the density of Tier 2, while by the growth of S_2 the suitability of densification in Tier 2 reduces. These results can be explained by noticing that by the growth of the multiplexing gain in a tier, the associated coverage probability can decrease. So, to preserve the required coverage probability it is advisable to densify the other tier while keeping its associated multiplexing gain as small as possible. This allows many UEs seek association with the densified tier, which is more probable to be fruitful.

In Fig. 2.14,[4] we demonstrate the best SINR thresholds for various values of multiplexing gains. It is seen that in many cases, close to minimum acceptable SINR thresholds are quite sufficient. This is because for the smaller values of SINR thresholds it is more probable to preserve the coverage requirements. Nevertheless, since ASE (the objective function of O_2) may also grow by increasing SINR thresholds, Fig. 2.14 shows that for some particular combinations of multiplexing gains it is possible to increase β_is.

Note that although we devise the optimization problem O_2 with the SINR thresholds as

[3]Here optimal densities stand for the deployment densities that are corresponding to the maximum value of objective function of (2.131).

[4]Here optimal SINR thresholds stand for the SINR thresholds that are corresponding to the maximum value of objective function of (2.131).

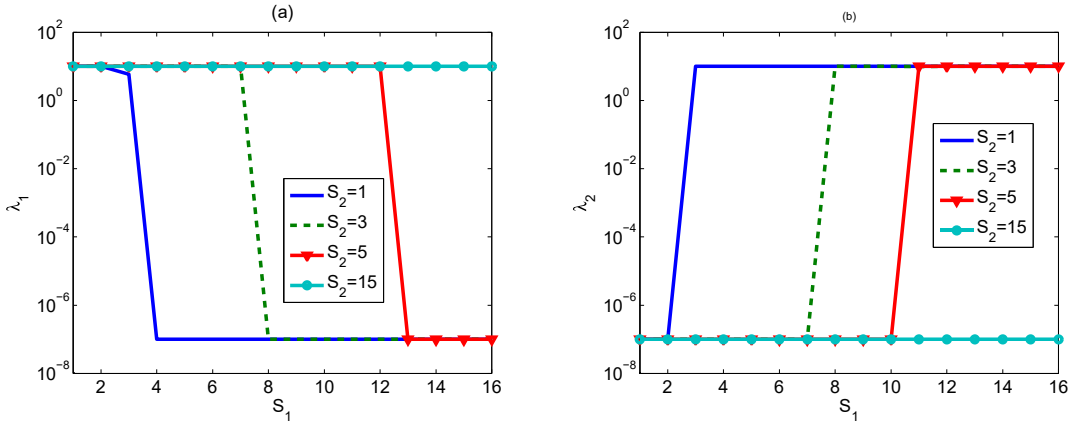

Figure 2.13: (a): Optimal λ_1 *vs.* S_1, (b): Optimal λ_2 *vs.* S_2, when $N^r = 16$.

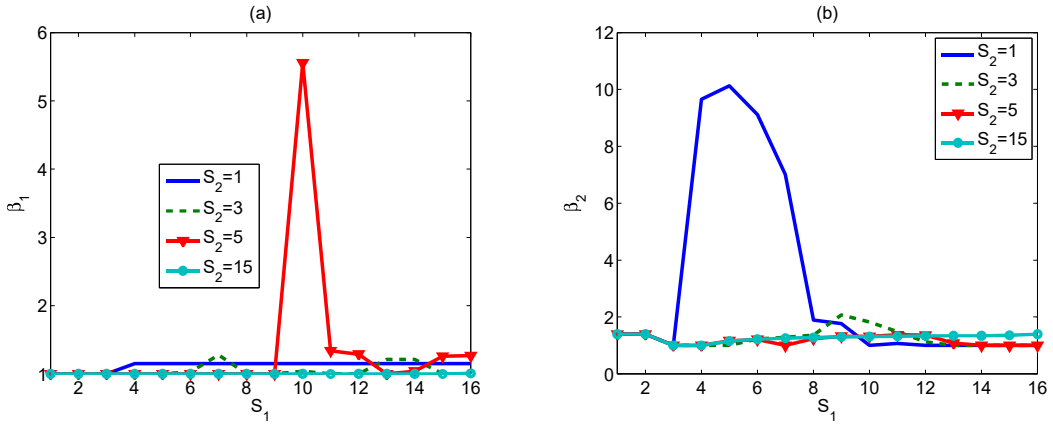

Figure 2.14: (a): Optimal β_1 *vs.* S_1, (b): Optimal β_2 *vs.* S_2, when $N^r = 16$.

variables, referring to Remark 2.2.5 one may assume β_is are given and solve the optimization problem to derive the best offloading biases.

We should highlight that both optimization problems $\mathcal{O}_1$ and $\mathcal{O}_2$ promote the network-level design. The deployment densities, which are basically the average number of BSs per unit area of the network, should be known (for the case of optimization problem $\mathcal{O}_1$) or desired to be known (for the case of optimization problem $\mathcal{O}_2$). Furthermore, for the design problem $\mathcal{O}_2$ if the network is already deployed (densities are given), one can treat the obtained densities obtained by solving $\mathcal{O}_2$ to specify the percentage of active BSs.

2.8.3 Design of Feedback Capacity

The provided coverage probability in our analysis can actually be interpreted as the CCDF of effective SINR. Consequently, it could be exploited to understand the capacity performance of the network *viz.* spatial throughput (ST), which measures the scheduled data rate per unit area. We formulate ST as

$$\eta^{\mathrm{ZF}} \triangleq \sum_{i} \lambda_i \overline{R}_i^{\mathrm{ZF}}, \tag{2.134}$$

where $\overline{R}_i^{\mathrm{ZF}}$ is the expected rate at the typical UE received from a BS in Tier i. However, for the serving BS x_i to estimate affordable data rate $\overline{R}_i^{\mathrm{ZF}}$, there must be feedback channel between UEs and their serving BS. Taking the capacity of the feedback channel into account and assuming Gaussian signaling, one may formulate $\overline{R}_i^{\mathrm{ZF}}$ as the following

$$\overline{R}_i^{\mathrm{ZF}} = S_i \mathbb{E} \log \left(1 + \mathcal{Q}_i \left(\max_{x_i \in \Phi_i} \min_{l_i = 1, \ldots, S_i} \mathrm{SINR}_{x_i, l_i}^{\mathrm{ZF}}, B_i \right) \right), \tag{2.135}$$

where the expectation operates over the SINRs. Since the typical UE is in coverage if all the data streams are received successfully and the transmission power is uniformly shared among data streams, $\overline{R}_i^{\mathrm{ZF}}$ is thus proportionally increased by the multiplexing gain S_i. In (2.135), B_i is the feedback capacity in bits per frame designated to each BS of Tier i (note that we assume that only one UE is served per each frame). Furthermore, $\mathcal{Q}_i(., B_i)$ is the scaler quantization function employed at the UEs to quantize the estimated SINR values—assuming the estimated values equal to the experienced ones—by B_i bits before feeding back the resultant to the serving BS. For the quantization purpose, consider 2^{B_i} quantization thresholds $\hat{\gamma}_{q_i,i} < \hat{\gamma}_{q_i+1,i}$ so that $\hat{\gamma}_{0,i} = \beta_i$ and $\hat{\gamma}_{2^{B_i},i} = \hat{\gamma}_{\max,i}$. Here, we assume that the quantization thresholds and $\hat{\gamma}_{\max,i}$ are pre-specified, based on PHY layer particulars including modulation and coding methods. We in the rest of this part simply assume that $\hat{\gamma}_{\max,i} = 1000$ $\forall i$, and assume the quantization thresholds are uniformly distributed. We set $\hat{\gamma}_{0,i} = \beta_i \geq 1$, thus the typical UE must be in the coverage in order to receive data.

Using Shannon capacity formula [14], (2.135) is simplified to

$$\overline{R}_i^{\mathrm{ZF}} = S_i \sum_{q_i=0}^{2^{B_i}-1} \left[\mathbb{P}\left\{ \max_{x_i \in \Phi_i} \min_{l_i=1,\ldots,S_i} \mathrm{SINR}_{x_i,l_i}^{\mathrm{ZF}} \geq \hat{\gamma}_{q_i,i} \right\} - \right.$$

$$\left. \mathbb{P}\left\{ \max_{x_i \in \Phi_i} \min_{l_i=1,\ldots,S_i} \mathrm{SINR}_{x_i,l_i}^{\mathrm{ZF}} > \hat{\gamma}_{q_i+1,i} \right\} \right] \log(1+\hat{\gamma}_{q_i,i}). \tag{2.136}$$

Using (2.136), ST defined in (2.134) is ultimately formulated as

$$\eta^{\mathrm{ZF}} = \sum_i \lambda_i S_i \sum_{q_i=0}^{2^{B_i}-1} \left[\mathbb{P}\left\{ \max_{x_i \in \Phi_i} \min_{l_i=1,\ldots,S_i} \mathrm{SINR}_{x_i,l_i}^{\mathrm{ZF}} \geq \hat{\gamma}_{q_i,i} \right\} \right.$$

$$\left. -\mathbb{P}\left\{ \max_{x_i \in \Phi_i} \min_{l_i=1,\ldots,S_i} \mathrm{SINR}_{x_i,l_i}^{\mathrm{ZF}} > \hat{\gamma}_{q_i+1,i} \right\} \right] \log(1+\hat{\gamma}_{q_i,i}), \tag{2.137}$$

Now, using Proposition 2.6.1, we are able to suggest the following approximation (recall that Proposition 2.6.1 provides an upper-bound on the coverage probability) of ST:

$$\eta^{\mathrm{ZF}} \approx \frac{2\pi}{\tilde{C}(\alpha)} \sum_{i \in \mathcal{K}} \frac{\lambda_i^2 S_i \left(\frac{P_i}{S_i^2}\right)^{\check{\alpha}} \left(\Gamma_i^{\mathrm{ZF}}\right)^{S_i}}{\sum_{j \in \mathcal{K}} \lambda_j \left(\frac{P_j}{S_j}\right)^{\check{\alpha}} \left(\frac{\Gamma(\frac{\check{\alpha}}{S_i}+S_j)}{\Gamma(S_j)}\right)^{S_i}} \sum_{q_i=0}^{2^{B_i}-1} (\hat{\gamma}_{q_i,i}^{-\check{\alpha}} - \hat{\gamma}_{q_i+1,i}^{-\check{\alpha}}) \log(1+\hat{\gamma}_{q_i,i}). \tag{2.138}$$

In Fig. 2.15 and Fig. 2.16, we show plots of ST vs. B_1 and B_2 for several settings of the deployment densities and multiplexing gains. As seen, by growing feedback capacity in each tier the ST proportionally increases before it reaches the plateau, which is partially due to parameters $\hat{\gamma}_{\max,i}$. For the case that $B_1 = B_2 = 1$, ST reduces to ASE [56]. Interestingly, we observe that by designating up to 8 bits feedback capacity per tier per frame, it is possible to boost the ST by more that 180% over the conventional scenario of 1-bit per frame per BS (i.e., the ASE performance).

On the other hand, comparing Fig. 2.15 and Fig. 2.16 we further observe that densification of Tier 1 may not necessarily add to the growth of ST. In fact, for the case that $S_1 = 2$,

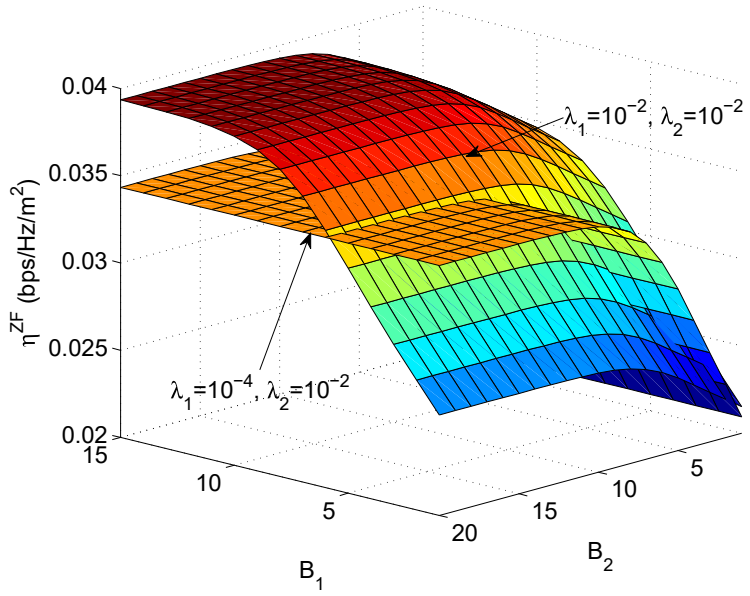

Figure 2.15: ST *vs.* B_1 and B_2 for $\beta_1 = \beta_2 = 5$, and $S_1 = S_2 = 2$.

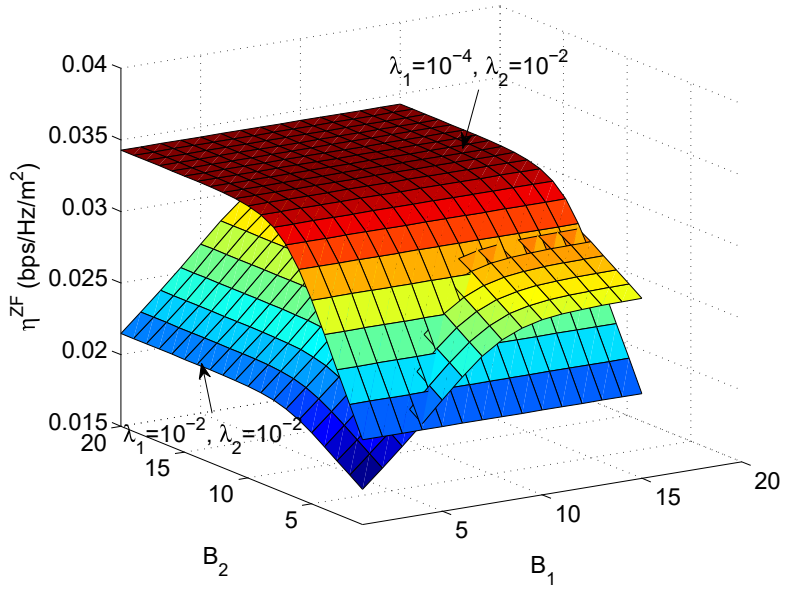

Figure 2.16: ST *vs.* B_1 and B_2 for $\beta_1 = \beta_2 = 5$, $S_1 = 6$ and $S_2 = 2$.

densifying Tier 1 boosts ST by nearly 147% (see, Fig. 2.15), while when $S_1 = 6$, it reduces ST almost by the same figure.

2.9 Extensions of the Analysis

Here we primarily aim at demonstrating how the above analysis can be exploited to discuss several relevant MIMO communication scenarios in HetNets. Further, our analysis in this section demonstrates that

- It is possible to decouple the design of HetNets from underlying spectrum sharing services, simply by adjusting equivalent noise power at the UEs and tuning the parameters of spectrum sharing system to produce the adjusted noise power;
- How to adjust CA parameters, e.g., the number of pilots and the way that is distributed across tiers, from a network level perspective.

2.9.1 Inclusion of Spectrum Sharing

In Remark 2.7.2, we highlight that one may exploit the analysis of this thesis to simplify the design of spectrum sharing scenarios, e.g., underlay D2D communications. To be able to do so, the prerequisite is that the contribution of D2D services be modelled through proper AWGN. In this section we firstly derive the coverage probability in a spectrum sharing environment by adopting the same models usually considered in the literature [79, 81, 167]. We then demonstrate how the analysis can be exploited to estimate the equivalent AWGN power.

Consider the structure shown in Fig. 2.17. Let us assume there are Q services, indexed by q, sharing the spectrum with HetNets in underlay mode. In [9], different scenarios of spectrum sharing in D2D networks are discussed. We denote λ_q and P_q as the density and transmission power of service q, respectively. Assume PPP $\Psi_q = z_q$ stands for the location

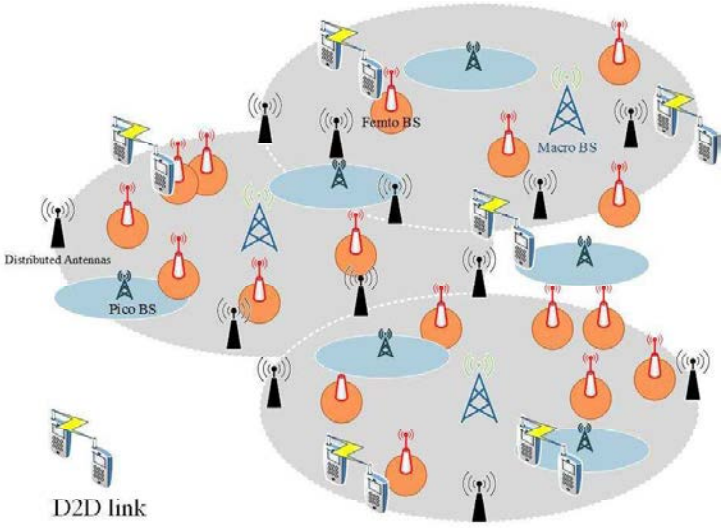

Figure 2.17: An illustration of a scenario where downlink HetNet is shared with a single D2D service in underlay setting.

of transmitter devices of service q. Denote $\Psi = \{\Psi_q\}_q$, and assume Ψ_qs are independent of each other. Moreover, let Ψ, Φ_U, Φ be mutually independent. We then denote W_{z_q,l_i} as the effective channel power gain between device z_q and the typical UE on stream l_i, which, for the sake of generality, is assumed to be chi-squared with M_q DoF. The post-processing SINR in (2.3) is then rewritten as

$$\mathrm{SINR}^{\mathrm{ZF}}_{x_i,l_i} = \frac{\frac{P_i}{S_i}\|x_i\|^{-\alpha} H^{\mathrm{ZF}}_{x_i,l_i}}{I_{\mathrm{ICI}} + \sum_{q=1}^{Q} \sum_{z_q \in \Psi_q} P_q \|z_q\|^{-\alpha} W_{z_q,l_i} + \sigma_i^2},$$

where I_{ICI} is the ICI, i.e., the interference contribution of cellular services; W_{z_q,l_i} is the effective channel power gain between transmitter z_q and the typical UE on stream l_i. The second term in the denominator represents the inter-service interference. Define

$$\Upsilon \triangleq \sum_q \lambda_q P_q^{\check{\alpha}} \frac{\Gamma(M_q + \check{\alpha})}{\Gamma(M_q)}. \tag{2.139}$$

Therefore, applying the method developed in the proof of Proposition 2.3.2, we can show

that the coverage probability is upper-bounded by

$$c^{\mathrm{ZF}} = \sum_{i\in\mathcal{K}} 2\pi\lambda_i \int_0^\infty r_i \mathbb{E}_\Psi \mathbb{E}_\Phi \prod_{l_i=1}^{S_i} \mathbb{P}\left\{\mathrm{SINR}^{\mathrm{ZF}}_{x_i,l_i} \geq \beta_i \middle| \Phi, \Psi\right\} \mathrm{d}r_i \tag{2.140}$$

$$= \sum_{i\in\mathcal{K}} 2\pi\lambda_i \int_0^\infty r_i \mathrm{d}r_i \int_0^\infty \ldots \int_0^\infty e^{-\beta_i \frac{S_i}{P_i} r_i^\alpha \sigma_i^2 \sum\limits_{l_i=1}^{S_i} t_{l_i}} \prod_{l_i=1}^{S_i} \mathcal{L}^{-1}_{\overline{F}_{H_i^{\mathrm{ZF}}}}(t_{l_i}) \mathrm{d}t_{l_i} \left(\prod_{j\in\mathcal{K}} \mathbb{E}_{\Phi_j} \prod_{x_j\in\Phi_j/x_i} \right.$$
$$\left. \times \mathbb{E}_{G^{\mathrm{ZF}}_{x_j}} e^{-\beta_i \frac{S_i}{P_i} r_i^\alpha \frac{P_j}{S_j} \|x_j\|^{-\alpha} \sum\limits_{l_i=1}^{S_i} G^{\mathrm{ZF}}_{x_j,l_i} t_{l_i}} \right) \left(\prod_{q=1}^{Q} \mathbb{E}_{\Psi_q} \prod_{z_q\in\Psi_q} \right.$$
$$\left. \times \mathbb{E}_{W_{z_q}} e^{-\beta_i \frac{S_i}{P_i} r_i^\alpha P_q \|z_q\|^{-\alpha} \sum\limits_{l_i=1}^{S_i} W_{z_q,l_i} t_{l_i}} \right) \tag{2.141}$$

$$= \sum_{i\in\mathcal{K}} 2\pi\lambda_i \int_0^\infty r_i \mathrm{d}r_i \int_0^\infty \ldots \int_0^\infty e^{-\beta_i \frac{S_i}{P_i} r_i^\alpha \sigma_i^2 \sum\limits_{l_i=1}^{S_i} t_{l_i}}$$
$$\times \prod_{l_i=1}^{S_i} \mathcal{L}^{-1}_{\overline{F}_{H_i^{\mathrm{ZF}}}}(t_{l_i}) \mathrm{d}t_{l_i} e^{-r_i^2 \left(\frac{S_i^2\beta_i}{P_i}\right)^{\check{\alpha}} \frac{\Lambda(\boldsymbol{S})+\Upsilon}{S_i} \sum\limits_{l_i=1}^{S_i} t_{l_i}^{\check{\alpha}}} \tag{2.142}$$

$$= \sum_{i\in\mathcal{K}} 2\pi\lambda_i \int_0^\infty e^{-\beta_i \frac{S_i^2}{P_i} r_i^\alpha \sigma_i^2} e^{-r_i^2 \left(\frac{S_i^2\beta_i}{P_i}\right)^{\check{\alpha}} (\Lambda(\boldsymbol{S})+\Upsilon)} \left(1 + \sum_{m_i=1}^{N^r-S_i} \sum_{m_i'=0}^{m_i} \frac{(-1)^{m_i'} \binom{m_i}{m_i'}}{m_i!} \times \right.$$
$$\left. \left(\beta_i \frac{S_i}{P_i} r_i^\alpha \sigma_i^2 \right)^{m_i-m_i'} \left[1 + \sum_{n=1}^{m_i'} \frac{\phi_n^{m_i'}}{n!} \left(\frac{S_i^2\beta_i}{P_i} \right)^{n\check{\alpha}} \frac{(\Lambda(\boldsymbol{S})+\Upsilon)^n}{S_i^n} r_i^{2n} \right] \right)^{S_i} r_i \mathrm{d}r_i. \tag{2.143}$$

Comparing (2.143) with Proposition 2.3.2, we can conclude that the coverage probability under spectrum sharing is straightforwardly derivable from Proposition 2.3.2 simply by replacing parameter $\Lambda(\boldsymbol{S})$ with $\Lambda(\boldsymbol{S}) + \Upsilon$.

On the other hand, for given value of Υ and background noise σ_i^2, we can exploit (2.143) and Proposition 2.3.2 to derive the equivalent AWGN contribution of inter-service interference, denoted by σ^2, which is unknown. One can simply devise an equation as (2.143)=(2.37), and then solve it for σ^2. This calculation allows to map the contribution of spectrum sharing devices through AWGN, without affecting the accuracy of the coverage analysis.

2.9.2 Coverage Performance under Nonhomogeneous Path-Loss Exponents

Here, we derive the coverage probability when path-loss exponents are nonhomogeneous. Let us denote α_j as the path-loss exponent associated with Tier j. Further, define $\check{\alpha}_j = 2/\alpha_j$. We first introduce parameter $Y_j(\alpha_i, \alpha_j)$ defined as

$$Y_j(\alpha_i, \alpha_j) \triangleq \lambda_j r_i^{2\frac{\alpha_i}{\alpha_j}} \left(\frac{S_i^2 \beta_i}{P_i}\right)^{\check{\alpha}_j} \left(\frac{P_j}{S_j}\right)^{\check{\alpha}_j} \frac{\Gamma(S_j + \check{\alpha}_j)}{S_i \Gamma(S_j)}. \tag{2.144}$$

Now, under nonhomogeneous path-loss model the expression (2.48) can be shown to be upper-bounded as

$$c^{\mathrm{ZF}} \leq \sum_{i \in \mathcal{K}} 2\pi\lambda_i \int_0^\infty r_i \mathrm{d}r_i \left(\int_0^\infty e^{-\beta_i \frac{S_i}{P_i} r_i^{\alpha_i} \sigma_i^2 t_i} \mathcal{L}^{-1}_{\overline{F}_{H_i^{\mathrm{ZF}}}}(t_i) e^{-\sum\limits_j Y_j(\alpha_i,\alpha_j) t_i^{\check{\alpha}_j}} \mathrm{d}t_i \right)^{S_i}. \tag{2.145}$$

Now analogous to (2.48), we should derive the inner integral through the following expression that requires the evaluation of higher-order differentiations:

$$\begin{aligned} \int_0^\infty e^{-\beta_i \frac{S_i}{P_i} r_i^{\alpha_i} \sigma_i^2 t_i} \mathcal{L}^{-1}_{\overline{F}_{H_i^{\mathrm{ZF}}}}(t_i) e^{-\sum\limits_j Y_j(\alpha_i,\alpha_j) t_i^{\check{\alpha}_j}} \mathrm{d}t_i \quad &= e^{-\beta_i \frac{S_i}{P_i} r_i^{\alpha_i} \sigma_i^2} e^{-\sum\limits_j Y_j(\alpha_i,\alpha_j)} + \sum_{m_i=1}^{N^r - S_i} \frac{(-1)^{m_i}}{m_i!} \\ &\times \sum_{m_i'=0}^{m_i} \binom{m_i}{m_i'} \underbrace{\frac{d^{m_i - m_i'}}{dt_i^{m_i - m_i'}} e^{-\beta_i \frac{S_i}{P_i} r_i^{\alpha_i} \sigma_i^2 t_i}\Big|_{t_i=1}}_{T_1} \underbrace{\frac{d^{m_i'}}{dt_i^{m_i'}} e^{-\sum\limits_j Y_j(\alpha_i,\alpha_j) t_i^{\check{\alpha}_j}}\Big|_{t_i=1}}_{T_2}. \end{aligned} \tag{2.146}$$

The evaluation of T_1 in closed-form expression is straightforward. However, the evaluation of T_2 is substantially more involved than the counterpart term (2.49) corresponding the homogenous path-loss model. To calculate T_2 we apply [112, Brunos formula Eq. (16)] to obtain

$$\frac{d^{m_i'}}{dt_i^{m_i'}} e^{-\sum\limits_j Y_j(\alpha_i,\alpha_j) t_i^{\check{\alpha}_j}}\Big|_{t_i=1} = \mathcal{B}_{m_i'}\left(y_i^{(1)}, \ldots, y_i^{(m_i')}\right) e^{-\sum\limits_j Y_j(\alpha_i,\alpha_j)}, \tag{2.147}$$

in which

$$y_i^{(m)} = \frac{d^m}{dt_i^m} \sum_j Y_i(\alpha_i, \alpha_j) t_i^{\breve{\alpha}_j}|_{t_i=1} = \sum_j Y_i(\alpha_i, \alpha_j) \left(\prod_{n=0}^{m-1} (\breve{\alpha}_j - n) \right). \tag{2.148}$$

Here, $B_m(z_1, \ldots, z_m)$ is the nth complete Bell polynomial. Plugging this back into (2.146) and substituting the resultant into (2.145) along with some manipulations and rearrangements, we eventually derive the following expression for the coverage probability

$$\begin{aligned} c^{\mathrm{ZF}} \quad & \leq \sum_{i \in \mathcal{K}} 2\pi\lambda_i \int_0^\infty e^{-\beta_i \frac{S_i}{P_i} r_i^{\alpha_i} \sigma_i^2} e^{-\sum_j Y_j(\alpha_i, \alpha_j)} \left(1 + \sum_{m_i=1}^{N^r - S_i} \sum_{m_i'=0}^{m_i} \frac{(-1)^{m_i'} \binom{m_i}{m_i'}}{m_i!} \left(\beta_i \frac{S_i}{P_i} r_i^{\alpha_i} \sigma_i^2 \right)^{m_i - m_i'} \right. \\ & \left. \times \left[1 + \mathcal{B}_{m_i'} \left(\sum_j Y_i(\alpha_i, \alpha_j), \ldots, \sum_j Y_i(\alpha_i, \alpha_j) \left(\prod_{n=0}^{m_i'-1} (\breve{\alpha}_j - n) \right) \right) \right] \right)^{S_i} r_i \mathrm{d}r_i. \end{aligned} \tag{2.149}$$

This expression resonates the same for that does the homogenous path-loss model in (2.37). Nevertheless, in this case, as explicitly recognizable, the coverage probability is computationally very expensive due to the integration as well as the computation of Bell polynomial.

2.9.3 Coverage Probability of MIMO-ZFBF Multiplexing under Practical Max-SINR CA Rule

Regarding the discussion provided in Section 1.2.3, the max-SINR CA rule relies upon an idealistic assumption: in each communication frame that the network's status changes—due for instance to mobility, handoff, and fading/shadowing—UEs are assumed stayed associated with the *best* BS, which is selected out of the entire pool of BSs across all tiers. The best BS is the one that provides the maximum SINR on the link. But, to find this so-called best BS large number of measurements of the emitted pilot signals from all the BSs is required, which is an unrealistic assumption and imposes staggering complexities and ultimately depletes the resources. In effect, the entire frame time might be simply designated for merely the CA mechanism, and unfortunately nothing will be left for actual data transmission—zero spectral

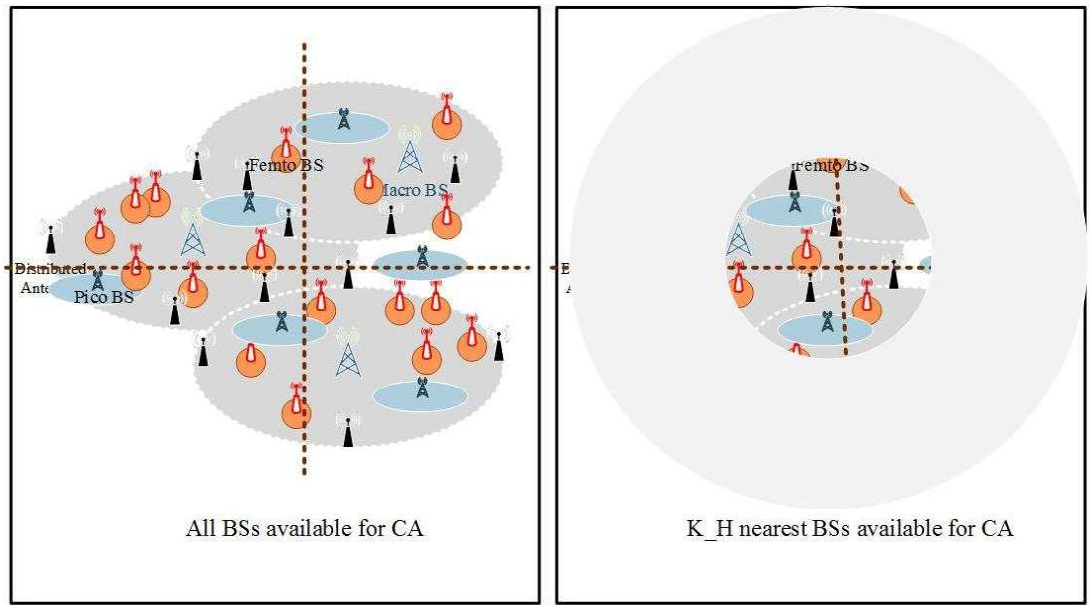

Figure 2.18: An illustration of limited max-SINR CA rule.

efficiency.

In practice however, UEs are advocated to check the feasibility of *a number of adjacent BSs for association* (see also Fig. 2.18). Accordingly, our goal in this section is to investigate the impact of practical CA rule on the performance of MIMO-ZFBF HetNets. To do this, we derive the coverage probability taking into account the maximum number of BSs across all tiers that UEs are allowed to assess for association, $K_H \geq 1$. This is inline with relevant issues dominating the practical scenarios, pilot's reuse factor, handoff rate, and network's resource constraints. Further, let $0 \leq n_i \leq K_H$ be the number of i-th tier pilots that the typical UE measures so that $\sum_i n_i = K_H$. We introduce set Φ_i^H as the index of BSs of tier i that UE assesses for CA procedure. Regarding the fact that in practice pilots corresponding to *nearby* BSs have a higher chance of being successfully detected, and network's configuration advocates handoff to adjacent cells rather far cells, set Φ_i^H is assumed to contain the n_i BSs nearest to the typical UE.

Accordingly, the typical UE is considered covered if $\mathcal{A}^{\mathrm{ZF}}$ is nonempty, where

$$\mathcal{A}^{\mathrm{ZF}} = \left\{ \exists i \in \mathcal{K} : \max_{x_i \in \Phi_i^H} \min_{l_i=1,\ldots,S_i} \mathrm{SINR}^{\mathrm{ZF}}_{x_i,l_i} \geq \beta_i \right\}. \tag{2.150}$$

Note that compared to (2.5) the maximization is over Φ_i^H. Thus, by increasing $K_H \to \infty$, so that $n_i \to \infty \ \forall i$, we have $\Phi_i^H \to \Phi_i \ \forall i$, which implies that the coverage of the network incrementally converges to the case that all BSs are available for CA.

Now, we derive the coverage probability under the devised max-SINR CA rule. Let $c^{\mathrm{ZF}} = \mathbb{P}\{\mathcal{A}^{\mathrm{ZF}} \neq \emptyset\}$ denote the coverage probability. To derive the coverage probability, we sort the BSs in Tier i such that $\|x_i^{(l)}\| \leq \|x_i^{(l+1)}\|$, where $x_i^{(l)}$ is the position of the lth closest BS to the origin. Note that r.v. $\pi\lambda_i \|x_i^{(l)}\|^2$ is distributed according to $2l$ chi-squared [121]. Thus, c^{ZF} can be lower-bounded as

$$\begin{aligned}
c^{\mathrm{ZF}} &= \sum_{i=1}^{K} \mathbb{E}\left[\sum_{x_i \in \Phi_i^H} 1\left(\min_{l_i=1,\ldots,S_i} \mathrm{SINR}^{\mathrm{ZF}}_{x_i,l_i} \geq \beta_i \right) \middle| \{\Phi_j^H\} \right] \\
&\overset{(a)}{\geq} \sum_{i=1}^{K} \mathbb{E}\left[\sum_{x_i \in \Phi_i^H} 1\left(\min_{l_i=1,\ldots,S_i} \mathrm{SINR}^{\mathrm{ZF}}_{x_i,l_i} \geq \beta_i \right) \middle| \Phi_i^H \right] \\
&\overset{(b)}{=} \sum_{i=1}^{K} \sum_{l=1}^{n_i} \mathbb{P}\left\{ \min_{l_i=1,\ldots,S_i} \mathrm{SINR}^{\mathrm{ZF}}_{x_i^{(l)},l_i} \geq \beta_i \right\} \\
&\overset{(c)}{\geq} \sum_{i=1}^{K} \sum_{l=1}^{n_i} \mathbb{P}\left\{ \min_{l_i=1,\ldots,S_i} \mathrm{SINR}^{\mathrm{ZF-FC}}_{x_i^{(l)},l_i} \geq \beta_i \right\} \\
&\overset{(d)}{=} \sum_{i=1}^{K} \sum_{l=1}^{n_i} \int_0^{\infty} f_{\chi^2_{2l}}(r_i) \mathbb{P}\left\{ H^{\mathrm{ZF}}_{i,\min} \geq \frac{\beta_i r_i^{\alpha/2} (I^{\mathrm{FC}} + \sigma_i^2)}{(\pi\lambda_i)^{\frac{\alpha}{2}} \frac{P_i}{S_i}} \right\} \mathrm{d}r_i \\
&\overset{(e)}{=} \sum_{i \in \mathcal{K}} \sum_{l=1}^{n_i} \overline{\sum_{i,\boldsymbol{k}}} \sum_{u=0}^{\tilde{S}_i(\boldsymbol{k})-1} \frac{2\pi\lambda_i (-1)^u S_i^{u+1} \Gamma(\tilde{S}_i(\boldsymbol{k}))}{\Gamma(S_i) u! \prod_{l=0}^{N^r - S_i} (l!)^{k_l}} \left(\psi^0_{0il} \right.
\end{aligned}$$

$$+\sum_{m_i=1}^{u}\sum_{m_i'=0}^{m_i}\frac{(-1)^{m_i'}}{m_i!}\binom{m_i}{m_i'}\left(\frac{\beta_i S_i\sigma_i^2}{(\pi\lambda_i)^{\frac{\alpha}{2}}P_i}\right)^{m_i-m_i'}\psi_{0il}^{m_i-m_i'}$$

$$+\sum_{m_i=1}^{u}\sum_{m_i'=0}^{m_i}\sum_{n=1}^{m_i'}\frac{(-1)^{m_i'}\binom{m_i}{m_i'}(\Lambda^{\mathrm{FC}})^n\phi_n^{m_i'}\psi_{0il}^{m_i-m_i'}}{m_i!n!\left(\frac{S_i\beta_i}{(\pi\lambda_i)^{\frac{\alpha}{2}}P_i}\right)^{-n\check{\alpha}}\left(\frac{\beta_i S_i\sigma_i^2}{(\pi\lambda_i)^{\frac{\alpha}{2}}P_i}\right)^{m_i'-m_i}}\Bigg),$$

where the inequality in Step (a) is because un-conditioning reduces the probability of an event, Step (b) is because at most n_i candidate BSs in Tier i are available for CA procedure, Step (c) is obtained by using the FC assumption, Step (d) is because the distance to the lth associative BS from Tier i is a chi-squared r.v. with $2l$ DoF [121], and Step (e) is based on the proof of Proposition 2.4. Here parameter ψ_{nil}^m is defined as

$$\psi_{nil}^m \triangleq \int_0^\infty f_{\chi^2_{2l}}(r_i)r_i^{m\alpha+2n+1}e^{-\frac{\beta_i S_i^2 r_i^{\alpha/2}\sigma_i^2}{(\pi\lambda_i)^{\frac{\alpha}{2}}P_i}}e^{-\frac{r_i}{\pi\lambda_i}\left(\frac{S_i^2\beta_i}{P_i}\right)^{\check{\alpha}}\Lambda^{\mathrm{FC}}}\mathrm{d}r_i.$$

The final result has a similar composition to the lower-bound (2.57). One then can select best K_H and n_is by maximizing c^{ZF} for given density of BSs and multiplexing gains.

Note that this practical CA model is still simplistic. In practice one can include the power of pilots, as weak pilots may not be detectable at UEs. Further, the share of power at the BSs for pilot transmission phase and signal transmission phase should be included too.

2.9.4 Other MIMO Techniques

The main focus of this chapter is on the evaluation of coverage performance in open-loop ZFBF multiplexing systems. However, as mentioned in Remark 2.2.2, the analysis is general enough and can be adopted to predict the coverage performance of other particular examples of MIMO systems. In this section, we provide instances to demonstrate how the derived analytical results in Section 2.6 can be employed to predict the coverage probability of other HetNets. For simplicity, here we only consider interference-limited scenario.

Single-Input Multiple-Output (SIMO) Systems

For the SIMO systems, we set $S_i = 1$, $\forall i$. Proposition 2.6.1 reduces to

$$c^{\text{SIMO}} = c^{\text{SISO}} \sum_{r=0}^{N^r-1} \frac{\Gamma(\breve{\alpha}+r)}{\Gamma(\breve{\alpha})\Gamma(1+r)}. \tag{2.151}$$

This is actually the coverage performance of single-stream MIMO-ZFBF (i.e., diversity system). Applying Kershaws inequality [62],[5] we observe that

$$\sum_{r=0}^{N^r-1} \left(r - 0.5 + \sqrt{\breve{\alpha}+0.25}\right)^{\breve{\alpha}-1} < \sum_{r=0}^{N^r-1} \frac{\Gamma(\breve{\alpha}+r)}{\Gamma(\breve{\alpha})\Gamma(1+r)} < \sum_{r=0}^{N^r-1} \left(r+0.5\breve{\alpha}\right)^{\breve{\alpha}-1} \tag{2.153}$$

or equivalently

$$\int_0^{N^r-1} \left(x - 0.5 + \sqrt{\breve{\alpha}+0.25}\right)^{\breve{\alpha}-1} \mathrm{d}x \lessapprox \sum_{r=0}^{N^r-1} \frac{\Gamma(\breve{\alpha}+r)}{\Gamma(\breve{\alpha})\Gamma(1+r)} \lessapprox \int_0^{N^r-1} \left(x+0.5\breve{\alpha}\right)^{\breve{\alpha}-1} \mathrm{d}x. \tag{2.154}$$

Therefore,

$$\frac{\alpha}{2}\left(N^r + \sqrt{\breve{\alpha}+0.25}\right)^{\breve{\alpha}-1} \lessapprox \frac{c^{\text{SIMO}}}{c^{\text{SISO}}} \lessapprox \frac{\alpha}{2}\left(N^r+0.5\breve{\alpha}\right)^{\breve{\alpha}-1} \tag{2.155}$$

This last expression indicates that

$$\frac{c^{\text{SIMO}}}{c^{\text{SISO}}} \propto (N^r)^{\breve{\alpha}} \tag{2.156}$$

which is an increasing function of N^r and decreasing function of path-loss exponent. This implies that the benefit of receive arrays in enhancing the coverage performance reduces when the path-loss exponent increases.

[5] Kershaws inequality:

$$\left(r - 0.5 + \sqrt{\breve{\alpha}+0.25}\right)^{s-1} < \frac{\Gamma(r+s)}{\Gamma(r+1)} < \left(r+0.5s\right)^{s-1} \tag{2.152}$$

Multiple-Input Single-Output (MISO) Systems

So far, we assumed that the CSIT is not available. However, some cases with CSIT known at the BSs can also be covered by our analysis. Let's consider a MISO system, where $N^r = 1$, and $S_i = 1$, $\forall i$, and assume that CSIT is available to the BSs for eigen beamforming, i.e., maximum ratio transmission (MRT) [16]. In such a system, assuming noise power is negligible, the SIR at the typical UE served by x_i is

$$\mathrm{SIR}_{x_i}^{\mathrm{MRT}} = \frac{P_i \|x_i\|^{-\alpha} H_{x_i}^{\mathrm{MRT}}}{\sum\limits_{j\in\mathcal{K}} \sum\limits_{x_j\in\Phi_j\setminus x_i} P_j \|x_j\|^{-\alpha} G_{x_j}^{\mathrm{MRT}}}, \tag{2.157}$$

where $H_{x_i}^{\mathrm{MRT}}$ and $G_{x_j}^{\mathrm{MRT}}$ are chi-squared with $2N_i^t$ DoF, and exponential r.v.s, respectively. Using Proposition 2.6.1, the coverage probability is thus

$$c^{\mathrm{MRT}} = \frac{\pi}{C(\alpha)} \frac{\sum_{i\in\mathcal{K}} \lambda_i \left(\frac{P_i}{\beta_i}\right)^{\check{\alpha}} \sum\limits_{m=0}^{N_i^t-1} \frac{\Gamma(\check{\alpha}+m)}{\Gamma(\check{\alpha})\Gamma(1+m)}}{\sum_{j\in\mathcal{K}} \lambda_j P_j^{\check{\alpha}}}. \tag{2.158}$$

We now observe that

$$\frac{c^{\mathrm{MRT}}}{c^{\mathrm{SISO}}} \leq \frac{\sum_{i\in\mathcal{K}} \lambda_i \left(\frac{P_i}{\beta_i}\right)^{\check{\alpha}} \sum\limits_{m=0}^{N_i^t-1} \frac{\Gamma(\check{\alpha}+m)}{\Gamma(\check{\alpha})\Gamma(1+m)}}{\sum_{i\in\mathcal{K}} \lambda_i \left(\frac{P_i}{\beta_i}\right)^{\check{\alpha}}}. \tag{2.159}$$

Using (2.159) we then have

$$\frac{c^{\mathrm{MRT}}}{c^{\mathrm{SISO}}} \propto \frac{\alpha}{2\Gamma(\alpha)} \frac{\sum_{i\in\mathcal{K}} \lambda_i \left(N_i^t \frac{P_i}{\beta_i}\right)^{\check{\alpha}}}{\sum_{i\in\mathcal{K}} \lambda_i \left(\frac{P_i}{\beta_i}\right)^{\check{\alpha}}}. \tag{2.160}$$

On the other hand, using (2.158) and (2.151) we can observe that

$$\frac{c^{\mathrm{MRT}}}{c^{\mathrm{SIMO}}} \propto \frac{\sum_{i\in\mathcal{K}} \lambda_i \left(\frac{N_i^t}{N^r} \frac{P_i}{\beta_i}\right)^{\check{\alpha}}}{\sum_{i\in\mathcal{K}} \lambda_i \left(\frac{P_i}{\beta_i}\right)^{\check{\alpha}}} \tag{2.161}$$

In practice, $N_i^t \geq N^r$, therefore we expect that

$$\frac{c^{\text{MRT}}}{c^{\text{SIMO}}} \geq 1, \tag{2.162}$$

which implies that eign-beamforming outperforms diversity system. This gain can be attributed to the CSIT.

MISO-SDMA Systems

Another example scenario in which the BSs have access to the CSIT, is the MISO-SDMA system. Let $N^r = 1$, and $S_i = 1, \forall i$. We further assume that each cell of tier i serves $U_i \leq N_i^t$ UEs adopting ZFBF at the transmitter (see [56, 114] for more information). Assuming a fixed transmit power, the SIR of the typical UE that is associated with BS x_i is

$$\text{SIR}_{x_i}^{\text{SDMA}} = \frac{\frac{P_i}{U_i}\|x_i\|^{-\alpha} H_{x_i}^{\text{SDMA}}}{\sum\limits_{j\in\mathcal{K}} \sum\limits_{x_j\in\Phi_j/x_i} \frac{P_j}{U_j}\|x_j\|^{-\alpha} G_{x_j}^{\text{SDMA}}}, \tag{2.163}$$

where $H_{x_i}^{\text{SDMA}}$ and $G_{x_j}^{\text{SDMA}}$ are both chi-squared r.v.s with $2(N_i^t - U_i + 1)$ and DoF of $2U_j$, respectively [56, 111]. Using Proposition 2.6.1, we then obtain (see also [168])

$$c^{\text{SDMA}} = \frac{\pi}{\tilde{C}(\alpha)} \frac{\sum_{i\in\mathcal{K}} \lambda_i \left(\frac{P_i}{U_i\beta_i}\right)^{\check{\alpha}} \sum\limits_{m=0}^{N_i^t - U_i} \frac{\Gamma(\check{\alpha}+m)}{\Gamma(\check{\alpha})\Gamma(1+m)}}{\sum_{j\in\mathcal{K}} \lambda_j (\frac{P_j}{U_j})^{\check{\alpha}} \frac{\Gamma(\check{\alpha}+U_j)}{\Gamma(U_j)}}. \tag{2.164}$$

2.10 Conclusions

This chapter dealt with a comprehensive analysis of the coverage performance of MIMO-ZFBF multiplexing HetNet when each multi-stream communication link is subject to noise, fading, and ICI. We specified our analysis for the max-SINR CA rule and successful reception of all of the transmitted data streams to declare coverage. Adopting PPP model, we derived an upper-bound and a lower-bound on the coverage probability. Our proposed expressions

of the coverage probability were easy-to-compute and explicitly captured impacts of various system parameters including densities of BSs, SIR thresholds, and multiplexing gains. The lower-bound was in a closed-form and very tight. We also proved that the lower-bound is achievable under the FC assumption. We then specified the coverage probability for the interference-limited system which admitted in closed-form.

We further demonstrated how the analysis of the chapter can be utilized to predict the coverage probability of some other pertinent MIMO systems, impact of practical CA, non-homogenous path-loss environment, and spectrum sharing systems.

Our analysis showed that 1) full correlation of ICI across data streams slightly reduces the coverage probability; 2) increasing multiplexing gains can reduce the coverage probability; and 3) MIMO multiplexing systems are well modelled by the interference-limited system.

We confirmed the accuracy of our analysis by the aid of simulations. We further studied a number of optimization problems demonstrating the relationship between densification and multiplexing gains. Our results demonstrate the importance of practicing densification with accordance to multiplexing gains as well as SINR thresholds. We also spotted a tradeoff between densification and multiplexing gain: if one is to increase the multiplexing gain in one tier, he is recommended to simultaneously densify the other tier.

Finally, we studied the spatial throughput of multiplexing systems when the quantized values of SINRs are made available at the serving BSs. Results demonstrated that by including feedback channels with capacity up to 8 bits per frame per BS, it is possible to increase the spatial throughput by nearly 180% over 1-bit feedback scenario.

Chapter 3

Analysis and Design of Multi-Stream MIMO-MRC Receivers in HetNets

3.1 Introduction

In the previous chapter, we explored the coverage probability of MMO-ZFBF multiplexing HetNets, and further explored various aspects of MIMO multiplexing systems. In Section 2.9.4, we also discussed the extension of the analysis to multi-user SDMA-ZFBF, MRT, and diversity systems. However, as we also discussed in Remark 2.2.2 ,the analysis is not directly applicable for the scenarios where the receiver suffers from intra-stream interference, which is the case of MRC multiplexing systems. Our main quest in this chapter is therefore to extend the analysis developed in the previous chapter to MIMO-MRC multiplexing systems.

We shall emphasize that despite the popularity and practical significance of MIMO-MRC for cellular communications, due to its simple implementation and near zero feedback overheads, its performance in HetNets has not yet investigated. Specifically, to our best knowledge, only [119] investigates the *stream-level coverage* analysis (which as we elaborated in Chapter 1 is not accurate) of MIMO-MRC multiplexing systems in a single-tier ad hoc network. For K-tier HenNets and under max-SINR CA rule, the *link-level coverage* probability of MIMO-MRC multiplexing system has not yet been explored.

Apart from the importance of such an extension, in this chapter, we enrich our system model to incorporate cases where UEs have partial CSIR, due to mobility and estimation error. This allows us to discuss the relationship between multiplexing, densification, and

CSI error estimation from a network-level perspective. This investigation demonstrates that as the CSIR estimation error grows the possible tradeoff rooms between densification and multiplexing gain shrinks.

For this model, we further obtain an easy-to-compute, tight upper-bound on the network coverage probability in closed-form. Our analytical results—supported by extensive simulation—provide significant practical insights on the impact of densification on the link-level coverage performance. We draw various relationships between densification and multiplexing gain in HetNets. Our results indicate that an increased CSI inaccuracy compromises the coverage advantage of multi-stream over single-stream systems.

We then demonstrate practical cases in which the high processing costs of ZFBF justifies using MRC, although ZFBF generally outperforms MRC in terms of coverage probability. We further provide quantitative insights on the coverage cost of adopting MRC compared to ZFBF, and techniques to control the shrinkage of coverage footprint.

We also analyze the cross-stream SIR correlation coefficient amongst multiple streams in a communication link. Our analysis provides quantitative insights on the impact of tiers' BSs density, path-loss exponent, CSI inaccuracy, and multiplexing gains on the SIR correlation among data streams.

Besides exploring the coverage probability of MIMO-MRC under FC assumption (see Section 2.4 for the definition), we in this chapter discuss another extreme correlation scenario: no SIR correlation (NC) assumption, whereby under it all data streams of a communication link are deemed to be entirely uncorrelated. We then show that the NC setting substantially over-estimates the coverage performance. Observing that the FC setting slightly underestimates the coverage probability reconfirms the conclusion that in multiplexing systems the data streams can be regarded as fully correlated.

The rest of the chapter is organized as follows. Section 3.2 presents the system model and Section 3.3 provides coverage evaluation. Section 3.4 investigates the SIR correlation and its impact on the coverage probability. The simulation results are provided in Section

3.6. Section 3.5 explores several insightful design issues, followed by conclusions in Section 3.7.

3.2 System Model and Assumptions

The network model in this chapter is similar to the one presented in Section 2.2. In the rest of this section, we only discuss the required upgrades regarding the MRC filter.

Here, we focus on the scenarios that only partial CSI is available at the receivers. As in [35, 169], the quantified measure for channel estimation error is considered to be the correlation coefficient between the actual fading channel coefficient and its estimated value as

$$\boldsymbol{H}_{x_i} = \sqrt{1-\epsilon_i^2}\,\widetilde{\boldsymbol{H}}_{x_i} + \epsilon_i \boldsymbol{E}_{x_i}, \tag{3.1}$$

where $\widetilde{\boldsymbol{H}}_{x_i}$ is the estimated channel which is a complex Gaussian random matrix with zero mean and identity covariance matrix; ϵ_i^2 measures the inaccuracy of channel estimation; and $\boldsymbol{E}_{x_i}$ is a complex Gaussian random matrix with zero mean and identity covariance matrix. Random matrices $\boldsymbol{E}_{x_i}$ and $\widetilde{\boldsymbol{H}}_{x_i}$ are assumed independent, e.g., in cases where CSI is estimated using a pilot-based MMSE [35, 169].

Similar to (2.1), for the typical UE associated with BS x_i transmitting S_i data streams, the received signal, $\boldsymbol{y}_{x_i} \in \mathbb{C}^{N^r \times 1}$, is:

$$\boldsymbol{y}_{x_i} = \|x_i\|^{-\frac{\alpha}{2}} \sqrt{1-\epsilon_i^2}\widetilde{\boldsymbol{H}}_{x_i}\boldsymbol{s}_{x_i} + \|x_i\|^{-\frac{\alpha}{2}}\epsilon_i \boldsymbol{E}_{x_i}\boldsymbol{s}_{x_i} + \sum_{j\in\mathcal{K}}\sum_{x_j\in\Phi_j\setminus x_0} \|x_i\|^{-\frac{\alpha}{2}}\boldsymbol{H}_{x_j}\boldsymbol{s}_{x_j}, \tag{3.2}$$

Note that here we exclude the impact of noise effect, which is supported by discussions presented in Section 2.7. The first term in (3.2) accounts for the useful signal, the second term represents the interference due to inaccuracy of CSI, and the last term is the ICI. At the receiver, MRC is adopted with decoding filter $\boldsymbol{U}_{x_i} = \boldsymbol{H}_{x_i} = [\boldsymbol{h}_{x_i,1} \dots \boldsymbol{h}_{x_i,S_i}]$ [119].

Post-processing SIR for data stream l_i is therefore

$$\mathrm{SIR}_{x_i,l_i}^{\mathrm{MRC}} = \frac{\frac{P_i}{S_i}\|x_i\|^{-\alpha}(1-\epsilon_i^2)\|\tilde{\boldsymbol{h}}_{x_i,l_i}\|^2}{\frac{P_i}{S_i\|x_i\|^{\alpha}}\left(\sum\limits_{l'\neq l_i}\frac{\|\tilde{\boldsymbol{h}}_{x_i,l_i}^{\dagger}\boldsymbol{h}_{x_i,l'}\|^2}{\|\tilde{\boldsymbol{h}}_{x_i,l_i}\|^2}+\epsilon_i^2\frac{\|\tilde{\boldsymbol{h}}_{x_i,l_i}^{\dagger}\boldsymbol{e}_{x_i,l_i}\|^2}{\|\tilde{\boldsymbol{h}}_{x_i,l_i}\|^2}\right)+\sum\limits_{j\in\mathcal{K}}\sum\limits_{x_j\in\Phi_j\setminus x_i}\frac{P_j}{S_j\|x_j\|^{\alpha}}\sum\limits_{l_j=1}^{S_j}\frac{\|\tilde{\boldsymbol{h}}_{x_i,l_i}^{\dagger}\boldsymbol{h}_{x_j,l_j}\|^2}{\|\tilde{\boldsymbol{h}}_{x_i,l_i}\|^2}}. \tag{3.3}$$

Let r.v. $H_{x_i,l_i}^{\mathrm{MRC}} \triangleq \|\tilde{\boldsymbol{h}}_{x_i,l_i}\|^2$ which is chi-squared with DoF $2N^r$; $\hat{H}_{x_i,l_i}^{\mathrm{MRC}} \triangleq \sum\limits_{l'\neq l_i}\frac{\|\tilde{\boldsymbol{h}}_{x_i,l_i}^{\dagger}\boldsymbol{h}_{x_i,l'}\|^2}{\|\tilde{\boldsymbol{h}}_{x_i,l_i}\|^2}$ which is also chi-squared with DoF $2(S_i-1)$; and $\tilde{H}_{x_i,l_i}^{\mathrm{MRC}} \triangleq \frac{\|\tilde{\boldsymbol{h}}_{x_i,l_i}^{\dagger}\boldsymbol{e}_{x_i,l_i}\|^2}{\|\tilde{\boldsymbol{h}}_{x_i,l_i}\|^2}$ which is an exponential r.v. Both $\hat{H}_{x_i,l_i}^{\mathrm{MRC}}$ and $\tilde{H}_{x_i,l_i}^{\mathrm{MRC}}$ are independent of $H_{x_i,l_i}^{\mathrm{MRC}}$. We further set $G_{x_j,l_i}^{\mathrm{MRC}} \triangleq \sum\limits_{l_j=1}^{S_j}\frac{\|\tilde{\boldsymbol{h}}_{x_i,l_i}^{\dagger}\boldsymbol{h}_{x_j,l_j}\|^2}{\|\tilde{\boldsymbol{h}}_{x_i,l_i}\|^2}$ which is also chi-squared with DoF $2S_j$ and independent of $\hat{H}_{x_i,l_i}^{\mathrm{MRC}}$, $\tilde{H}_{x_i,l_i}^{\mathrm{MRC}}$, and $H_{x_i,l_i}^{\mathrm{MRC}}$. Using the above notation, $H_{x_i,l_i}^{\mathrm{MRC}}$, $\hat{H}_{x_i,l_i}^{\mathrm{MRC}}$, $\tilde{H}_{x_i,l_i}^{\mathrm{MRC}}$, and $G_{x_j,l_i}^{\mathrm{MRC}}$, respectively stand for the channel power gains associated with the intending signal, the interference due to imperfect CSI estimation, the inter-stream interference caused by streams $l_i' \neq l_i$, and the ICI imposed by $x_j \neq x_i$ on the l_ith data stream. Post-processing SIR in (3.3) is then represented as

$$\mathrm{SIR}_{x_i,l_i}^{\mathrm{MRC}} = \frac{\frac{P_i}{S_i}\|x_i\|^{-\alpha}(1-\epsilon_i^2)H_{x_i,l_i}^{\mathrm{MRC}}}{\frac{P_i}{S_i}\|x_i\|^{-\alpha}\left(\hat{H}_{x_i,l_i}^{\mathrm{MRC}}+\epsilon_i^2\tilde{H}_{x_i,l_i}^{\mathrm{MRC}}\right)+\sum\limits_{j\in\mathcal{K}}\sum\limits_{x_j\in\Phi_j\setminus x_i}\frac{P_j}{S_j}\|x_j\|^{-\alpha}G_{x_j,l_i}^{\mathrm{MRC}}}. \tag{3.4}$$

Comparing (3.4) with (2.3) and observing that both $G_{x_j,l_i}^{\mathrm{MRC}}$ and $G_{x_j,l_i}^{\mathrm{ZF}}$ are chi-squared with $2S_j$ DoF, we conclude that similar to ZFBF, under MRC receiver the ICI is similarly distributed (refer to (2.11) for its Laplace transform). However, compared to ZFBF, in MRC the DoF of the intended signal is boosted from $2(N^r-S_j+1)$ to $2N^r$, while each data stream suffers from inter-stream interference as well as CISR inaccuracy. Our main objective in this chapter is to develop analytical tools allowing us understanding the effect of both these interference sources on the coverage performance of the HetNet.

3.3 Analyzing the Coverage Performance

As in the previous chapter, we consider the max-SIR CA rule as defined in Definition 2.2.2, which implies that the typical UE is in coverage if the set

$$\mathcal{A}^{\mathrm{MRC}} = \left\{ \exists i \in \mathcal{K} : \max_{x_i \in \Phi_i} \min_{l_i = 1, \ldots, S_i} \mathrm{SIR}^{\mathrm{MRC}}_{x_i, l_i} \geq \beta_i \right\}, \tag{3.5}$$

is nonempty. The coverage probability is therefore defined as $c^{\mathrm{MRC}} = \mathbb{P}\{\mathcal{A}^{\mathrm{MRC}} \neq \emptyset\}$. In the following proposition, we provide an upper-bound on the coverage probability.

Proposition 3.3.1 (Upper-Bound). *In the MIMO-MRC multiplexing HetNet adopting the max-SIR CA rule, the coverage probability is upper-bounded as:*

$$c^{\mathrm{MRC}} \leq \frac{\pi}{\tilde{C}(\alpha)} \sum_{i \in \mathcal{K}} \frac{\lambda_i \left(\frac{P_i (1 - \epsilon_i^2)}{S_i^2 \beta_i} \right)^{\check{\alpha}} \left(\Gamma_i^{\mathrm{MRC}} \right)^{S_i}}{\sum_{j=1}^{K} \lambda_j \left(\frac{P_j}{S_j} \right)^{\check{\alpha}} \left(\frac{\Gamma(\frac{\check{\alpha}}{S_j} + S_j)}{\Gamma(S_j)} \right)^{S_i}}, \tag{3.6}$$

where

$$\Gamma_i^{\mathrm{MRC}} \triangleq \sum_{r_i=0}^{N^r - 1} \sum_{q_i=0}^{r_i} \sum_{p_i=0}^{q_i} \frac{(-1)^{q_i - p_i} \beta_i^{2q_i - p_i}}{\epsilon_i^{-4q_i + 2p_i} (1 - \epsilon_i^2)^{S_i}} \frac{(1 - \epsilon_i^2 + \beta_i)^{-q_i - S_i + 1} \left(1 + \epsilon_i^2 (\beta_i - 1)\right)^{-q_i + p_i - 1}}{p_i \mathrm{B}(S_i - 1, p_i)(r_i - q_i) \mathrm{B}(\frac{\check{\alpha}}{S_i}, r_i - q_i)}, \tag{3.7}$$

and $\mathrm{B}(a, b) = \frac{\Gamma(a)\Gamma(b)}{\Gamma(a+b)}$ *is the beta function.*

Proof. To prove this proposition we apply the developed methods in the proof of Proposition 2.3 and the proof of Proposition 2.6. Denote $r_i = \|x_i\|$. We use Slivnyak's Theorem and Campbell's Theorem along with [47, Lemma 1] as $\beta_i \geq 1$, $\forall i$, and then write

$$\begin{aligned} c^{\mathrm{MRC}} &= \sum_{i \in \mathcal{K}} \mathbb{E} \sum_{x_i \in \Phi_i} 1 \left(\min_{l_i = 1, \ldots, S_i} \mathrm{SIR}^{\mathrm{MRC}}_{x_i, l_i} \geq \beta_i \right) && (3.8) \\ &= \sum_{i \in \mathcal{K}} 2\pi \lambda_i \int_0^{\infty} r_i \mathbb{E}_{\Phi} \mathbb{P} \left\{ \mathrm{SIR}^{\mathrm{MRC}}_{x_i, l_i} \geq \beta_i : \forall l_i \middle| \Phi \right\} dr_i && (3.9) \end{aligned}$$

$$= \sum_{i\in\mathcal{K}} 2\pi\lambda_i \int_0^\infty r_i \mathbb{E}_\Phi \prod_{l_i=1}^{S_i} \mathbb{P}\left\{\mathrm{SIR}_{x_i,l}^{\mathrm{MRC}} \geq \beta_i \middle| \Phi\right\} dr_i. \tag{3.10}$$

We then note that conditioned on processes Φ_js, the SIR values across streams are statistically independent. Now we use Lemma 2.3.2. For x_i, we have

$$\begin{aligned}
\mathbb{P}\left\{\mathrm{SIR}_{x_i,l_i}^{\mathrm{MRC}} \geq \beta_i \middle| \Phi\right\} &= \mathbb{P}\Big\{ H_{x_i,l_i}^{\mathrm{MRC}} \geq \frac{\beta_i(\epsilon_i^2 \tilde{H}_{x_i,l_i}^{\mathrm{MRC}} + \hat{H}_{x_i,l_i}^{\mathrm{MRC}})}{1-\epsilon_i^2} \\
&\quad + \frac{S_i \beta_i x_i^\alpha}{P_i(1-\epsilon_i^2)} \sum_{j\in\mathcal{K}} \sum_{x_j\in\Phi_j\setminus x_i} \frac{P_j}{S_j} \|x_j\|^{-\alpha} G_{x_j,l_i}^{\mathrm{MRC}} \Big| \{\Phi_j\} \Big\} \qquad (3.11) \\
&= \int_0^\infty \mathcal{L}^{-1}_{\overline{F}_{H_i^{\mathrm{MRC}}}}(t_i) \prod_{j\in\mathcal{K}} \prod_{x_j\in\Phi_j/x_i} \mathbb{E}_{G_{x_j,l_i}^{\mathrm{MRC}}} e^{-t_i \frac{\beta_i S_i x_i^\alpha}{P_i(1-\epsilon_i^2)} \frac{P_j}{S_j} \|x_j\|^{-\alpha} G_{x_j,l_i}^{\mathrm{MRC}}} \\
&\quad \times \mathbb{E} e^{-t_i \frac{\beta_i(\epsilon_i^2 \tilde{H}_{x_i,l_i}^{\mathrm{MRC}} + \hat{H}_{x_i,l_i}^{\mathrm{MRC}})}{1-\epsilon_i^2}} dt_i \qquad (3.12) \\
&= \int_0^\infty \frac{\mathcal{L}^{-1}_{\overline{F}_{H_i^{\mathrm{MRC}}}}(t_i)}{\left(1+\frac{t_i\beta_i}{1-\epsilon_i^2}\right)^{S_i-1} (1+\frac{t_i\epsilon_i^2\beta_i}{1-\epsilon_i^2})} \\
&\quad \times \prod_{j\in\mathcal{K}} \prod_{x_j\in\Phi_j\setminus x_i} \mathbb{E}_{G_{x_j,l_i}^{\mathrm{MRC}}} e^{-t_i \frac{\beta_i S_i x_i^\alpha}{P_i(1-\epsilon_i^2)} \frac{P_j}{S_j \|x_j\|^\alpha} G_{x_j,l_i}^{\mathrm{MRC}}} dt_i, \qquad (3.13)
\end{aligned}$$

where $\mathcal{L}^{-1}_{\overline{F}_{H_i^{\mathrm{MRC}}}}(t_i)$ is the inverse Laplace transform of H_i^{MRC}, $\mathcal{L}^{-1}_{\overline{F}_{H_i^{\mathrm{MRC}}}}(t_i) = \sum_{m=0}^{N^r-1} \frac{1}{m!}\delta^{(m)}(t-1)$ (see Lemmas 2.14), and $\delta^{(m)}(t)$ is the m-th derivative of the Dirac delta function. Substituting (3.13) into (3.10) followed by straightforward derivations yields

$$\begin{aligned}
c^{\mathrm{MRC}} &= \sum_{i\in\mathcal{K}} 2\pi\lambda_i \int_0^\infty r_i \mathbb{E}_\Phi \prod_{l_i=1}^{S_i} \int_0^\infty \frac{\mathcal{L}^{-1}_{\overline{F}_{H_i^{\mathrm{MRC}}}}(t_i)}{\left(1+\frac{t_i\beta_i}{1-\epsilon_i^2}\right)^{S_i-1} (1+\frac{t_i\epsilon_i^2\beta_i}{1-\epsilon_i^2})} \\
&\quad \times \prod_{j\in\mathcal{K}} \prod_{x_j\in\Phi_j/x_i} \mathbb{E}_{G_{x_j,l_i}^{\mathrm{MRC}}} e^{-t_i \frac{\beta_i S_i r_i^\alpha}{P_i(1-\epsilon_i^2)} \frac{P_j}{S_j} \|x_j\|^{-\alpha} G_{x_j,l_i}^{\mathrm{MRC}}} dt_i dr_i \qquad (3.14) \\
&= \sum_{i\in\mathcal{K}} 2\pi\lambda_i \int_0^\infty r_i dr_i \mathbb{E}_\Phi \int_0^\infty \cdots \int_0^\infty \prod_{l_i=1}^{S_i} \frac{\mathcal{L}^{-1}_{\overline{F}_{H_i^{\mathrm{MRC}}}}(t_{l_i}) dt_{l_i}}{\left(1+\frac{t_{l_i}\beta_i}{1-\epsilon_i^2}\right)^{S_i-1} (1+\frac{t_{l_i}\epsilon_i^2\beta_i}{1-\epsilon_i^2})}
\end{aligned}$$

$$\times \prod_{j\in\mathcal{K}} \prod_{x_j\in\Phi_j/x_i} \mathbb{E}_{G_{x_j}^{\mathrm{MRC}}} \prod_{l_i=1}^{S_i} e^{-\frac{\beta_i S_i r_i^{\alpha}}{P_i(1-\epsilon_i^2)} \frac{P_j G_{x_j,l_i}^{\mathrm{MRC}} t_{l_i}}{S_j \|x_j\|^{\alpha}}}, \tag{3.15}$$

as r.v.s $G_{x_j,l_i}^{\mathrm{zf}}$ are i.i.d. across the streams. Thus,

$$\begin{aligned}
c^{\mathrm{MRC}} &= \sum_{i\in\mathcal{K}} 2\pi\lambda_i \int_0^{\infty} r_i dr_i \int_0^{\infty} \cdots \int_0^{\infty} \prod_{l_i=1}^{S_i} \frac{\mathcal{L}^{-1}_{\overline{F}_{H_i^{\mathrm{MRC}}}}(t_i) dt_{l_i}}{\left(1+\frac{t_i\beta_i}{1-\epsilon_i^2}\right)^{S_i-1}(1+\frac{t_i\epsilon_i^2\beta_i}{1-\epsilon_i^2})} \\
&\quad \times \prod_{j\in\mathcal{K}} \mathbb{E}_{\Phi_j} \prod_{x_j\in\Phi_j/x_i} \mathbb{E}_{G_{x_j}^{\mathrm{MRC}}} e^{-\frac{\beta_i S_i r_i^{\alpha}}{P_i(1-\epsilon_i^2)} \frac{P_j \sum_{l_i=1}^{S_i} G_{x_j,l_i}^{\mathrm{MRC}} t_{l_i}}{S_j \|x_j\|^{\alpha}}} \qquad (3.16) \\
&= \sum_{i\in\mathcal{K}} 2\pi\lambda_i \int_0^{\infty} r_i dr_i \int_0^{\infty} \cdots \int_0^{\infty} \prod_{l_i=1}^{S_i} \frac{\mathcal{L}^{-1}_{\overline{F}_{H_i^{\mathrm{MRC}}}}(t_i) dt_{l_i}}{\left(1+\frac{t_i\beta_i}{1-\epsilon_i^2}\right)^{S_i-1}(1+\frac{t_i\epsilon_i^2\beta_i}{1-\epsilon_i^2})} \\
&\quad \times e^{-r_i^2\tilde{C}(\alpha)\left(\frac{\beta_i S_i}{P_i(1-\epsilon_i^2)}\right)^{\check{\alpha}} \sum_{j=1}^{K} \lambda_j \left(\frac{P_j}{S_j}\right)^{\check{\alpha}} \mathbb{E}_{G_j^{\mathrm{MRC}}}\left[(\sum_{l_i=1}^{S_i} G_{j,l_i}^{\mathrm{MRC}} t_{l_i})^{\check{\alpha}}\right]} \qquad (3.17) \\
&= \sum_{i\in\mathcal{K}} 2\pi\lambda_i \int_0^{\infty} \cdots \int_0^{\infty} \prod_{l_i=1}^{S_i} \frac{\mathcal{L}^{-1}_{\overline{F}_{H_i^{\mathrm{MRC}}}}(t_i) dt_{l_i}}{\left(1+\frac{t_i\beta_i}{1-\epsilon_i^2}\right)^{S_i-1}(1+\frac{t_i\epsilon_i^2\beta_i}{1-\epsilon_i^2})} \\
&\quad \times \int_0^{\infty} r_i e^{-r_i^2\tilde{C}(\alpha)\left(\frac{\beta_i S_i}{P_i(1-\epsilon_i^2)}\right)^{\check{\alpha}} \sum_{j=1}^{K} \lambda_j \left(\frac{P_j}{S_j}\right)^{\check{\alpha}} \mathbb{E}\left[(\sum_{l_i=1}^{S_i} G_{j,l_i}^{\mathrm{MRC}} t_{l_i})^{\check{\alpha}}\right]} dr_i \qquad (3.18) \\
&= \sum_{i\in\mathcal{K}} \frac{\pi}{\tilde{C}(\alpha)} \int_0^{\infty} \cdots \int_0^{\infty} \frac{\lambda_i \left(\frac{P_i(1-\epsilon_i^2)}{S_i\beta_i}\right)^{\check{\alpha}}}{\sum_{j\in\mathcal{K}} \lambda_j \left(\frac{P_j}{S_j}\right)^{\check{\alpha}} \mathbb{E}_{G_j^{\mathrm{MRC}}}\left[(\sum_{l_i=1}^{S_i} G_{j,l_i}^{\mathrm{MRC}} t_{l_i})^{\check{\alpha}}\right]} \\
&\quad \times \prod_{l_i=1}^{S_i} \frac{\mathcal{L}^{-1}_{\overline{F}_{H_i^{\mathrm{MRC}}}}(t_i) dt_{l_i}}{\left(1+\frac{t_i\beta_i}{1-\epsilon_i^2}\right)^{S_i-1}(1+\frac{t_i\epsilon_i^2\beta_i}{1-\epsilon_i^2})}, \qquad (3.19)
\end{aligned}$$

which is not easily tractable due to $\mathbb{E}_{G_j^{\mathrm{MRC}}}\left[(\sum_{l_i=1}^{S_i} G_{j,l_i}^{\mathrm{MRC}} t_{l_i})^{\check{\alpha}}\right]$. To make the analysis tractable, we transform $\sum_{l_i=1}^{S_i} G_{j,l_i}^{\mathrm{MRC}} t_{l_i}$ into a multiplicative form $\prod_{l_i=1}^{S_i} G_{j,l_i}^{\mathrm{MRC}} t_{l_i}$ so that expectation operation on G_{j,l_i}^{MRC} becomes effective irrespective of variables t_{l_i}s. To do this, we adopt the arithmetic-geometric inequality, which results in the following upper-bound on the coverage

probability:

$$
\begin{aligned}
c^{\mathrm{MRC}} \quad & \leq \sum_{i\in\mathcal{K}} \frac{\frac{\pi}{\tilde{C}(\alpha)}\left(\frac{P_i(1-\epsilon_i^2)}{S_i\beta_i}\right)^{\check{\alpha}}\frac{\lambda_i}{S_i^{\check{\alpha}}}}{\sum_{j=1}^{K}\lambda_j\left(\frac{P_j}{S_j}\right)^{\check{\alpha}}\mathbb{E}_{G_j^{\mathrm{MRC}}}\prod_{l_i=1}^{S_i}(G_{j,l_i}^{\mathrm{MRC}})^{\frac{\check{\alpha}}{S_i}}} \\
& \times \int_0^\infty \cdots \int_0^\infty \prod_{l_i=1}^{S_i} \frac{t_{l_i}^{-\frac{\check{\alpha}}{S_i}}\mathcal{L}^{-1}_{\overline{F}_{H_i^{\mathrm{MRC}}}}(t_{l_i})dt_{l_i}}{\left(1+\frac{t_i\beta_i}{1-\epsilon_i^2}\right)^{S_i-1}(1+\frac{t_i\epsilon_i^2\beta_i}{1-\epsilon_i^2})} \qquad (3.20) \\
& = \sum_{i\in\mathcal{K}} \frac{\frac{\pi}{\tilde{C}(\alpha)}\left(\frac{P_i(1-\epsilon_i^2)}{S_i\beta_i}\right)^{\check{\alpha}}\frac{\lambda_i}{S_i^{\check{\alpha}}}}{\sum_{j=1}^{K}\lambda_j\left(\frac{P_j}{S_j}\right)^{\check{\alpha}}\left(\mathbb{E}_{G_j^{\mathrm{MRC}}}(G_j^{\mathrm{MRC}})^{\frac{\check{\alpha}}{S_i}}\right)^{S_i}}\left(\int_0^\infty \frac{t_i^{-\frac{\check{\alpha}}{S_i}}\mathcal{L}^{-1}_{\overline{F}_{H_i^{\mathrm{MRC}}}}(t_i)}{\left(1+\frac{t_i\beta_i}{1-\epsilon_i^2}\right)^{S_i-1}(1+\frac{t_i\epsilon_i^2\beta_i}{1-\epsilon_i^2})}\right)^{S_i} \qquad (3.21)
\end{aligned}
$$

where the last step is due to the fact that rv.s $G_{x_j,l_i}^{\mathrm{MRC}}$ are i.i.d. across streams. We now evaluate the integral in (3.21). Using (B.2), we write

$$
\begin{aligned}
\int_0^\infty \frac{t_i^{-\frac{\check{\alpha}}{S_i}}\mathcal{L}^{-1}_{\overline{F}_{H_i^{\mathrm{MRC}}}}(t_i)}{\left(1+\frac{t_i\beta_i}{1-\epsilon_i^2}\right)^{S_i-1}(1+\frac{t_i\epsilon_i^2\beta_i}{1-\epsilon_i^2})}dt_i \quad &= \quad \sum_{r_i=0}^{N^r-1}\frac{1}{r_i!}\int_0^\infty \frac{\delta^{(r_i)}(t_i-1)t_i^{-\frac{\check{\alpha}}{S_i}}}{\left(1+\frac{t_i\beta_i}{1-\epsilon_i^2}\right)^{S_i-1}(1+\frac{t_i\epsilon_i^2\beta_i}{1-\epsilon_i^2})}dt_i \qquad (3.22) \\
&= \quad \sum_{r_i=0}^{N^r-1}\frac{(-1)^{r_i}}{r_i!}\frac{d^{r_i}}{dt^{r_i}}\frac{t^{-\frac{\check{\alpha}}{S_i}}}{\left(1+\frac{t_i\beta_i}{1-\epsilon_i^2}\right)^{S_i-1}(1+\frac{t_i\epsilon_i^2\beta_i}{1-\epsilon_i^2})}\Big|_{t=1} \qquad (3.23)
\end{aligned}
$$

Applying the Leibniz rule along with straightforward mathematical derivation, we get

$$
\begin{aligned}
\frac{d^{r_i}}{dt^{r_i}}\frac{t^{-\frac{\check{\alpha}}{S_i}}}{\left(1+\frac{t\beta_i}{1-\epsilon_i^2}\right)^{S_i-1}\left(1+\frac{t\epsilon_i^2\beta_i}{1-\epsilon_i^2}\right)} \quad &= \sum_{q_i=0}^{r_i}\binom{r_i}{q_i}\frac{d^{q_i}}{dt^{q_i}}\frac{1}{\left(1+\frac{t\beta_i}{1-\epsilon_i^2}\right)^{S_i-1}\left(1+\frac{t\epsilon_i^2\beta_i}{1-\epsilon_i^2}\right)}\frac{d^{r_i-q_i}}{dt^{r_i-q_i}}t^{-\frac{\check{\alpha}}{S_i}} \\
&= \sum_{q_i=0}^{r_i}\binom{r_i}{q_i}\sum_{p_i=0}^{q_i}\binom{q_i}{p_i}\frac{d^{p_i}}{dt^{p_i}}\frac{1}{\left(1+\frac{t\beta_i}{1-\epsilon_i^2}\right)^{S_i-1}} \\
&\times\frac{d^{q_i-p_i}}{dt^{q_i-p_i}}\frac{1}{\left(1+\frac{t\epsilon_i^2\beta_i}{1-\epsilon_i^2}\right)}\frac{d^{r_i-q_i}}{dt^{r_i-q_i}}t^{-\frac{\check{\alpha}}{S_i}}. \qquad (3.24)
\end{aligned}
$$

We then employ the following formulas:

$$\frac{d^n}{dt^n}\frac{1}{(1+ta)^S} = \frac{(-a)^n \prod_{u=0}^{n-1}(S+u)}{(1+ta)^{S+n}} \tag{3.25}$$

$$\frac{d^n}{dt^n}t^{-b} = (-1)^n t^{-b-n}\prod_{u=0}^{n-1}(b+u), \tag{3.26}$$

thus (3.24) is further reduced to which is

$$\begin{aligned}
(3.24) &= \sum_{q_i=0}^{r_i}\sum_{p_i=0}^{q_i} \frac{\binom{r_i}{q_i}\binom{q_i}{p_i}\prod_{m_i=0}^{p_i-1}(S_i-1+m_i)}{(\frac{-\beta_i}{1-\epsilon_i^2})^{-q_i}\left(1+\frac{t\beta_i}{1-\epsilon_i^2}\right)^{q_i+S_i-1}} \frac{\prod_{u_i=0}^{q_i-p_i-1}(1+u_i)}{(\frac{-\beta_i\epsilon_i^2}{1-\epsilon_i^2})^{-q_i+p_i}\left(1+\frac{t\beta_i\epsilon_i^2}{1-\epsilon_i^2}\right)^{q_i-p_i+1}} \frac{\prod_{n_i=0}^{r_i-q_i-1}(\frac{\check{\alpha}}{S_i}+n_i)}{(-1)^{-r_i+q_i}t^{\frac{\check{\alpha}}{S_i}+r_i-q_i}} \\
&= (-1)^{r_i}\sum_{q_i=0}^{r_i}\sum_{p_i=0}^{q_i} \frac{(-1)^{q_i-p_i}\binom{r_i}{q_i}\binom{q_i}{p_i}\prod_{m_i=0}^{p_i-1}(S_i-1+m_i)}{\left(\frac{\beta_i}{1-\epsilon_i^2}\right)^{-q_i}\left(1+\frac{\beta_i}{1-\epsilon_i^2}\right)^{q_i+S_i-1}} \frac{\prod_{u_i=0}^{q_i-p_i-1}(1+u_i)}{\left(\frac{\beta_i\epsilon_i^2}{1-\epsilon_i^2}\right)^{-q_i+p_i}\left(1+\frac{\beta_i\epsilon_i^2}{1-\epsilon_i^2}\right)^{q_i-p_i+1}} \prod_{n_i=0}^{r_i-q_i-1}(\frac{\check{\alpha}}{S_i}+n_i) \\
&= \sum_{q_i=0}^{r_i}\sum_{p_i=0}^{q_i} \frac{(-1)^{r_i+q_i-p_i}\binom{r_i}{q_i}\binom{q_i}{p_i}\Gamma(S_i-1+p_i)\Gamma(q_i-p_i+1)\Gamma(\frac{\check{\alpha}}{S_i}+r_i-q_i)}{\epsilon_i^{2p_i-4q_i}\left(1+\frac{\beta_i}{1-\epsilon_i^2}\right)^{q_i+S_i-1}\left(\frac{\beta_i}{1-\epsilon_i^2}\right)^{p_i-2q_i}\left(1+\frac{\beta_i\epsilon_i^2}{1-\epsilon_i^2}\right)^{q_i-p_i+1}\Gamma(S_i-1)\Gamma(\frac{\check{\alpha}}{S_i})}
\end{aligned} \tag{3.27}$$

Using this expression, (3.24) is then rewritten as

$$(3.24) = \sum_{r_i=0}^{N^r-1}\sum_{q_i=0}^{r_i}\sum_{p_i=0}^{q_i} \frac{(-1)^{q_i-p_i}\beta_i^{2q_i-p_i}}{\epsilon_i^{-4q_i+2p_i}} \frac{(1-\epsilon_i^2+\beta_i)^{-q_i-S_i+1}(1+\epsilon_i^2(\beta_i-1))^{-q_i+p_i-1}}{(1-\epsilon_i^2)^{S_i}p_i\mathrm{B}(S_i-1,p_i)(r_i-q_i)\mathrm{B}(\frac{\check{\alpha}}{S_i},r_i-q_i)}. \tag{3.28}$$

Finally, by substituting (3.28) into (3.21), and noticing that $G_{x_j,l_i}^{\mathrm{MRC}}$ is chi-squared with $2S_j$ DoF, the desired result follows.

□

Despite significant model complexities, Proposition 3.3.1 provides a closed-form upper-bound for the coverage probability. Our simulation results in Section 3.6 indicate that the upper-bound of Proposition 3.3.1 is accurate and representative. We further notice a striking resemblance between the coverage probability under MRC receiver and that of ZFBF in

(2.116). For the case that CSI is accurately known at the receiver, one can simply exchange Γ_i^{MRC} with Γ_i^{ZF} to derive the coverage probability of ZFBF from Proposition 3.3.1. This resemblance is perhaps attributable to the fact that in both systems ICI is similarly distributed. Further, in both systems the post-processed fading gains on intending communication link are Chi-squared random variables, but with different DoFs. The only substantial difference between these two receivers is that in the case of MRC the intra-stream interference is not cancelled out. This extra source of interference is captured by Γ_i^{MRC}.

3.4 Cross-Stream SIR Correlation

In Chapter 2.4, we demonstrated the significance of cross-stream interference correlation on the MIMO-ZFBF multiplexing systems, by showing that under the FC assumption the coverage probability slightly declines. In this section, we explore other aspects of cross-stream interference correlation under MRC receiver, by characterizing the correlation coefficient and analyzing the impact on SIR correlation on the system coverage performance. We shall emphasize that although we investigate these issues under MRC receiver, by straightforward manipulations and simple adjustments, it is possible to extend the results to the case of ZFBF.

3.4.1 SIR Correlation Coefficient

The focus in the related literature (e.g., [78, 170]) is often on understanding the interference correlation among antennas. In contrast, we here focus on the SIR correlation among data streams, as in a link the coverage probability is related to the joint SIRs' CDF of the streams. To quantify the SIR correlation, the Pearson correlation coefficient is used:

$$\rho_{x_i}^{\mathrm{MRC}}(l_i, l_i') = \frac{\mathbb{E}\left[\mathrm{SIR}_{x_i,l_i}^{\mathrm{MRC}}\mathrm{SIR}_{x_i,l_i'}^{\mathrm{MRC}}\right] - \overline{\mathrm{SIR}}_{x_i,l_i}^{\mathrm{MRC}}\overline{\mathrm{SIR}}_{x_i,l_i'}^{\mathrm{MRC}}}{\sqrt{\mathrm{Var}\left(\mathrm{SIR}_{x_i,l_i}^{\mathrm{MRC}}\right)\mathrm{Var}\left(\mathrm{SIR}_{x_i,l_i'}^{\mathrm{MRC}}\right)}} \tag{3.29}$$

$$= \frac{\mathbb{E}\left[\mathrm{SIR}^{\mathrm{MRC}}_{x_i,l_i}\mathrm{SIR}^{\mathrm{MRC}}_{x_i,l'_i}\right] - (\overline{\mathrm{SIR}}^{\mathrm{MRC}}_{x_i,l_i})^2}{\mathrm{Var}\left(\mathrm{SIR}^{\mathrm{MRC}}_{x_i,l_i}\right)}, \tag{3.30}$$

where $\overline{\mathrm{SIR}}^{\mathrm{MRC}}_{x_i,l_i}$ is the average SIR on data stream l_i.

Proposition 3.4.1. *For a typical UE receiving data from BS x_i in a MIMO-MRC multiplexing system, the correlation coefficient between data streams l_i and l'_i, $\forall l_i, l'_i, l_i \neq l'_i$ is:*

$$\rho^{\mathrm{MRC}}_{x_i}(l_i,l'_i) = \frac{\int_0^\infty\int_0^\infty \frac{\frac{e^{-\tilde{C}(\alpha)\sum_j \lambda_j (\frac{P_j}{S_j})^{\check{\alpha}}\overline{W}_j(t,\tau)}}{1+(t+\tau)\frac{P_i}{S_i}x_i^{-\alpha}} - \frac{e^{-(t^{\check{\alpha}}+\tau^{\check{\alpha}})\Lambda(\boldsymbol{S})}}{(1+t\frac{P_i}{S_i}x_i^{-\alpha})(1+\tau\frac{P_i}{S_i}x_i^{-\alpha})}}{\left(1+t\frac{P_i}{S_i}\epsilon_i^2 x_i^{-\alpha}\right)\left(1+\tau\frac{P_i}{S_i}\epsilon_i^2 x_i^{-\alpha}\right)\left((1+t\frac{P_i}{S_i}x_i^{-\alpha})(1+\tau\frac{P_i}{S_i}x_i^{-\alpha})\right)^{S_i-2}} dt d\tau}{\int_0^\infty\int_0^\infty \left[\frac{\frac{N^r+1}{N^r}e^{-(t+\tau)^{\check{\alpha}}\Lambda(\boldsymbol{S})}}{\left(1+\frac{(t+\tau)P_i\epsilon_i^2}{S_i x_i^\alpha}\right)\left(1+\frac{(t+\tau)P_i}{S_i x_i^\alpha}\right)^{S_i-1}} - \frac{e^{-(t^{\check{\alpha}}+\tau^{\check{\alpha}})\Lambda(\boldsymbol{S})}}{\left(1+\frac{tP_i}{S_i x_i^\alpha}\epsilon_i^2\right)\left(1+\frac{P_i\epsilon_i^2\tau}{S_i x_i^\alpha}\right)\left((1+\frac{tP_i}{S_i x_i^\alpha})(1+\frac{P_i\tau}{S_i x_i^\alpha})\right)^{S_i-1}}\right] dt d\tau}, \tag{3.31}$$

where

$$\overline{W}_j(t,\tau) \triangleq \sum_{l=0}^{S_j-1} \frac{\binom{S_j-1}{l}(-1)^{S_j-1-l}}{\tau^{S_j-\check{\alpha}-1-l}t^{S_j}\Gamma(S_j)^2} \times \int_0^\infty \Gamma(\check{\alpha}+l+1,\frac{v}{\tau})e^{-v(\frac{1}{t}-\frac{1}{\tau})}v^{2S_j-2-l}dv, \tag{3.32}$$

and $\Gamma(a,b) = \int_b^\infty z^{a-1}e^{-z}dz$ is the upper incomplete Gamma function.

Proof. We start with the evaluation of $\overline{\mathrm{SIR}}^{\mathrm{MRC}}_{x_i,l_i}$. Due to the independence of the intended and interfering signals, and noting that $H^{\mathrm{MRC}}_{x_i,l_i}$ is a chi-squared distributed with $2N^r$ DoF, we write

$$\overline{\mathrm{SIR}}^{\mathrm{MRC}}_{x_i,l_i} = \frac{P_i N^r(1-\epsilon_i^2)}{S_i x_i^\alpha}\mathbb{E}\left(\frac{P_i}{S_i x_i^\alpha}(\epsilon_i^2\tilde{H}^{\mathrm{MRC}}_{x_i,l_i} + \hat{H}^{\mathrm{MRC}}_{x_i,l_i}) + \sum_{j\in\mathcal{K}}\sum_{x_j\in\Phi_j\setminus x_i}\frac{P_j G^{\mathrm{MRC}}_{x_j,l_i}}{S_j\|x_j\|^\alpha}\right)^{-1}. \tag{3.33}$$

Using $\int_0^\infty e^{-sz}ds = z^{-1}$, the expectation in (3.33) is evaluated as

$$\begin{aligned}
&\mathbb{E}\int_0^\infty e^{-t\frac{P_i}{S_i x_i^\alpha}(\epsilon_i^2\tilde{H}^{\mathrm{MRC}}_{x_i,l_i}+\hat{H}^{\mathrm{MRC}}_{x_i,l_i})-t\sum\limits_{j\in\mathcal{K}}\sum\limits_{x_j\in\Phi_j\setminus x_i}\frac{P_j G^{\mathrm{MRC}}_{x_j,l_i}}{S_j\|x_j\|^\alpha}}dt \\
&\overset{(a)}{=}\int_0^\infty \mathbb{E}e^{-t\frac{P_i}{S_i x_i^\alpha}\epsilon_i^2\tilde{H}^{\mathrm{MRC}}_{x_i,l_i}}\mathbb{E}e^{-t\frac{P_i}{S_i x_i^\alpha}\hat{H}^{\mathrm{MRC}}_{x_i,l_i}}\mathbb{E}_{\{\Phi_j\}}\mathbb{E}_{\{G^{\mathrm{MRC}}_{x_j,l_i}\}_{\forall x_j}}\prod_{j\in\mathcal{K}}\prod_{x_j\in\Phi_j\setminus x_i}e^{-t\frac{P_j}{S_j}\|x_j\|^{-\alpha}G^{\mathrm{MRC}}_{x_j,l_i}}dt \qquad (3.34)\\
&\overset{(b)}{=}\int_0^\infty \frac{\prod\limits_{j\in\mathcal{K}}\mathbb{E}_{\Phi_j}\prod\limits_{x_j\in\Phi_j\setminus x_i}\mathbb{E}_{G^{\mathrm{MRC}}_{x_j,l_i}}e^{-t\frac{P_j}{S_j}\|x_j\|^{-\alpha}G^{\mathrm{MRC}}_{x_j,l_i}}}{\left(1+t\frac{P_i}{S_i x_i^\alpha}\epsilon_i^2\right)\left(1+t\frac{P_i}{S_i x_i^\alpha}\right)^{S_i-1}}dt \qquad (3.35)\\
&=\int_0^\infty \frac{e^{-t^{\check{\alpha}}\tilde{C}(\alpha)\sum\limits_j\lambda_j(\frac{P_j}{S_j})^{\check{\alpha}}\frac{\Gamma(\check{\alpha}+S_j)}{\Gamma(S_j)}}}{\left(1+t\frac{P_i}{S_i x_i^\alpha}\epsilon_i^2\right)\left(1+t\frac{P_i}{S_i x_i^\alpha}\right)^{S_i-1}}dt, \qquad (3.36)
\end{aligned}$$

where in Step (a) the independence of r.v.s is used, and in Step (b) we insert the Laplace transforms of r.v.s $\tilde{H}^{\mathrm{MRC}}_{x_i,l_i}$ which is a chi-square distributed with $2(S_i-1)$ DoF, and $\tilde{H}^{\mathrm{MRC}}_{x_i,l_i}$ which is exponentially distributed, at point $\frac{P_i}{S_i}x_i^{-\alpha}$. In the last step, we use $\mathbb{E}(G_j^{\mathrm{MRC}})^{\check{\alpha}} = \frac{\Gamma(\check{\alpha}+S_j)}{\Gamma(S_j)}$ is substituted as G_j^{MRC} is a chi-squared r.v. with $2S_j$ DoF. Finally, substituting $\Lambda(\boldsymbol{S})$ (2.12) yields

$$\overline{\mathrm{SIR}}^{\mathrm{MRC}}_{x_i,l_i} = \frac{P_i N^r(1-\epsilon_i^2)}{S_i x_i^\alpha}\int_0^\infty \frac{e^{-t^{\check{\alpha}}\Lambda(\boldsymbol{S})}}{\left(1+t\frac{P_i}{S_i x_i^\alpha}\epsilon_i^2\right)\left(1+t\frac{P_i}{S_i x_i^\alpha}\right)^{S_i-1}}dt. \qquad (3.37)$$

To evaluate $\mathrm{Var}(\mathrm{SIR}^{\mathrm{SVD}}_{x_i,l_i})$, we first need to evaluate $\mathbb{E}\left[\left(\mathrm{SIR}^{\mathrm{SVD}}_{x_i,l_i}\right)^2\right]$, which can be done applying the same steps above:

$$\begin{aligned}
&\mathbb{E}\left[\left(\mathrm{SIR}^{\mathrm{MRC}}_{x_i,l_i}\right)^2\right]\\
&=\frac{(1-\epsilon_i^2)^2\mathbb{E}[(H^{\mathrm{MRC}}_{x_i,l_i})^2]}{P_i^{-2}S_i^2x_i^{2\alpha}}\mathbb{E}\left(\frac{P_i}{S_i x_i^\alpha}(\epsilon_i^2\tilde{H}^{\mathrm{MRC}}_{x_i,l_i}+\hat{H}^{\mathrm{MRC}}_{x_i,l_i})+\sum_{j\in\mathcal{K}}\sum_{x_j\in\Phi_j\setminus x_i}\frac{P_j G^{\mathrm{MRC}}_{x_j,l_i}}{S_j\|x_j\|^\alpha}\right)^{-2} \qquad (3.38)
\end{aligned}$$

$$= \frac{(1-\epsilon_i^2)^2 N^r (N^r+1)}{P_i^{-2} S_i^2 x_i^{2\alpha}} \mathbb{E} \int_0^\infty \int_0^\infty e^{-(t+\tau)\frac{P_i}{S_i x_i^\alpha}(\epsilon_i^2 \tilde{H}^{\mathrm{MRC}}_{x_i,l_i} + \hat{H}^{\mathrm{MRC}}_{x_i,l_i}) - (t+\tau) \sum\limits_{j\in\mathcal{K}} \sum\limits_{x_j \in \Phi_j \setminus x_i} \frac{P_j G^{\mathrm{MRC}}_{x_j,l_i}}{S_j \|x_j\|^\alpha}} dt d\tau \quad (3.39)$$

$$= \frac{(1-\epsilon_i^2)^2 N^r (N^r+1)}{P_i^{-2} S_i^2 x_i^{2\alpha}} \int_0^\infty \int_0^\infty \frac{e^{-(t+\tau)^{\check{\alpha}} \Lambda(\boldsymbol{S})}}{\left(1+(t+\tau)\frac{P_i}{S_i x_i^\alpha}\epsilon_i^2\right)\left(1+(t+\tau)\frac{P_i}{S_i x_i^\alpha}\right)^{S_i-1}} dt d\tau. \quad (3.40)$$

Combining (3.37) and (3.40), $\mathrm{Var}(\mathrm{SIR}^{\mathrm{SVD}}_{x_i,l_i})$ is then obtained as

$$\mathrm{Var}(\mathrm{SIR}^{\mathrm{SVD}}_{x_i,l_i}) = \frac{(1-\epsilon_i^2)^2 N^r}{P_i^{-2} S_i^2 x_i^{2\alpha}} \left[(N^r+1) \int_0^\infty \int_0^\infty \frac{e^{-(t+\tau)^{\check{\alpha}} \Lambda(\boldsymbol{S})} dt d\tau}{\left(1+(t+\tau)\frac{P_i}{S_i x_i^\alpha}\epsilon_i^2\right)\left(1+(t+\tau)\frac{P_i}{S_i x_i^\alpha}\right)^{S_i-1}} \right. \quad (3.41)$$
$$\left. - N^r \left(\int_0^\infty \frac{e^{-t^{\check{\alpha}} \Lambda(\boldsymbol{S})}}{\left(1+t\frac{P_i}{S_i x_i^\alpha}\epsilon_i^2\right)\left(1+t\frac{P_i}{S_i x_i^\alpha}\right)^{S_i-1}} dt \right)^2 \right].$$

On the other hand,

$$\mathbb{E}\left[\mathrm{SIR}^{\mathrm{MRC}}_{x_i,l_i} \mathrm{SIR}^{\mathrm{MRC}}_{x_i,l_i'}\right] = \frac{(P_i(1-\epsilon_i^2)N^r)^2}{S_i^2 x_i^{2\alpha}} \mathcal{I}, \quad (3.42)$$

where

$$\mathcal{I} = \mathbb{E}\left[\left(\frac{P_i}{S_i x_i^\alpha}(\epsilon_i^2 \tilde{H}^{\mathrm{MRC}}_{x_i,l_i} + \hat{H}^{\mathrm{MRC}}_{x_i,l_i}) + \sum_{j\in\mathcal{K}} \sum_{x_j\in\Phi_j\setminus x_i} \frac{P_j G^{\mathrm{MRC}}_{x_j,l_i}}{S_j \|x_j\|^\alpha} \right)^{-1} \right. \quad (3.43)$$
$$\left. \times \left(\frac{P_i}{S_i x_i^\alpha}(\epsilon_i^2 \tilde{H}^{\mathrm{MRC}}_{x_i,l_i'} + \hat{H}^{\mathrm{MRC}}_{x_i,l_i'}) + \sum_{j\in\mathcal{K}} \sum_{x_j\in\Phi_j\setminus x_i} \frac{P_j G^{\mathrm{MRC}}_{x_j,l_i'}}{S_j \|x_j\|^\alpha} \right)^{-1} \right] \quad (3.44)$$
$$= \int_0^\infty \int_0^\infty \frac{\mathbb{E}e^{-\sum\limits_{j\in\mathcal{K}} \sum\limits_{x_j\in\Phi_j\setminus x_i} \frac{P_j}{S_j\|x_j\|^\alpha}(tG^{\mathrm{MRC}}_{x_j,l_i'} + \tau G^{\mathrm{MRC}}_{x_j,l_i'})}}{\left(1+t\frac{P_i}{S_i}\epsilon_i^2 x_i^{-\alpha}\right)\left(1+\tau\frac{P_i}{S_i}\epsilon_i^2 x_i^{-\alpha}\right)} \mathbb{E}e^{-\frac{P_i}{S_i x_i^\alpha}(t\hat{H}^{\mathrm{MRC}}_{x_i,l_i} + \tau \hat{H}^{\mathrm{MRC}}_{x_i,l_i'})} dt d\tau. \quad (3.45)$$

It is also straightforward to show that

$$\mathbb{E}e^{-\frac{P_i}{S_i x_i^\alpha}(t\hat{H}^{\mathrm{MRC}}_{x_i,l_i} + \tau \hat{H}^{\mathrm{MRC}}_{x_i,l_i'})}$$
$$= \mathbb{E}e^{-\frac{P_i}{S_i x_i^\alpha}\left(t \sum\limits_{l'\neq l_i} \frac{\|\tilde{\boldsymbol{h}}^\dagger_{x_i,l_i} \boldsymbol{h}_{x_i,l'}\|^2}{\|\boldsymbol{h}_{x_i,l_i}\|^2} + \tau \sum\limits_{l''\neq l_i'} \frac{\|\tilde{\boldsymbol{h}}^\dagger_{x_i,l_i'} \boldsymbol{h}_{x_i,l''}\|^2}{\|\boldsymbol{h}_{x_i,l_i'}\|^2} \right)} \quad (3.46)$$

$$= \mathbb{E}e^{-\frac{P_i}{S_i x_i^{\alpha}}\left(t\sum\limits_{l'\neq l_i,l'_i}\frac{\|\tilde{\boldsymbol{h}}^{\dagger}_{x_i,l_i}\boldsymbol{h}_{x_i,l'}\|^2}{\|\tilde{\boldsymbol{h}}_{x_i,l_i}\|^2}+\tau\sum\limits_{l''\neq l'_i,l_i}\frac{\|\tilde{\boldsymbol{h}}^{\dagger}_{x_i,l'_i}\boldsymbol{h}_{x_i,l''}\|^2}{\|\tilde{\boldsymbol{h}}_{x_i,l'_i}\|^2}+t\frac{\|\tilde{\boldsymbol{h}}^{\dagger}_{x_i,l_i}\boldsymbol{h}_{x_i,l'_i}\|^2}{\|\tilde{\boldsymbol{h}}_{x_i,l_i}\|^2}+\tau\frac{\|\tilde{\boldsymbol{h}}^{\dagger}_{x_i,l_i}\boldsymbol{h}_{x_i,l'_i}\|^2}{\|\tilde{\boldsymbol{h}}_{x_i,l'_i}\|^2}\right)} \tag{3.47}$$

$$= \mathbb{E}e^{-\frac{P_i}{S_i x_i^{\alpha}}\left(t\sum\limits_{l'\neq l_i,l'_i}\frac{\|\tilde{\boldsymbol{h}}^{\dagger}_{x_i,l_i}\boldsymbol{h}_{x_i,l'}\|^2}{\|\tilde{\boldsymbol{h}}_{x_i,l_i}\|^2}+\tau\sum\limits_{l''\neq l'_i,l_i}\frac{\|\tilde{\boldsymbol{h}}^{\dagger}_{x_i,l'_i}\boldsymbol{h}_{x_i,l''}\|^2}{\|\tilde{\boldsymbol{h}}_{x_i,l'_i}\|^2}+(t+\tau)\frac{\|\tilde{\boldsymbol{h}}^{\dagger}_{x_i,l_i}\boldsymbol{h}_{x_i,l'_i}\|^2}{\|\tilde{\boldsymbol{h}}_{x_i,l_i}\|^2}\right)} \tag{3.48}$$

$$= \mathbb{E}e^{-\frac{P_i}{S_i x_i^{\alpha}}\left(t\sum\limits_{l'\neq l_i,l'_i}\frac{\|\tilde{\boldsymbol{h}}^{\dagger}_{x_i,l_i}\boldsymbol{h}_{x_i,l'}\|^2}{\|\tilde{\boldsymbol{h}}_{x_i,l_i}\|^2}+\tau\sum\limits_{l''\neq l'_i,l_i}\frac{\|\tilde{\boldsymbol{h}}^{\dagger}_{x_i,l'_i}\boldsymbol{h}_{x_i,l''}\|^2}{\|\tilde{\boldsymbol{h}}_{x_i,l'_i}\|^2}\right)}\mathbb{E}e^{-(t+\tau)\frac{\|\tilde{\boldsymbol{h}}^{\dagger}_{x_i,l_i}\boldsymbol{h}_{x_i,l'_i}\|^2}{\|\tilde{\boldsymbol{h}}_{x_i,l_i}\|^2}} \tag{3.49}$$

$$= \frac{1}{\left((1+t\frac{P_i}{S_i}x_i^{-\alpha})(1+\tau\frac{P_i}{S_i}x_i^{-\alpha})\right)^{S_i-2}}\frac{1}{1+(t+\tau)\frac{P_i}{S_i}x_i^{-\alpha}}. \tag{3.50}$$

Inserting (3.50) in (3.45) yields:

$$\mathcal{I} = \int_0^{\infty}\int_0^{\infty}\frac{\left(1+(t+\tau)\frac{P_i}{S_i}x_i^{-\alpha}\right)^{-1}\prod\limits_{j\in\mathcal{K}}\mathbb{E}_{\Phi_j}\prod\limits_{x_j\in\Phi_j/x_i}\mathbb{E}_{G^{\mathrm{MRC}}_{x_j,l_i},G^{\mathrm{MRC}}_{x_j,l'_i}}e^{-\frac{P_j(tG^{\mathrm{MRC}}_{x_j,l'_i}+\tau G^{\mathrm{MRC}}_{x_j,l'_i})}{S_j\|x_j\|^{\alpha}}}}{\left(1+t\frac{P_i}{S_i}\epsilon_i^2x_i^{-\alpha}\right)\left(1+\tau\frac{P_i}{S_i}\epsilon_i^2x_i^{-\alpha}\right)\left((1+t\frac{P_i}{S_i}x_i^{-\alpha})(1+\tau\frac{P_i}{S_i}x_i^{-\alpha})\right)^{S_i-2}}dtd\tau \tag{3.51}$$

$$= \int_0^{\infty}\int_0^{\infty}\frac{\left(1+(t+\tau)\frac{P_i}{S_i}x_i^{-\alpha}\right)^{-1}e^{-\tilde{C}(\alpha)\sum\limits_j\lambda_j(\frac{P_j}{S_j})^{\check{\alpha}}\bar{W}_j(t,\tau)}dtd\tau}{\left(1+t\frac{P_i}{S_i}\epsilon_i^2x_i^{-\alpha}\right)\left(1+\tau\frac{P_i}{S_i}\epsilon_i^2x_i^{-\alpha}\right)\left((1+t\frac{P_i}{S_i}x_i^{-\alpha})(1+\tau\frac{P_i}{S_i}x_i^{-\alpha})\right)^{S_i-2}}, \tag{3.52}$$

where in the last step $\overline{W}_j(t,\tau)$ is defined as

$$\overline{W}_j(t,\tau) = \mathbb{E}\left[(tG^{\mathrm{MRC}}_{x_j,l'_i}+\tau G^{\mathrm{MRC}}_{x_j,l'_i})^{\check{\alpha}}\right] \tag{3.53}$$

$$= \int_0^{\infty}\int_0^{\infty}(tg_1+\tau g_2)^{\check{\alpha}}\frac{(g_1g_2)^{S_j-1}}{\Gamma^2(S_j)}e^{-(g_1+g_2)}dg_1dg_2 \tag{3.54}$$

$$= \sum_{l=0}^{S_j-1}\frac{\binom{S_j-1}{l}(-1)^{S_j-1-l}}{\tau^{S_j-\check{\alpha}-1-l}t^{S_j}\Gamma(S_j)^2}\times\int_0^{\infty}\Gamma(\check{\alpha}+l+1,\frac{v}{\tau})e^{-v(\frac{1}{t}-\frac{1}{\tau})}v^{2S_j-2-l}dv. \tag{3.55}$$

To derive (3.55), we note the independence of $G^{\mathrm{MRC}}_{x_j,l'_i}$ and $G^{\mathrm{MRC}}_{x_j,l'_i}$. The proof is completed by obtaining (3.30) through combining (3.41), (3.42) and (3.52).

□

As shown in (3.31), the ICI affects the correlation coefficient mainly through $\Lambda(\boldsymbol{S})$, defined in (2.12), where $\Lambda(\boldsymbol{S})$ is a function of BSs' density, transmission powers and multiplexing

gains, and path-loss exponents[6]. It is further shown in (3.31) that the multiplexing gains and the CSI estimation inaccuracy may affect the correlation by imposing self-interference.

To highlight the impact of various parameters on the SIR correlation, we now investigate the behavior of $\rho_{x_i}^{\mathrm{MRC}}(l_i, l_i')$ in a two-tier HetNet for different settings in Figs. 3.1, 3.2, 3.3, and 3.4.

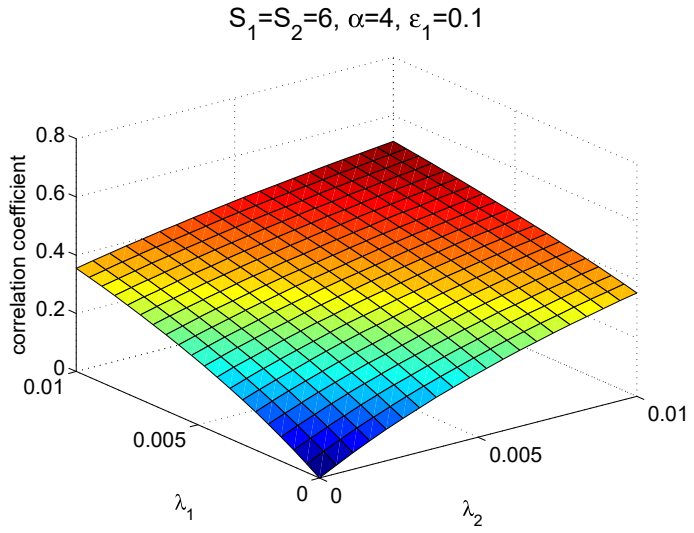

Figure 3.1: Correlation coefficient *vs.* λ_1 and λ_2, when $P_1 = 10$W and $P_2 = 10$W. We set $K = 2$, $N^r = 8$, $\epsilon_1 = 0.1$, $\alpha = 4$, and $x_i = 20$.

Effect of the Density of BSs

Figs. 3.1 and Fig. 3.2 show the impact of λ_1 and λ_2 on $\rho_{x_i}^{\mathrm{MRC}}(l_i, l_i')$. As seen, for a sparse network, where $\lambda_1 \to 0$ and $\lambda_2 \to 0$, the correlation coefficient is very close to 0. In other words, the network behaves like an isolated link, where BSs are sparse in the coverage area. By increasing the density of BSs $\rho_{x_i}^{\mathrm{MRC}}(l_i, l_i')$ gets proportionally increased such that in an extreme case of high density of BSs where $\lambda_1 \approx 0.01$ and/or $\lambda_2 \approx 0.01$, the SIRs of data streams become highly correlated. In such a case, if a data stream, l_i, experiences outage

[6]Note that for the case that CSIR is accurate it is straightforward to calculate the SIR correlation for ZFBF following steps developed in the proof of Proposition 3.4.1. However, if one considers CSIR inaccuracy, one then urges to recalculate the SIR correlation, since under ZFBF the CSIR inaccuracy affects the attending fading gain as well as induces extra source of interference on each data stream.

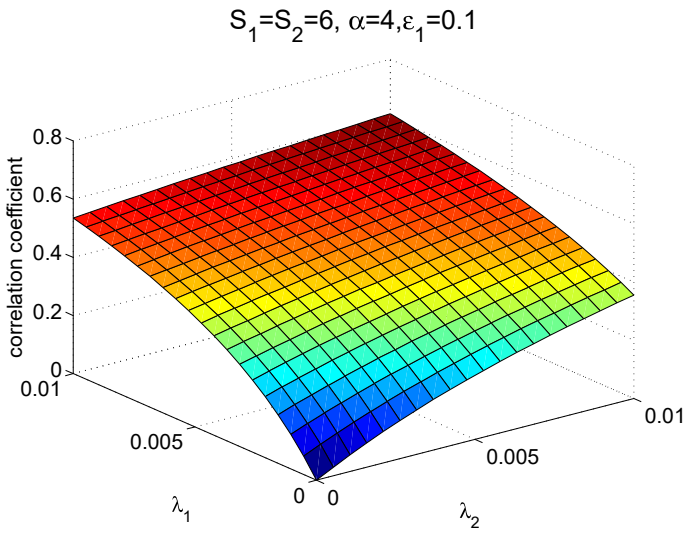

Figure 3.2: Correlation coefficient *vs.* λ_1 and λ_2, when $P_1 = 50$W and $P_2 = 10$W. We set $K = 2$, $N^r = 8$, $\epsilon_1 = 0.1$, $\alpha = 4$, and $x_i = 20$.

due to a close-by interfering BS, then other data streams $l_i' \neq l_i$ will most likely experience the same.

Effect of Transmit Power

A further comparison of Fig. 3.1 and Fig. 3.2 suggests that increasing the transmit power results in a substantial increase of $\rho_{x_i}^{\mathrm{MRC}}(l_i, l_i')$. In fact, by increasing P_1 from 10W to 50W, the correlation coefficient increases almost 125%. When $P_1 > P_2$, the increase of $\rho_{x_i}^{\mathrm{MRC}}(l_i, l_i')$ due to the increase of the density of Tier 1 BSs, λ_1, is larger than that of λ_2.

Impact of the Multiplexing Gains

The impact of multiplexing gains on the correlation coefficient is shown in Fig. 3.3. The higher the multiplexing gains, the greater the correlation coefficient among data streams. In this particular example, S_2 shows a greater impact on increasing $\rho_{x_i}^{\mathrm{MRC}}(l_i, l_i')$ than S_1 since $\lambda_2 > \lambda_1$. This is due mainly to the fact that increasing S_2 increases the level of ICI at the typical UE receiver which, in return, increases the SIR correlation.

Impact of Path-Loss Exponent and CSI Estimation Error

The impact of path-loss exponent is also seen in Fig. 3.4. For a lower α, even a small number of moderately close interferers induce a substantial level of interference. This reduces the SIR for all data streams at the same time, thus causing large correlation among data streams. For a higher value of α, the collective impact of the ICI received from the BSs located far from the receiver causes correlation, and hence unless the density of interferers is very high, the correlation is negligible. From Fig. 3.4, we further observe that the imposed correlation due to the CSI estimation error seems negligible. This is because each individual data stream receives $S_i - 1$ inter-stream interference which is much more powerful than the interference imposed by the CSI estimation error.

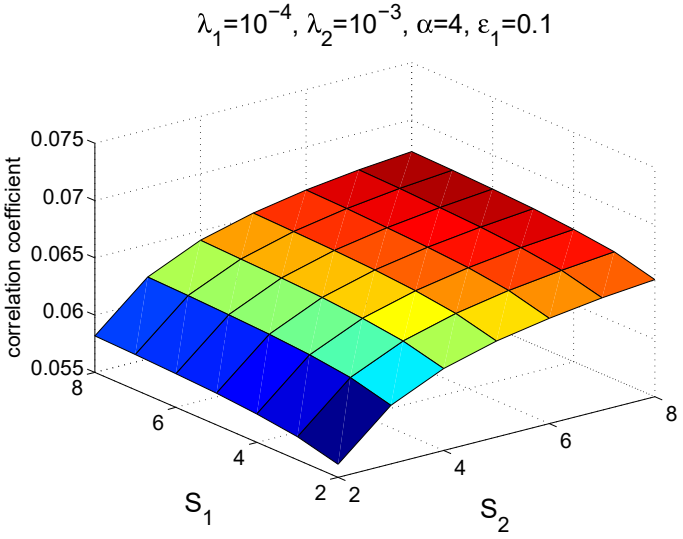

Figure 3.3: Correlation coefficient *vs* S_1 and S_2.

3.4.2 Impact of SIR Correlation on the Coverage Performance under FC Assumption

As Definition 2.4.1, we can also construct FC assumption to analyze the impact of the cross-stream SIR correlation on the coverage performance. Assuming a typical UE is associated

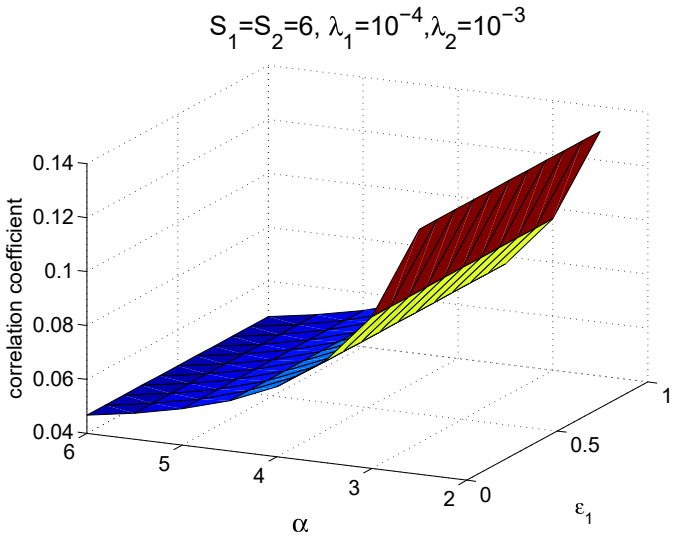

Figure 3.4: Correlation coefficient *vs* α and ϵ_1. Parameters are: $S_1 = S_2 = 6$, $\lambda_1 = 10^{-4}$, and $\lambda_2 = 10^{-3}$

with BS x_i, the corresponding post-processing SIR for stream l_i is

$$\mathrm{SIR}_{x_i,l_i}^{\mathrm{MRC-FC}} = \frac{\frac{P_i}{S_i}\|x_i\|^{-\alpha}(1-\epsilon_i^2)H_{x_i,l_i}^{\mathrm{MRC}}}{\frac{P_i}{S_i\|x_i\|^{\alpha}}\left(\hat{H}_{x_i,l_i}^{\mathrm{MRC}} + \epsilon_i^2\tilde{H}_{x_i,l_i}^{\mathrm{MRC}}\right) + I^{\mathrm{FC}}}. \tag{3.56}$$

We then derive the coverage probability under the FC assumption in the following corollary:

Proposition 3.4.2 (FC Assumption). *In the FC setting, the coverage probability of MIMO-MRC Multiplexing system is upper-bounded as:*

$$c^{\mathrm{MRC-FC}} \leq \frac{\pi}{\Lambda^{\mathrm{FC}}}\sum_{i\in\mathcal{K}}\lambda_i\left(\frac{P_i(1-\epsilon_i^2)}{S_i^2\beta_i}\right)^{\check{\alpha}}\left(\Gamma_i^{\mathrm{MRC}}\right)^{S_i}, \tag{3.57}$$

where Λ^{FC} *is given by* (2.56) *in Proposition 2.4.1.*

Proof. We prove the proposition by following the same line of argument as in the proof of Proposition 3.3.1. In the FC setting, (3.10) is reduced to

$$c^{\mathrm{MRC-FC}} = \sum_{i\in\mathcal{K}} 2\pi\lambda_i \int_0^{\infty} x_i \mathbb{E}_{\{I^{\mathrm{FC}}\}} \prod_{l_i=1}^{S_i} \mathbb{P}\left\{\mathrm{SIR}_{x_i,l}^{\mathrm{MRC-FC}} \geq \beta_i \middle| I^{\mathrm{FC}}\right\} dx_i \tag{3.58}$$

$$= \sum_{i\in\mathcal{K}} 2\pi\lambda_i \int_0^\infty x_i \prod_{l_i=1}^{S_i} \int_0^\infty \frac{\mathcal{L}^{-1}_{\overline{F}_{H_i^{\mathrm{MRC}}}}(t_i)}{\left(1+\frac{t_i\beta_i}{1-\epsilon_i^2}\right)^{S_i-1}(1+\frac{t_i\epsilon_i^2\beta_i}{1-\epsilon_i^2})}$$
$$\times \prod_{j\in\mathcal{K}} \mathbb{E}_{\Phi_j} \prod_{x_j\in\Phi_j\setminus x_i} e^{-t_i\frac{\beta_i S_i x_i^\alpha}{P_i(1-\epsilon_i^2)}P_j\|x_j\|^{-\alpha}} dt_i \tag{3.59}$$

$$\overset{(a)}{=} \sum_{i\in\mathcal{K}} 2\pi\lambda_i \int_0^\infty x_i \int_0^\infty \dots \int_0^\infty e^{-x_i^2\tilde{C}(\alpha)\left(\frac{\beta_i S_i}{P_i(1-\epsilon_i^2)}\right)^{\breve{\alpha}} \sum_{j=1}^{K}\lambda_j P_j^{\breve{\alpha}}(\sum_{l_i=1}^{S_i} t_{l_i})^{\breve{\alpha}}}$$
$$\times \prod_{l_i=1}^{S_i} \frac{\mathcal{L}^{-1}_{\overline{F}_{H_i^{\mathrm{MRC}}}}(t_{l_i})}{\left(1+\frac{t_{l_i}\beta_i}{1-\epsilon_i^2}\right)^{S_i-1}(1+\frac{t_{l_i}\epsilon_i^2\beta_i}{1-\epsilon_i^2})} dt_{l_i} \tag{3.60}$$

$$\overset{(b)}{=} \frac{\pi}{\Lambda^{\mathrm{FC}}} \sum_{i\in\mathcal{K}} \lambda_i \left(\frac{P_i(1-\epsilon_i^2)}{\beta_i S_i^2}\right)^{\breve{\alpha}} \int_0^\infty \dots \int_0^\infty (\sum_{l_i=1}^{S_i} t_{l_i})^{-\breve{\alpha}}$$
$$\times \prod_{l_i=1}^{S_i} \frac{\mathcal{L}^{-1}_{\overline{F}_{H_i^{\mathrm{MRC}}}}(t_{l_i})}{\left(1+\frac{t_{l_i}\beta_i}{1-\epsilon_i^2}\right)^{S_i-1}(1+\frac{t_{l_i}\epsilon_i^2\beta_i}{1-\epsilon_i^2})} dt_{l_i} \tag{3.61}$$

$$\overset{(c)}{\leq} \frac{\pi}{\Lambda^{\mathrm{FC}}} \sum_{i\in\mathcal{K}} \lambda_i \left(\frac{P_i(1-\epsilon_i^2)}{\beta_i S_i^2}\right)^{\breve{\alpha}} \int_0^\infty \dots \int_0^\infty \prod_{l_i=1}^{S_i} \frac{t_{l_i}^{-\frac{\breve{\alpha}}{S_i}}\mathcal{L}^{-1}_{\overline{F}_{H_i^{\mathrm{MRC}}}}(t_{l_i})dt_{l_i}}{\left(1+\frac{t_{l_i}\beta_i}{1-\epsilon_i^2}\right)^{S_i-1}(1+\frac{t_{l_i}\epsilon_i^2\beta_i}{1-\epsilon_i^2})} \tag{3.62}$$

$$\overset{(d)}{=} \frac{\pi}{\Lambda^{\mathrm{FC}}} \sum_{i\in\mathcal{K}} \lambda_i \left(\frac{P_i(1-\epsilon_i^2)}{\beta_i S_i^2}\right)^{\breve{\alpha}} \prod_{l_i=1}^{S_i} \int_0^\infty \frac{t_{l_i}^{-\frac{\breve{\alpha}}{S_i}}\mathcal{L}^{-1}_{\overline{F}_{H_i^{\mathrm{MRC}}}}(t_{l_i})}{\left(1+\frac{t_{l_i}\beta_i}{1-\epsilon_i^2}\right)^{S_i-1}(1+\frac{t_{l_i}\epsilon_i^2\beta_i}{1-\epsilon_i^2})} dt_{l_i} \tag{3.63}$$

$$\overset{(e)}{=} \frac{\pi}{\Lambda^{\mathrm{FC}}} \sum_{i\in\mathcal{K}} \lambda_i \left(\frac{P_i(1-\epsilon_i^2)}{\beta_i S_i^2}\right)^{\breve{\alpha}} \left(\int_0^\infty \frac{t_i^{-\frac{\breve{\alpha}}{S_i}}\mathcal{L}^{-1}_{\overline{F}_{H_i^{\mathrm{MRC}}}}(t_i)dt_i}{\left(1+\frac{t_i\beta_i}{1-\epsilon_i^2}\right)^{S_i-1}\left(1+\frac{t_i\epsilon_i^2\beta_i}{1-\epsilon_i^2}\right)}\right)^{S_i}, \tag{3.64}$$

where in Step (a) we insert the Laplace transform of I^{FC}, and in Step (b) the integrals are reordered and we integrate the inner integral with respect to x_i. In Step (c), arithmetic-geometric inequality is applied, followed by Step (d) and Step (e) where the fading gains, $H^{\mathrm{MRC}}_{x_i,l_i}$, are i.i.d.. Applying the method we developed in (3.21), Step (e) then completes the proof. □

Comparing Propositions 3.3.1 and 3.4.2, we realize that in general for the FC assumption,

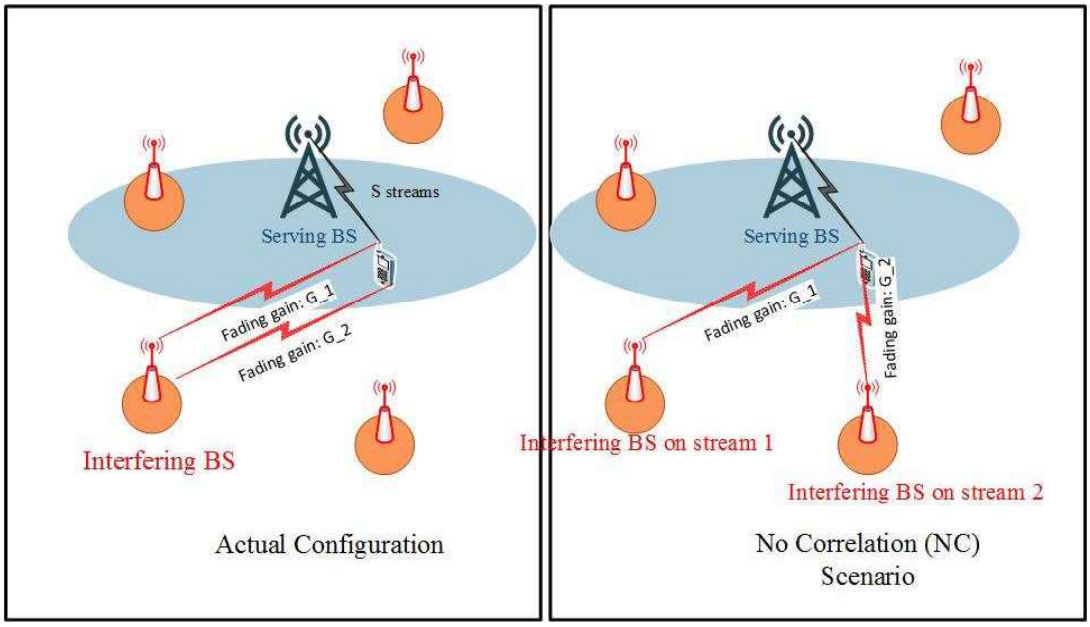

Figure 3.5: This illustration shows an example of the No-correlation (NC) scenario in comparison with the actual configuration of PPP.

the coverage probability has a more simplified form. On the other hand, the upper-bound of the coverage performance of a MIMO-MRC HetNet system is (almost) always higher than the same system assuming the FC assumption. This is because for $\frac{\check{\alpha}}{S_i} \in (0,1)$, there holds $\frac{\Gamma(\frac{\check{\alpha}}{S_i}+S_j)}{\Gamma(S_j)} \lesssim S_j^{\frac{\check{\alpha}}{S_i}}$ [78]. Therefore, since (3.6) and (3.57) have the same numerator while the denominator of the former is larger than that of the latter, we reach the following

$$c^{\mathrm{MRC-FC}} \lesssim c^{\mathrm{MRC}}. \tag{3.65}$$

Consequently, we can conclude that, similar to the case of ZFBF (see Proposition 2.4.2), increased correlation among the data streams of a communication link can reduce the coverage probability. Although this result is based on the derived upper-bounds on the coverage probabilities in (3.6) and (3.57), our simulation results in Section 3.6 confirm its credibility.

3.4.3 What If the Cross-Stream SIR Correlation Is Overlooked?

The above analysis shows that approximating a practical scenario based on the FC setting results in underestimation of the coverage probability. Another way to grasp the impact of cross-stream SIR correlation on the coverage analysis is to simply ignore the cross stream SIR correlation, i.e., statistically independent SIR values. We refer to this case as *no-correlation* (NC) assumption. For an illustrative example refer to Fig. 3.5. As seen, subject to association with BS x_i the location of interfering BSs across data streams is different under the NC assumption. Starting from (3.10) and assuming the NC setting, the coverage probability in (3.10) is written as

$$c^{\mathrm{MRC-NC}} = \sum_{i\in\mathcal{K}} 2\pi\lambda_i \int_0^\infty x_i \prod_{l_i=1}^{S_i} \mathbb{E}_\Phi \mathbb{P}\left\{\mathrm{SIR}^{\mathrm{MRC}}_{x_i,l_i} \geq \beta_i \middle| \Phi\right\} dx_i. \tag{3.66}$$

Note that in (3.66) we move in the expectation operator into the product operator relying upon the NC assumption. The coverage probability in (3.66) can then be written as:

$$\begin{aligned}
c^{\mathrm{MRC-NC}} \quad & \sum_{i\in\mathcal{K}} 2\pi\lambda_i \int_0^\infty x_i \prod_{l_i=1}^{S_i} \int_0^\infty \frac{\mathcal{L}^{-1}_{\overline{F}_{H_i^{\mathrm{MRC}}}}(t_i)}{\left(1+\frac{t_i\beta_i}{1-\epsilon_i^2}\right)^{S_i-1}(1+\frac{t_i\epsilon_i^2\beta_i}{1-\epsilon_i^2})} \\
& \times \prod_{j\in\mathcal{K}} \mathbb{E}_{\Phi_j} \prod_{x_j\in\Phi_j/x_i} \mathbb{E}_{G^{\mathrm{MRC}}_{x_j,l_i}} e^{-t_{l_i}\frac{\beta_i S_i x_i^\alpha}{P_i(1-\epsilon_i^2)}\frac{P_j G^{\mathrm{MRC}}_{x_j,l_i}}{S_j\|x_j\|^\alpha}} dt_i \qquad (3.67) \\
& \overset{(a)}{=} \sum_{i\in\mathcal{K}} 2\pi\lambda_i \int_0^\infty x_i \int_0^\infty \cdots \int_0^\infty e^{-x_i^2\Lambda(\boldsymbol{S})\left(\frac{\beta_i S_i}{P_i(1-\epsilon_i^2)}\right)^{\check{\alpha}}(\sum_{l_i=1}^{S_i} t_{l_i}^{\check{\alpha}})} \\
& \times \prod_{l_i=1}^{S_i} \frac{\mathcal{L}^{-1}_{\overline{F}_{H_i^{\mathrm{MRC}}}}(t_{l_i})}{\left(1+\frac{t_{l_i}\beta_i}{1-\epsilon_i^2}\right)^{S_i-1}(1+\frac{t_{l_i}\epsilon_i^2\beta_i}{1-\epsilon_i^2})} dt_{l_i} \qquad (3.68) \\
& = \frac{\pi}{\Lambda(\boldsymbol{S})} \sum_{i\in\mathcal{K}} \lambda_i \left(\frac{P_i(1-\epsilon_i^2)}{\beta_i S_i^2}\right)^{\check{\alpha}} \int_0^\infty \cdots \int_0^\infty \left(\prod_{l_i=1}^{S_i} t_{l_i}\right)^{-\check{\alpha}} \\
& \times \prod_{l_i=1}^{S_i} \frac{\mathcal{L}^{-1}_{\overline{F}_{H_i^{\mathrm{MRC}}}}(t_{l_i})}{\left(1+\frac{t_{l_i}\beta_i}{1-\epsilon_i^2}\right)^{S_i-1}(1+\frac{t_{l_i}\epsilon_i^2\beta_i}{1-\epsilon_i^2})} dt_{l_i} \qquad (3.69)
\end{aligned}$$

$$= \frac{\pi}{\Lambda(\boldsymbol{S})} \sum_{i\in\mathcal{K}} \lambda_i \left(\frac{P_i(1-\epsilon_i^2)}{\beta_i S_i^2}\right)^{\breve{\alpha}} \prod_{l_i=1}^{S_i} \int_0^\infty \frac{t_{l_i}^{-\breve{\alpha}} \mathcal{L}^{-1}_{\overline{F}_{H_i^{\mathrm{MRC}}}}(t_{l_i})}{\left(1+\frac{t_{l_i}\beta_i}{1-\epsilon_i^2}\right)^{S_i-1}(1+\frac{t_{l_i}\epsilon_i^2\beta_i}{1-\epsilon_i^2})} dt_{l_i} \quad (3.70)$$

$$\overset{(b)}{=} \frac{\pi}{\Lambda(\boldsymbol{S})} \sum_{i\in\mathcal{K}} \lambda_i \left(\frac{P_i(1-\epsilon_i^2)}{\beta_i S_i^2}\right)^{\breve{\alpha}} \left(\int_0^\infty \frac{t_i^{-\breve{\alpha}} \mathcal{L}^{-1}_{\overline{F}_{H_i^{\mathrm{MRC}}}}(t_i)}{\left(1+\frac{t_i\beta_i}{1-\epsilon_i^2}\right)^{S_i-1}(1+\frac{t_i\epsilon_i^2\beta_i}{1-\epsilon_i^2})} dt_i \right)^{S_i} \quad (3.71)$$

where in Step (a) we insert the Laplace transform of the ICI and further notice the definition of $\Lambda(\boldsymbol{S})$ from (2.12). Denoting the integral in Step (b) by $\Gamma_i^{\mathrm{MRC-NC}}$ we then have

$$\Gamma_i^{\mathrm{MRC-NC}} \triangleq \sum_{r_i=0}^{N^r-1} \sum_{q_i=0}^{r_i} \sum_{p_i=0}^{q_i} \frac{(-1)^{q_i-p_i}\beta_i^{2q_i-p_i}}{\epsilon_i^{-4q_i+2p_i}(1-\epsilon_i^2)^{S_i}} \frac{(1-\epsilon_i^2+\beta_i)^{-q_i-S_i+1}\left(1+\epsilon_i^2(\beta_i-1)\right)^{-q_i+p_i-1}}{p_i \mathrm{B}(S_i-1,p_i)(r_i-q_i)\mathrm{B}(\breve{\alpha},r_i-q_i)}. \quad (3.72)$$

We then have

$$c^{\mathrm{MRC-NC}} = \frac{\pi}{\Lambda(\boldsymbol{S})} \sum_{i\in\mathcal{K}} \lambda_i \left(\frac{P_i(1-\epsilon_i^2)}{S_i\beta_i}\right)^{\breve{\alpha}} \left(\Gamma_i^{\mathrm{MRC-NC}}\right)^{S_i}. \quad (3.73)$$

Note that the NC setting is in fact an impractically extreme case and thus $c^{\mathrm{MRC-NC}}$ is not achievable. This is because it does not comply with the max-SIR CA rule as in the NC setting, an independent set of interferers appears on each data stream. On the other hand, there might be cases where the typical UE becomes associated with different BSs for different data streams. This, however, contradicts the reality of the MIMO signal model as presented in (3.2).

Utilizing Proposition 3.4.2, we further note that, as $\breve{\alpha} \in (0,1)$, by using $\frac{\Gamma(\breve{\alpha}+S_j)}{\Gamma(S_j)} \lesssim S_j^{\breve{\alpha}}$ a lower-bound on $c^{\mathrm{MRC-NC}}$ is therefore

$$c^{\mathrm{MRC-NC}} \gtrsim \frac{\pi \sum_{i\in\mathcal{K}} \lambda_i \left(\frac{P_i(1-\epsilon_i^2)}{S_i^2\beta_i}\right)^{\breve{\alpha}} \left(\Gamma_i^{\mathrm{MRC-NC}}\right)^{S_i}}{\Lambda^{\mathrm{FC}}} \quad (3.74)$$

$$\geq \frac{\pi \sum_{i\in\mathcal{K}} \lambda_i \left(\frac{P_i(1-\epsilon_i^2)}{S_i^2\beta_i}\right)^{\breve{\alpha}} \left(\Gamma_i^{\mathrm{MRC}}\right)^{S_i}}{\Lambda^{\mathrm{FC}}} \quad (3.75)$$

$$= c^{\mathrm{MRC-FC}}, \quad (3.76)$$

where the second inequality is because $\Gamma_i^{\mathrm{MRC-NC}} \geq \Gamma_i^{\mathrm{MRC}}$. To confirm this, we notice that the beta function is a decreasing function of its arguments, and observing that by comparing $\Gamma_i^{\mathrm{MRC-NC}}$ in (3.72) and Γ_i^{MRC} in (3.7), we note that for a given positive number a, we have

$$\Gamma_i^{\mathrm{MRC-NC}} - \Gamma_i^{\mathrm{MRC}} \propto \frac{1}{\mathrm{B}(\check{\alpha}, a)} - \frac{1}{\mathrm{B}(\frac{\check{\alpha}}{S_i}, a)}. \tag{3.77}$$

On the other hand, since $\frac{\check{\alpha}}{S_i} \in (0,1)$, there holds [78]

$$\frac{\Gamma(\frac{\check{\alpha}}{S_i} + S_j)}{\Gamma(S_j)} > S_j^{\frac{\check{\alpha}}{S_i}} \Gamma(1 + \frac{\check{\alpha}}{S_i}). \tag{3.78}$$

Applying this, c^{MRC} in (3.6) can further be upper-bounded as

$$\begin{aligned} c^{\mathrm{MRC}} &\leq \frac{\pi \sum\limits_{i \in \mathcal{K}} \lambda_i \left(\frac{P_i(1-\epsilon_i^2)}{S_i^2 \beta_i}\right)^{\check{\alpha}} \left(\Gamma_i^{\mathrm{MRC}} \Gamma(1 + \frac{\check{\alpha}}{S_i})\right)^{S_i}}{\Lambda^{\mathrm{FC}}} && (3.79) \\ &\leq \frac{\pi \sum\limits_{i \in \mathcal{K}} \lambda_i \left(\frac{P_i(1-\epsilon_i^2)}{S_i^2 \beta_i}\right)^{\check{\alpha}} \left(\Gamma_i^{\mathrm{MRC}}\right)^{S_i}}{\Lambda^{\mathrm{FC}}} && (3.80) \\ &\leq c^{\mathrm{MRC-NC}}, && (3.81) \end{aligned}$$

where the last line is because $\Gamma(1 + \frac{\check{\alpha}}{S_i}) \leq 1$ for $\frac{\check{\alpha}}{S_i} \in (0,1)$. Consequently, using the NC setting, the coverage probability is basically overestimated. This implies that the common approach that focuses on either isolated scenarios or non-isolated scenarios but with emphasis on characterization of MIMO communications from the perspective of a data stream is essentially an overestimation of the actual performance of the network[7].

[7]We should mention that since our focus here is on the interference-limited scenario and inaccurate CSIR, the method we used to derive the coverage probability and its relationship with the actual coverage performance under the FC assumption is different from the method we adopted in the previous chapter. However, as we noticed a striking resemblance between the coverage probability under MRC receiver and that of ZFBF in (2.116), it is then possible to reach the conclusions of this section for the case of interference-limited ZFBF too.

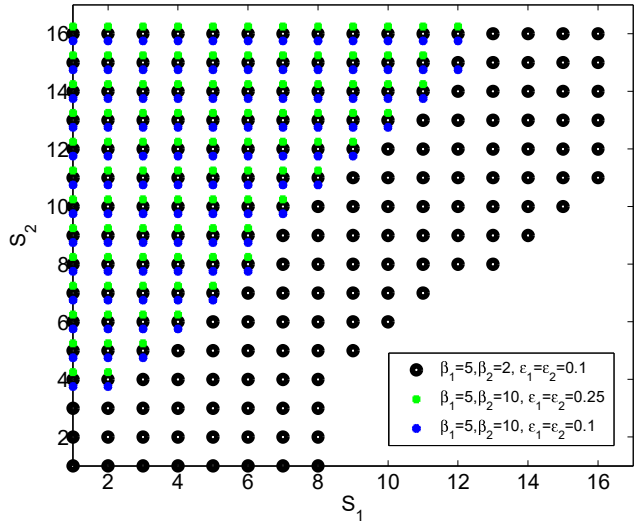

Figure 3.6: Combinations of multiplexing gains for which $\frac{\partial c^{\mathrm{MRC}}}{\partial \tilde{\lambda}_1} > 0$. Parameters are $\alpha = 4$, $P_1 = 50$W, and $P_2 = 1$W.

3.5 Design Issues

Here we explore various design issues related to the developed analysis in Section 3.3. Throughout this section, we then consider max-SIR CA rule and consider the actual coverage probability derived in Proposition 3.3.1.

3.5.1 Is Densification Always Beneficial?

Does Densification Always Improve the Coverage Probability?

We investigate the impact of densification on the coverage probability. We are interested in combinations of system parameters for which the coverage probability is increased by increasing the density of the BS in a given tier, namely Tier 1: $\frac{\partial c^{\mathrm{MRC}}}{\partial \tilde{\lambda}_1} > 0$. For brevity, we set $K = 2$, and $\tilde{\lambda}_1 = \lambda_1 (P_1/S_1)^{\check{\alpha}}$, $\tilde{\lambda}_2 = \lambda_2 (P_2/S_2)^{\check{\alpha}}$, $A_{ji} = \left(\frac{\Gamma(\frac{\check{\alpha}}{S_i} + S_j)}{\Gamma(S_j)} \right)^{S_i}$. In this case, it can be shown that for $\frac{\partial c^{\mathrm{MRC}}}{\partial \tilde{\lambda}_1} > 0$, it is necessary to have $\frac{\tilde{\lambda}_2}{\tilde{\lambda}_1}(A_{21} - BA_{22}) < A_{12}B - A_{11}$, where $B = \sqrt{\left(\frac{(1-\epsilon_1^2)\beta_2 S_2}{(1-\epsilon_2^2)\beta_1 S_1} \right)^{\check{\alpha}} \frac{(\Gamma_1^{\mathrm{MRC}})^{S_1} A_{21}}{(\Gamma_2^{\mathrm{MRC}})^{S_2} A_{12}}}$.

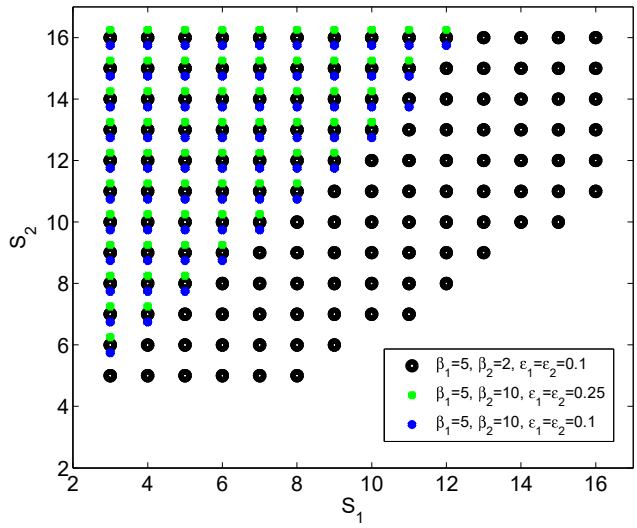

Figure 3.7: Combinations of multiplexing gains for which $\frac{\partial \mathrm{ASE}_{\mathrm{all}}^{\mathrm{MRC}}}{\partial \tilde{\lambda}_1} > 0$. Parameters are $\alpha = 4$, $P_1 = 50$W, and $P_2 = 1$W.

Fig. 3.6 shows various combinations of the multiplexing gains that guarantee $\frac{\tilde{\lambda}_2}{\tilde{\lambda}_1}(A_{21} - BA_{22}) < A_{12}B - A_{11}$. In general, for densification of Tier 1 to be effective in improving coverage performance, we need $S_2 > S_1$. In fact, as decoding S_2 data streams is more unlikely than S_1 data streams, densification of Tier 1 allows UEs to be more frequently associated with Tier 1, thus improving the coverage probability. Moreover, as β_1 or CSI inaccuracy increases, we get a smaller number of multiplexing gain combinations, (S_1, S_2), in which densification improves the coverage probability.

Does Densification Always Improve the Area Spectral Efficiency?

ASE is an essential performance metric which indicates efficiency of spectral usage throughout the coverage area of a wireless network. In a MIMO HetNet, the data rate of tier i is $S_i \log(1 + \beta_i)$, therefore,

$$\mathrm{ASE}^{\mathrm{MRC}} = \sum_i \lambda_i S_i c_i^{\mathrm{MRC}} \log(1 + \beta_i), \tag{3.82}$$

where c_i^{MRC} denotes the probability that a BS in Tier i is being successfully associated with the typical UE. Using Proposition 3.3.1, we then write

$$c_i^{\mathrm{MRC}} \leq \frac{\pi}{\tilde{C}(\alpha)} \frac{\lambda_i \left(\frac{P_i}{S_i^2 \beta_i}\right)^{\check{\alpha}} (\Gamma_i^{\mathrm{MRC}})^{S_i}}{\sum_{j=1}^{K} \lambda_j \left(\frac{P_j}{S_j}\right)^{\check{\alpha}} \left(\frac{\Gamma(\frac{\check{\alpha}}{S_i}+S_j)}{\Gamma(S_j)}\right)^{S_i}}. \tag{3.83}$$

Here we are interested in system parameters combinations so that $\frac{\partial \mathrm{ASE}^{\mathrm{MRC}}}{\partial \tilde{\lambda}_1} > 0$, i.e., densification in Tier i, increases the ASE. Straightforward mathematical derivations lead to $\tilde{B}\frac{\frac{\tilde{\lambda}_1}{\lambda_2}A_{12}+A_{22}}{A_{12}} \geq \frac{\frac{\tilde{\lambda}_1}{\lambda_2}A_{11}+A_{21}}{\frac{\tilde{\lambda}_1}{\lambda_2}A_{12}+2A_{21}}$, where $\tilde{B} \triangleq \sqrt{\left(\frac{(1-\epsilon_1^2)\beta_2 P_2}{(1-\epsilon_2^2)\beta_1 P_1}\right)^{\check{\alpha}} \frac{(\Gamma_1^{\mathrm{MRC}})^{S_1}\log(1+\beta_1)}{(\Gamma_2^{\mathrm{MRC}})^{S_2}\log(1+\beta_2)}}$.

Fig. 3.7 shows the combinations of multiplexing gains in which the densification of Tier 1 results in an ASE improvement. For $S_2 \geq S_1$, even for small β_1, it is still possible to have a higher multiplexing gain, S_1, while densifying Tier 1. Comparison of Figs. 3.6 and 3.7 further suggests that to improve ASE by densification in Tier 1, i.e., increasing λ_1, one needs to have a higher multiplexing gain in Tier 2, $S_2 > S_1$.

3.5.2 Selecting the Transceiver Technique

We first compare two prevalent open-loop techniques: ZFBF and MRC from the coverage probability perspective. Here we assume perfect CSIR, i.e., $\epsilon_i = 0\ \forall i$. Using (2.116) and Proposition 3.3.1, we can now inspect whether ZFBF outperforms MRC. For clarity, we set $K = 1$. It is then straightforward to confirm that $c^{\mathrm{ZF}} > c^{\mathrm{MRC}}$ if $\Gamma_1^{\mathrm{ZF}} > \Gamma_1^{\mathrm{MRC}}$.

Fig. 3.8 shows that, in general, ZFBF yields a higher coverage probability than MRC. This is mainly because the MRC receivers suffer from inter-stream interference. Furthermore, as shown in Fig. 3.8-(a), by increasing the multiplexing gain, ZFBF becomes even more efficient than MRC. For a larger N^r, the superiority of ZFBF over MRC is shown to be reduced because the MRC receivers can harness diversity more effectively than ZFBF. Noticing that the ZFBF receiver complexity of a large array can be very high (because of the required matrix inversion operation), MRC provides room for compromising coverage performance

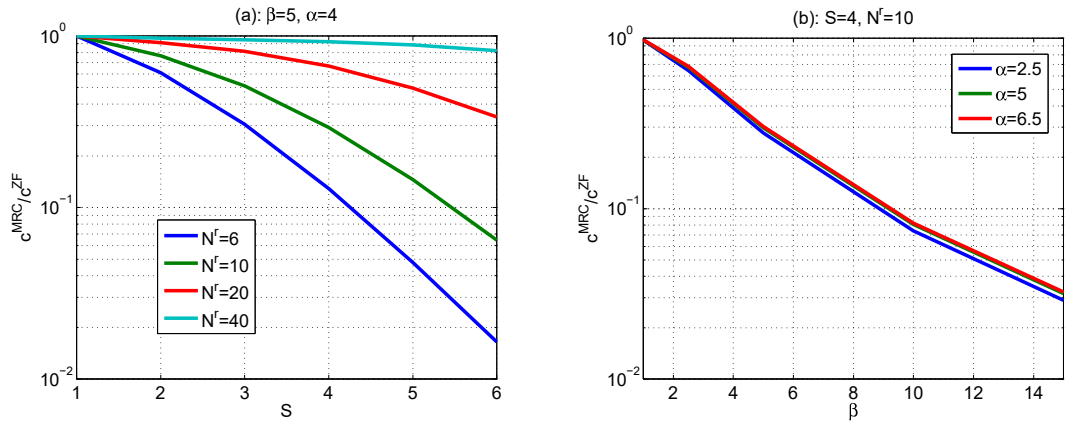

Figure 3.8: (a) $\frac{c^{\mathrm{MRC}}}{c^{\mathrm{ZF}}}$, *vs.* the multiplexing gain S; (b) $\frac{c^{\mathrm{MRC}}}{c^{\mathrm{ZF}}}$ *vs.* the SIR threshold β. Parameters are: $\alpha = 4$, $K = 2$, $P_1 = 50$ W, $P_2 = 10$ W.

(in fact, slightly for larger arrays) over computational complexity. Such aspects can be exploited in the design of HetNets. For instance, it is plausible to adaptively select either ZFBF or MRC in order to keep the prescribed coverage performance intact, while minimizing the complexity and energy consumption of the signal processing modules at the receivers.

Remark 3.5.1. *For the adaptive selection amongst ZFBF or MRC, one requires to know the density of BSs and other relevant system parameters, e.g., multiplexing gain, SIR thresholds, and the like. In general, since such a design problem requires network-level performance metrics, e.g., coverage probability and ASE, the design problem can be solved once a while (e.g., each 10 minutes or so). This is because, the average behavior of the network may not considerably change during a short period of time. In practice, a centralized entity is responsible for gathering relevant system parameters and solving the optimization problem. Nevertheless, it is also possible to solve the optimization problem in a distributed fashion via distributed algorithms and allowing singnaling/handshaking across adjacent BSs.*

Fig. 3.8-(b) also indicates that for a larger SIR threshold, β, ZFBF significantly outperforms MRC, while for small to moderate values of β, ZFBF is only slightly better than MRC. This observation suggests that for low-rate scenarios (e.g., for the cell-edge UEs) one can trade off a slightly higher performance for a significantly lower computational complexity.

Fig. 3.8 further indicates that the relative performance of ZFBF and MRC is not related to the path-loss exponent.

Now we explore if there is any benefit in adopting MRC over ZFBF, despite the above discussion that the former in general renders the shrinkage of coverage footprint. We here consider ASE as the main performance indicator. Given the simplicity of MRC receivers, we are specifically interested in seeing whether there are cases in which considering both spectral efficiency and the associated computational complexity, it is justifiable to use MRC over ZFBF. We consider the following optimization problem:

$$\mathcal{O}_1: \quad \eta^*(\zeta_1,\zeta_2) = \max \frac{\sum\limits_i \lambda_i S_i c_i^{\mathrm{MRC}} \log(1+\beta_i)}{\sum\limits_i \lambda_i S_i c_i^{\mathrm{ZF}} \log(1+\beta_i)} \left(\sum_i \chi_{\frac{\mathrm{ZF}}{\mathrm{MRC}}}(N^r, S_i)\right)^{\zeta_2} \tag{3.84}$$

$$s.t. \;\; \lambda_i \geq 0, \beta_i \geq 1, 1 \leq S_i \leq \min\{N^r, N_i^t\}, \;\; \forall i \tag{3.85}$$

$$c^{\mathrm{ZF}} - c^{\mathrm{MRC}} \leq \zeta_1. \tag{3.86}$$

In $\mathcal{O}_1$, $\chi_{\frac{\mathrm{ZF}}{\mathrm{MRC}}}(N^r, S_i)$ represents the computational cost (number of arithmetic operations) of adopting ZFBF in Tier i over MRC. This parameter incorporates the corresponding computational cost of the required extra matrix multiplication and inversion while using ZFBF. The computational cost $\chi_{\frac{\mathrm{ZF}}{\mathrm{MRC}}}(N^r, S_i)$ of Tier i is formulated as $\chi_{\frac{\mathrm{ZF}}{\mathrm{MRC}}}(N^r, S_i) \propto \mathcal{O}(S_i^2 N^r) + \mathcal{O}((S_i)^{2+c_{\mathrm{inv}}})$ [171]—The first (resp. second) term is associated with the computational cost of matrix multiplication (resp. matrix inversion). For optimized CW-like algorithm's matrix inversion, we have c_{inv} =0.373 [171, Section 28]. In $\mathcal{O}_1$, $\zeta_2 \geq 0$ represents the level of importance of the computational cost as part of the performance objective. A larger ζ_2 indicates that a designer imposes more stress regarding the computational cost in the system design, due to battery life, energy consumption, processing power, etc.

In $\mathcal{O}_1$, $\sum\limits_i \lambda_i S_i c_i^{\mathrm{MRC}} \log(1+\beta_i)$ (resp. $\sum\limits_i \lambda_i S_i c_i^{\mathrm{ZF}} \log(1+\beta_i)$) further represents the ASE of MRC (resp. ZFBF) techniques, respectively, assuming per cell per frame each tier designates merely one feedback bit to convey back whether it is in the coverage or not. Recall that since in Tier i, the number of transmitted data streams is S_i, then the ASE is proportionally

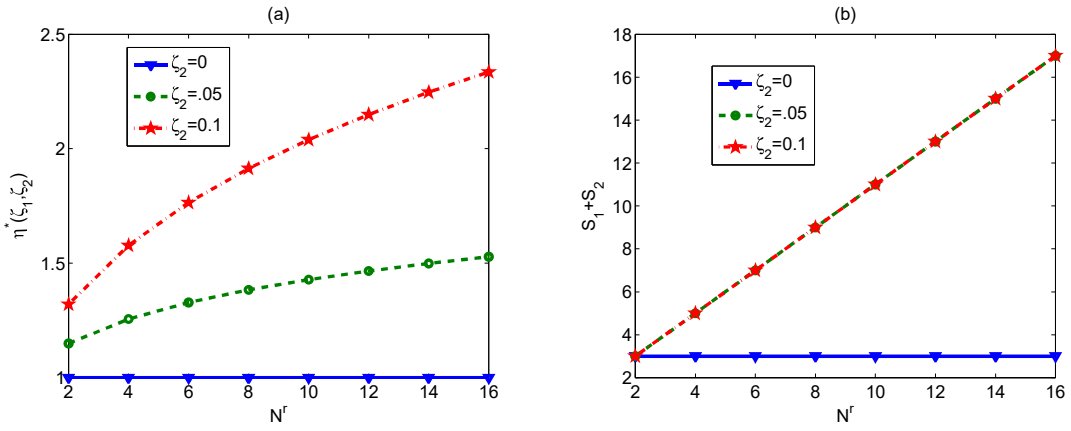

Figure 3.9: (a) $\eta^*(\zeta_1, \zeta_2)$ *vs.* N^r; (b) $S_1 + S_2$ *vs.* N^r; Parameters are: $\alpha = 4$, $K = 2$, $P_1 = 50$ W, $P_2 = 10$ W.

increased by increasing S_i. However, since the coverage probability in each tier is also proportionally reduced by increasing S_i, the growth of S_i may not necessarily result in a higher ASE.

The objective of $\mathcal{O}_1$ is to maximize a performance objective including the relative ASE of MRC over ZFBF and the associated computational cost of using ZFBF. This optimization is subject to the required coverage constraint of MRC system over ZFBF, i.e., $c^{\text{ZF}} - c^{\text{MRC}} \leq \zeta_1$, where $\zeta_1 \in (0, 1)$ is the maximum acceptable coverage loss compared to ZFBF due to the adoption of MRC. Optimization variables in $\mathcal{O}_1$ are the SIR thresholds, deployment densities, and multiplexing gains.

In Fig. 3.9-(a) and Fig. 3.9-(b), we respectively present $\eta^*(\zeta_1 = 0.05, \zeta_2)$, and the total transmitted data streams across tiers, $S_1 + S_2$, versus N^r. In Fig. 3.9-(a), for $\zeta_2 = 0$ (computational cost is not of importance to the system designer) ZFBF does not show any advantage over MRC as both systems have the same ASE. For $\zeta_2 > 0$, however, Fig. 3.9-(a) shows that MRC makes a significant performance gain over ZFBF, where the performance measure $\eta^*(\zeta_1 = 0.05, \zeta_2 > 0)$ grows by increasing N^r as well as ζ_2. Fig. 3.9-(b) further indicates that S_1+S_2 (accumulated multiplexing gains across tiers) is increased by increasing N^r. However, by increasing ζ_2 from 0.05 to 0.1, an increase of $\eta^*(\zeta_1 = 0.05, \zeta_2 > 0)$ does not

increase the accumulated multiplexing gains, $S_1 + S_2$ (see Fig. 3.9-(b)), which is due to the coverage constraint.

The above results suggest that when the computational cost is incorporated, as is the case in practice, MRC appears to be a better option.

3.5.3 Optimizing the Aggregate Multiplexing Gains

As we did in Section 2.8, here, we also investigate whether or not one can increase multiplexing gains in MRC without compromising the coverage performance compared to a single-stream system (SIMO). Similar to the optimization problem in (2.131), we derive the best combinations of multiplexing gains S_1 and S_2 that guarantee $c^{\text{SIMO}} - c^{\text{MRC}} < \xi_3$, where $\xi_3 \in (0, 1)$ is a given threshold:

$$O_2 : \quad \max_{S_1, S_2} (S_1 + S_2) \tag{3.87}$$

$$s.t. \quad c^{\text{SIMO}} - c^{\text{MRC}} \leq \xi_3.$$

This optimization provides the maximum number of data streams across tiers, subject to an acceptable level of coverage degradation compared to SIMO. Note that compared to (2.131), the above optimization also allows to explore the impact of estimation error on the multiplexing gain of the network.

In Figs. 3.10-(a) and 3.10-(b) for $\epsilon_i = \epsilon = 0.1$ $\forall i$ (lower inaccuracy level), and Figs.3.11-(a) and 3.11-(b) for $\epsilon_i = \epsilon = 0.25$, $\forall i$ (higher inaccuracy level), we derive the optimal values for several values of deployment densities where $\zeta_3 = 0.05$ (Here optimal values of multiplexing gains are the ones that maximize the objective function in optimization problem 3.87). For $\epsilon_i = \epsilon = 0.1$, Figs. 3.10-(a) and 3.10-(b) show that multi-stream MIMO communications with large multiplexing gains across tiers can be adopted without degrading the coverage probability compared to SIMO. It is, however, important to carefully select the multiplexing gains in each tier according to deployment densities. For instance, Fig. 3.10-

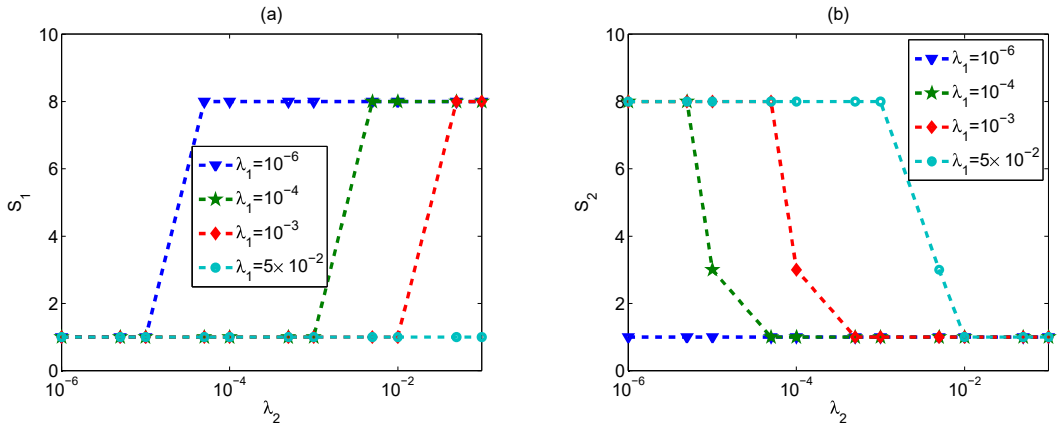

Figure 3.10: (a) S_1, *vs.* λ_2 when $\epsilon_i = \epsilon = 0.1$; (b) S_2, *vs.* λ_2 when $\epsilon_i = \epsilon = 0.1$.

(a) implies that by increasing λ_2 it is possible to increase S_1, but by densification of Tier 1 a smaller S_1 should be selected. Therefore, a large S_1 is suitable only when Tier 2 is highly densified. Fig. 3.10-(b) also shows that simultaneous densification and increasing multiplexing in Tier 2 compromise the coverage probability. Similarly, with densification in Tier 1, one should select a smaller multiplexing gain in Tier 2.

We then conclude that by increasing the multiplexing gain in a tier, the coverage performance might be compromised, and thus densification in the other tier is required to preserve the coverage performance. This is because by increasing the multiplexing gain of a tier, it becomes harder to preserve the required coverage performance. Therefore, the potential coverage loss needs to be compensated for through densification in the other tier while keeping its multiplexing gain as small as possible such that a larger number of UEs is getting associated with this tier. Similar conclusion is also derived from our previous numerical analysis in Chapter 2.8 in optimization problem (2.131).

We further consider the cases with a higher level of CSI inaccuracy ($\epsilon_i = \epsilon = 0.25$), see Figs. 3.11-(a) and 3.11-(b). Comparison of Figs. 3.10-(a) and 3.10-(b) shows that increasing the level of CSI inaccuracies reduces the suitability of multi-stream communications. Fig. 3.11-(a) also indicates that there is no setting for which multi-stream communications in

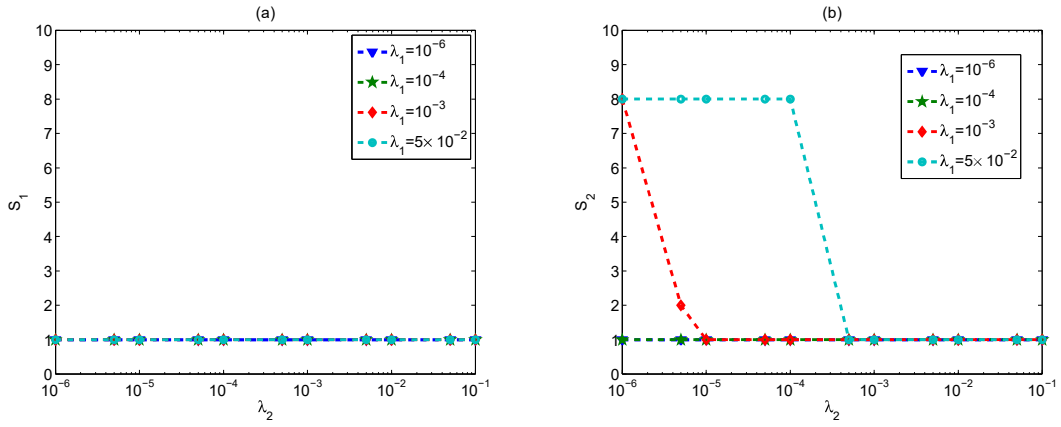

Figure 3.11: (a) S_1, *vs.* λ_2 when $\epsilon_i = \epsilon = 0.25$; (b) S_2, *vs.* λ_2 when $\epsilon_i = \epsilon = 0.25$.

Tier 1 can improve the coverage while according to Fig. 3.11-(b), Tier 2 can still support multi-stream communications. Consistent with the low-level inaccuracy in Figs. 3.10-(a) and 3.10-(b), we also observe that a simultaneous increase of λ_2 and S_2 does not improve coverage.

3.6 Simulation Results

The simulation setup in the following is exactly the one already discussed in Section 2.7, with the difference that in the following the CSI is inaccurately known at the receivers.

Impact of Path-loss Exponent, CSI Estimation Error, and SIR Threshold

Fig. 3.12 shows the coverage probability versus the estimation error, $\epsilon = \epsilon_i$, $\forall i$, for several values of the path-loss exponent, α. The upper-bound is shown to be close to the simulation result. Also, increased CSI inaccuracy is shown to reduce the coverage performance. This is because the interference on each data stream is increased due to the CSI inaccuracy. It is also seen in Fig. 3.12 that increasing the path-loss exponent improves the outage performance.

Remark 3.6.1. *Finding out that "the larger is the path-loss exponent, the larger will be the coverage probability" may come with surprise. However, note that while growing α reduces*

the effective received power of attending signal per data stream, it also weakens the aggregate interference. As seen, the latter takes precedence, thus the coverage probability improves. On the other hand, noting that a larger α implies a smaller signal strength, the improved outage performance suggests that the ICI is one of the main limiting factor in HetNets.

Fig. 3.12 also shows that in contrast to the cases with a smaller path-loss exponent (e.g., outdoor communications), the coverage is not significantly affected by the CSI inaccuracy when the path-loss exponent is high (e.g., indoor communications). This suggests that a simpler signaling protocol (that may cause higher CSI inaccuracy) can be used when the path-loss exponent is large without any significant compromise of the coverage probability.

Remark 3.6.2. *In our simulation setup we do not distinguish between indoor and outdoor. Yet, in practice the coverage area is partially covered by buildings and other obstacles. As a result, the considered path-loss exponent in the simulation setup should be regarded as the mean value of path-loss exponent. Thus, one can argue that the larger path-loss exponent is more akin to the scenarios that a larger portion of the network is covered by buildings. Accordingly, as it is more likely that the typical user is located indoor, this regime is representing the indoor communication setup.*

Fig. 3.13 shows the coverage probability versus β_2. The upper-bound obtained in Proposition 3.3.1 is shown to be sufficiently accurate even for small values of β_2 (see also Remark 2.3.2 in Chapter 2). It also shows that a higher β_2 results in a lower coverage performance.

Impact of Densification and Multiplexing Gains

In Figs. 3.14, 3.15, 3.16 and 3.17 the coverage probability is given versus λ_1. We consider 5 settings (Stg) of multiplexing gains between two tiers, where Stg1, Stg2, Stg3, Stg4, and Stg5, respectively, refer to $(S_1 = 1, S_2 = 1)$, $(S_1 = 4, S_2 = 1)$, $(S_1 = 4, S_2 = 2)$, $(S_1 = 1, S_2 = 2)$, and $(S_1 = 8, S_2 = 2)$. Figs. 3.14 and 3.15 show the coverage performance for Stg1, Stg2, and Stg3. The results of Stg1, Stg4, and Stg5 are plotted in Fig. 3.16 and Fig. 3.17. All figures

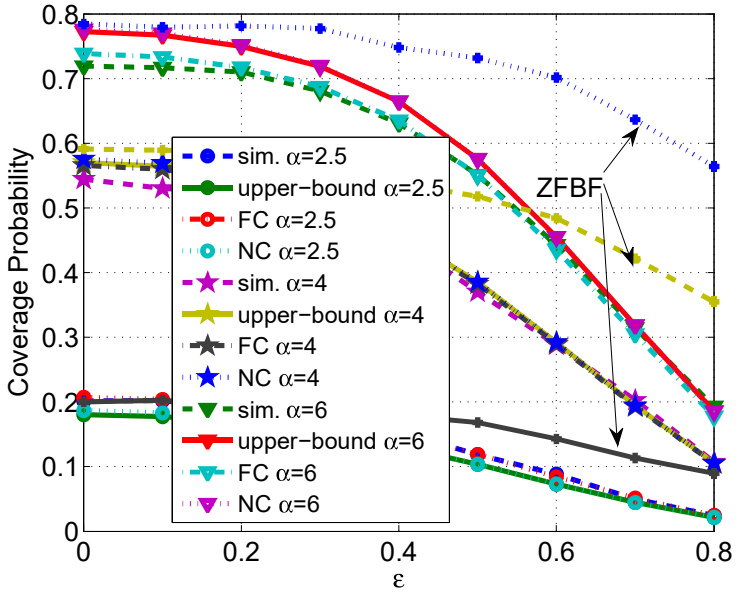

Figure 3.12: Coverage probability *vs.* the CSI estimation error. Parameters are: $S_1 = 4$, $S_2 = 1$, $\lambda_1 = 10^{-4}$, $\lambda_2 = 10^{-2}$, $\beta_1 = 5$, and $\beta_2 = 10$.

demonstrate the outage performance for two values of densities $\lambda_2 = 10^{-3}$ and $\lambda_2 = 10^{-2}$.

It is seen in Figs. 3.14, 3.15, 3.16 and 3.17 that the analytical result presented in Proposition 3.3.1 closely follows the simulation results. It is also observed that a single stream communications, Stg1, generally outperforms the other combinations of multiplexing gains, regardless of the density of the BSs in both tiers. For the single stream case, it is also seen that densification in Tier 1 always results in a higher improvement in the coverage probability. Nevertheless, comparison of Fig. 3.14 with Fig. 3.15 (resp. Fig. 3.16 with Fig. 3.17) suggests that the improvement of the coverage probability by increasing λ_1 is reduced if Tier 2 is also densified at the same time.

Fig. 3.14 and Fig. 3.15 also show that for a small to moderate λ_1, increasing S_1 from 1 to 4 (Stg1 $\rightarrow$ Stg2) does not compromise coverage performance. However, for a sufficiently large λ_1, the coverage performance in Stg2 is significantly reduced. Comparing Fig. 3.14 with Fig. 3.15, we further observe that for a higher value of λ_2, the positive impact of having

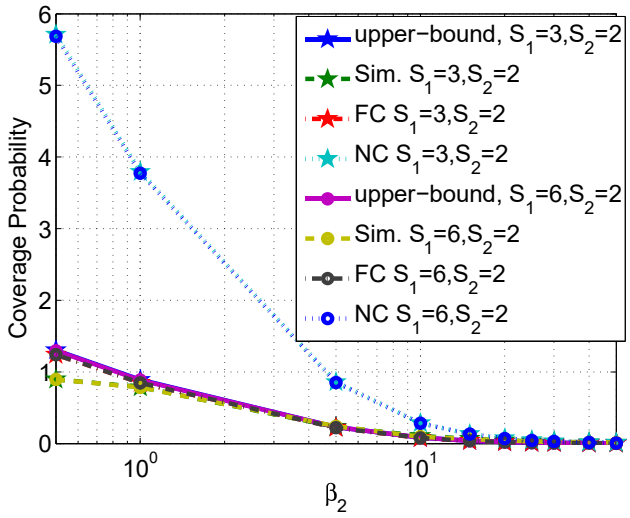

Figure 3.13: Coverage probability *vs.* β_2. Parameters are: $\lambda_1 = 10^{-4}$, $\lambda_2 = 10^{-2}$, $\beta_1 = 5$, and $\epsilon = 0.1$.

a larger S_1 on the coverage performance is lower. Therefore, densification in Tier 2 allows the growth of multiplexing gain in Tier 1.

These can be understood by noting that for a larger λ_2, the UEs are more likely to be associated with the BSs in Tier 2. This is because the successful decoding of a data streams where $S_2 = 1$ is more probable than that of $S_1 = 4$, so the coverage probability is improved.

Results in Fig. 3.16 and Fig. 3.17 show that for a small to moderate λ_1, increasing S_2 from 1 to 2 (Stg1 $\rightarrow$ Stg4) substantially reduces the coverage performance. To tackle this problem, one may consider increasing λ_1 which reduces the performance gap. For a very dense Tier 1, the coverage performance of Stg1 and Stg4 are then converged. Comparing Fig. 3.16 with Fig. 3.17, one can see that by increasing λ_2, the impact of S_2 on the coverage performance is increased. Therefore, when densifying Tier 2, increasing its multiplexing gain is not recommended. This is because for a larger λ_2, the UEs are more likely to be associated with the BSs in Tier 2. The chance of successful decoding of $S_2 = 2$ is less than that of $S_2 = 1$, and hence the coverage probability is reduced. To address this issue, one is ought to densify Tier 1. By increasing λ_1, UEs are more often associated with the BSs in Tier 1,

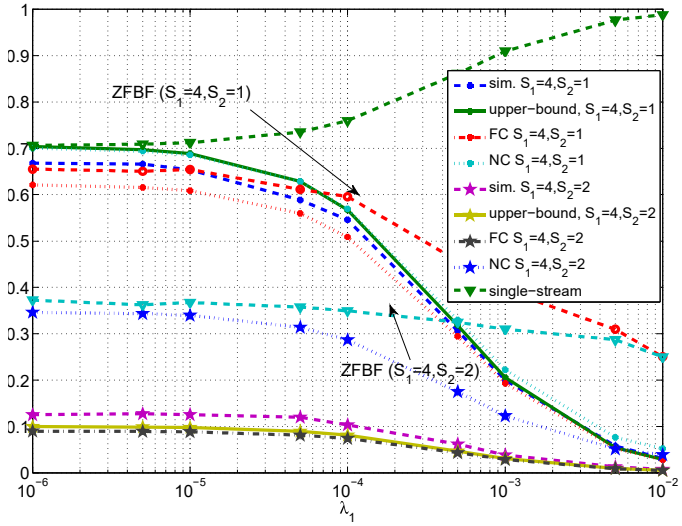

Figure 3.14: Coverage Probability *vs.* λ_1 when $\lambda_2 = 10^{-3}$ where $\beta_1 = 5$, $\beta_2 = 10$, and $N^r = 10$.

where $S_1 = 1$ and it is more likely for the data stream to be successfully decoded.

It is further seen in Figs. 3.14, 3.15, 3.16 and 3.17 that both Stg3 and Stg4 similarly perform with a low coverage performance, where densification neither in Tier 1 nor in Tier 2, can compensate the significant coverage reduction compared to Stg1. This is because in cases where both S_1 and S_2 are high, successful decoding of data streams is less likely, even for a high density of the BSs. For such cases, reducing the multiplexing gains seems the only way to improve the coverage performance.

Impact of the SIR Correlation

In Section 3.4, we quantitatively investigated the impact of SIR correlation on the coverage probability. We showed that under the FC assumption the the coverage probability is underestimated, whereas by ignoring the SIR correlation, the coverage probability is overestimated. These results are confirmed through simulations in Fig. 3.12 and Fig. 3.13, and also Figs. 3.14, 3.15, 3.16, and 3.17.

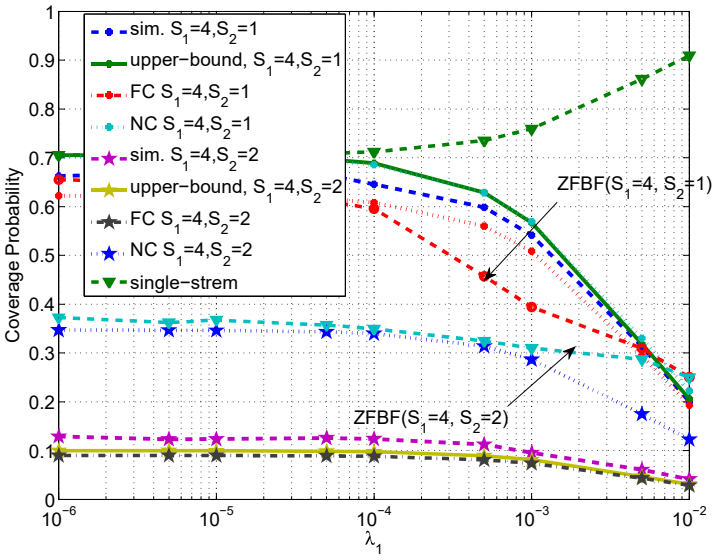

Figure 3.15: Coverage Probability *vs.* λ_1 when $\lambda_2 = 10^{-2}$, where $\beta_1 = 5$, $\beta_2 = 10$, and $N^r = 10$.

Comparison with ZFBF

Fig. 3.12 shows the coverage performance of ZFBF versus the level of CSI inaccuracy ϵ. ZFBF is, in general, shown to be more resilient to CSI inaccuracy than MRC. However, for small to moderate CSI inaccuracy levelsi.e., $\epsilon \lessapprox 0.3$, both systems perform almost the same, while MRC has a much lower computational complexity. Since MRC already suffers from uncancelled intra-stream interference on each data stream, it is very susceptible to extra source of interference that is originated from CSIR inaccuracy. On the other hand, ZFBF cancels the intra-stream interference out entirely, thus the new source of interference, due to CSIR inaccuracy, is not that powerful to considerably reduce its coverage probability.

Furthermore, as shown in Figs. 3.14, 3.15, 3.16, and 3.17, there exist combinations of multiplexing gains and deployment densities in which, compared to MRC, ZFBF does not improve coverage performance, see, e.g., Fig. 3.14 for $(S_1, S_2) = (4, 1)$ where $\lambda_1 < 10^{-4}$, and Fig. 3.16 for $(S_1, S_2) = (1, 2)$ where $\lambda_1 > 10^{-3}$. In such cases, it would be preferable to use the latter.

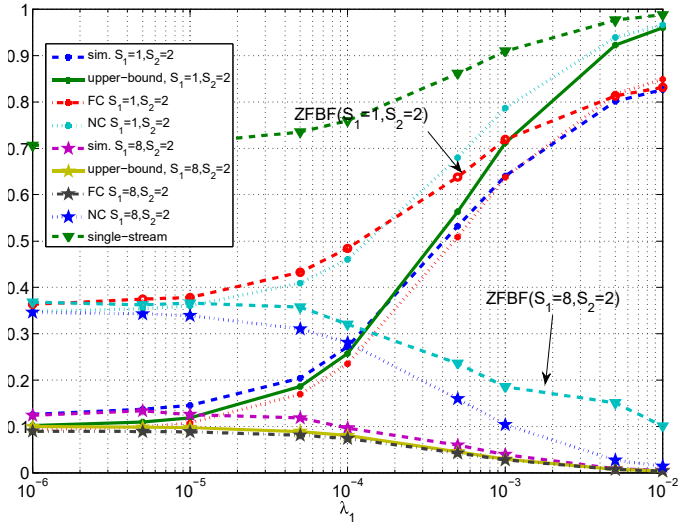

Figure 3.16: (a): Coverage probability *vs.* λ_1 when $\lambda_2 = 10^{-3}$ where $\beta_1 = 5$, $\beta_2 = 10$, and $N^r = 10$.

3.7 Conclusions

Adopting tools of stochastic geometry, we studied the coverage probability of MIMO-MRC multiplexing systems in HetNets. Our analysis incorporated impacts of many important system parameters including the density of BSs, transmission powers, SIR thresholds, multiplexing gains, and CSI inaccuracies on the coverage performance. We derived an accurate upper-bound on the coverage probability in a closed-form.

Important engineering insights were derived from scrutinizing our analytical and simulation results:

- Densification in multiplexing systems should be practiced in conjunction with multiplexing gains, else dramatic coverage loss might be inevitable. Furthermore, by growing the CSIR inaccuracy, it becomes less suitable to densify the network.

- In indoor scenarios (high path-loss exponent regimes) it is possible to reduce the pilot signaling overhead, designated for CSI estimation, without imposing noticeable coverage loss compared to the outdoor coverage performance. This implies that one can save

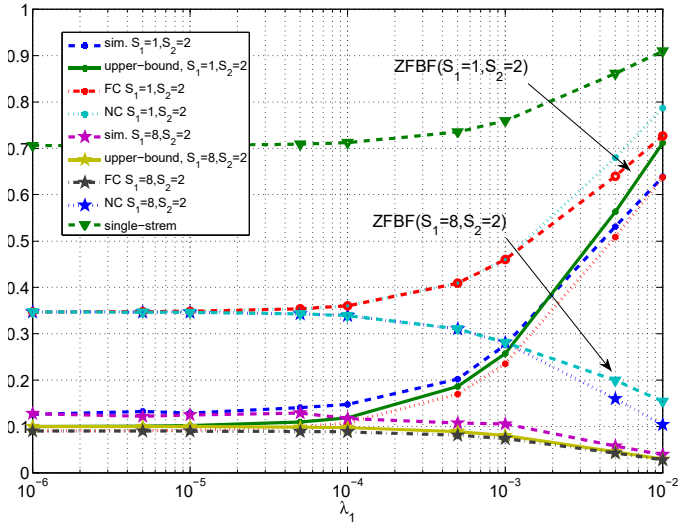

Figure 3.17: Coverage probability *vs.* λ_1 when $\lambda_2 = 10^{-2}$, where $\beta_1 = 5$, $\beta_2 = 10$, and $N^r = 10$.

pilot resources in indoor environments without loosing coverage probability compared to outdoors.

- Although MRC suffers from intra-stream interference in comparison to more complex receivers such as ZFBF, the relative coverage loss in large array scenarios and/or for cell edge users (e.g., small SIR thresholds) is barely noticeable. Furthermore, when the complexity of ZFBF is included, a properly designed configuration may recommend MRC over ZFBF with slightly loosing coverage probability.

We also developed analytical tools facilitating thorough investigations of the impact of cross-stream SIR correlation on the coverage performance of multi-stream systems. Specifically, by focusing on the communication scenarios that the successful decoding of all transmitted data streams are required for the coverage, assuming full correlation among data streams is shown to yield a slightly smaller coverage performance. On the other hand, our analysis proved that by neglecting such correlation, as commonly assumed in the literature, one should expect a substantial overestimation of the coverage probability.

Chapter 4

Analysis of MIMO-SVD Multiplexing HetNets

4.1 Introduction

In Chapter 2 and Chapter 3, we studied the coverage performance of ZFBF and MRC systems, respectively. These receiver filters are among prominent examples of open-loop techniques, as the transmitters do not rely upon the availability of CSIT, either complete or quantized, to construct the pre-coding matrices—each BS simply turns of a subset of its transmission antennas and divides the transmission power equally among them. In the present chapter, we aim at exploring the scenario where the CSIT is completely available at BSs, by deriving the coverage performance of MIMO-SVD multiplexing communications.

Analogous to the analytical sprit of the previous chapters, here we are aiming at providing analytical result on the coverage performance of MIMO-SVD multiplexing systems in HetNets. We evaluate the cross-stream SIR correlation and observe that while in the isolated scenario the data streams are negatively correlated, ICI causes positive correlation among data streams. On the other hand, when ICI is included by the growth of the receive antennas he cross-stream SIR correlation. This is opposite of the isolated scenario in which the cross-stream SIR correlation converges to zero by the growth of the receive antennas. Consequently, ICI substantially affects the statistical behavior of SIRs in SVD systems.

Furthermore, we derive easy-to-compute, closed-form approximations of the coverage probability as a function of deployment density, transmission power of BSs, SIR thresholds,

the number of antennas and data streams. Extensive simulations corroborate the analysis. We also compare the coverage performance of full-MUX system—transmitting as many data streams as the number of receive antennas at the UEs—under SVD, ZFBF, and MRC. Our results demonstrate that *i*) the SVD configuration can provide a substantial coverage performance growth, which highlights the importance of CSIT in enhancing the coverage performance of HetNets. For instance, we observe that under the SVD systems up to 450% (resp. almost 1000%) coverage growth over the ZFBF (resp. MRC) can be achieved while as many as the minimum number of transmit-receive antennas data streams are transmitted. *ii*) Importantly, for the full-MUX scenario, while both ZFBF and MRC are entirely oblivious to the growth of the number of antennas at the BSs, SVD systems can harness considerable coverage gain. In our view, this suggests the vital value of SVD for large-array antenna systems. *iii*) However, it may not always be recommendable to increase the number of antennas at the macro BSs in particular when the network is densifyed in Tier 2. We observe that if the network is densified in Tier 2, increasing the number of antennas in Tier 1 does not provide coverage enhancement.

Note that the base of our analysis is built upon the one previously developed in Chapter 2. However, compared to ZFBF as well as MRC systems, under SVD procedure, besides the correlation of ICI across data streams of a given communication link, the effective power of attending signals are also correlated across data streams, due to the correlation of eigenvalues of intending channel matrix. This renders new analytical complexities, which require upgrading the developed analysis in the previous chapters. Since, to our best knowledge, the coverage performance of MIMO-SVD multiplexing system in cellular networks (an also ad hoc communications) has not been investigated so far, in this chapter we set our goal to tackle this issue.

One should also note that the common methods of the literature [33, 37, 38] are inherently unsuitable to capture the randomness of the interference, and suffer from lack of scalability. In fact, it is substantially complex to accurately account for the max-SIR CA, densification,

and heterogeneity in the analysis of the literature.

On the other hand, as we also thoroughly discuss in Section 1.3, the analysis of [33, 37, 38] is not applicable here, since the analytical results are provided in very complex forms of determinants of matrices with entries in the term of special mathematical functions (e.g., hypergeometric functions), prohibiting further expectation operation required to deal with random location of interferes. We in this section utilized the FC assumption to considerably reduce the complexity of the analysis.

The rest of this chapter is organized as the following. In Section 4.2 we elaborate on the SVD model in HetNet. In Section 4.3, we evaluate the cross-stream SIR correlation. Then, in Section 4.4, we analyze the coverage probability under max-SIR CA rule. In Section 4.5, we present simulation results and compare the performance of SVD, ZFBF, and MRC systems. Finally Section 4.6 concludes the chapter.

4.2 System Model

The network model in this chapter is quite similar to the one presented in Section 2.2, we therefore only discuss the required upgrades.

Under SVD configuration, the N^r-dimensional equivalent low-pass received signal, after matched filtering and sampling, at the output of receiver antennas, $\boldsymbol{y}_{x_i} \in \mathbb{C}^{N^r \times 1}$, can be expressed as

$$\boldsymbol{y}_{x_i} = \|x_i\|^{-\frac{\alpha}{2}} \boldsymbol{H}_{x_i} \boldsymbol{V}_{x_i} \boldsymbol{s}_{x_i} + \sum_{j \in \mathcal{K}} \sum_{x_j \in \Phi_j \setminus x_i} \|x_j\|^{-\frac{\alpha}{2}} \boldsymbol{H}_{x_j} \boldsymbol{V}_{x_j} \boldsymbol{s}_{x_j}, \tag{4.1}$$

in which $\boldsymbol{V}_x \in \mathbb{C}^{N^t \times S_i}$ is the pre-coding matrix applied at any BS x, which is constructed according to SVD method [14], [16]. In fact, by applying SVD the communication channel between BS x_i and the typical UE can be decomposed into spatial modes so that $\boldsymbol{H}_{x_i} = \boldsymbol{U}_{x_i} \boldsymbol{\Gamma}_{x_i} \boldsymbol{V}_{x_i}^{\dagger}$ in which $\boldsymbol{V}_{x_i} = [\boldsymbol{v}_{x_i,1} \dots \boldsymbol{v}_{x_i,S_i}]$ is the unitary pre-coding matrix of right (input) eigenvectors, $\boldsymbol{U}_{x_i} = [\boldsymbol{u}_{x_i,1} \dots \boldsymbol{u}_{x_i,S_i}]$ is the unitary post-coding (combining) matrix of left (output) eigenvector, and $\boldsymbol{\Gamma}_{x_i}$ is a $S_i \times S_i$ diagonal matrix of eigenvalues [14], [16]. More

specifically, $\boldsymbol{v}_{x_i,l_i}$ is associated with the l_ith eigenvalue of the corresponding central Wishart matrix $\boldsymbol{W}_{x_i}^{S_i\times S_i}$, where

$$\boldsymbol{W}_{x_i}=\begin{cases}\boldsymbol{H}_{x_i}\boldsymbol{H}_{x_i}^{\dagger} & N^r\leq N_i^t\\ \boldsymbol{H}_{x_i}^{\dagger}\boldsymbol{H}_{x_i} & N^r>N_i^t.\end{cases} \tag{4.2}$$

Note that non-zero eigenvalues of matrices $\boldsymbol{H}_{x_i}\boldsymbol{H}_{x_i}^{\dagger}$ and $\boldsymbol{H}_{x_i}^{\dagger}\boldsymbol{H}_{x_i}$ are the same and consequently distributed statistically equal [163]. We denote ϕ_{x_i,l_i} as the (unordered) l_ith non-zero eigenvalue of $\boldsymbol{W}_{x_i}$.

The typical UE multiplies the received signal $\boldsymbol{y}_{x_i}$ with $\boldsymbol{U}_{x_i}^{\dagger}$ in order to collect post-processing signal vector $\boldsymbol{z}_{x_i}=\boldsymbol{U}_{x_i}^{\dagger}\boldsymbol{y}_{x_i}$, which using (4.1) is

$$\boldsymbol{z}_{x_i}=\|x_i\|^{-\frac{\alpha}{2}}\boldsymbol{\Gamma}_{x_i}\boldsymbol{s}_{x_i}+\sum_{j\in\mathcal{K}}\sum_{x_j\in\Phi_j\setminus x_i}\|x_j\|^{-\frac{\alpha}{2}}\boldsymbol{U}_{x_i}^{\dagger}\boldsymbol{H}_{x_j}\boldsymbol{V}_{x_j}\boldsymbol{s}_{x_j}.$$

It is then seen that the signal power associated with data stream l_i is equal to $\frac{P_i}{S_i}\|x_i\|^{-\alpha}\phi_{x_i,l_i}$. Also, the interference power related to the data stream l_i imposed from BS $x_j\neq x_i$ is $\frac{P_j}{S_j}\|x_j\|^{-\alpha}\|\boldsymbol{u}_{x_i,l_i}^{\dagger}\boldsymbol{H}_{x_j}\boldsymbol{V}_{x_j}\|^2$. Define $Y_{x_j,l_j}^{\mathrm{SVD}}\triangleq\left|\boldsymbol{u}_{x_i,l_i}^{\dagger}\boldsymbol{H}_{x_j}\boldsymbol{v}_{x_j,l_j}\right|^2$, and denote r.v. $G_{x_j,l_i}^{\mathrm{SVD}}$ by $G_{x_j,l_i}^{\mathrm{SVD}}\triangleq\sum_{l_j=1}^{S_j}Y_{x_j,l_j}^{\mathrm{SVD}}$. Thus, the imposed interference from BS $x_j\neq x_i$ on data stream l_i is in effect obtained from $\frac{P_j}{S_j}\|x_j\|^{-\alpha}G_{x_j,l_i}^{\mathrm{SVD}}$. Finally, the SIR associated with the l_ith data stream from BS x_i is formulated by

$$\mathrm{SIR}_{x_i,l_i}^{\mathrm{SVD}}=\frac{\frac{P_i}{S_i}\|x_i\|^{-\alpha}\phi_{x_i,l_i}}{\sum\limits_{j\in\mathcal{K}}\sum\limits_{x_j\in\Phi_j\setminus x_i}\frac{P_j}{S_j\|x_j\|^{\alpha}}G_{x_j,l_i}^{\mathrm{SVD}}}. \tag{4.3}$$

Conditioned on $\boldsymbol{H}_{x_i}$, $\boldsymbol{u}_{x_i,l_i}^{\dagger}\boldsymbol{H}_{x_j}\boldsymbol{v}_{x_j,l_j}$ is a complex Gaussian r.v. with mean zero and variance 1 [33]. So, each term of $Y_{x_j,l_j}^{\mathrm{SVD}}$ is distributed exponentially and independent of $\boldsymbol{H}_{x_i}$ [33]. Regarding the independencies of r.v.s $Y_{x_j,l_j}^{\mathrm{SVD}}$ across stream l_js, it is straightforward to confirm that r.v. $G_{x_j,l_i}^{\mathrm{SVD}}$ is chi-squared with DoF $2S_j$ [118, 134].

Note that $G_{x_j,l_i}^{\mathrm{SVD}}$ is independent across streams l_i and further across BSs [123]. In addition,

$G^{\mathrm{SVD}}_{x_j,l_i}$ and ϕ_{x_i,l_i} are independent. Furthermore, the denominator of (4.3) is the ICI denoted by I^{l_i} (see also (2.6)), and its Laplace transform is given by (2.11). This is because similar to ZFBF and MRC systems, r.v. $G^{\mathrm{SVD}}_{x_j,l_i}$ is also a chi-squared with $2S_j$ DoF.

4.3 Derivation of Cross-Stream SIR Correlation

As the case of MRC receivers studied in Chapter 3, one can also straightforwardly derive the cross-stream SIR correlation, defined as

$$\rho^{\mathrm{SVD}}_{x_i}(l_i,l_i') = \frac{\mathbb{E}\left[\mathrm{SIR}^{\mathrm{SVD}}_{x_i,l_i}\mathrm{SIR}^{\mathrm{SVD}}_{x_i,l_i'}\right] - \overline{\mathrm{SIR}}^{\mathrm{SVD}}_{x_i,l_i}\overline{\mathrm{SIR}}^{\mathrm{SVD}}_{x_i,l_i'}}{\sqrt{\mathrm{Var}\left(\mathrm{SIR}^{\mathrm{SVD}}_{x_i,l_i}\right)\mathrm{Var}\left(\mathrm{SIR}^{\mathrm{SVD}}_{x_i,l_i'}\right)}} \tag{4.4}$$

$$= \frac{\mathbb{E}\left[\mathrm{SIR}^{\mathrm{SVD}}_{x_i,l_i}\mathrm{SIR}^{\mathrm{SVD}}_{x_i,l_i'}\right] - (\overline{\mathrm{SIR}}^{\mathrm{SVD}}_{x_i,l_i})^2}{\mathrm{Var}\left(\mathrm{SIR}^{\mathrm{SVD}}_{x_i,l_i}\right)}, \tag{4.5}$$

In the following, we firstly evaluate constituents of (4.5), which are $\overline{\mathrm{SIR}}^{\mathrm{svd}}_{x_i,l_i}$, $\mathrm{Var}(\mathrm{SIR}^{\mathrm{svd}}_{x_i,l_i})$, and $\mathbb{E}\left[\mathrm{SIR}^{\mathrm{svd}}_{x_i,l_i}\mathrm{SIR}^{\mathrm{svd}}_{x_i,l_i'}\right]$. We further discuss a numerical evaluation of $\rho^{\mathrm{SVD}}_{x_i}(l_i,l_i')$. To derive $\rho^{\mathrm{SVD}}_{x_i}(l_i,l_i')$, we follow the same method already developed in the proof of Proposition 3.4.1.

Evaluation of $\overline{\mathrm{SIR}}^{\mathrm{svd}}_{x_i,l_i}$

Under the premises of independencies of PPPs as well as of the intended and interfering channel matrices, and noting that $\mathbb{E}[\phi_{x_i,l_i}] = N^r$ [130], we have

$$\overline{\mathrm{SIR}}^{\mathrm{svd}}_{x_i,l_i} = \frac{P_i N^r}{S_i} x_i^{-\alpha}\mathbb{E}\frac{1}{\sum\limits_{j\in\mathcal{K}}\sum\limits_{x_j\in\Phi_j\setminus x_i}\frac{P_j}{S_j}\|x_j\|^{-\alpha}G^{\mathrm{svd}}_{x_j,l_i}} \tag{4.6}$$

$$= \frac{P_i N^r}{S_i x_i^{\alpha}}\mathbb{E}\int_0^{\infty} e^{-t\sum\limits_{j\in\mathcal{K}}\sum\limits_{x_j\in\Phi_j\setminus x_i}\frac{P_j}{S_j}\|x_j\|^{-\alpha}G^{\mathrm{svd}}_{x_j,l_i}}dt \tag{4.7}$$

$$\overset{(a)}{=} \frac{P_i N^r}{S_i x_i^{\alpha}}\int_0^{\infty}\mathcal{L}_{I^{l_i}}(t)dt \tag{4.8}$$

$$= \frac{P_i N^r}{S_i x_i^{\alpha}} \int_0^{\infty} e^{-t^{\breve{\alpha}} \Lambda(\boldsymbol{S})} dt \tag{4.9}$$

$$= \frac{P_i N^r \Gamma(\frac{\alpha}{2}+1)}{S_i x_i^{\alpha}} \left(\Lambda(\boldsymbol{S})\right)^{-\frac{\alpha}{2}}, \tag{4.10}$$

where in step (a) $\mathcal{L}_{I^{l_i}}(t)$ is the Laplace transform of the interference at the typical UE, which is obtained in (2.11).

Evaluation of $\mathrm{Var}(\mathrm{SIR}^{\mathrm{svd}}_{x_i,l_i})$

To evaluate $\mathrm{Var}(\mathrm{SIR}^{\mathrm{svd}}_{x_i,l_i})$ we firstly require to evaluate $\mathbb{E}\left[\left(\mathrm{SIR}^{\mathrm{svd}}_{x_i,l_i}\right)^2\right]$ which is carried out in the following:

$$\mathbb{E}\left[\left(\mathrm{SIR}^{\mathrm{svd}}_{x_i,l_i}\right)^2\right] = \frac{\mathbb{E}[(\phi_{x_i,l_i})^2]}{P_i^{-2} S_i^2 x_i^{2\alpha}} \int_0^{\infty}\int_0^{\infty} e^{-\tilde{C}(\alpha)(t+\tau)^{\breve{\alpha}} \sum_j \lambda_j (\frac{P_j}{S_j})^{\breve{\alpha}} \frac{\Gamma(\breve{\alpha}+S_j)}{\Gamma(S_j)}} dt d\tau \tag{4.11}$$

$$\overset{(a)}{=} \frac{N^r(N^r+S_j)}{P_i^{-2} S_i^2 x_i^{2\alpha}} \int_0^{\infty}\int_{t_2}^{\infty} e^{-t_1^{\breve{\alpha}} \Lambda(\boldsymbol{S})} dt_1 dt_2 \tag{4.12}$$

$$= \frac{N^r(N^r+S_j)}{P_i^{-2} S_i^2 x_i^{2\alpha}} \int_0^{\infty} t_1 e^{-t_1^{\breve{\alpha}} \Lambda(\boldsymbol{S})} dt_1 \tag{4.13}$$

$$= \frac{N^r(N^r+S_j)}{P_i^{-2} S_i^2 x_i^{2\alpha}} \frac{\frac{\alpha}{2}\Gamma(\alpha)}{\left(\Lambda(\boldsymbol{S})\right)^{\alpha}}, \tag{4.14}$$

where in Step (a) we apply $\mathbb{E}[(\phi_{x_i,l_i})^2] = N^r(N^r+S_j)$ [130], and introduce new variables $t_2 = t$ and $t_1 = t+\tau$. Using (4.14) and (4.10), $\mathrm{Var}(\mathrm{SIR}^{\mathrm{svd}}_{x_i,l_i})$ is then obtained as

$$\mathrm{Var}(\mathrm{SIR}^{\mathrm{svd}}_{x_i,l_i}) = \frac{N^r}{(\frac{S_i}{P_i})^2 x_i^{2\alpha}} \frac{\frac{\alpha(N^r+S_j)}{2}\Gamma(\alpha) - \Gamma(\frac{\alpha}{2}+1)^2}{\left(\Lambda(\boldsymbol{S})\right)^{\alpha}}. \tag{4.15}$$

Evaluation of $\mathbb{E}\left[\mathrm{SIR}^{\mathrm{svd}}_{x_i,l_i}\mathrm{SIR}^{\mathrm{svd}}_{x_i,l'_i}\right]$

Since $\mathbb{E}[\phi_{x_i,l_i}\phi_{x_i,l'_i}] = N^r(N^r-1)$ [130], we can write

$$\begin{aligned}
\mathbb{E}\left[\mathrm{SIR}^{\mathrm{svd}}_{x_i,l_i}\mathrm{SIR}^{\mathrm{svd}}_{x_i,l'_i}\right] &= \frac{P_i^2\mathbb{E}[\phi_{x_i,l_i}\phi_{x_i,l'_i}]}{S_i^2 x_i^{2\alpha}} && (4.16)\\
&\times \mathbb{E}\frac{1}{\sum\limits_{j\in\mathcal{K}}\sum\limits_{x_j\in\Phi_j\setminus x_i}\frac{P_j}{S_j}\|x_j\|^{-\alpha}G^{\mathrm{svd}}_{x_j,l_i}}\frac{1}{\sum\limits_{j\in\mathcal{K}}\sum\limits_{x_j\in\Phi_j\setminus x_i}\frac{P_j}{S_j}\|x_j\|^{-\alpha}G^{\mathrm{svd}}_{x_j,l'_i}} && (4.17)\\
&= \frac{P_i^2N^r(N^r-1)}{S_i^2x_i^{2\alpha}}\mathbb{E}\int_0^\infty e^{-t\sum\limits_{j\in\mathcal{K}}\sum\limits_{x_j\in\Phi_j\setminus x_i}\frac{P_j}{S_j}\|x_j\|^{-\alpha}G^{\mathrm{svd}}_{x_j,l_i}}dt && (4.18)\\
&\times \int_0^\infty e^{-\tau\sum\limits_{j\in\mathcal{K}}\sum\limits_{x_j\in\Phi_j\setminus x_i}\frac{P_j}{S_j}\|x_j\|^{-\alpha}G^{\mathrm{svd}}_{x_j,l'_i}}d\tau && (4.19)\\
&= \frac{P_i^2N^r(N^r-1)}{S_i^2x_i^{2\alpha}}\int_0^\infty\int_0^\infty \mathbb{E}\exp\Big(-\sum_{j\in\mathcal{K}}\sum_{x_j\in\Phi_j\setminus x_i}\frac{P_j}{S_j}\|x_j\|^{-\alpha} && (4.20)\\
&\times (tG^{\mathrm{svd}}_{x_j,l_i}+\tau G^{\mathrm{svd}}_{x_j,l'_i})\Big)dtd\tau && (4.21)\\
&= \frac{P_i^2N^r(N^r-1)}{S_i^2x_i^{2\alpha}}\int_0^\infty\int_0^\infty\prod_{j\in\mathcal{K}}\mathbb{E}_{\Phi_j}\prod_{x_j\in\Phi_j\setminus x_i}\mathbb{E}_{G^{\mathrm{svd}}_{x_j,l_i}}\mathbb{E}_{G^{\mathrm{svd}}_{x_j,l'_i}} && (4.22)\\
&\times e^{-\frac{P_j}{S_j}\|x_j\|^{-\alpha}(tG^{\mathrm{svd}}_{x_j,l_i}+\tau G^{\mathrm{svd}}_{x_j,l'_i})}dtd\tau && (4.23)\\
&= \frac{N^r(N^r-1)}{P_i^{-2}S_i^2x_i^{2\alpha}}\int_0^\infty\int_0^\infty e^{-\tilde{C}(\alpha)\sum\limits_j\lambda_j(\frac{P_j}{S_j})^\alpha\overline{W}_j(t,\tau)}dtd\tau, && (4.24)
\end{aligned}$$

where in the last step the function $\overline{W}_j(t,\tau)$ is given by (3.55). Note that in this case we require to apply numerical integration to evaluate (4.24).

Evaluation of $\rho^{\mathrm{svd}}_{x_i,(l_i,l'_i)}$

Finally, combining (4.15), (4.10), and (4.24) an expression for $\rho^{\mathrm{svd}}_{x_i,(l_i,l'_i)}$ is derived as

$$\rho^{\mathrm{SVD}}_{x_i}(l_i,l'_i) = \frac{(N^r-1)\left(\Lambda(\boldsymbol{S})\right)^\alpha\int_0^\infty\int_0^\infty e^{-\tilde{C}(\alpha)\sum\limits_j\lambda_j(\frac{P_j}{S_j})^\alpha\overline{W}_j(t,\tau)}dtd\tau - N^r(\Gamma(\frac{\alpha}{2}+1))^2}{\frac{\alpha(N^r+S_j)}{2}\Gamma(\alpha)-\Gamma(\frac{\alpha}{2}+1)^2} \quad (4.25)$$

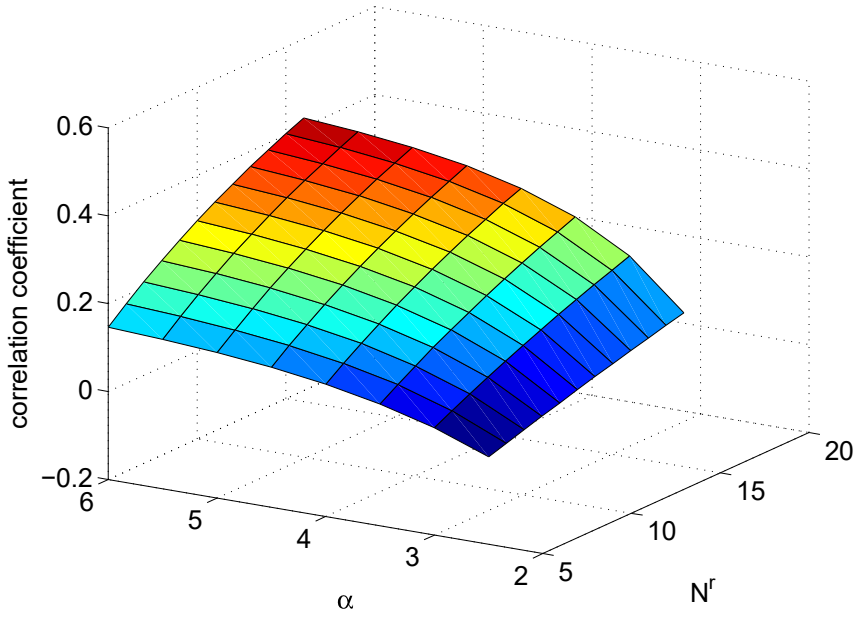

Figure 4.1: $\rho^{\text{svd}}_{x_i,(l_i,l'_i)}$ *vs.* α and N^r. Parameters are $P_1 = 50$ Watts, $P_2 = 1$ Watt, $\lambda_1 = 10^{-4}$, $\lambda_2 = 10^{-3}$, $N^t_1 = N^t_2 = 16$, $S_2 = N_r$, and $S_1 = N^r$.

For the purpose of illustration an example of $\rho^{\text{svd}}_{x_i,(l_i,l'_i)}$ vs. α and N^r is depicted in Fig. 4.1. Here we have assumed that the typical UE is attached to a BS of Tier 1 located at $\|x_1\| = 10$. Note that regarding the results of [130] we already know that the correlation coefficient among two randomly picked eigenvalues (isolated scenario) is $-1/N^r$, which it is vanishing by growing N^r. But with the consideration of ICI, Fig. 4.1 reveals that the correlation coefficient is an increasing function of N^r and the rate of increment is increasing with α. Furthermore, the larger the path-loss exponent is, the higher the correlation coefficient will be. It is interesting to note that for some particular choices of α and N^r the data streams can be actually uncorrelated ($\alpha \approx 3$ and $N^r \approx 6$). Finally, while in the isolated scenario the data streams are negatively correlated, ICI renders in many cases positive correlation among data streams.

4.4 Analyzing the Coverage Performance

As the previous chapters, we also consider the max-SIR CA rule as defined in Definition 2.2.2, which implies that the typical UE is in the coverage if the set

$$\mathcal{A}_{\text{SVD}} = \left\{ \exists i \in \mathcal{K} : \max_{x_i \in \Phi_i} \min_{l_i = 1,\ldots,S_i} \text{SIR}_{x_i,l_i}^{\text{SVD}} \geq \beta_i \right\}, \tag{4.26}$$

is nonempty. The coverage probability is defined as $c^{\text{SVD}} = \mathbb{P}\{\mathcal{A}^{\text{SVD}} \neq \emptyset\}$.

We now derive the coverage probability. Let us denote $r_i = \|x_i\|$. Since $\beta_i \geq 1$ is assumed, referring to (4.26) and applying the same procedure developed in the proof of Proposition 2.3.2, we can write

$$\begin{aligned}
c^{\text{SVD}} &= \sum_{i \in \mathcal{K}} \mathbb{E} \sum_{x_i \in \Phi_i} 1\left(\min_{l_i = 1,\ldots,S_i} \text{SIR}_{x_i,l_i}^{\text{SVD}} \geq \beta_i \right) && (4.27)\\
&= \sum_{i \in \mathcal{K}} 2\pi\lambda_i \int_0^\infty r_i \mathbb{P}\left\{ \min_{l_i = 1,\ldots,S_i} \text{SIR}_{x_i,l_i}^{\text{SVD}} \geq \beta_i \right\} dr_i && (4.28)\\
&= \sum_{i \in \mathcal{K}} 2\pi\lambda_i \int_0^\infty r_i \mathbb{E}_\Phi \mathbb{P}\left\{ \text{SIR}_{x_i,l_i}^{\text{SVD}} \geq \beta_i : \forall l_i \middle| \Phi \right\} dr_i && (4.29)\\
&= \sum_{i \in \mathcal{K}} 2\pi\lambda_i \int_0^\infty r_i \mathbb{E}_\Phi \mathbb{P}\Big\{ \phi_{x_i,1} \geq \frac{S_i \beta_i r_i^\alpha}{P_i} I^1, \ldots, \\
&\qquad\qquad \phi_{x_i,S_i} \geq \frac{S_i \beta_i r_i^\alpha}{P_i} I^{S_i} \middle| \Phi \Big\} dr_i && (4.30)\\
&= \sum_{i \in \mathcal{K}} 2\pi\lambda_i \int_0^\infty r_i \mathbb{E}_{\{I^{l_i}\}} \int_{\frac{S_i \beta_i r_i^\alpha}{P_i} I^1}^\infty \cdots \int_{\frac{S_i \beta_i r_i^\alpha}{P_i} I^{S_i}}^\infty \\
&\qquad\qquad \times \text{f}\left(\phi_{x_i,1}, \ldots, \phi_{x_i,S_i}\right) \prod_{l_i=1}^{S_i} d\phi_{x_i,l_i} dr_i. && (4.31)
\end{aligned}$$

in which $\text{f}\left(\phi_{x_i,1}, \ldots, \phi_{x_i,S_i}\right)$ is the joint PDF of unordered eigenvalues $\phi_{x_i,1}, \ldots, \phi_{x_i,S_i} > 0$. If

$N^r \leq N_i^t$, $S_i = N^r$ and thus the joint PDF is [163]

$$\mathrm{f}\left(\phi_{x_i,1},\ldots,\phi_{x_i,S_i}\right) = \frac{1}{S_i! Q_i}\left(\prod_{l_i=1}^{S_i}\phi_{r_i,l_i}\right)^{N_i^t-S_i} e^{-\sum\limits_{l_i=1}^{S_i}\phi_{x_i,l_i}} \prod_{1\leq l_i\leq l_{i'}\leq S_i}\left(\phi_{x_i,l_i}-\phi_{x_i,l_{i'}}\right)^2, \quad (4.32)$$

where $Q_i = \prod\limits_{l_i=1}^{S_i}(N_i^t - l_i)!(S_i - l_i)!$. Note that for the case that $N^r \leq N_i^t$, by exchanging N_i^t with N^r and letting $S_i = N_i^t$, (4.32) yields the joint PDF. Unfortunately, due to the complicated form of (4.32) and the lower-bounds of the integrals, which are statistically correlated r.v.s, the form of (4.31) does not lend itself into a tractable form. In fact, a term-by-term integration of (4.31), assuming it is pursuable, can even cause divergence. As a result, in the following we attempt to approximate (4.31) by adopting the FC assumption introduced in Section (2.4).

Recall from Definition 2.4.1, the ICI under FC assumption is denoted by I^{FC} given by 2.51. We are then able to approximate the coverage probability (4.31) as the following

$$\begin{aligned} c^{\mathrm{SVD}} \approx c^{\mathrm{SVD-FC}} &= \sum_{i\in\mathcal{K}} 2\pi\lambda_i \int_0^\infty r_i \mathbb{E}_{I^{\mathrm{FC}}} \int_{\frac{S_i\beta_i r_i^\alpha}{P_i} I^{\mathrm{FC}}}^\infty \cdots \int_{\frac{S_i\beta_i r_i^\alpha}{P_i} I^{\mathrm{FC}}}^\infty \\ &\qquad \times \mathrm{f}\left(\phi_{x_i,1},\ldots,\phi_{x_i,S_i}\right) \prod_{l_i=1}^{S_i} d\phi_{x_i,l_i} dr_i \qquad (4.33) \\ &= \sum_{i\in\mathcal{K}} 2\pi\lambda_i \int_0^\infty r_i \mathbb{E}_\Phi \mathbb{P}\Big\{\phi_{x_i,1} \geq \frac{S_i\beta_i r_i^\alpha}{P_i} I^{\mathrm{FC}}, \ldots \\ &\qquad , \phi_{x_i,S_i} \geq \frac{S_i\beta_i r_i^\alpha}{P_i} I^{\mathrm{FC}} \Big| \Phi \Big\} dr_i \qquad (4.34) \\ &= \sum_{i\in\mathcal{K}} 2\pi\lambda_i \int_0^\infty r_i \mathbb{E}_\Phi \mathbb{P}\left\{\phi_{x_i,\min} \geq \frac{S_i\beta_i r_i^\alpha}{P_i} I^{\mathrm{FC}} \Big| \Phi \right\} dr_i. \qquad (4.35) \end{aligned}$$

Accordingly, to evaluate $c^{\mathrm{SVD-FC}}$ we require the PDF of $\phi_{x_i,\min}$. This is analogous to the analysis under the FC assumption for ZFBF conducted in Section 2.4, in which the effective attending channel power gain is $H_{x_i,\min}^{\mathrm{ZF}}$. Note that statistics of the smallest eigenvalue of

Wishart matrices are broadly investigated in the literature [32] allowing us to borrow the results for furthering the evaluation of (4.35). The expression in [32] is in a determinant form of some matrix in which entries are special mathematical functions, which makes it unsuitable for our analytical purposes. In effect, using this determinant expression it becomes entirely intractable to apply expectation over the point processes. We, therefore, adopt an alternative polynomial expression for the PDF of $\phi_{x_i,\min}$ proposed in [172].

Let first define tensor determinant [163, 172]. For three-dimensional matrices (rank 3 tensors) $\boldsymbol{A} = \{a_{k_1,k_2,k_3}\}_{k_1,k_2,k_3=1,2,\ldots,N}$, operator $\mathtt{T}(\boldsymbol{A})$, which is the determinant of $\boldsymbol{A}$, is defined as

$$\mathtt{T}(\boldsymbol{A}) \triangleq \sum_{\boldsymbol{\mu}} \mathrm{sgn}(\boldsymbol{\mu}) \sum_{\boldsymbol{\eta}} \mathrm{sgn}(\boldsymbol{\eta}) \prod_{k=1}^{N} a_{\mu_k,\eta_k,k}, \tag{4.36}$$

where the sum is over all the permutations $\boldsymbol{\mu}$ and $\boldsymbol{\eta}$ over the integers $1, 2, \ldots, N$. Here, sgn(.) is the signature of the corresponding permutation and takes value 1 if the permutation is even (i.e., whenever the reordering given by the permutation is accomplished through successively interchanging two entries an even number of times), otherwise -1 if the permutation is odd. Define matrix $\boldsymbol{A} \triangleq \{(l_i' + l_i'' + k_{l_i})!\}_{l_i',l_i'',k_{l_i}=1,\ldots,S_i-1}$. We introduce operator $\mathtt{T}_{\{k_{l_i}\}}$ as

$$\mathtt{T}_{\{k_{l_i}\}} \triangleq \mathtt{T}\left(\boldsymbol{A}\right) \prod_{k_{l_i}=1}^{S_i-1} \binom{N_i^t - S_i}{k_{l_i}}. \tag{4.37}$$

Using $\mathtt{T}_{\{k_{l_i}\}}$, we then introduce

$$\overline{\sum_{\{k_{l_i}\}}} \mathtt{T}_{\{k_{l_i}\}} \triangleq \sum_{k_1=0}^{N_i^t-S_i} \cdots \sum_{k_{S_i-1}=0}^{N_i^t-S_i} \mathtt{T}_{\{k_{l_i}\}}. \tag{4.38}$$

Utilizing the results of [172], the PDF of $\phi_{x_i,\min}$ can finally be specified in the following polynomial form:

$$\mathrm{f}_{\phi_{x_i,\min}}(z) = \frac{e^{-S_i z}}{Q_i \Gamma(S_i)} \overline{\sum_{\{k_{l_i}\}}} \mathtt{T}_{\{k_{l_i}\}} z^{\hat{\Theta}_{\{k_{l_i}\}}-1}, \tag{4.39}$$

where $\hat{\Theta}_{\{k_{l_i}\}} = S_i(N_i^t - S_i) - \sum_{l_i=1}^{S_i-1} k_{l_i} + 1$. Furthermore, the CCDF of $\phi_{x_i,\min}$, denoted by $\bar{\mathrm{F}}_{\phi_{x_i,\min}}(.)$, is

$$\bar{\mathrm{F}}_{\phi_{x_i,\min}}(z) = \overline{\sum_{\{k_{l_i}\}}} \mathtt{T}_{\{k_{l_i}\}} \tilde{\Theta}_{\{k_{l_i}\}} \int_z^\infty e^{-S_i w} \frac{S_i^{\hat{\Theta}_{\{k_{l_i}\}}} w^{\hat{\Theta}_{\{k_{l_i}\}}-1}}{\Gamma(\hat{\Theta}_{\{k_{l_i}\}})} dw \tag{4.40}$$

$$= \overline{\sum_{\{k_{l_i}\}}} \mathtt{T}_{\{k_{l_i}\}} \tilde{\Theta}_{\{k_{l_i}\}} e^{-S_i z} \sum_{m_i=0}^{\hat{\Theta}_{\{k_{l_i}\}}-1} \frac{S_i^{m_i} z^{m_i}}{m_i!}, \tag{4.41}$$

where $\tilde{\Theta}_{\{k_{l_i}\}} = \frac{\Gamma(\hat{\Theta}_{\{k_{l_i}\}})}{Q_i \Gamma(S_i) S_i^{\hat{\Theta}_{\{k_{l_i}\}}}}$, which admits the following inverse Laplace transform

$$\mathcal{L}^{-1}_{\bar{\mathrm{F}}_{\phi_{x_i,\min}}}(t) = \overline{\sum_{\{k_{l_i}\}}} \mathtt{T}_{\{k_{l_i}\}} \tilde{\Theta}_{\{k_{l_i}\}} \sum_{m_i=0}^{\hat{\Theta}_{\{k_{l_i}\}}-1} \frac{S_i^{m_i}}{m_i!} \delta^{(m_i)}(t - S_i). \tag{4.42}$$

Now, we only require to adopt Lemma 2.3.2 to evaluate (4.35) as follows

$$c^{\mathrm{SVD-FC}} = \sum_{i\in\mathcal{K}} 2\pi\lambda_i \int_0^\infty r_i \mathbb{E}_{I^{\mathrm{FC}}} \left[\bar{\mathrm{F}}_{\phi_{x_i,\min}} \left(\frac{S_i \beta_i r_i^\alpha}{P_i} I^{\mathrm{FC}} \right) \right] dr_i \tag{4.43}$$

$$= \sum_{i\in\mathcal{K}} 2\pi\lambda_i \int_0^\infty r_i \mathbb{E}_{I^{\mathrm{FC}}} \int_0^\infty e^{-t\frac{S_i\beta_i r_i^\alpha}{P_i} I^{\mathrm{FC}}} \mathcal{L}^{-1}_{\bar{\mathrm{F}}_{\phi_{x_i,\min}}}(t) dt dr_i \tag{4.44}$$

$$= \sum_{i\in\mathcal{K}} 2\pi\lambda_i \int_0^\infty r_i \int_0^\infty e^{-r_i^2 t^{\tilde{\alpha}} \tilde{C}(\alpha) (\frac{\beta_i S_i}{P_i})^{\tilde{\alpha}} \Lambda^{\mathrm{FC}}} \tag{4.45}$$

$$\times \overline{\sum_{\{k_{l_i}\}}} \mathtt{T}_{\{k_{l_i}\}} \tilde{\Theta}_{\{k_{l_i}\}} \sum_{m_i=0}^{\hat{\Theta}_{\{k_{l_i}\}}-1} \frac{S_i^{m_i}}{m_i!} \delta^{(m_i)}(t - S_i) dt dr_i \tag{4.46}$$

$$= \sum_{i\in\mathcal{K}} 2\pi\lambda_i \int_0^\infty \overline{\sum_{\{k_{l_i}\}}} \mathtt{T}_{\{k_{l_i}\}} \tilde{\Theta}_{\{k_{l_i}\}} \sum_{m_i=0}^{\hat{\Theta}_{\{k_{l_i}\}}-1} \frac{S_i^{m_i}}{m_i!}$$

$$\delta^{(m_i)}(t - S_i) \int_0^\infty r_i e^{-r_i^2 t^{\tilde{\alpha}} \tilde{C}(\alpha) (\frac{\beta_i S_i}{P_i})^{\tilde{\alpha}} \Lambda^{\mathrm{FC}}} dr_i dt \tag{4.47}$$

$$= \sum_{i\in\mathcal{K}} \pi\lambda_i \int_0^{\infty} \overline{\sum_{\{k_{l_i}\}} \mathtt{T}_{\{k_{l_i}\}} \tilde{\Theta}_{\{k_{l_i}\}}} \sum_{m_i=0}^{\hat{\Theta}_{\{k_{l_i}\}}-1} \frac{\frac{S_i^{m_i}}{m_i!}\delta^{(m_i)}(t-S_i)}{t^{\breve{\alpha}}\tilde{C}(\alpha)(\frac{\beta_i S_i}{P_i})^{\breve{\alpha}}\Lambda^{\mathrm{FC}}} dt \tag{4.48}$$

$$= \sum_{i\in\mathcal{K}} \frac{\pi\lambda_i(\frac{P_i}{\beta_i S_i})^{\breve{\alpha}}}{\tilde{C}(\alpha)\Lambda^{\mathrm{FC}}} \overline{\sum_{\{k_{l_i}\}} \mathtt{T}_{\{k_{l_i}\}} \tilde{\Theta}_{\{k_{l_i}\}}} \sum_{m_i=0}^{\hat{\Theta}_{\{k_{l_i}\}}-1} \frac{S_i^{m_i}}{m_i!} \int_0^{\infty} \delta^{(m_i)}(t-S_i)\frac{1}{t^{\breve{\alpha}}} dt \tag{4.49}$$

$$= \frac{\pi}{\tilde{C}(\alpha)\Lambda^{\mathrm{FC}}} \sum_{i\in\mathcal{K}} \lambda_i \left(\frac{P_i}{\beta_i S_i^2}\right)^{\breve{\alpha}} \overline{\sum_{\{k_{l_i}\}} \mathtt{T}_{\{k_{l_i}\}} \tilde{\Theta}_{\{k_{l_i}\}}} \sum_{m_i=0}^{\hat{\Theta}_{\{k_{l_i}\}}-1} \frac{\Gamma(\breve{\alpha}+m_i)}{m_i!\Gamma(\breve{\alpha})}, \tag{4.50}$$

where Λ^{FC} is given by (2.56). The significance of the above analysis is that it provides an approximation for the coverage probability of a complex system in a closed-form expression. One can explicitly recognize the impact of various important system parameters such as the density of BSs, transmission powers, SIR thresholds, number of transmit and receive antennas on the coverage probability. In addition, the required numerical cost of $c^{\mathrm{SVD-FC}}$ given in (4.50) to evaluate the coverage probability for each set of network's parameter is fairly low. This is because in comparison to [33, 37, 38], here we do not need to numerically evaluate infinite integrals, determinant of matrices, and higher order differentiations (see also Remark 1.3.1).

4.5 Simulation Results

The considered simulation setup is similar to the one proposed in Section 2.7. In all our experiments we assume $S_1 = S_2 = N^r$, thus the number of data streams the BSs in both tiers transmit is as many as the number of antennas that UEs are equipped with, e.g., full-MUX scenario.

4.5.1 Impact of SIR Thresholds

We start with examining the accuracy of our analysis versus SIR thresholds β_1 and β_2. Fig. 4.2 and Fig. 4.3 illustrate the coverage probability versus β_1 and β_2, respectively. Both

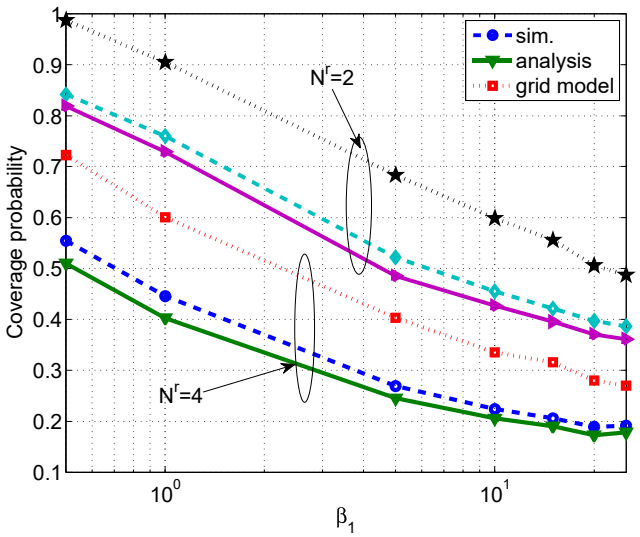

Figure 4.2: Coverage probability *v.s.* β_1 where $\beta_2 = 5$. Parameters are $\lambda_1 = 10^{-4}$, $\lambda_2 = 5 \times 10^{-3}$, $N_1^t = 16$, $N_2^t = 8$, and $P_1 = 50$ W.

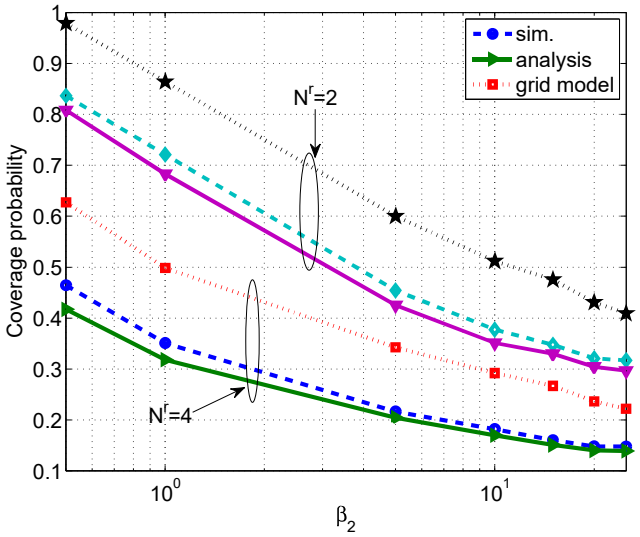

Figure 4.3: Coverage probability *v.s.* β_2 where $\beta_1 = 10$. Parameters are $\lambda_1 = 10^{-4}$, $\lambda_2 = 5 \times 10^{-3}$, $N_1^t = 16$, $N_2^t = 8$, and $P_1 = 50$ W.

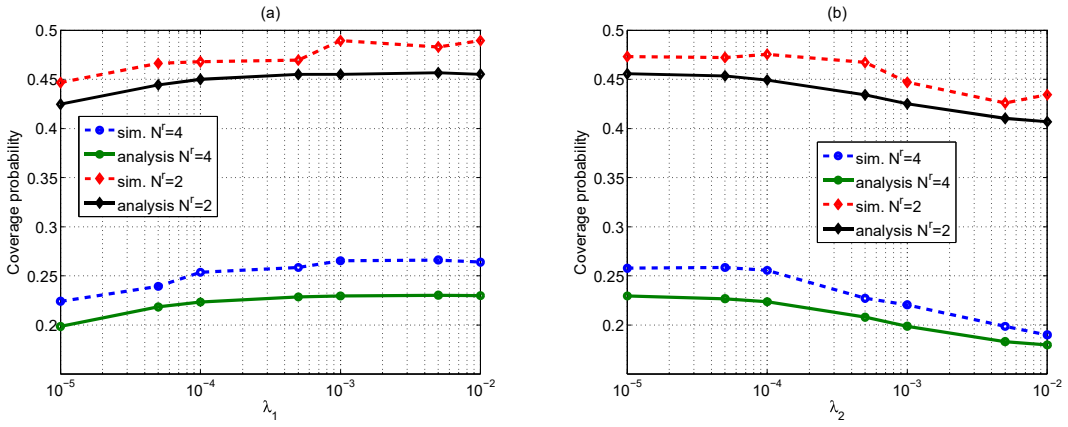

Figure 4.4: (a) Coverage probability *v.s.* λ_1 where $\lambda_2 = 10^{-3}$, (b) Coverage probability *v.s.* λ_2 where $\lambda_1 = 10^{-4}$. Parameters are $\beta_1 = 10$, $\lambda_2 = 5$, $N_1^t = 16$, $N_2^t = 8$, $P_1 = 50$ W.

of these illustrations confirm that our analysis accurately match those from the Monte-Carlo simulation, which is also inline with the discussion of Remark 2.3.2. Apart from accuracy perspective, the trends spotted in Fig. 4.2 and Fig. 4.3 are otherwise intuitive as by increasing SIR thresholds it is generally becoming more difficult for the typical UE to successfully decode all data streams, which in turn renders smaller coverage probability.

More interestingly, we observe that for smaller values of N^r the coverage probability is higher. In fact, increasing the number of receive antennas from $N^r = 2$ to $N^r = 4$ causes 50% reduction of coverage probability. Recalling that MIMO-SVD multiplexing system is a full-MUX scenario, this can be understood by noticing that in the all-coverage probability perspective of the communication link it is generally becoming less likely to detect a greater number of streams.

In Fig. 4.2 and Fig. 4.3 we also include the simulation results of grid model whereby the location of BSs in Tier 1 is based of hexagonal layout while the location of BSs in Tier 2 is still based on PPP model. As expected, the grid model provides an upper-bound on the coverage probability.

4.5.2 Impact of Densification

In Fig. 4.4-(a), we study the coverage probability v.s. λ_1 assuming $\lambda_2 = 10^{-3}$, and in Fig. 4.4-(b), we study the coverage probability vs. λ_2 assuming $\lambda_1 = 10^{-4}$.

First, both panels show that approximation $c^{\mathrm{SVD-FC}}$ can quite accurately predict the coverage probability for wide range of density of BSs. As expected, this approximation yields a tight lower-bound on the coverage probability. Second, both panels indicate that by doubling the number of receive antennas (and thus the number of data streams) the coverage probability reduces by nearly 50%. Third, Fig. 4.4-(a) shows that by densifying Tier 1 (increasing the number of macro BSs per unit area) the coverage probability increases almost 125%. On the other hand, as seen from Fig. 4.4-(b), densifying Tier 2 (installing more femto BSs) causes more than 50% reduction of the coverage probability.

The negative effect of densification of femto-tier (Tier 2) on the coverage probability can be reasoned noticing that by increasing λ_2, albeit it is becoming more probable for the typical UE to consider association from Tier 2, the association is not guaranteed to be fruitful. This is because the severity of ICI from interfering femto cells is simultaneously increased by practicing the densification. Moreover, femto BSs should yet compete with Macro BSs that are equipped with greater number of antennas.

On the other hand, the coverage probability increases by densifying Tier 1 because for larger densities i) it becomes more probable for the typical UE to select one of the macro BSs for the association, and 2) since Macro BSs are equipped with large number of transmit antennas, the detection of all the N^r data streams transmitted from a Macro BS stays effectively probable. In this way, it is plausible to argue that the negative impact of growing ICI due to increasing λ_1 is effectively compensated for.

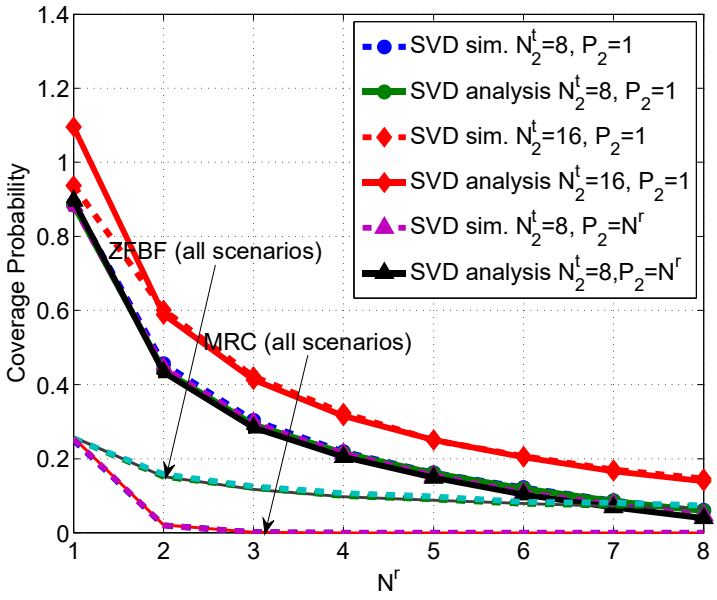

Figure 4.5: Coverage probability *v.s.* N^r. Parameters are $\beta_1 = 10$, $\beta_2 = 5$, $\lambda_1 = 10^{-4}$, $\lambda_2 = 10^{-3}$, $N_1^t = 16$, $N_2^t = 8$, $P_1 = 50$ W.

4.5.3 Impact of Number of Data Streams

Let us increase N^r. Analytical and simulation results are illustrated in Fig. 4.5. For comparison we also report the results of MRC and ZFBF. For the MRC and ZFBF systems, BSs randomly turn on N^r transmit antennas and switch the rest off. Fig. 4.5 shows the coverage performance vs. N^r.

Remark 4.5.1 (Remark 2.3.2 Cont.). *As seen from Fig. 4.5, the analytical result of the coverage probability may become larger than 1. We already discuss this issue in Remark 2.3.2. In fact, if the average power of the fading of the attending channel is much higher than that of the fading of the interfering channel (for this scenario the former is 16 while the latter is one), it becomes highly probable that more than one BS can support the typical UE, which makes* (4.31) *an upper-bound of the actual coverage probability.*

MIMO-SVD System

From Fig. 4.5 we observe that the theoretical and simulation results match-up closely. Now, consider the case that $N_2^t = 8$ and $P_2 = 1$ W. As seen, by increasing N^r the coverage probability dramatically reduces. In fact, by moving from $N^r = 1$ to $N^r = 2$ we experience almost 50% coverage reduction. This is due to the rapid increase of ICI and the decrease of intended signal strength by growing N^r. However, the rate of reduction of coverage probability versus N^r is reduced for larger values of N^r. One may ask does increasing the transmission power help to compensate for the larger values of N^r? To inspect this, we let the value of P_2 increase by N^r. Fig. 4.5 shows that with higher transmission power the coverage probability does not improve. Finally, let us increase the number of transmit antennas of femto BSs to $N_2^t = 16$. Fig. 4.5 confirms 10% coverage growth compared to two previously considered setups.

MRC and ZFBF Systems

As it is seen from Fig. 4.5 MRC system is very vulnerable to the growth of multiplexing gain (increase of N^r). In fact, for $N^r \geq 2$ its coverage probability is almost zero. Unfortunately, neither increasing P_2 nor increasing N_2^t can enhance the robustness of MRC systems against large values of N^r. Compared to MRC system, ZFBF system is more robust against the growth of N^r (see also Fig. 2.6). In fact, Fig. 4.5 shows that by increasing N^r the coverage probability is reduced, but with much lower rate compared to MRC system. Surprisingly, for the case that $N_2^t = 8$ and $N^r = 8$ the coverage probability of ZFBF system is almost equal to that of SVD system.

Note that as the case of MRC system, ZFBF system also does not respond to neither the growth of transmission power nor the growth of N_2^t.

Comparison Between SVD and MRC/ZFBF Systems

For the case of $N^r = 1$, we observe that SVD system introduces growths more that 450% in the coverage compared to MRC system. For $2 \leq N^r \leq 6$ and $N_2^t = 16$ these values are higher than 1000%. On the other hand, for the case of $N^r = 1$, we measure that SVD system increases the coverage probability by 450% against ZFBF system.

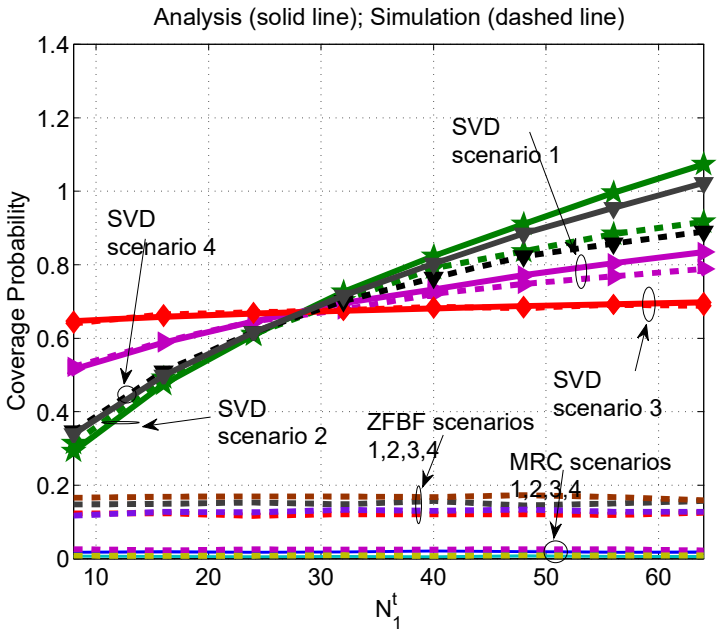

Figure 4.6: Coverage probability *v.s.* N_1^t. Parameters are $N^r = 2$, $\beta_1 = 10$, $\beta_2 = 5$, $P_1 = 50$ W, and $N_2^t = 8$.

4.5.4 Impact of Transmit Antennas

Here, we are mainly interested to investigate the net effect of equipping BSs with sufficiently large number of antennas in conjunction with densification. We consider four scenarios: (1) both tiers are sparse, $\lambda_1 = 10^{-4}$ and $\lambda_2 = 10^{-3}$, (2) only Tier 1 is densified, $\lambda_1 = 10^{-2}$ and $\lambda_2 = 10^{-3}$, (3) only Tier 2 is densified, $\lambda_1 = 10^{-4}$ and $\lambda_2 = 10^{-2}$, and (4) both tiers are densified, $\lambda_1 = 10^{-2}$ and $\lambda_2 = 10^{-2}$. Note that here the introduction of terms "sparse" and "dense" are merely used to make the discussion succinct.

Impact of N_1^t

We start by studying N_1^t. The results are reported in Fig. 4.6. For this experiment we set $N_2^t = 8$ and $N^r = 2$.

Scenario (1): First consider scenario (1) in which both tiers are sparse, i.e., $\lambda_1 = 10^{-4}$ and $\lambda_2 = 10^{-3}$. Coverage probability is shown in Fig. 4.6. As seen from this illustration, the coverage probability of SVD increases by increasing N_1^t. Specifically, increasing N_1^t by 8 folds results in 160% enhancement of the coverage probability. On the other hand, for ZFBF and MRC systems, we observe that N_1^t does not have any impact on the coverage probability. These observations are inline with our intuition: in the SVD system by increasing the number of transmit antennas and keeping the receive antennas fixed the power of signal strength on each data streams grows while the ICI is kept stable, thus, the coverage enhances by increasing N_1^t. However, in the open-loop systems both signal power and ICI on each data stream are irresponsive to the amount of N_1^t, hence the resultant coverage probability stays stable against the growth of N_1^t.

Scenario (2): Now, let us densify Tier 1 to $\lambda_1 = 10^{-2}$ while keeping the density of Tier 2 as the scenario 1 equal to $\lambda_2 = 10^{-3}$. For the SVD system, as seen, increasing N_1^t monotonically increases the coverage probability. From Fig. 4.6, we further measure that increasing N_1^t by 8 folds increases the coverage probability by 334%. Interestingly, for $N_1^t = 64$ almost 95% coverage is guaranteed, which is impressive. For the systems of ZFBF and MRC, results indicate that the coverage probability is unaffected by densification of Tier 1 and/or the growth of N_1^t.

Scenario (3): We densify Tier 2 and keep the density of Tier 1 low, i.e., $\lambda_1 = 10^{-4}$ and $\lambda_2 = 10^{-2}$. When SVD system is considered, we observe from Fig. 4.6 that (similar to MRC and ZFBF systems) the coverage probability does not respond to the growth of N_1^t. On the other hand, for small to moderate values of N_1^t (more specifically $N_1^t \leq 32$) this scenario results in the highest coverage performance. However, for moderate to large values of N_1^t (more specifically $N_1^t > 32$) this Scenario yields the smallest performance. Consequently,

massively increasing the number of antennas in the tier of macro BSs while the network in Tier 2 is immensely densified does not provide any appreciable performance value.

Scenario (4): Finally, we observe that when both tiers are densified, almost no performance enhancement is introduced in terms of coverage probability compared to Scenario (2). This observation holds true for all SVD, MRC, and ZFBF systems. Thus, only densifying Tier 1 is deemed adequate.

Remark 4.5.2 (Remark 2.3.2 Cont.). *We also observe from Fig. 4.6 that for sufficiently large N_1^t the coverage probability obtained from analysis takes values slightly larger than 1. For this case, the average power of the fading of the attending channel is larger than 50, which is much higher than that of the fading of the interfering channel that is around 8. Therefore, it becomes highly probable that more than 1 BS can support the typical UE, which makes* (4.31) *an upper-bound of the actual coverage probability.*

Impact of N_2^t

We now study impact of N_2^t in Fig. 4.7. Here we set $N^r = 2$ and $N_1^t = 64$. First consider Scenario (1). As seen, the coverage probability monotonically increases with N_2^t. Specifically, increasing N_2^t by 8 folds results in 150% enhancement of the coverage probability.

Now let us densify Tier 2 (i.e., Scenario (3)). It is seen that the coverage probability increases by increasing N_2^t, so that increasing N_2^t by 8 folds results in 350% enhancement of the coverage probability.

On the other hand, when densification is practiced in Tier 1 (i.e., Scenario (2)) we observe that the coverage probability stays stable against the growth of N_2^t. However, compared to both previous scenarios, we here recognize that this scenario renders the highest coverage probability.

In the case of Scenario (4), i.e., both tiers are densified, a slightly smaller coverage probability to that of Scenario (2) is reported. Furthermore, the coverage is not affected by increasing N_2^t.

Finally, we see from Fig. 4.7 that the MRC and ZFBF systems do not respond to the growth of N_2^t in all the considered scenarios. In addition, in all the scenarios SVD adds huge performance boost compared to these open-loop systems.

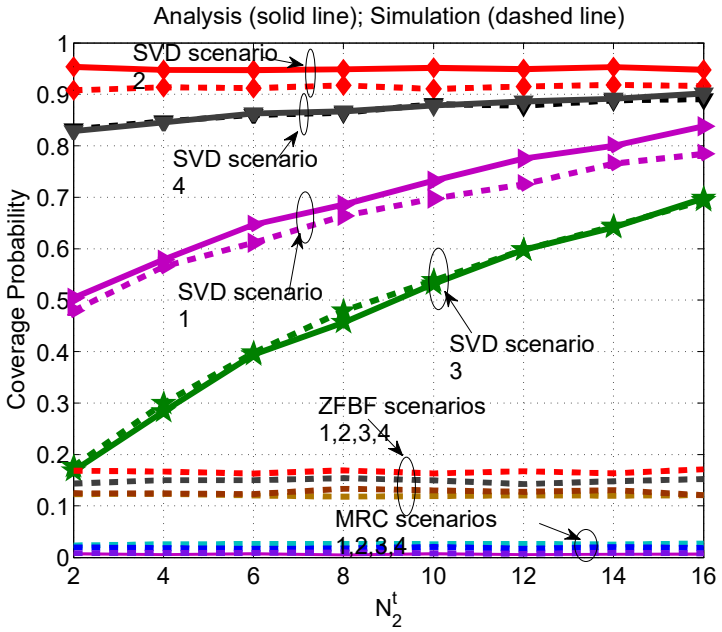

Figure 4.7: Coverage probability *v.s.* N_2^t. Parameters are $N^r = 2$, $\beta_1 = 10$, $\beta_2 = 5$, $\lambda_2 = 5$, and $N_1^t = 64$.

4.6 Conclusions

In this chapter, we studied the coverage performance of MIMO-SVD multiplexing system. We adopted tool of random matrix theory to provide an expression for the coverage probability in a closed-form, as a function of main system parameters. Our simulation result confirmed the accuracy of the analysis. We also observed that the MIMO-SVD full-MUX system has huge benefits in enhancing the coverage performance against the open-loop MIMO multiplexing systems (MRC and ZFBF). We further noticed that as the cases of MRC and ZFBF systems, in SVD system it is important to cautiously densify the network with accordance to multiplexing gain to improve the coverage performance. In effect, we observed

that it is not recommended to simultaneously densify the network in Tier 2 while massively adding to the number of transmit antennas in Tier 1.

Chapter 5

Conclusions and Future Research Directions

In this final chapter, in Section 5.1, we summarize our results and highlight the contributions of this thesis. Section 5.2 highlights important engineering insights we have drawn from our investigations. In Section 5.3, we propose ideas for future research.

5.1 Conclusions

In this thesis, we have developed analytical tools for investigating the coverage performance and ASE of MIMO multiplexing HetNets. The focus of the thesis is mainly on down-link communications. The analysis of the thesis is based on stochastic geometry theory. We have chiefly considered the max-SINR CA rule and focused on the scenario that the successful reception of all of the transmitted data-streams is required for the coverage.

- In Chapter 2, we have introduced a K-tier PPP model for MIMO multiplexing HetNets and formulated the coverage probability. We have derived an upper-bound and a lower-bound on the coverage probability. Our proposed expressions of the coverage probability are easy-to-compute and explicitly capture impacts of various system parameters including densities of BSs, SIR thresholds, and multiplexing gains. The lower-bound is in closed-form and very tight. We have also proved that the lower-bound is achievable under the full-correlation (FC) assumption. We have specified the coverage probability for the interference-limited system. We have exploited the

analysis to study a number of optimization problems demonstrating the relationship between densification and multiplexing gains. We have studied the spatial throughput of multiplexing systems when the quantized values of SINRs are available at the serving BSs.

We have further explored the coverage probability of some other pertinent MIMO systems, a more practical variation of the max-SINR CA rule, and non-homogenous path-loss environments. We have also extended the analysis for the case of spectrum-sharing D2D HetNets and demonstrated how one can adjust the noise power at the receiver based on the D2D communication parameters. This allows a very straightforward and decoupled design of the operating regimes of the D2D and HetNet only based on a number of statistical parameters.

Our analysis in this chapter have shown that 1) full correlation of ICI across data streams slightly reduces the coverage probability; 2) increasing multiplexing gains can reduce the coverage probability; 3) MIMO multiplexing systems are well modelled by the interference-limited system; 4) the existence of a tradeoff between densification and multiplexing gain: if one is to increase the multiplexing gain in a tier, it is recommended to simultaneously densify the other tier in order to preserve a level of coverage performance against diversity system; and 5) by including feedback channels with capacity up to 8 bits per frame per BS, it is possible to increase the spatial throughput by nearly 180% over 1-bit feedback scenario.

- In Chapter 3 the main focus is on MRC multiplexing systems. Our analysis incorporats CSI inaccuracies on the coverage performance. We have derived an accurate upper-bound on the coverage probability in closed-form. We have also developed analytical tools facilitating thorough investigations of the impact of cross-stream SIR correlation on the coverage performance of multi-stream systems. Full correlation among data streams has been shown to yield a slightly smaller coverage performance. On the other

hand, our analysis has proved that by neglecting such correlation, as commonly assumed in the literature, one should expect a substantial overestimation of the coverage probability.

Important engineering insights have been derived from optimizing the performance along with the simulation results: 1) densification in multiplexing systems should be practiced based on multiplexing gains; otherwise a dramatic coverage loss might be inevitable; 2) in indoor scenarios (high path-loss exponent regimes) it is possible to reduce the pilot signaling overhead designated for CSI estimation without imposing noticeable coverage loss compared to the outdoor coverage performance; and 3) although MRC suffers from intra-stream interference in comparison to more complex receivers such as ZFBF, the relative coverage loss in large-array scenarios and/or for cell edge users (e.g., small SIR thresholds) is barely noticeable.

- In Chapter 4, we have derived the coverage performance of MIMO-SVD multiplexing system. We have adopted tool of random matrix theory to provide an approximation of the coverage probability in an easy-to-use closed-form expression as a function of main system parameters. We have also observed that the MIMO-SVD full-MUX system has huge benefits in enhancing the coverage performance against MRC and ZFBF systems. Our results also shed lights on the relationship between network densification and massive MIMO-SVD communications: 1) it is not recommended to simultaneously densify the network in small cell tier while also adding to its number of transmit antennas at the BSs, as it may not introduce coverage gain; 2) one can keep tier of Macro BSs sparse and massively add to the number of antennas they are equipped with to proportionally increase coverage performance with the number of antennas even when the operating point is full multiplexing.

5.2 Network-Level Insights and Recommendations

Here, we enumerate important design guidelines and engineering insights that our investigations have achieved. Note that our system model includes max-SINR CA rule along with all-coverage probability.

- It is important to correctly account for the traits of MIMO multiplexing systems in the stage of CA. Otherwise, potentials of MIMO systems — enhancing communication reliability and increasing data rate — may not be fully realizable. We observe that the max-SINR CA rule can, at least to some extents, achieve this goal without sacrificing analytical tractability.

- To correctly model MIMO multiplexing systems for a network-level analysis, one should define coverage probability from the perspective of the communication link. This is because, due to severe ICI in HetNets, a substantial correlation across the data steams of a communication link is inevitable. In effect, a stream-level coverage probability inaccurately overestimates the correct coverage performance.

- Densification in multiplexing systems should be practiced in conjunction with considerations of multiplexing gains, else dramatic coverage loss might be inevitable. Furthermore, when the CSIR is not accurately available at the receivers, the network densification becomes less attractive as the inaccuracy of CSIR increases.

- Substantial coverage probability growth under the SVD configuration is attainable, which highlights the importance of CSIT in enhancing the coverage performance of HetNets. Further, SVD systems can harness considerable coverage gain in large-array antenna systems. However, if the network is densified in Tier 2, increasing the number of antennas in Tier 1 does not provide coverage enhancement.

5.3 Future Research Directions

In this section, we propose some possible research directions that can be followed from this thesis.

- *Receive Antenna Correlation:* Throughout the thesis, we assumed that receive antennas are uncorrelated. This assumption substantially simplified our analysis. Nevertheless, in practice receive antennas may exhibits levels of row correlation due, for instance, to the space limitation at the devices. As a promising direction, we believe it is important to extend the analysis of this thesis to account for receive antenna correlation.

- *Inaccurate CSIR for ZFBF and SVD Systems:* This thesis commonly assumed that accurate CSIR is available at the receiver. The only exception was the case of MRC systems in Chapter 3. For the other two multiplexing systems (ZFBF and SVD) it is more involved to incorporate the CSIR inaccuracies into the analysis. From a practical standpoint it is interesting to investigate how robust is the performance gain of SVD over ZFBF or ZFBF over MRC is when CSIR is inaccurate.

- *Correlated Shadowing:* Our analysis is valid when large-scale shadowing independently affects attending signal and interfering signals. In reality however, large obstacles cause distance-dependent correlated shadowing; see Fig. 5.1. This implies that the received signals from interfering BSs may be correlated with the level of correlation influenced by the size and density of large obstacles. Therefore, a substantial improvement of the analysis is required to incorporate such practical case.

- *More Practical Point Process Models to Incorporate Repulsion:* Throughput the analysis of this thesis, we let BSs be located arbitrarily in the coverage space. However, in reality BSs may demonstrate minimum separation distance, in particular across macro BSs. Further, there might be some limitations in the installation location of small cells,

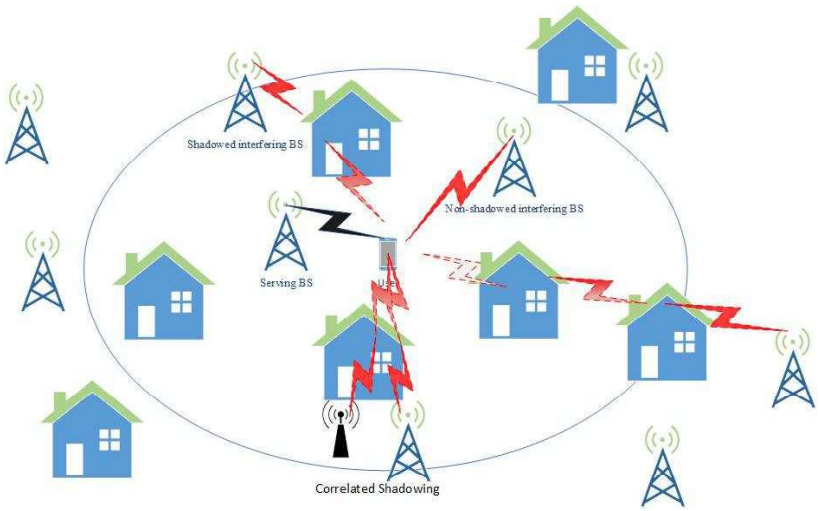

Figure 5.1: An example of correlated shadowing.

e.g., dead zones, cell edges, and hot spots. We believe it is practically appealing to extend the analysis of this thesis for more sophisticated yet practically accurate point process models.

- *Adaptive Cross-Stream Power Allocation in MIMO SVD System:* For the case of SVD systems, we let the power be equally shared across data streams. However, in reality, thanks to the availability of CSIT, the BS can adaptively share power across data streams according to the strength of eigenvalues. One may also enforce zero power allocation to the weakest channel associated with the weakest eigenvalue to preserve the transmission power for stronger eigenvalues. For both cases it is then a promising research direction to extend the method of Chapter 4.

Bibliography

[1] J. G. Andrews, F. Baccelli, and R. K. Ganti, "A tractable approach to coverage and rate in cellular networks," *IEEE Trans. Commun.*, vol. 59, pp. 3122–3134, Nov. 2011.

[2] 3GPP, "Technical specification group radio access network; evolved universal terrestrial radio access (E-UTRA); further advancements for E-UTRA physical layer aspects (Release 9). TR 36.814," 2010.

[3] F. Boccardi, R. W. Heath, A. Lozano, T. L. Marzetta, and P. Popovski, "Five disruptive technology directions for 5G," *IEEE Commun. Magazine*, vol. 54, pp. 74–80, Feb. 2014.

[4] J. G. Andrews, H. Claussen, M. Dohler, S. Rangan, and M. C. Reed, "Femtocells: Past, present, and future," *IEEE J. Select. Areas Commun.*, vol. 30, pp. 497–508, Apr. 2012.

[5] E. Castaneda, A. Silva, A. Gameiro, and M. Kountouris, "An overview on resource allocation techniques for multi-user MIMO systems," *IEEE Commun. Surveys & Tutorials*, vol. 19, pp. 239–284, First Quarter 2017.

[6] J. G. Andrews, S. Buzzi, W. Choi, S. V. Hanly, A. Lozano, A. C. K. Soong, and J. C. Zhang, "What will 5G be?," *IEEE J. Select. Areas Commun.*, vol. 32, pp. 1065–1082, Jun. 2014.

[7] T. L. Marzetta, "Noncooperative cellular wireless with unlimited numbers of base station antennas," *IEEE Trans. Wireless Commun.*, vol. 9, pp. 3590–3600, Nov. 2010.

[8] D. Gesbert, S. Hanly, H. Huang, S. Shamai, O. Simeone, and W. Yu, "Multi-cell MIMO cooperative networks: A new look at interference," *IEEE J. Sel. Areas Commun.*, vol. 28, pp. 1380–1408, Dec. 2010.

[9] A. Asadi, Q. Wang, and V. Mancuso, "A survey on device-to-device communication in cellular networks," *IEEE Commun. Surveys & Tutorials,*, vol. 16, no. 4, pp. 1801–1819, 2014.

[10] Q. Li, G. Li, W. Lee, M. Lee, D. Mazzarese, B. Clerckx, and Z. Li, "MIMO techniques in WiMAX and LTE: A feature overview," *IEEE Commun. Magazine*, vol. 48, pp. 86–92, May 2010.

[11] C. Lim, T. Yoo, B. L. B. Clerckx, and B. Shim, "Recent trend of multiuser MIMO in LTE-Advanced," *IEEE Commun. Mag.*, vol. 51, pp. 127–135, Mrc. 2013.

[12] Cisco, "Visual networking index," Feb. 2014. white paper at Cisco.com.

[13] D. Gesbert, M. Shafi, D. Shiu, P. J. Smith, and A. Naguib, "From theory to practice: An overview of MIMO spacetime coded wireless systems," *IEEE J. Sel. Areas Commun.*, vol. 21, pp. 281–302, Apr. 2003.

[14] D. Tse and P. Viswanath, *Fundamentals of Wireless Communication*. Cambridge University Press, September 2004.

[15] E. Telatar, "Capacity of multi-antenna gaussian channels," *Europ. Trans. Telecomm.*, vol. 10, pp. 585–595, Nov.Dec. 1999.

[16] A. J. Goldsmith, *Wireless Communications*. Cambridge University Press, 2005.

[17] L. Liu, R. Chen, S. Geirhofer, K. Sayana, Z. Shi, and Y. Zhou, "Downlink MIMO in LTE-advanced: SU-MIMO vs. MU-MIMO," *IEEE Commun. Mag.*, vol. 50, pp. 140–147, Feb. 2012.

[18] A. Lozano, R. W. Heath, and J. G. Andrews, "Fundamental limits of cooperation," *IEEE Trans. Inform. Theory*, vol. 59, pp. 5213–5226, Sep. 2013.

[19] K. Hosseini, W. Yu, and R. S. Adve, "A stochastic analysis of network MIMO systems," *IEEE Trans. Signal Proc.*, vol. 64, pp. 4113–4126, Aug. 2016.

[20] P. Marsch and G. Fettweis, *Coordinated Multi-Point in Mobile Communications*. Cambridge University Press, Cambridge, England, 2011.

[21] D. Lee, H. Seo, B. Clerckx, E. Hardouin, D. Mazzarese, S. Nagata, and K. Sayana, "Coordinated multipoint transmission and reception in LTE-Advanced: Deployment scenarios and operational challenges," *IEEE Commun. Mag.*, vol. 50, pp. 148–155, Feb. 2012.

[22] M. Sawahashi, Y. Kishiyama, A. Morimoto, D. Nishikawa, and M. Tanno, "Coordinated multipoint transmission/reception techniques for LTE-Advanced," *IEEE Wireless Commun. Mag.*, vol. 3, pp. 26–34, Jun. 2010.

[23] D. Liu, L. Wang, Y. Chen, M. Elkashlan, K.-K. Wong, R. Schober, and L. Hanzo, "User association in 5g networks: A survey and an outlook," *IEEE Commun. Surveys & Tutorials*, vol. 18, pp. 1018–1044, Second Quarter 2016.

[24] L. P. Qian, A. Zhang, Y. Wu, and J. Chen, "Joint base station association and power control via benders decompostition," *IEEE Trans. Wireless Commun.*, vol. 4, pp. 1651–1665, Apr. 2013.

[25] K. Shen and W. Yu, "Distributed pricing-based user association for downlink heterogeneous cellular networks," *IEEE J. Select. Areas Commun.*, vol. 32, pp. 1100–1113, Jun. 2014.

[26] X. Y. H. Kim, G. de Veciana and M. Venkatachalam, "Distributed α-optimal user association and cell load balancing in wireless networks," *IEEE/ACM Trans. Networking*, vol. 59, pp. 3122–3134, Nov. 2011.

[27] A. D. Wyner, "Shannon-theoretic approach to a gaussian cellular multi-access channel," *IEEE Trans. Inf. Theory*, vol. 40, pp. 1713–1727, Nov. 1994.

[28] M. A. Wigger, R. Timo, and S. Shamai, "Conferencing in Wyner's asymmetric interference network: Effect of number of rounds," *IEEE Trans. Inf. Theory*, vol. 63, pp. 1199–1226, Feb. 2017.

[29] A. Lapidoth, N. Levy, S. Shamai, and M. A. Wigger, "Cognitive wyner networks with clustered decoding," *IEEE Trans. Inf. Theory*, vol. 60, pp. 6342–6367, Nov. 2014.

[30] F. Baccelli, B. Blaszczyszyn, and P. Muhlethaler, "Stochastic analysis of spatial and opportunistic ALOHA," *IEEE J. Select. Areas Commun.*, vol. 27, pp. 1105–1119, Sep. 2009.

[31] P. A. Dighe, R. K. Mallik, and S. S. Jamuar, "Analysis of transmit-receive diversity in rayleigh fading," *IEEE Trans. Commun.*, vol. 51, pp. 694–703, Apr. 2003.

[32] A. Zanella, M. Chiani, and M. Z. Win, "On the marginal distribution of the eigenvalues of wishart matrices," *IEEE Trans. Commun.*, vol. 57, pp. 1050–1060, Apr. 2009.

[33] M. Kang and M. S. Alouini, "A comparative study on the performance of MIMO MRC systems with and without cochannel interference," *IEEE Trans. Commun.*, vol. 52, pp. 1417–1425, Aug. 2004.

[34] Y. Li, L. Zhang, L. J. Cimini, and H. Zhang, "Statistical analysis of MIMO beamforming with co-channel unequal-power MIMO interferers under path-loss and rayleigh fading," *IEEE Trans. Signal Proc.*, vol. 59, pp. 3738–3748, Aug. 2011.

[35] K. S. Ahn, "Performance analysis of MIMO-MRC systems with channel estimation error in the presence of cochannel interferences," *IEEE Signal Proc. Let.*, vol. 15, pp. 445–448, 2008.

[36] J. Mietzner, R. Schober, L. Lampe, W. H. Gerstacker, and P. A. Hoeher, "Multiple-antenna techniques for wireless communications: A comprehensive literature survey," *IEEE Commun. Surveys & Tutorials*, vol. 11, pp. 87–105, Second Quarter 2009.

[37] M. Z. W. M. Chiani and H. Shin, "MIMO networks: The effects of interference," *IEEE Trans. Inform. Theory*, vol. 56, pp. 336–349, Jan. 2010.

[38] D.-W. Yue and Q. T. Zhang, "Generic approach to the performance analysis of correlated transmit/receive diversity MIMO systems with/without co-channel interference," *IEEE Trans. Inform. Theory*, vol. 56, pp. 1147–1157, Mrc. 2010.

[39] Y. Chen and M. R. McKay, "Coulumb fluid, painleve transcendents, and the information theory of MIMO systems," *IEEE Trans. Inform. Theory*, vol. 58, pp. 4594–4634, Jul. 2012.

[40] J. F. C. Kingman, *Poisson Processes.* Oxford University Press, 1993.

[41] M. Haenggi and R. K. Ganti, *Interference in large wireless networks.* NOW: Foundations and Trends in Networking, 2009.

[42] H. ElSawy, A. Sultan-Salem, and M.-S. Alouini, "Modeling and analysis of cellular networks using stochastic geometry: A tutorial," *IEEE Commun. Surveys & Tutorials,*, vol. 19, pp. 167–203, Firstquarter 2017.

[43] W. C. Ao and K.-C. Chen, "Bounds and exact mean node degree and node isolation probability in interference-limited wireless ad hoc networks with general fading," *IEEE Trans. Veh. Tech.*, vol. 61, pp. 2342–2348, Jun. 2012.

[44] F. Baccelli and B. Blaszczyszyn, *Stochastic geometry and wireless networks, vol. I-II.* No. 2, NOW: Foundations and Trends in Networking, 2009.

[45] M. D. Renzo and W. Lu, "The equivalent-in-distribution EiD-based approach: On the analysis of cellular networks using stochastic geometry," *IEEE Commun. Lett.*, vol. 18, pp. 761–764, May 2014.

[46] A. Ghosh, "Mixture-based modeling of spatially correlated interference in a poisson field of interferers," *IEEE Commun. Lett.*, vol. 21, pp. 2496–2499, Nov. 2017.

[47] H. S. Dhillon, R. K. Ganti, F. Baccelli, and J. G. Andrews, "Modeling and analysis of K-tier downlink heterogeneous cellular networks," *IEEE J. Select. Areas Commun.*, vol. 30, pp. 550–560, Apr. 2012.

[48] S. Mukherjee, "Distribution on downlink SINR in heterogeneous cellular network," *IEEE J. Select. Areas Commun.*, vol. 30, pp. 575–585, Apr. 2012.

[49] H. S. Jo, Y. J. Sang, P. Xia, and J. G. Andrews, "Heterogeneous cellular networks with flexible cell association: A compehensive downlink SINR analysis," *IEEE Trans. Wireless Commun.*, vol. 11, pp. 3484–3495, Oct. 2012.

[50] H. S. Dhillon and J. G. Andrews, "Downlink rate distribution in heterogenous cellular networks under generalized cell association," *IEEE Wireless Commun. Letters*, vol. 3, pp. 42–45, Feb. 2014.

[51] H. S. Dhillon, J. G. Andrews, and A. Ghosh, "Load-aware modeling and analysis of heterogenous cellular networks," *IEEE Trans. Commun.*, vol. 12, pp. 1666–1677, Apr. 2013.

[52] Y. Lin, W. Bao, W. Yu, and B. Liang, "Optimizing user association and spectrum allocation in hetnets: A utility perspective," *IEEE J. Select. Areas Commun.*, vol. 33, pp. 1025–1039, Jun. 2015.

[53] H. Yang, G. Geraci, and T. Q. S. Quek, "Energy efficient design of MIMO heterogeneous networks with wireless backhaul," *IEEE Trans. Wireless Commun.*, vol. 15, pp. 4914–4927, Jul. 2016.

[54] J. Zhu, S. Govindasamy, and J. Hwang, "Perforamnce of multiantenna linear MMSE receivers in doubly stochastic networks," *IEEE Trans. Commun.*, vol. 62, pp. 2825–2839, Aug. 2014.

[55] R. Tanbourgi, H. S. Dhillon, and F. K. Jondral, "Analysis of joint transmit-receive diversity in downlink MIMO heterogeneous cellular networks," *IEEE Trans. Wireless Commun.*, vol. 14, pp. 6695–6709, Jul. 2015.

[56] H. S. Dhillon, M. Kountouris, and J. G. Andrews, "Downlink MIMO hetnets: Modeling, ordering results and performance analysis," *IEEE Trans. Wireless Commun.*, vol. 12, pp. 5208–5222, Oct. 2013.

[57] G. George, R. K. Mungara, A. Lozano, and M. Haenggi, "Ergodic spectral efficiency in MIMO cellular networks," *IEEE Trans. Wireless Commun.*, vol. 16, pp. 2835–2849, May. 2017.

[58] V. Suryaprakash, P. Rost, and G. Fettweis, "Are heterogeneous cloudbased radio access networks cost effective?," *IEEE J. Sel. Areas Commun.*, vol. 33, pp. 2239–2251, Oct. 2015.

[59] Y. Zhong, T. Q. S. Quek, and W. Zhang, "Complementary networking for C-RAN: Spectrum efficiency delay and system cost," *IEEE Trans. Wireless Commun.*, vol. 16, pp. 4639–4653, Jul. 2017.

[60] C. Li, J. Zhang, M. Haenggi, and K. B. Letaief, "User-centric intercell interference nulling for downlink small cell networks," *IEEE Trans. Commun.*, vol. 63, pp. 1419–1431, Apr. 2015.

[61] S. Akoum and R. W. Heath, "Interference coordination: Random clustering and adaptive limited feedback," *IEEE Trans. Signal Proc.*, vol. 61, pp. 1822–1834, Apr. 2013.

[62] K. Huang, and J. G. Andrews, and D. Guo, and R. W. Heath Jr., and R. A. Berry, "Spatial interference cancellation for multiantenna mobile ad hoc networks," *IEEE Trans. Inform. Theory*, vol. 58, pp. 1660–1676, Mrc. 2012.

[63] S. Yu, H.-B. Kong, Y.-T. Kim, S.-H. Park, , and I. Lee, "Novel feedback bit allocation methods for multi-cell joint processing systems," *IEEE Trans. Wireless Commun.*, vol. 11, pp. 3030–3036, Sep. 2012.

[64] M. N. Kulkarni, A. Ghosh, and J. G. Andrews, "A comparison of MIMO techniques in downlink millimeter wave cellular networks with hybrid beamfrming," *IEEE Trans. Commun.*, vol. 54, pp. 1952 – 1967, May 2016.

[65] J. G. Andrews, T. Bai, M. N. Kulkarni, A. Alkhateeb, A. K. Gupta, and R. W. Heath, "Modeling and analyzing millimeter wave cellular systems," *IEEE Trans. Commun.*, vol. 65, pp. 403–430, Jan. 2017.

[66] C. Galiotto, N. K. Pratas, N. Marchetti, and L. Doyle, "A stochastic geometry framework for LOS/NLOS propagation in dense small cell networks," in *Proc. of IEEE International Conferene on Communiations (ICC)*, pp. 2851 – 2856, Jun. 2015.

[67] I. A. J. Arnau and M. Kountouris, "Impact of LOS/NLOS propagation and path loss in ultra-dense cellular networks," in *Proc. of IEEE International Conferene on Communiations (ICC)*, Jun. 2016.

[68] M. Ding, P. Wang, D. Lopez-Perez, G. Mao, and Z. Lin, "Performance impact of LoS and NLoS transmissions in dense cellular networks," *IEEE Trans. Wireless Commun.*, vol. 15, pp. 2365–2380, Mar. 2016.

[69] J. Liu, M. Sheng, L. Liu, and J. Li, "Effect of densification on cellular network performance with bounded pathloss model," *IEEE Commun. Letters*, vol. 21, pp. 346–349, Feb. 2017.

[70] R. V. T. Bai and R. W. Heath Jr., "Analysis of blockage effects on urban cellular networks," *IEEE Trans. Wireless Commun.*, vol. 13, pp. 5070–5083, Sep. 2014.

[71] M. Taranetz, R. W. Heath Jr. and M. Rupp, "Analysis of urban two-tier heterogeneous mobile networks with small cell partitioning," *IEEE Trans. Wireless Commun.*, vol. 15, pp. 7044–2613, Oct. 2016.

[72] T. Ding, M. Ding, Z. L. G. Mao, D. Lopez-Perez, and A. Y. Zomaya, "Uplink performance analysis of dense cellular networks with LoS and NLoS transmissions," *IEEE Trans. Wireless Commun.*, vol. 16, pp. 2601–2613, Apr. 2017.

[73] M. D. Renzo and P. Guan, "Stochastic geometry modeling, system-level analysis and optimization of uplink heterogeneous cellular networks with multi-antenna base stations," *IEEE Trans. Commun.*, vol. 64, pp. 2453–2476, Jun. 2016.

[74] M. Sheng, W. Jiao, X. Wang, and G. Liu, "Effect of power control on performance of users in an interference-limited network with unsaturated traffic," *IEEE Trans. Veh. Tech.*, vol. 66, pp. 2740–2755, Mrc. 2017.

[75] W. Bao and B. Liang, "Stochastic geometric analysis of user mobility in heterogeneous wireless networks," *IEEE J. Sel. Areas Commun.*, vol. 14, pp. 2212– 2225, Oct. 2015.

[76] S. Sadr and R. Adve, "Handoff rate and coverage analysis in multitier heterogeneous networks," *IEEE Trans. Wireless Commun.*, vol. 14, pp. 2626–2638, May 2015.

[77] R. Arshad, H. ElSawy, S. Sorour, T. Y. Al-Naffouri, and M.-S. Alouini, "Velocity-aware handover management in two-tier cellular networks," *IEEE Trans. Wireless Commun.*, vol. 16, pp. 1851–1867, Mrc. 2017.

[78] M. Haenggi, "Diversity loss due to interference correlation," *IEEE Commun. Letters*, vol. 16, pp. 1600–1603, Oct. 2012.

[79] M. G. Khoshkholgh, Y. Zhang, K.-C. Chen, K. G. Shin, and S. Gjessing, "Connectivity of cognitive device-to-device communications underlying cellular networks," *IEEE J. Select. Areas Commun.*, vol. 33, pp. 81–99, Jan. 2015.

[80] X. Lin, R. Ratasuk, A. Ghosh, and J. G. Andrews, "Modeling, analysis, and optimization of multicast device-to-device transmisisons," *IEEE Trans. Wireless Comm.*, vol. 13, pp. 4346–4359, Aug. 2014.

[81] Y. J. Chun, S. L. Cotton, H. S. Dhillon, A. Ghrayeb, and M. O. Hasna, "A stochastic geometric analysis of Device-to-Device communications operating over generalized fading channels," *IEEE Trans. Wireless Commun.*, vol. 16, pp. 4151 – 4165, Jul. 2017.

[82] S. Amuru, H. S. Dhillon, and R. M. Buehrer, "On jamming against wireless networks," *IEEE Trans. Wireless Commun.*, vol. 16, pp. 412–428, Jan. 2017.

[83] J. Yao, X. Zhou, Y. Liu, and S. Feng, "The intensity matching approach: A tractable stochastic geometry approximation to system-level analysis of cellular networks," *IEEE Trans. Wireless Commun.*, vol. 17, pp. 822–834, Feb. 2018.

[84] K. Lee, Y. Park, M. Na, H. Wang, and D. Hong, "Aligned reverse frame structure for interference mitigation in dynamic TDD systems," *IEEE Trans. Wireless Commun.*, vol. 16, pp. 6967–6978, Oct. 2017.

[85] J. Lee and T. Q. S. Quek, "Hybrid full-/half-duplex system analysis in heterogeneous wireless networks," *IEEE Trans. Wireless Commun.*, vol. 14, pp. 2883–2895, May 2014.

[86] R. Hernandez-Aquino, S. A. R. Zaidi, D. McLernon, and M. Ghogho, "Energy efficiency analysis of two-tier MIMO diversity schemes in Poisson cellular networks," *IEEE Trans. Commun.*, vol. 63, pp. 3898–3911, Oct. 2015.

[87] P. Guan and M. D. Renzo, "Stochastic geometry analysis of the energy efficiency of downlink MIMO cellular networks," in *Proc. of IEEE Veh. Technol. Conf. (VTC Spring)*, 2015.

[88] Y. Kwon, T. Hwang, and X. Wang, "Energy-efficient transmit power control for multi-tier MIMO HetNets," *IEEE J. Select. Areas in Commun.*, vol. 33, pp. 2070–2086, Oct. 2015.

[89] M. D. Renzo and W. Lu, "System-level analysis and optimization of cellular networks with simultaneous wireless information and power transfer: Stochastic geometry modeling," *IEEE Trans. Veh. Tech.*, vol. 66, pp. 2251–2275, Mrc. 2017.

[90] M. D. Renzo, W. Lu, and P. Guan, "The intensity matching approach: A tractable stochastic geometry approximation to system-level analysis of cellular networks," *IEEE Trans. Wireless Commun.*, vol. 15, pp. 5963–5983, Sep. 2016.

[91] A. Guo and M. Haenggi, "Spatial stochastic models and metrics for the structure of base stations in cellular networks," *IEEE Trans. Wireless Commun.*, vol. 12, pp. 5800–5812, Nov. 2013.

[92] W. Lu and M. D. Renzo, "Stochastic geometry modeling of cellular networks: Analysis, simulation and experimental validation," in *Proceedings of the 18th ACM International Conference on Modeling, Analysis and Simulation of Wireless and Mobile Systems (MSWiM '15)*, pp. 179–188, Nov. 2015.

[93] A. Ghosh, N. Mangalvedhe, R. Ratasuk, B. Mondal, M. Cudak, E. Visotsky, T. A. Thomas, J. G. Andrews, P. Xia, H. S. Jo, H. S. Dhillon, and T. D. Novlan, "Heterogeneous cellular networks: from theory to practice," *IEEE Commun. Mag.*, vol. 50, pp. 54–64, Jun. 2012.

[94] N. Miyoshi and T. Shirai, "Downlink coverage probability in a cellular network with Ginibre deployed base stations and Nakagami-m fading channels," in *13th International Symposium on Modeling and Optimization in Mobile, Ad Hoc, and Wireless Networks (WiOpt)*, pp. 483 – 489, 2015.

[95] Y. Li, F. Baccelli, H. S. Dhillon, and J. G. Andrews, "Statistical modeling and probabilistic analysis of cellular networks with determinantal point processes," *IEEE Trans. Commun.*, vol. 63, pp. 3405–3422, Sep. 2015.

[96] A. Guo and M. Haenggi, "Spatial stochastic models and metrics for the structure of base stations in cellular networks," *IEEE Trans. Wireless Commun.*, vol. 12, pp. 5800–5812, Nov. 2013.

[97] H. Wei, N. Deng, W. Zhou, and M. Haenggi, "Approximate sir analysis in general heterogeneous cellular networks," *IEEE Trans. Commun.*, vol. 54, pp. 1259 – 1273, Mrc. 2016.

[98] R. K. Ganti and M. Haenggi, "Asymptotics and approximation of the SIR distribution in general cellular networks," *IEEE Trans. Wireless Commun.*, vol. 15, pp. 2130–2143, Mrc. 2016.

[99] B. Blaszczyszyn, M. K. Karray, and H. P. Keeler, "Wireless networks appear poissonian due to strong shadowing," *IEEE Trans. Wireless Commun.*, vol. 14, pp. 4379–4390, Aug. 2015.

[100] B. Blaszczyszyn and M. K. Karray, "Using poisson processes to model lattice cellular networks," in *Proc. of IEEE INFOCOM*, pp. 773–781, 2013.

[101] F. Baccelli and X. Zhang, "A correlated shadowing model for urban wireless networks," in *Proc. of IEEE INFOCOM*, pp. 801–809, Apr. 2015.

[102] D. B. Taylor, H. S. Dhillon, T. D. Novlan, and J. G. Andrews, "Pairwise interaction processes for modeling cellular network topology," in *IEEE Global Communications Conference (GLOBECOM)*, pp. 4524 – 4529, Dec. 2012.

[103] H. S. Dhillon, R. K. Ganti, and J. G. Andrews, "Load-aware modeling and analysis of heterogeneous cellular networks," *IEEE Trans. Wireless Commun.*, vol. 12, pp. 1666–1677, Apr. 2013.

[104] M. Haenggi, J. G. Andrews, F. Baccelli, O. Dousse, and M. Franceschetti, "Stochastic geometry and random graphs for the analysis and design of wireless networks," *IEEE J. Select. Areas Commun.*, vol. 27, pp. 1029–1046, Sep. 2009.

[105] H. ElSawy, A. Sultan-Salem, M.-S. Alouini, and M. Z. Win, "Modeling and analysis of cellular networks using stochastic geometry: A tutorial," *IEEE Commun. Surveys & Tutorials*, vol. 19, no. 1, pp. 167–203, 2017.

[106] H. P. Keeler, B. Blaszczyszyn, and M. K. Karray, "SINR-based k-coverage probability in cellular networks with arbitrary shadowing," in *IEEE international symposium on information theory*, Jul. 2013.

[107] B. Blaszczyszyn and H. P. Keeler, "Studying the SINR process of the typical user in poisson networks using its factorial moment measures," *IEEE Trans. Inf. Theory*, vol. 61, pp. 6774–6794, Dec. 2015.

[108] P. Herath, W. A. Krzymien, and C. Tellambura, "Coverage and rate analysis for limited information cell association in stochastic-layout cellular networks," *IEEE Trans. Veh. Tech.*, vol. 65, pp. 6962–6971, Sep. 2016.

[109] A. Sankaraman, J. w. Cho, and F. Baccelli, "Performance-oriented association in large cellular networks with technology diversity," in *28th International Teletraffic Congress (ITC 28)*, 2016. [Online]. http://arxiv.org/abs/1603.06928.

[110] A. K. Gupta, H. S. Dhillon, S. Vishwanath, and J. G. Andrews, "Downlink multi-antenna heterogeneous cellular network with load balancing," *IEEE Trans. Commun.*, vol. 62, pp. 4052–4067, Nov. 2014.

[111] V. Chandrasekhar, M. Kountouris, and J. G. Andrews, "Coverage in multi-antenna two-tier networks," *IEEE Trans. Wireless Commun.*, vol. 8, pp. 5314–5327, Oct. 2009.

[112] R. Tanbourgi, H. S. Dhillon, J. G. Andrews, and F. K. Jondral, "Dual-branch MRC receivers in the cellular downlink under spatial interference correlation," in *Proc. 20th Eur. Wireless Conf.*, pp. 13–18, May 2014.

[113] Y. L. P. Madhusudhanan, J. G. Restrepo and T. X. Brown, "Analysis of downlink connectivity models in aheterogenous cellular network via stochastic geometry," *IEEE Trans. Wireless Commun.*, vol. 15, pp. 3895–3907, Jun. 2016.

[114] C. Li, J. Zhang, J. G. Andrews, and K. B. Letaief, "Success probability and area spectral efficiency in multiuser MIMO HetNets," *IEEE Trans. Commun.*, vol. 64, pp. 1544–1556, Apr. 2016.

[115] G. V. S. S. P. Varma, G. V. V. Sharma, and A. Kumar, "Closed-form approximations for coverage and rate in a multi-tier heterogeneous network in Nakagami-m fading," 2016. Available at https://arxiv.org/abs/1604.07157.

[116] U. Schilcher, S. Toumpis, M. Haenggi, A. Crismani, G. Brandner, and C. Bettstetter, "Interference functionals in poisson networks," *IEEE Trans. Inform. Theory*, vol. 62, pp. 370–383, Jan. 2016.

[117] A. Shojaeifard, K. A. Hamdi, E. Alsusa, D. K. C. So, and J. Tang, "Exact SINR statistics in the presence of heterogeneous interferers," *IEEE Trans. Inform. Theory*, vol. 61, pp. 6759–6773, Dec. 2015.

[118] R. Vaze and R. W. Heath, "Transmission capacity of ad-hoc networks with multiple antennas using transmit stream adaptation and interference cancellation," *IEEE Trans. Inform. Theory*, vol. 58, pp. 780–792, Feb. 2012.

[119] R. H. Y. Louie, M. R. McKay, and I. B. Collings, "Open-loop spatial multiplexing and diversity communications in ad hoc networks," *IEEE Trans. Inform. Theory*, vol. 57, pp. 317–344, Jan. 2011.

[120] A. Hunter, J. G. Andrews, and S. Weber, "Transmission capacity of ad hoc networks with spatial diversity," *IEEE Trans. Wireless Commun.*, vol. 7, pp. 5058–5071, Dec. 2008.

[121] N. Jindal, J. G. Andrews, and S. Weber, "Multi-antenna communication in ad hoc networks: Achieving MIMO gains with SIMO transmission," *IEEE Trans. Commun.*, vol. 59, pp. 529–540, Feb. 2011.

[122] N. Lee, F. Baccelli, and R. W. Heath, "Spectral efficiency scaling laws in dense random wireless networks with multiple receive antennas," *IEEE Trans. Inform. Theory*, vol. 62, pp. 1344–1359, Mrc. 2016.

[123] Y. Wu, R. H. Y. Louie, M. R. McKay, and I. B. Collings, "Generalized framework for the analysis of linear MIMO transmission schemes in decentralized wireless ad hoc networks," *IEEE Trans. Wireless Commun.*, vol. 11, pp. 2815–2827, Aug. 2012.

[124] N. Lee, F. Baccelli, and R. W. Heath, "Spectral efficiency scaling laws in dense random networks with multiple receive antennas," *IEEE Trans. Inf. Theory*, vol. 62, pp. 1344–1359, Mrc. 2016.

[125] W. Shi and J. A. Ritcey, "Performance of MMSE multi-antenna receiver under hierarchical poisson random fields of interferences," in *46th Asilomar Conference on Signals, Systems and Computers (ASILOMAR)*, pp. 1167–1171, Nov. 2012.

[126] R. Tanbourgi, H. S. Dhillon, J. G. Andrews, and F. K. Jondral, "Dual-branch MRC receivers under spatial interference correlation and Nakagami fading," *IEEE Trans. Commun.*, vol. 62, pp. 1830–1844, Jun. 2014.

[127] R. H. Y. Louie, M. R. McKay, N. Jindal, and I. B. Collings, "Spatial multiplexing with MMSE receivers in ad hoc networks," in *IEEE International Conference on Communications (ICC)*, Jun. 2011.

[128] K. R. Kumar, G. Caire, and A. L. Moustakas, "Asymptotic performance of linear receivers in MIMO fading channels," *IEEE Trans. Inform. Theory*, vol. 55, pp. 4398–4418, Oct. 2009.

[129] A. Hedayat and A. Nosratinia, "Outage and diversity of linear receivers in flat-fading MIMO channels," *IEEE Trans. Signal Proc.*, vol. 55, pp. 5868–5873, Dec. 2007.

[130] B. M. Hochwald, T. L. Marzetta, and V. Tarokh, "Multiple-antenna channel hardening and its implications for rate feedback and scheduling," *IEEE Trans. Inf. Theory*, vol. 50, pp. 1893–1909, Sep. 2004.

[131] Z. Wang and G. B. Giannakis, "Outage mutual information of space-time MIMO channels," *IEEE Trans. Inform. Theory*, vol. 50, pp. 657–662, Apr. 2004.

[132] K. Stamatiou, J. G. Proakis, and J. R. Zeidler, "Spatial multiplexing in random wireless networks," *Advances In Electronics And Telecommunications*, vol. 1, pp. 5–12, Apr. 2010. [Online]. https://pdfs.semanticscholar.org/5463/1a4c7d645fc034cc0bd50edf49e940067d32.pdf.

[133] G. J. Foschini and M. J. Gans, "On limits of wireless communications in a fading environment when using multiple antennas," *Wireless Personal Communications*, vol. 6, pp. 311–335, 1998.

[134] A. M. Hunter and J. G. Andrews, "Adaptive rate control over multiple spatial channels in ad hoc networks," in *6th International Symposium of IEEE WiOPT*, pp. 469–474, Apr. 2008.

[135] T.-X. Zheng, H.-M. Wang, and M. H. Lee, "Multi-antenna transmission in downlink heterogeneous cellular networks under a threshold-based mobile association policy," *IEEE Trans. Commun.*, vol. 65, pp. 244–256, Feb. 2017.

[136] S. Park, W. Seo, S. Choi, and D. Hong, "A beamforming codebook restriction for cross-tier interference coordination in two-tier femtocell networks," *IEEE Trans. Veh. Tech.*, vol. 60, pp. 1651–1663, May 2011.

[137] J. Park, and N. Lee, and J. G. Andrews, and R. W. Heath Jr., "On the optimal feedback rate in interference-limited multi-antenna cellular systems," *IEEE Trans. Wireless Commun.*, vol. 15, pp. 5748–5762, Aug. 2016.

[138] M. D. Renzo and P. Guan, "Stochastic geometry modeling of coverage and rate of cellular networks using the Gil-Pelaez inversion theorem," *IEEE Commun. Letters*, vol. 18, pp. 1575–1578, Sep. 2014.

[139] M. D. Renzo and P. Guan, "A mathematical framework to the computation of the error probability of downlink MIMO cellular networks by using stochastic geometry," *IEEE Trans. Commun.*, vol. 62, pp. 2860–2879, Aug. 2014.

[140] W. Lu and M. D. Renzo, "Stochastic geometry analysis of multi-user mimo cellular networks using zero-forcing precoding," in *IEEE International Conference on Communications (ICC)*, pp. 1477 – 1482, Jun. 2015.

[141] M. D. Renzo and W. Lu, "Stochastic geometry modeling and performance evaluation of MIMO cellular networks using the equivalentin- distribution EiD-based approach," *IEEE Trans. Commun.*, vol. 63, pp. 977–996, Mar. 2015.

[142] L. H. Afify, H. ElSawy, T. Y. Al-Naffouri, and M.-S. Alouini, "Unified stochastic geometry model for MIMO cellular networks with retransmissions," *IEEE Trans. Wireless Commun.*, vol. 15, pp. 8595–8609, Dec. 2016.

[143] A. Shojaeifard, K. A. Hamdi, E. Alsusa, D. K. C. So, J. Tang, and K.-K. Wong, "Design, modeling, and performance analysis of multi-antenna heterogeneous cellular networks," *IEEE Trans. Commun.*, vol. 64, pp. 3104–3118, Jul. 2016.

[144] S. T. Veetil, "Performance of PZF and MMSE receivers in cellular networks with multi-user spatial multiplexing," *IEEE Trans. Wireless Commun.*, vol. 14, pp. 4867–34878, Sep. 2015.

[145] Z. Chen, L. Qiu, and X. Liang, "Area spectral efficiency analysis and energy consumption minimization in multi-antenna poisson distributed networks," *IEEE Trans. Wireless Commun.*, vol. 15, pp. 4862–4874, Jul. 2016.

[146] H. H. Yang, G. Geraci, and T. Q. S. Quek, "Energy-efficient design of MIMO heterogeneous networks with wireless backhaul," *IEEE Trans. Wireless Commun.*, vol. 15, pp. 4914–4927, Jul. 2016.

[147] Y. Wu, Y. Cui, and B. Clerckx, "Analysis and optimization of inter-tier interference coordination in downlink multi-antenna hetnets with offloading," *IEEE Trans. Wireless Commun.*, vol. 14, pp. 6550–6564, Dec. 2015.

[148] C. S. Chen, V. M. Nguyen, and L. Thomas, "On small cell network deployment: A comparative study of random and grid topologies," in *Proc. of IEEE Vehicular Technolgy Conferance (VTC Fall)*, 2012.

[149] R. Cai, W. Zhang, and P. C. Ching, "Cost-efficient optimization of base station densities for multitier heterogeneous cellular networks," *IEEE Trans. Wireless Commun.*, vol. 15, pp. 2381–2393, Mrc. 2016.

[150] j. Wen, M. Sheng, X. Wang, J. Li, and H. Sun, "On the capacity of downlink multi-hop heterogeneous cellular networks," *IEEE Trans. Wireless Commun.*, vol. 13, pp. 4092–4103, Aug. 2014.

[151] L. G. Ordonez, D. P. Palomar, and J. R. Fonollosa, "Ordered eigenvalues of a general class of hermitian random matrices with application to the performance analysis of MIMO systems," *IEEE Trans. Signal Proc.*, vol. 57, pp. 672–689, Feb. 2006.

[152] R. W. Heath Jr., and D. J. Love, "Multimode antenna selection for spatial multiplexing systems with linear receivers," *IEEE Trans. Signal Proc.*, vol. 53, pp. 3042–3056, Aug. 2005.

[153] C. B. Papadias and G. J. Foschini, "On the capacity of certain spacetime coding schemes," *EURASIP J. Appl. Signal Proc.*, vol. 5, pp. 447–458, May 2002.

[154] S. Jin, M. R. Mckay, X. Gao, and I. B. Collings, "MIMO multichannel beamforming: SER and outage using new eigenvalue distributions of complex noncentral wishart matrices," *IEEE Trans. Commun.*, vol. 56, pp. 424–434, Mrc. 2008.

[155] J. G. Andrews, A. K. Gupta, and H. S. Dhillon, "A primer on cellular network analysis using stochastic geometry," *arXiv*, 2016.

[156] M. G. Khoshkholgh, K. G. Shin, K. Navaie, and V. C. M. Leung, "Coverage performance in multi-stream MIMO-ZFBF heterogeneous networks," *IEEE Trans. Veh. Tech.*, vol. 66, pp. 6801–6818, Aug. 2017.

[157] B. Blaszczyszyn, M. K. Karray, and H. P. Keeler, "Wireless networks appear Poissonian due to strong shadowing," *IEEE Trans. Wireless Commun.*, vol. 14, pp. 4379–4390, Aug. 2015.

[158] L. J. Greenstein, S. S. Ghassemzadeh, V. Erceg, and D. G. Michelson, "Rician K-factor in narrow-band fixed wireless channels: theory, experiments, and statistical models," *IEEE Trans. Veh. Tech.*, vol. 58, pp. 4000–4011, Oct. 2009.

[159] L. G. Greenstein, S. Ghassemzadeh, V. Erceg, and D. G. Michelson, "Ricean K-factors in narrowband fixed wireless channels," in *Proc. WPMC Conf.*, Sep. 1999.

[160] V. Erceg, P. Soma, D. S. Baum, and S. Catreux, "Multiple-input multiple-output fixed wireless radio channel measurements and modeling using dual-polarized antennas at 2.5 GHz," *IEEE Trans. Wireless Commun.*, vol. 3, pp. 2288–2298, Nov. 2004.

[161] S. Dey and J. Evans, "Optimal power control over multiple time-scale fading channels with service outage constraints," *IEEE Trans. Commun.*, vol. 53, pp. 708–717, Apr. 2005.

[162] H. Shin and j. H. Lee, "Capacity of multiple-antenna fading channels: spatial fading correlation, double scattering, and keyhole," *IEEE Trans. Inform. Theory*, vol. 49, pp. 2636–2647, Oct. 2003.

[163] M. Chiani, M. Z. Win, and A. Zanella, "On the capacity of spatially correlated MIMO rayleigh-fading channels," *IEEE Trans. Inform. Theory*, vol. 49, pp. 2363–2371, Oct. 2003.

[164] C. Siriteanu, S. Kuriki, D. Richards, and A. Takemura, "Chi-square mixture representations for the distribution of the scalar Schur complement in a noncentral Wishart matrix," *Statistics and Probability Letters*, vol. 115, pp. 70–87, Aug. 2017.

[165] S. Boyd and L. Vandenberghe, *Convex Optimization*. Cambridge University Press, Cambridge, England, 2004.

[166] K. Stamatiou, J. G. Proakis, and J. R. Zeidler, "Channel diversity in random wireless networks," *IEEE Trans. Wireless Commun.*, vol. 9, pp. 2280–2289, Jul. 2010.

[167] X. Lin, J. G. Andrews, and A. Ghosh, "Spectrum sharing for Device-to-Device communication in cellular networks," *IEEE Trans. Wireless Commun.*, vol. 13, pp. 6727–6740, Dec. 2014.

[168] M. G. Khoshkholgh, K. Navaie, K. G. Shin, and V. C. M. Leung, "Performance evaluation of MISO-SDMA in heterogenous networks with practical cell association," in *IEEE 84th Veh. Technol. Conf. (VTC-Fall)*, Sep. 2016.

[169] Y. Chen and C. Tellambura, "Performance analysis of maximum ratio transmission with imperfect channel estimation," *IEEE Commun. Let.*, vol. 9, pp. 322–324, Apr. 2005.

[170] R. Tanbourgi, H. S. Dhillon, and F. K. Jondral, "Analysis of joint transmitreceive diversity in downlink MIMO heterogeneous cellular networks," *IEEE Trans. Wireless Commun.*, vol. 14, pp. 6695–6709, Dec. 2015.

[171] T. Cormen, C. Leiserson, R. Rivest, and C. Stein, *Introduction to Algorithms*. MIT Press, Cambridge, MA, 3 ed., 2009.

[172] H. Zhang, F. Niu, H. Yang, X. Zhang, and D. Yang, "Polynomial expression for distribution of the smallest eigenvalue of Wishart matrices," in *Proc. of 68th IEEE Veh. Technol. Conf. (VTC-Fall)*, Jun. 2008.

Appendix A

A Brief Introduction to Stochastic Geometry

In this appendix, we review several important concepts of stochastic geometry that are commonly used in the thesis. The materials are mainly reported from [40, 41, 42, 44, 104, 105].

A.1 Basic Concepts

Definition A.1.1 (Point Process (PP)). *A Point process* $\Phi = \{X_i : i \in \mathbb{N}\}$ *is a random collection of points in* $\mathbb{R}^d$ *(or any measure space), where* d *is the dimension. From a counting measure viewpoint, for a set* $A \in \mathbb{R}^d$ *the measure* $\#(A) = \sum_{X_i \in \Phi} 1(X_i \in A)$ *counts the number of points fallen in set* A*, the distribution of which depends on* Φ*.*

Definition A.1.2 (Poisson Point Process (PPP)). *A given Point process* $\Phi = \{X_i : i \in \mathbb{N}\}$ *is PPP if 1) for any set* $A \in \mathbb{R}^d$ *counting measure* $\#(A)$ *is a Poisson r.v. with mean* $\mu(A) = \mathbb{E}[\#(A)]$*, and 2) for countable disjoint sets* A_j*, counting measures* $\#(A_j)$ *are independent.*

Definition A.1.3 (Homogenous PPP). *For Homogenous PPP there holds* $\mu(A) = \lambda l(A)$*, where* λ *is the intensity or density of the PPP, and* $l(A)$ *is the size of set* A*, e.g., if* A *is a disk with radius* r *in* $\mathbb{R}^2$*, then* $l(A) = \pi r^2$*. This implies that*

$$P\{\#(A) = n\} = \frac{(\lambda \pi r^2)^n}{n!} e^{-\lambda \pi r^2}, \quad n = 0, 1, \ldots. \tag{A.1}$$

Theorem A.1.1 (Campbell's Theorem). *Consider function $g : \mathbb{R}^d \to R^+$, thus for PPP set $\Phi = \{X_i : i \in \mathbb{N}\}$ with density λ we have*

$$\mathbb{E}\left[\sum_{X_i \in \Phi} g(X_i)\right] = \lambda \int\limits_{\boldsymbol{x} \in \mathbb{R}^d} g(\boldsymbol{x}) \mathrm{d}\boldsymbol{x}. \tag{A.2}$$

Definition A.1.4 (Probability Generating Functional (PGFL) of PPP). *Consider function $g : \mathbb{R}^d \to R^+$, thus for PPP set $\Phi = \{X_i : i \in \mathbb{N}\}$ with density λ, PGFL of the PPP Φ with respect to g is defined as*

$$\begin{aligned} \mathrm{PGFL}_g &= \mathbb{E} \prod_{X_i \in \Phi} g(X_i) && \text{(A.3)} \\ &= e^{-\lambda \int\limits_{\boldsymbol{x} \in \mathbb{R}^d} (1 - g(\boldsymbol{x})) \mathrm{d}\boldsymbol{x}}. && \text{(A.4)} \end{aligned}$$

Definition A.1.5 (Marked PPP and Superposition). *For a homogenous PPP $\Phi = \{X_i : i \in \mathbb{N}\}$ with density λ:*

1. *One can assign mark Q_i, which can be randomly distributed according to a given distribution, say Rayleigh with mean 1, to each point to produce marked PPP $\hat{\Phi} = \{(X_i, Q_i), X_i \in \Phi\}$.*

2. *This implies that if one independently thin a PPP set Φ with probability p (i.e., retaining each point X_i with probability p and collecting only the points that are retained), the resultant process is still homogenous PPP but with density $p\lambda$.*

3. *Consider another homogenous PPP set Φ' independent of Φ, with density λ', the superposition $\Phi \bigcup \Phi'$ is again a homogenous PPP, with density $\lambda + \lambda'$.*

Definition A.1.6 (Stationary and Isotropic PPP). *A PPP set $\Phi = \{X_i : i \in \mathbb{N}\}$ is stationary if under transition the law of the process stays unaffected. Also, if rotation does not change the law of the process, the process is known as isotropic. A PPP set which is stationary and isotropic is motion-invariant.*

Definition A.1.7 (Palm Distribution). *For homogenous PPP $\Phi = \{X_i : i \in \mathbb{N}\}$ with density λ, the Palm distribution represents the conditional distribution assuming there is a point at location $\boldsymbol{x}$.*

Theorem A.1.2 (Slivnyak's Theorem). *Conditioned on having a point at $\boldsymbol{x}$, the distribution of the Point process does not change. Thus, a property of the network observed from this point will be the same all over the set irrespective of conditioning on this point.*

A.2 Interference/Shot Noise Process

Consider a homogenous PPP $\Phi = \{X_i : i \in \mathbb{N}\}$ with density λ. Let assign to each point X_i countless marks $(h_{i1}, h_{i2}, \ldots)$, where r.v. h_{ij}, drawn from PDF $f(h_1, h_2, \ldots)$, is independent across indices. For any r.v. I that is represented as $I = \sum_{X_i \in \Phi} g(X_i, (h_{i1}, h_{i2}, \ldots))$, one is able to use PGFL (A.4) to calculate the Laplace transform of I as follows

$$\begin{aligned}
\mathcal{L}_I(t) &= \mathbb{E}e^{-tI} && \text{(A.5)}\\
&= \mathbb{E}e^{-t\sum\limits_{X_i\in\Phi} g(X_i,(h_{i1},h_{i2},\ldots))} && \text{(A.6)}\\
&= \mathbb{E}_{\Phi}\mathbb{E}_{(h_{i1},h_{i2},\ldots)}\prod_{X_i\in\Phi} e^{-tg(X_i,(h_{i1},h_{i2},\ldots))} && \text{(A.7)}\\
&= \mathbb{E}_{\Phi}\prod_{X_i\in\Phi}\mathbb{E}_{(h_{i1},h_{i2},\ldots)}e^{-tg(X_i,(h_{i1},h_{i2},\ldots))} && \text{(A.8)}\\
&= e^{-\lambda\int\limits_{\boldsymbol{x}\in\mathbb{R}^d}(1-\mathbb{E}_{(h_1,h_2,\ldots)}e^{-tg(\boldsymbol{x},(h_1,h_2,\ldots))})\mathrm{d}\boldsymbol{x}}. && \text{(A.9)}
\end{aligned}$$

For the particular case that the function $g(X_i, (h_{i1}, h_{i2}, \ldots))$ is governed by the form

$$L(\|X_i\|)\hat{g}(h_{i1}, h_{i2}, \ldots),$$

where $\|X_i\|$ is the Euclidean norm, $L(\|X_i\|)$ is the path-loss function (e.g., power-law/standard path-loss function $\|X_i\|^{-\alpha}$ where $\alpha > 2$ is the path-loss exponent), and $\hat{g}(h_{i1}, h_{i2}, \ldots)$ is a

function, the r.v. I is known as interference. This r.v. is the accumulated imposed interference from all the points X_i at the origin. For this scenario a mark such as (h_{i1}, h_{i2}, h_{i3}) can be encapsulating the interfering fading power gain, designated power at point X_i, and MAC status.

Example A.2.1 (Rayleigh Fading). *Assume each point $X_i \subseteq \mathbb{R}^2$ is marked by single r.v. h_i, standing for the fading power gain between X_i and origin of exponential PDF with mean one. This implies that each transmitter is always transmitting (i.e., no MAC protocol) with constant power 1 (i.e., no power control). Further, let us consider standard path-loss function. Thus, the Laplace transform* (A.9) *is simplified to*

$$\begin{aligned} \mathcal{L}_I(t) &= e^{-2\pi\lambda \int_0^\infty x(1-\mathbb{E}_h e^{-tx^{-\alpha}h})\mathrm{d}x} && \text{(A.10)} \\ &= e^{-2\pi\lambda \int_0^\infty x(1-\frac{1}{1+tx^{-\alpha}})\mathrm{d}x} && \text{(A.11)} \\ &= e^{-\lambda C(\alpha) t^{\breve{\alpha}}}, && \text{(A.12)} \end{aligned}$$

where $C(\alpha) = \pi\Gamma(1-\breve{\alpha})\Gamma(1+\breve{\alpha})$ and $\breve{\alpha} = 2/\alpha$.

Example A.2.2 (General Fading). *In Example A.2.1, let us keep all the settings intacted, except the distribution of the mark $f(h)$ that is now assumed to be any legitimate continuous PDF. Thus, the Laplace transform* (A.9) *is*

$$\mathcal{L}_I(t) = e^{-\lambda \tilde{C}(\alpha) t^{\breve{\alpha}} \mathbb{E}[h^{\breve{\alpha}}]}, \quad \text{(A.13)}$$

where $\tilde{C}(\alpha) = \pi\Gamma(1-\breve{\alpha})$. It is easy to check that when the PDF of h is exponential, (A.13) *reduces to* (A.12).

Appendix B

Proofs for Chapter 2

B.1 Proof of Lemma 2.3.1

Adopting [43, Proof of Corollary 1], it is straightforward to show that the CCDF of r.v. H, $\overline{F}_H(z) = e^{-Mz} \sum_{m=0}^{M-1} \frac{M^m z^m}{m!}$, admits the inverse Laplace transform

$$\mathcal{L}^{-1}_{\overline{F}_{H_i}}(s) = \sum_{m=0}^{M_i-1} \frac{1}{m!} \delta^{(m)}(s-1), \tag{B.1}$$

where $\delta^{(m)}(s-1)$ is the mth derivative of Delta Dirac function, satisfying

$$\int_{-\infty}^{\infty} \delta^{(m)}(s) f(s) ds = (-1)^m \frac{d^m}{ds^m} f(s)\Big|_{s=1}. \tag{B.2}$$

On the other hand, it is a matter of straightforward differentiation to show that

$$\frac{d^m}{ds^m} s^{-\check{\alpha}}\Big|_{s=1} = (-1)^m \prod_{u=0}^{m-1} (\check{\alpha}+1) = (-1)^m \frac{\Gamma(m+\check{\alpha})}{\Gamma(\check{\alpha})}, \tag{B.3}$$

which is then used to show that

$$\int_0^{\infty} \frac{\mathcal{L}^{-1}_{\overline{F}_H(z)}(t)}{t^{\check{\alpha}}} \mathrm{d}t = \int_0^{\infty} \sum_{m=0}^{M_i-1} \frac{(-1)^m}{m!} \frac{d^m}{ds^m} s^{-\check{\alpha}}\Big|_{s=1} \tag{B.4}$$

$$= \sum_{m=0}^{M-1} \frac{\Gamma(\check{\alpha}+m)}{\Gamma(\check{\alpha})\Gamma(m+1)}, \tag{B.5}$$

where $\Gamma(.)$ is the Gamma function.

B.2 Proof of Lemma 2.3.2

Due to the independency of processes Φ_is, we can write

$$\mathbb{P}\{H \geq \Delta I\} = \mathbb{E}\int_0^\infty \mathcal{L}^{-1}_{\overline{F}_H}(t) e^{-t\Delta \sum_{j\in\mathcal{K}} I_j} \mathrm{d}t \tag{B.6}$$

$$= \int_0^\infty \mathcal{L}^{-1}_{\overline{F}_H}(t) \prod_{j\in\mathcal{K}} \mathcal{L}_{I_j}(t\Delta)\,\mathrm{d}t, \tag{B.7}$$

where $\mathcal{L}_{I_j}(t)$ is the Laplace transform of r.v. I_j, which is a shot noise process, see Appendix A. According to Example A.2.2, we then have

$$\mathcal{L}_{I_j}(t\Delta) = \mathbb{E}e^{-t\Delta \sum_{x_j\in\Phi_j} P_j \|x_j\|^{-\alpha} H_{x_j}} \tag{B.8}$$

$$= \mathbb{E}_{\Phi_j} \prod_{x_j\in\Phi_j} \mathbb{E}_{H_{x_j}} e^{-t\Delta P_j \|x_j\|^{-\alpha} H_{x_j}} \tag{B.9}$$

$$= e^{-2\pi\lambda_j \int_0^\infty [1-(1+t\Delta P_j x_j^{-\alpha})^{-M_j}] x_j dx_j} \tag{B.10}$$

$$= e^{-\pi\lambda_j (t\Delta P_j)^{\check{\alpha}} \Psi(M_j,\alpha)}, \tag{B.11}$$

where

$$\Psi(M_j,\alpha) = \int_0^\infty [1-(1+w_j^{-\alpha/2})^{-M_j}]\mathrm{d}w_j. \tag{B.12}$$

Applying (A.2.2) to the Laplace transform of the shot noise process I_j, we then obtain

$$\mathcal{L}_{I_j}(t\Delta) = e^{-\tilde{C}(\alpha)\lambda_j (t\Delta P_j)^{\check{\alpha}} \mathbb{E}[(H_j)^{\check{\alpha}}]} \tag{B.13}$$

$$= e^{-\tilde{C}(\alpha)\lambda_j (t\Delta P_j)^{\check{\alpha}} \frac{\Gamma(\check{\alpha}+M_j)}{\Gamma(M_j)}}, \tag{B.14}$$

noticing that for a ci-squared r.v. with M_j DoF $\mathbb{E}[(H_j)^{\check{\alpha}}] = \frac{\Gamma(\check{\alpha}+M_j)}{\Gamma(M_j)}$. Substituting (B.14) into (B.7) completes the proof. By comparing (B.14) and (B.11), it can be shown that

$$\Psi(M_j, \alpha) = \frac{\tilde{C}(\alpha)}{\pi} \frac{\Gamma(\check{\alpha} + M_j)}{\Gamma(M_j)}. \tag{B.15}$$

Appendix C

Other Contributions

- Mohammad G. Khoshkholgh and Victor C. M. Leung, "Characterizing mutual information of multi-stream MIMO-SVD systems in heterogeneous random networks," *IEEE Transactions on Vehicular Technology*, vol. 67, no. 1, pp. 436-453, Mar. 2017.

- Mohammad G. Khoshkholgh, Kang and Victor C. M. Leung, "Analysis of multi-stream MIMO-ZFBF communications in K-Tier HetNets under LOS/NLOS path-loss model," *submitted to IEEE Transactions on Mobile Computing*, 2017.

- Mohammad G. Khoshkholgh, Kang and Victor C. M. Leung, "Mean delay analysis of MIMO-ZFBF multiplexing in random networks under LOS/NLOS path-loss model," *to appear in IEEE Transactions on Wireless Communications*, 2018.

- Mohammad G. Khoshkholgh and Victor C. M. Leung, "Analyzing coverage probability of multi-tier heterogeneous networks under quantized multi-user ZF beamforming," *IEEE Transactions on Vehicular Technology*, vol. 67, no. 4, pp. 3319-3338, April 2018.

- Mohammad G. Khoshkholgh and Victor C. M. Leung, "Adaptive CDI-CQI feedback bit partitioning for quantized MISO-SDMA in downlink HetNets," in *Proc. of IEEE 86th Vehicular Technology Conference (VTC-Fall)*, 2017.

- Mohammad G. Khoshkholgh and Victor C. M. Leung, "Impact of LOS/NLOS propagation on the coverage performance of multi-stream MIMO-ZFBF cellular downlink," in *Proc. of IEEE 86th Vehicular Technology Conference (VTC-Fall)*, 2017.

- Mohammad G. Khoshkholgh and Victor C. M. Leung, "Evaluation of local transmission delay of MIMO-ZFBF multiplexing receivers under correlated interference," in *Proc. of IEEE PIMRC*, 2017.

- Mohammad G. Khoshkholgh, Victor C. M. Leung: "Effective capacity of multi-stream MIMO-ZFBF communications in large wireless networks," in *Proc. of IEEE 86th Vehicular Technology Conference (VTC-Fall)*, 2017

- Mohammad G. Khoshkholgh, Ali A. Haghighi, Victor C. M. Leung: "Evaluation of multicast efficiency in random clustered networks under antenna selection combining," in *Proc. of IEEE PIMRC*, 2017.

- Mohammad G. Khoshkholgh, Nader Mokari Yamchi, Keivan Navaie, Halim Yanikomeroglu, Victor C. M. Leung, Kang G. Shin: "Radio resource allocation for OFDM-based dynamic spectrum sharing: duality gap and time averaging," *IEEE Journal on Selected Areas in Communications*, vol. 33, no. 5, pp. 848-864, 2015.

- Mohammad G. Khoshkholgh, Keivan Navaie, Kang G. Shin, C.-H. Liu, Yongguang Zhang, Victor C. M. Leung, Stein Gjessing: "On the impact of delay constraint on the multicast outage in wireless fading environment.," in *Proc. ICC*, pp. 3714-3719, 2015.

- Mohammad G. Khoshkholgh, Victor C. M. Leung, Kang G. Shin: "Fast and accurate cardinality estimation in cellular-based wireless communications," in *Proc. WCNC* pp. 1119-1123, 2015.

- Mohammad G. Khoshkholgh, Yan Zhang, Kang G. Shin, Victor C. M. Leung, Stein Gjessing: "Modeling and characterization of transmission energy consumption in Machine-to-Machine networks," in *Proc. WCNC* pp. 2073-2078, 2015.

- Mohammad G. Khoshkholgh, Keivan Navaie, Kang G. Shin, Victor C. M. Leung: "Provisioning statistical QoS for coordinated communications with limited feedback," in *Proc. GLOBECOM*, 2016.

- Mohammad G. Khoshkholgh, Ali A. Haghighi, Keivan Navaie, Kang G. Shin, Victor C. M. Leung: "Exploiting quantization uncertainty for enhancing capacity of limited-feedback MISO Ad Hoc networks," in *Proc. GLOBECOM*, 2016.